Understanding the responses of marine phytoplankton to experimental warming

Submitted by

Samuel Barton

To the University of Exeter as a thesis for the degree of

Doctor of Philosophy in Biological Sciences

October 2018

I certify that all material in this thesis which is not my own work has been identified and that any material that has previously been submitted and approved for the award of a degree by this or any other University has been acknowledged

Signature: ……

Acknowledgements

This research is dedicated to my late father, Dr Andrew Barton-Breck. He was incredibly supportive of my academic journey and was especially delighted by my decision to study for a PhD. From a young age, the upbringing he provided for my brothers and I most definitely nurtured our respect and appreciation for the natural world. It is memories of him and his eternal optimism that helped me through the hardest of times over the last couple of years.

I wouldn't be anywhere without the loving support of my Mum, Julie. Thanks for always being there and everything you have done for me.

To my big brothers, Mark and Jack. Thanks for sticking together and supporting the little nerd in the family. You are always there for me to call upon.

Thanks to my wider family, in particular my Grandfather, Bert. He was a humble gentleman and a fantastic role model. He too taught me great lessons about respecting nature and the people around me.

Thank you to my partner in crime, Adeline, for all of your support these last few years and the many adventures we've shared.

Extra special thanks go to my main research supervisor, Gabriel Yvon-Durocher. I've learnt an awful lot since you first introduced me to joys of the Oxylab way back when I was studying for my MSc. Thanks for our many great discussions and being so passionate about all of my experiments and results. It has been an incredibly rewarding experience and I am extremely grateful to have had this opportunity, spending four years asking big questions and honing my skills as a researcher. I hope that we can share in the joys of seeing some of the findings from this thesis published in the near future. Beyond research, thanks for always having an open door and being there at times of difficulty.

I would also like to thank Angus Buckling and Nicholas Smirnoff for their advice, guidance and wisdom as secondary supervisors.

I have had the privilege of working in a research group with some fantastic individuals; Elisa Schaum aka The Dark Lord, Elvire Bestion, Daniel Padfield (the wizaRd), Ben Makin, Ruth Warfield and Francisca Garcia. Thanks for making long days in the lab more bearable, for sharing ideas, offering constructive feedback and for the many thought provoking conversations. I also had the pleasure of helping a handful of undergraduates with their final year projects; I am grateful to them for putting up with the thorough lab protocols and for directly assisting with some of my experiments.

Lastly, I'd likely to thank all the friends that I have made along the way, for the great memories and for making coming into work every day so much easier.

Author Contributions

My main supervisor, Professor Gabriel Yvon-Durocher, assisted with the experimental design, data analysis and offered constructive advice for the writing of all three data chapters. My secondary supervisors, Professor Angus Buckling and Professor Nicholas Smirnoff also provided advice for the experimental design and constructive feedback for the writing of Chapter 2. Professor Angus Buckling provided guidance for the experimental design of the evolution study, Chapter 4.

Lab Assistance

Carrying out these experiments was a great undertaking and required many hours spent in the lab, often at unsociable times of the day. I was lucky enough to work with a few very enthusiastic undergraduates who partially assisted with some of the data collection; James Jenkins assisted with the metabolism measurements for Chapter 2, and Abby Masterson assisted with measuring long term changes in algal growth rate for Chapter 4. I was also greatly supported in the lab by Elisa Schaum who provided invaluable assistance with culturing techniques during the early days of this research, and Ruth Warfield who often assisted with maintenance of my many cultures. In terms of data analysis I was fortunate to be working alongside Daniel Padfield who was able to share a great deal of useful R script, in particular for modelling thermal tolerance curves and thermal performance curves. Lastly, I am grateful to Ben Makin who assisted with confocal microscope imaging that was used for Chapter 3 to derive estimates of cell volume.

Abstract

Understanding how marine phytoplankton will fare in response to the expected increases in ocean temperature over the next century is crucial for improving their inclusion in models of ocean biogeochemistry. Marine phytoplankton plays an essential role for the global carbon cycle, accounting for approximately 50% of global primary production, and provides the base of all aquatic food webs. There is currently poor understanding of what sets the limits of thermal tolerance and how quickly different species of phytoplankton can adapt to changes in environmental temperature. Furthermore, models that have previously factored for the response of phytoplankton to warming have tended to generalise their inclusion by applying the Eppley coefficient to make predictions about future ocean productivity; this is an across-species characterisation of the thermal sensitivity of phytoplankton growth rates, which assumes a monotonic, exponential, increase in maximal growth rates with temperature. To enhance our understanding of the responses of marine phytoplankton to warming we first investigated the limits of thermal tolerance, as well as the thermal performance of both photosynthesis and respiration rates, for an array of phytoplankton taxa, representing key functional groups, including: cyanobacteria, diatoms, coccolithophores, dinoflagellates and chlorophytes. We identify, qualitatively, that the limits of thermal tolerance are likely to be underpinned by the thermal performance of metabolism, whereby across all taxa respiration was more temperature dependent, and generally had a higher optimal temperature, than photosynthesis. Next, using the understanding of thermal tolerance at the species level we estimated an across-species temperature dependence of maximal growth rates that was lower than the within-species average, supporting the “partial compensation” mechanism of thermal adaptation and highlighting that the canonical Eppley coefficient is likely to under or overestimate the temperature dependence in ocean regions where particular species, or phylogenetic groups, may dominate. With this finding we were also able to associate greater thermal tolerance with covariance of other ecologically important physiological and morphological traits, highlighting that the likely restructuring of phytoplankton communities in response to warming will have strong implications for ecosystem function and biogeochemical cycles. Lastly, we investigated the pace and magnitude of thermal adaptation to a

stressful supra-optimal temperature across three very different but ecologically important phytoplankton species. We found that across the three taxa there was clear variance in the rate and magnitude of thermal adaptation, with the least complex and smallest of the three taxa showing the fastest rates of thermal adaptation and the greatest improvement in thermal tolerance. Underpinning thermal adaptation across the taxa were clear metabolic adjustments, likely to be associated with overcoming the constraints of carbon allocation to growth due to the differing thermal sensitivities of photosynthesis and respiration. We conclude that each of the main findings from this research can help improve the inclusion of marine phytoplankton in models of ocean biogeochemistry and as part of wider Earth systems models, thereby aiding predictions of the likely reorganisation of phytoplankton communities and the impact of warming on the critical ecosystem services and biogeochemical cycles that phytoplankton mediate.

Table of Contents

List of Figures and Tables

Chapter 1: Introduction

Since the evolution of the first oxygenic - photosynthesising prokaryotes, roughly 2.5 to 3 billion years ago (Allen & Martin 2007; Frei *et al.* 2009; Schirrmeister *et al.* 2013), planetary oceanic and climatic perturbations have shaped the diversity of marine phytoplankton; channelling their prominence in global biogeochemical cycling and reducing atmospheric levels of carbon dioxide, becoming unconscious slaves (or dictators) to the successes of more complex life on Earth (Falkowski *et al.* 2004; Keeling 2004). Today phytoplankton are thought to be responsible for approximately 50% of global net primary production, and play a crucial role for the "biological carbon pump" whereby organically fixed carbon in the phytoplankton biomass sinks to the ocean floor and is subsequently sequestered for millions of years (Falkowski *et al.* 1998; Field *et al.* 1998). Thus, these microscopic unicellular organisms, whilst accounting for less than 1% of all photo-autotrophic biomass (Falkowski *et al.* 1998, 2004), are unequivocally important for the seemingly self-maintained Earth systems that we, and other complex life, rely on. However, we have now entered what has been labelled a human induced geological epoch, the 'Anthropocene' (Ruddiman *et al.* 2015); the roles have been reversed and humans are now causing an unprecedented increase in levels of atmospheric carbon dioxide. The associated climate change is raising sea surface temperatures and model projections suggest levels of ocean warming beyond natural variability by the end of the century (Wohlers *et al.* 2009; IPCC 2013). Crucial to understanding the implications this will have for marine ecology and the associated biogeochemical cycles is the ability of phytoplankton to adjust to warming and the associated physiological trade-offs.

What are phytoplankton?

Marine phytoplankton are an assorted group of pelagic, mostly unicellular, prokaryotic and eukaryotic photo-autotrophs with similar metabolic functions but very diverse evolutionary histories (Quigg *et al.* 2003). The word 'phytoplankton' simply translates to 'drifting (planktos) plants (phyto)'; however they are far more than subtle 'drifters'. Today they form the base of all aquatic food webs and play a fundamental role in key nutrient cycles; notably maintaining the balance of C (Carbon), N (Nitrogen) and P (Phosphorus) in marine environments, characterised by the canonical Redfield ratio of 106(C):16(N):1(P) (Redfield 1958; Toseland *et al.* 2013). The role that phytoplankton plays in bio-geochemical cycles, and for marine food webs, is largely dependent on the physiological traits of the particular phytoplankton that dominate under different thermal regimes, at different latitudes, and under varying levels of nutrient availability (Follows *et al.* 2007; Litchman *et al.* 2007; Litchman & Klausmeier 2008; Barton *et al.* 2010, 2013). Subsequently, different phylogenetic groups of phytoplankton can be found across natural environmental gradients, and this reflects the diversity of marine phytoplankton found in today's oceans. The proposed story(ies) for the evolution of phytoplankton, climaxing with the emergence of the diverse eukaryotic phytoplankton that are prevalent today is of great relevance for appreciating just how important these organisms have been for shaping the atmospheric composition and development of more complex life, but also how phytoplankton have succeeded in spite of previous global geophysical and climatic perturbations.

The phytoplankton story begins roughly 3Ga (billion years ago), when Earth's early atmosphere resembled that of today's atmosphere on Venus or Mars; with high levels of carbon dioxide, methane, nitrogen, water vapour and ammonium. The earliest life in this anaerobic greenhouse is thought to have been simple unicellular, prokaryotic, archaea and anaerobic bacteria. These were autotrophs that used rocks and minerals to generate their energy (Lenton & Watson 2012). From ~ 2.4Ga the fossil records start to show evidence of an increase in atmospheric oxygen content; there is much dispute over exactly when and how but this period marks the arrival of the first photo-autotrophs (Falkowski *et al.* 2004; Lenton & Watson 2012). This crucial event, or series of events,

represents the evolution of an anaerobic bacterium into a cyanobacterium through the development of the key photosynthetic proteins. Essentially this gave the organism the ability to use photons to efficiently split water, producing electrons to drive the fixation of atmospheric carbon dioxide into chemical energy (and biomass) with oxygen as a waste product (Allen & Martin 2007). As a result, atmospheric oxygen levels gradually rose and this led to the eventual evolution of aerobic bacteria. This was followed by the first key endosymbiosis event whereby a phagocytic archaea is thought to have engulfed an aerobic bacterium, forming a symbiotic relationship and eventual transfer of DNA with the host. These were the first eukaryotic cells with the aerobic 'slave' becoming the first mitochondria (Sagan 1967; Knoll 1992). Roughly 1.6-1.8Ga a further symbiotic event occurred when a eukaryote engulfed a cyanobacterium (Falkowski *et al.* 2004); DNA was transferred to the host nucleus and the relationship became permanent – the cyanobacterium 'slave' became the plastid and the first eukaryotic phytoplankton had evolved (see Figure.1.1). In phycology literature this is referred to as primary endosymbiosis (Falkowski *et al.* 2004; Keeling 2004); the phytoplankton primary endosymbionts can be divided into green algae, red algae and glaucophytes.

All green land plants evolved from the green algae and most marine and freshwater phytoplankton with a green plastid in today's oceans are primary endosymbionts (Lewis & McCourt 2004). Red algae on the other hand are not associated with land plants; they are more commonly associated with seaweeds (macro-algae) and with the exception of a few mesophilic open ocean dwellers most unicellular species are thermo-acido-philes (Saunders & Hommersand 2004; Bhattacharya *et al.* 2013). However, In terms of evolutionary history it is the red algae that have gone on to form a much greater diversity through secondary endosymbiosis compared to the greens (Falkowski *et al.* 2004; Saunders & Hommersand 2004). As with primary endosymbionts, the evolution of all secondary endosymbiont phyla is thought to be a result of a eukaryotic cell engulfing and exchanging DNA with a red or green alga. It is estimated the first secondary endosymbionts evolved ~1-1.2Ga and have continued to evolve and diversify throughout major climatic and tectonic earth systems perturbations until present day (Falkowski *et al.* 2004).

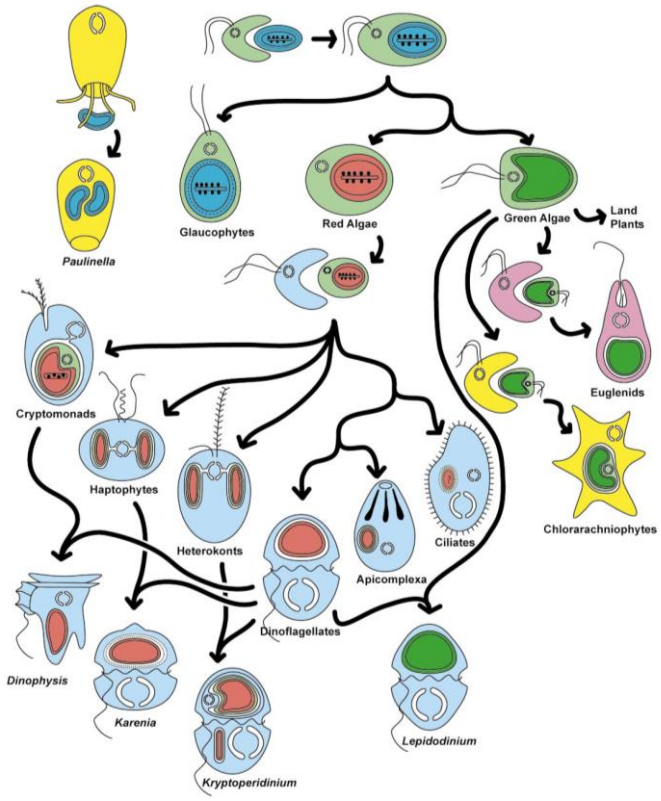

Figure 1.1 The history of marine phytoplankton evolution; a series of endosymbiosis events (taken from Keeling (2004)):The diagram illustrates the primary endosymbiosis event that give rise to Glaucophytes, Red algae and Green algae (colour coded: blue, red, green respectively) and the secondary endosymbiosis events that followed. This demonstrates the greater diversity of secondary endosymbiotic phyla of the red lineage compared to the green lineage. Keeling (2004), as shown here, favour the theory that there was just one secondary symbiosis event with a red alga – from which the lineage diverged into the 6 secondary phyla. This is contested by Falkowski *et al* (2004) who suggest the idea that there were many secondary endosymbiosis events in the red lineage- primarily because of a competitive advantage by forming a symbiotic relationship with a red alga because of the greater retention of DNA in red plastids.

In marine environments there are only two well established secondary endosymbionts of the green lineage: Euglenids and Chlorarachniophytes. Throughout the Palaeozoic, ~542-252Ma (Ma; millions of years ago), it was the primary and secondary green algae that would have dominated aquatic ecosystems. However, in today's oceans these secondary species, of the green lineage are fairly underrepresented in comparison to secondary endosymbionts of the red lineage (Grzebyk *et al.* 2003; Lewis & McCourt 2004). Following the Great Permian-Triassic extinction (~252Ma) the secondary red algae became

much more prevalent globally (Grzebyk *et al.* 2003). In the red lineage there are 6 major secondary phyla: Apicomplexa, Cilliates, Cryptomonads, Dinoflagellates, Haptophytes (coccolithophores) and Heterokonts (diatoms) (Keeling 2004). Contrary to green secondary phyla, the red secondary phyla play a far greater role in marine ecosystems and the functioning of the carbon sink than their primary counterparts (Grzebyk *et al.* 2003; Falkowski *et al.* 2004). Diatoms alone are estimated to be responsible for approximately 40% of carbon burial by the oceans biological carbon pump (Tréguer & Pondaven 2000; Bopp *et al.* 2005), and in combination with coccolithophores and dinoflagellates it is these three phylogenetic groups that are responsible for most of the export of organic carbon to ocean sediments (Falkowski *et al.* 2004). Furthermore, it is bloom forming phytoplankton such as diatoms, coccolithophores and dinoflagellates that under episodes of high nutrient concentration are essential for the feeding of higher trophic levels and thus the wider functioning of marine ecosystems.

After the rise in prevalence of these phylogenetic groups, along with the expansion of the Atlantic Ocean Basin and increased nutrient input (particularly silica) from weathering of continental land masses (Retallack 2001; Falkowski *et al.* 2004), there was generally greater primary production by marine phytoplankton, and thus the increased carbon uptake by the oceans resulted in much greater depletion of carbon dioxide from the atmosphere. Subsequently, since the Early Jurassic period (~205Ma), this was correlated with a gradual increase in atmospheric oxygen concentration; which is deemed a key contributing factor to the eventual evolution and increase in size of placental mammals (Falkowski *et al.* 2005).

Given the evolutionary history and diversity of marine phytoplankton outlined above, this provides rationale to investigate the largely unexplored metabolic thermal performance and tolerance for a wide range of phytoplankton isolates - encompassing cyanobacteria and both the red and green plastid types (Grzebyk *et al.* 2003; Falkowski *et al.* 2004; Keeling 2004, 2010). This would enable enhanced predictions for the likely responses of these diverse organisms to elevated temperature, by determining whether in spite of their facetted evolutionary histories there are similar or contrasting temperature

sensitivities and mechanisms of thermal adaptation across a wide range of species.

Responses of phytoplankton to warming

Due to anthropogenic burning of fossil fuels and land use change, increases in greenhouse gases since the industrial revolution, and arguably much earlier than that (Ruddiman *et al.* 2015), have resulted in an increase of global average temperatures. Subsequently the planet's oceans are experiencing unprecedented rates of change (Henson *et al.* 2017); the past 50 years have seen average sea surface temperatures increase by approximately 0.1ºC per decade (IPCC 2013), with projections suggesting a further average increase of 3 ºC by the end of the century (Collins *et al.* 2013). Warming of the oceans is considered to be a key factor behind recent declines in global phytoplankton productivity (Behrenfeld *et al.* 2006; Boyce *et al.* 2010; Capuzzo *et al.* 2018), and furthermore ecosystem models predict further declines in marine primary production over this century (Laufkotter *et al.* 2015).

A key mechanistic factor driving the decrease in primary production is that warming leads to increased ocean stratification, which consequently increases nutrient limitation, and thus this results in reduced phytoplankton growth (Falkowski *et al.* 1998; Behrenfeld *et al.* 2006; Irwin & Oliver 2009; Martinez *et al.* 2009; Boyce *et al.* 2010; Laufkotter *et al.* 2015). It is also expected that warming increases the rate of grazing by micro-zooplankton (Chen *et al.* 2012; Laufkotter *et al.* 2015), and this will also be a contributing factor to overall declines in productivity. Of more relevance however for understanding the direct effects of warming on phytoplankton fitness is the implication that primary production may decrease due to temperatures exceeding the limits of thermal tolerance for many taxa, resulting in local extinctions and potential migrations (Thomas *et al.* 2012, 2016; Boyd *et al.* 2013). This is attributable to the fact that marine phytoplankton exhibit large variability in their thermal tolerance, typically characterised by thermal tolerance curves, which reflect the specialisation of an organism to a thermal niche (see Figures 1.2 and 1.3). Like most ectothermic organisms, phytoplankton demonstrate a unimodal response of growth rate to

increase in temperature with left-skew, meaning that growth rates decline more rapidly beyond the thermal optima than below (Thomas *et al.* 2012). It has been demonstrated that optimal temperatures of phytoplankton growth can range between 2 and 38°C and that this large range in performance is directly correlated with the average temperatures of the environment, thus thermal optima can somewhat reflect the latitudinal gradient in average sea surface temperatures (Thomas *et al.* 2012, 2016). As a result of this, taxa that are specialised to particular thermal regimes, may well encounter temperatures in excess of their thermal optima as a result of warming and more extreme weather events (IPCC 2013). This is likely to be problematic, especially at lower latitudes and in tropical regions because many species exist at, or regularly experience, temperatures close to their limits of thermal tolerance. Therefore diversity of phytoplankton in these regions is most at risk to the expected increases in sea surface temperatures (Thomas *et al.* 2012, 2016).

With extinctions comes reorganisation of communities. As different phytoplankton have vastly different physiological traits, potential community restructuring is likely to have significant knock-on effects for bio-geochemical cycles and ecosystem functioning that is mediated by phytoplankton assemblages (Follows *et al.* 2007; Litchman *et al.* 2007; Litchman & Klausmeier 2008; Barton *et al.* 2013). As an example, cell size is a physiological trait that may well co-vary with greater thermal tolerance, however size is also 'master trait' that can drive many other physiological properties, such as: nutrient affinity, carbon storage, sinking velocities, resistance to grazing and light utilisation, all of which implicate primary productivity, trophic energy transfer and functioning of bio-geochemical cycles (Raven 1998; Litchman & Klausmeier 2008).

Although expected extinctions and resultant community reorganisation has been predicted, recent experimental evidence suggests that phytoplankton have the ability to rapidly adapt to abrupt warming of their environment (Listmann *et al.* 2016; Padfield *et al.* 2016; Baker *et al.* 2018; O'Donnell *et al.* 2018; Schaum *et al.* 2018). This knowledge is useful for reassessing the levels extinction, and subsequent reductions in primary production inferred from previous predictions (Thomas *et al.* 2012; Laufkotter *et al.* 2015); however, greater empirical

research is needed that covers a wider range species, representing the diversity of marine phytoplankton, but also that encompasses the effect of different ancestral environments i.e. how the potential for adaptation may vary across a range of latitudes for a particular species. Furthermore, thermal adaptation in itself can result in intra-specific physiological trait trade-offs and therefore despite the ability for phytoplankton to rapidly adapt there could still be strong implications for the ecosystem functioning.

Inclusion of phytoplankton in models

Despite recent research demonstrating that phytoplankton taxa show large variation in their thermal tolerance (Thomas *et al.* 2012, 2016; Boyd *et al.* 2013), and that they can rapidly adapt to changes in environmental temperature (Listmann *et al.* 2016; Padfield *et al.* 2016; Baker *et al.* 2018; O'Donnell *et al.* 2018; Schaum *et al.* 2018), the current inclusion of marine phytoplankton in climate change related ecosystem and biogeochemical models is simplified and likely to under or over predict the effects of warming on phytoplankton performance. To date, most models that have attempted to encompass the effects of warming on phytoplankton performance have applied the canonical Eppley coefficient to describe the temperature dependent responses of phytoplankton growth rates (Thomas *et al.* 2012; Laufkotter *et al.* 2015).

The Eppley coefficient describes the exponential increase in maximal growth rates observed from a meta-analyses of both marine and freshwater phytoplankton taxa (Eppley 1972). The thermal performance curve from which the Eppley coefficient is derived is therefore an across-species interpretation of how maximal growth rates increase with temperature (see Figure. 1.2a), defined by a Q_{10} value of 1.88 (which factors for the increase in rate per 10°C temperature increase). Generally, ecosystem and biogeochemical models have used the Eppley coefficient to directly factor for the thermal sensitivity of phytoplankton growth rates (Laufkotter *et al.* 2015) and to indirectly predict the thermal sensitivity of net primary production across global scales (Stock *et al.* 2014; Laufkotter *et al.* 2015). Other model based studies have used the Eppley curve to constrain predictions of growth rate and thermal tolerance for a wide-range of phytoplankton strains, with an emphasis on understanding the impact

of warming on community structure and latitudinal biodiversity of phytoplankton (Thomas *et al.* 2012). Overall, though application of the Eppley coefficient provides a quantitative estimate of how phytoplankton are likely to respond to warming, and it has since been supported by more robust statistical analyses (Bissinger *et al.* 2008), there are a number of assumptions made by such an application, and thus its inclusion in models is likely to reflect a limited foresight.

Firstly, as the Eppley coefficient stems from a meta-analysis of both freshwater and marine phytoplankton species, this overlooks the possibility that specific taxa, adapted to a particular environment, may well demonstrate thermal sensitivity to temperature increase that is less than, or greater than the Eppley coefficient. As different phylogenetic groups of phytoplankton are more prevalent in some regions, or latitudes, than others the subsequent use of a single coefficient to describe all phytoplankton growth responses to temperature increase not only has the potential to misrepresent particular taxa but entire ocean regions where specific taxa may dominate the phytoplankton assemblages (Follows *et al.* 2007; Barton *et al.* 2010, 2013). Furthermore, as the Eppley curve is based on a meta-analysis it is likely to have intrinsic limitations and uncertainties as a result of combining data from different laboratories where different methods were employed (e.g. different light regimes, nutrient concentrations and culture regimes).

In addition to this, application of the Eppley curve assumes that species that have adapted to have higher thermal optima will also have higher maximal growth rates. This assumption disregards the potential that in some environments, or for some taxa, the mechanism of thermal adaptation may be very different. The Eppley curve, is in itself reflective of the “hotter is better” mechanism of thermal adaptation (Kingsolver 2009; Knies *et al.* 2009; Angilletta *et al.* 2010). This mechanism supports the ‘thermo-dynamic constraint hypothesis’ whereby individuals adapted to warmer temperatures express higher performance than cold adapted individuals because low temperatures suppress biochemical reactions, and thus individuals that are adapted to cooler temperatures are likely to have a weaker maximal performance at their optimal temperature relative to warm adapted individuals (Savage *et al.* 2004b; Frazier *et al.* 2006; Knies *et al.* 2009; Angilletta *et al.* 2010). Therefore, under the “hotter is better” understanding, there is a positive effect of temperature on

maximal growth rates, and thus across species there is an observable temperature dependence of maximal growth rate (see Figure. 1.2b). Contrary to this mechanism, it is also possible that differences in maximal growth rate across individuals may reflect a 'complete compensation' or 'biochemical adaption' mechanism, whereby individuals up-regulate or down-regulate metabolic function to counter-balance the effect of temperature, and thus individuals adapt to warm environments by reducing maximal growth rates and conversely in cool environments by increasing maximal growth rates (Somero & Hochachka 1971; Clarke 2003; Angilletta *et al.* 2010). Consequently, under "complete compensation" there is temperature invariance of maximal growth rates, and thus across species there is no observable temperature dependence of maximal growth rate (see Figure. 1.2c).

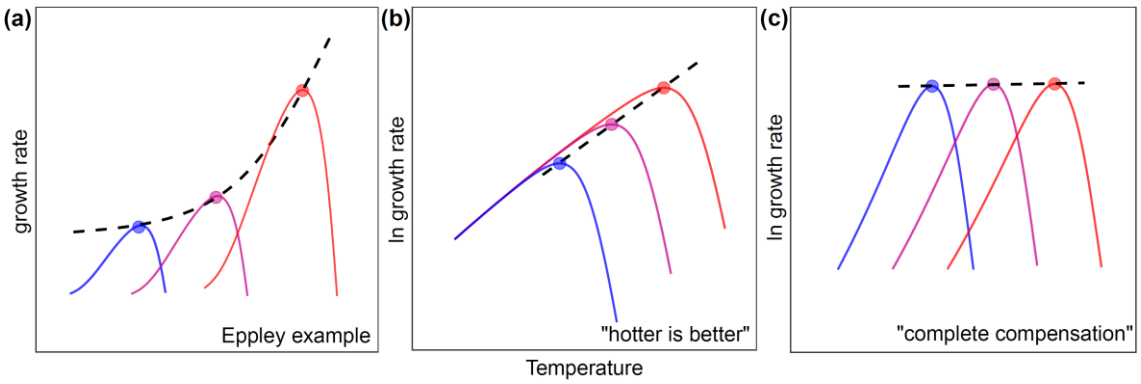

Figure 1.2 An illustration of the unimodal responses of phytoplankton growth rates to temperature increase, the proposed mechanisms of thermal adaptation and the consequential across-species temperature dependence, adapted from Padfield et al (2017). Blue colouring denotes thermal tolerance of cold adapted species and red colouring denotes warm adapted species, data points represent maximal growth rate at the thermal optima of each species. For visualisation purposes the black dashed line demonstrates the across-species temperature dependence modelled from the maximal growth rates in each plot.**(a)** A toy-diagram of the monotonic Eppley curve, which reflects the finding that phytoplankton taxa adapted to have higher thermal optima also express higher optimal growth rates, consequently a monotonic, exponential thermal sensitivity of maximal growth rates is modelled across-species (Eppley 1972) **(b)** reflects a "hotter is better" mechanism of thermal adaptation, similarly to the Eppley curve this implies that those taxa that have higher optimal temperatures tend to also have higher maximal growth rates, therefore there is a positive across-species temperature dependence of log transformed maximal growth rates, that is indistinguishable from the temperature dependence at the species level. **(c)** reflects the "complete compensation" mechanism of thermal adaptation where either warm adapted taxa have down-regulated their maximal rates and/or cold adapted taxa have upregulated their maximal rates, thus resulting in an across species

temperature dependence of log transformed maximal rates that is temperature invariant.

A further critique of the application of the Eppley coefficient is that it also overlooks the possibility that difference in maximal growth rates may also be driven by differences in size of the individuals. It is widely agreed that growth rates, and mass-specific metabolism, scale negatively with increases in cell size. This is typified by the ¾ power allometric scaling exponent (Kleiber 1932, 1947), whereby per-capita metabolic rate increases sub-linearly with body mass, and therefore mass-specific metabolic rates (and growth rates) scale negatively with body mass with a scaling exponent of -1/4. Whilst some studies have demonstrated a similar scaling for phytoplankton growth rates and metabolism (Banse 1976; Savage *et al.* 2004a; Edwards *et al.* 2012), there is a general consensus that there is divergence to a weaker size scaling for phytoplankton than expected (Banse 1982; Sommer 1989; Tang 1995; Maranón *et al.* 2007; Huete-Ortega *et al.* 2012; Sal *et al.* 2015; Kremer *et al.* 2017). Nonetheless, regardless of the magnitude of the size scaling, to accurately understand what is driving the “hotter is better” phenomenon that is portrayed by the Eppley curve it is necessary to consider the effect of cell size. If not corrected for, the effect of mass (or size) is likely to inflate or reduce the overall across-species temperature dependence, and therefore this provides further uncertainty when trying to use an across-species temperature dependence to describe community responses to temperature change where particular taxa dominate. So far only one recent study has attempted to reconcile the Eppley coefficient by including a correction for size (Kremer *et al.* 2017). Using metabolic theory of ecology (MTE), Kremer et al (2017) corrected the Eppley curve for the effect of cell size (albeit with a weaker size scaling than the ¾ power) and derived a Q_{10} value of 1.53, which is lower than the previous Eppley estimates (Eppley 1972; Bissinger *et al.* 2008); concluding that the Eppley coefficient may well over-estimate the temperature dependence of maximal phytoplankton growth, and postulating that metabolic theory provides a more accurate approach for deriving across-species temperature-scaling predictions.

From a modelling perspective, it could be argued that the application of a general thermal sensitivity, such as the Eppley coefficient, which captures the

temperature response across a broad range of species is a suitable approach for inclusion of phytoplankton in global scale models, where it is not entirely necessary to characterise the responses of specific taxa or phylogenetic groups in particular global regions. However, contrary to this, it could also be argued that the only way to improve global models is to better incorporate what happens at more regional scales where different phytoplankton taxa are more prevalent (Le Quere *et al.* 2005).

Whilst it is not clear how the assumptions surrounding the application of the Eppley coefficient effect the accuracy of the overall output of large-scale global models, it is recognised in the literature that an area for improvement to global models is to reduce the uncertainties around phytoplankton thermal sensitivity (Laufkotter *et al.* 2015; Chen & Laws 2017). Furthermore, it is not just the thermal sensitivity that could be misrepresented, it is also the fact that many models consider phytoplankton growth rates to be monotonic without an upper limit beyond which rates decrease; with the assumption that if temperatures exceed the optima of one species then there will always be another species to replace it with a greater thermal optima and maximal performance (Laufkotter *et al.* 2015). However, it has been demonstrated that in some global regions this is unlikely to be the case as many taxa are already living at temperatures close to, or beyond their thermal optima, and thus warming is likely to result in possible extinctions with uncertain species replacements and migrations. This raises concerns about the impacts of warming on phytoplankton biodiversity, and community restructuring, particularly in the tropics where many species are experiencing temperatures close to or beyond their optima (Thomas *et al.* 2012). In relation to the misrepresentation of thermal sensitivity in models, a recent study by Chen and Laws (2017) has also shown that the temperature dependence across key functional groups of phytoplankton can vary substantially, and moreover that such sensitivities deviate from the average temperature sensitivity across all functional groups; highlighting that a general temperature dependence does not do a sufficient job of representing more specific taxa. In conclusion of their findings, Chen and Laws (2017) emphasise the need for Earth system models to explicitly represent the thermal sensitivity of different phytoplankton functional groups, but acknowledge that this will require careful statistical analyses and a greater mechanistic understanding of the likely responses of different phyla to warming.

In order to accurately incorporate the variable thermal sensitivities for functional groups, or specific species, in biogeochemical models this would also require gaining a handle on the total biomass represented by such groups, alongside estimates of the change in sea surface temperature for the respective ocean regions where the groups dominate (Le Quere *et al.* 2005; Laufkotter *et al.* 2015). Furthermore, given the limits of thermal tolerance for different taxa and the likely community restructuring in response to warming (Thomas *et al.* 2012), such model adaptations would also require a firm understanding of the consequential implications of warming for ecosystem dynamics and biogeochemical cycles. This is because different functional groups of phytoplankton, for example cyanobacteria, diatoms and dinoflagellates play very different roles from a biogeochemical perspective. Cyanobacteria and other pico-phytoplankton species are known to dominate in the nutrient deplete oligotrophic ocean due to their greater nutrient affinity, which is associated with their smaller cell size (Raven 1998; Litchman *et al.* 2007). Whereas, dinoflagellates and diatoms are more commonly associated with bloom formation in ocean regions where phases of nutrient upwelling are common, or along coastal regions where there are generally greater nutrient concentrations (Litchman *et al.* 2007). These different phyla have variable functional traits (hence the term 'functional groups'); these are physiological (e.g. metabolic performance, thermal tolerance and nutrient uptake), morphological (e.g. size and shape) or behavioural (e.g. motility) traits that impact on the functioning of aquatic ecosystems and biogeochemical cycling (Litchman & Klausmeier 2008). For example the larger cell size of diatoms, with their dense silica frustules, gives them a greater sinking velocity; playing a critical role in benthic remineralisation and the oceans' biological carbon pump. Whereas, cyanobacteria, are smaller in cell size and have much lower sinking velocities, but are more nitrogen rich per unit biomass and are more susceptible to planktonic grazing (Litchman & Klausmeier 2008). Therefore, gaining a handle on the thermal sensitivity and thermal tolerance of different functional groups of phytoplankton is not just important for improving understanding of how ocean primary productivity (and phytoplankton growth) is impacted by warming, but also predicting outcomes of interspecific competition and the likely biogeochemical implications associated with changes in diversity of phytoplankton communities (Thomas *et al.* 2012). Thus, firmer understanding of

such dynamics at a species level (or functional group level) is crucial for improving model inclusion of phytoplankton in global ocean biogeochemistry models (Le Quere *et al.* 2005; Laufkotter *et al.* 2015; Chen & Laws 2017).

Applying metabolic theory of ecology (MTE) to phytoplankton responses to warming

Use of MTE can provide an alternative approach to modelling the thermal sensitivity of phytoplankton metabolism and growth rates to increasing temperature. MTE is a quantitative theory that was developed under the premise that metabolic rates are the most fundamental biological rates because they set the pace in which organisms uptake, transform and obtain energy from substrates in their surroundings. Therefore, by understanding what determines metabolic rate at the most fundamental level, this can subsequently be used to understand ecological processes across a range of scales from individuals, to communities, to ecosystems and arguably to the global biosphere (Brown *et al.* 2004). Specifically, MTE considers both body size (or mass) and temperature as the two fundamental variables that determine metabolic functioning of an individual (Gillooly 2001; Brown *et al.* 2004). This theory is encompassed by the following equation, adapted from Brown et al (2004) to be in alignment with its use in later chapters:

$$b(T) = b(T_c)M^{\alpha}e^{E_a\left(\frac{1}{kT_c}-\frac{1}{kT}\right)} \quad (1.1)$$

Where b is metabolic rate at temperature T in Kelvin (K), $b(T_c)$ is metabolic rate at a common temperature, T_c, also in Kelvin, M is mass (or another proxy for size), α is the allometric scaling exponent that describes how metabolic rate changes with M, k is the Boltzmann's constant (8.62×10^{-5} eV K^{-1}) and E_a is the activation energy which is used to describe the temperature dependence of the rate.

In light of this, much of the work that has applied ideas of MTE across diverse groups of organisms, including; microbes, ectotherms, endotherms and plants, has derived constants for α and E_a that are somewhat "universal"; with a value

for α of ~0.75 (or ¾), in agreement with earlier studies (Kleiber 1947; Gillooly 2001; Savage *et al.* 2004a; Banavar *et al.* 2010), and a value for E_a of ~0.65eV (Gillooly 2001; Allen *et al.* 2005). It has also been demonstrated that this can be scaled up to entire ecosystems, and whilst there are temporal variations to consider, short term temperature dependence of total ecosystem respiration on average has also been shown to fall close to ~0.65eV (Yvon-Durocher *et al.* 2010, 2012). However, there is also work that questions the universality of both E_a and α when applied beyond metazoans. Mass scaling of metabolic rates very much depends on the size range of organisms that have been included in its derivation. When size scaling covers major evolutionary transitions of life, encompassing prokaryotes, protists and metazoans, then a universal approach is likely to under or overestimate the size scaling (DeLong *et al.* 2010; Huete-Ortega *et al.* 2012). For example, prokaryotes have been shown to have a size scaling of >1 (DeLong *et al.* 2010; García *et al.* 2016) and protists have a scaling close to 1 (DeLong *et al.* 2010; Huete-Ortega *et al.* 2012). Specifically for phytoplankton, size scaling of growth rates and metabolic rates has also been observed to deviate from the "universal" allometric scaling (Banse 1982; Sommer 1989; Tang 1995; Maranón *et al.* 2007; Huete-Ortega *et al.* 2012; Sal *et al.* 2015; Kremer *et al.* 2017). Considering the large range of magnitudes in phytoplankton size, whereby taxa can range from 0.1 to 10^6 μm^3 in cell volume, it has been demonstrated by some studies that, similarly to the differences in size scaling observed between prokaryotes and metazoans, there are similar deviations between the size scaling of picophytoplankton (phytoplankton less than 2µm in diameter) and larger taxa such as diatoms and dinoflagellates (up to 200 µm in diameter), and this is characterised by a unimodal size scaling of phytoplankton growth rates and mass-specific rates (Marañón *et al.* 2013; López-Sandoval *et al.* 2014; Sal *et al.* 2015). Similarly to divergence away from a "universal" value for α, E_a has also been shown to vary from its "universal" value ~0.65eV. It can vary across taxa (Dell *et al.* 2011), across different ecosystems (Yvon-Durocher *et al.* 2012) and critically for the this discussion across different biological rates e.g. respiration and photosynthesis (Lopez-Urrutia *et al.* 2006; Yvon-Durocher *et al.* 2010; Regaudie-De-Gioux & Duarte 2012; Padfield *et al.* 2016). Furthermore, all estimates of temperature dependence that use standard Boltzmann-Arrhenius, functions, in accordance with Eq.1.1, are likely to show deviation in activation energy when compared to

other studies where estimates have been made over a different ranges of temperatures. This is because rates will vary depending on the activation and deactivation of particular rate limiting enzymes, so unless the range of temperatures used to derive estimates are broad enough and comparable enough across studies, there is likely to be intrinsic differences in the sensitives derived (Pawar *et al.* 2016).

Previous work that has derived activation energies for both respiration ($E_a{}^R$) and photosynthesis ($E_a{}^P$) at an ecosystem level has found that $E_a{}^R$ can fall close to the value of ~0.65eV (Allen *et al.* 2005; Yvon-Durocher *et al.* 2012) but $E_a{}^P$ is generally much lower, and variable, ranging from ~0.3eV to 0.55eV (Allen *et al.* 2005; Lopez-Urrutia *et al.* 2006; Yvon-Durocher *et al.* 2010; Regaudie-De-Gioux & Duarte 2012). A possible explanation for the greater variation and lower activation energy of photosynthesis, relative to respiration is that photosynthesis in C3 photo-autotrophs is a more diverse process whereby both carbon dioxide and oxygen compete for the active site of the enzyme Rubisco, through the processes of carboxylation (carbon dioxide fixation) and photorespiration (oxygen fixation). Thus, higher rates of photorespiration can result in less efficient photosynthesis and carbon dioxide uptake. The balance between these two processes is dependent on the partial pressures of both oxygen and carbon dioxide but also temperature (Chollet & Ogren 1975; Ehleringer *et al.* 1977; Farquhar *et al.* 1980; Bernacchi *et al.* 2001). At high temperatures the ratio of carboxylation to photorespiration is thought to decrease (Bernacchi *et al.* 2001), due to reduced affinity at the active site of rubisco for carbon dioxide relative to oxygen (Chollet & Ogren 1975). In combination with high-temperature enzyme inactivation this is an additional explanation for the unimodal relationship observed between photosynthesis rates and temperature (Farquhar *et al.* 1980; Bernacchi *et al.* 2001; Medlyn *et al.* 2002; Kattge & Knorr 2007). Therefore the derived activation energy for photosynthesis is dictated by these two competing processes in C3 plants (Farquhar *et al.* 1980; Bernacchi *et al.* 2001; Allen *et al.* 2005). This means there is an intrinsic inefficiency of photosynthesis that is likely to cause the observed higher activation energy for respiration relative to photosynthesis, $E_a{}^R > E_a{}^P$. This is why 'effective' activation energy is commonly used to term $E_a{}^P$ for previous derivations (Allen *et al.* 2005; Yvon-Durocher *et al.* 2010).

(Yvon-Durocher et al 2010b). Indeed, Allen et al (2005) modelled an $E_a{}^P$, based on carboxylation alone and the outcome was an activation energy comparable to $E_a{}^R$ (0.68eV), illustrating the negative effect of photorespiration on the temperature dependence of photosynthesis. On the other hand, when they modelled with partial pressures of carbon dioxide and oxygen set to Michaelis-Menten constants (Farquhar *et al.* 1980) and with atmospheric concentrations of carbon dioxide set to 70% of ambient levels the observed $E_a{}^P$ of 0.32ev was reproducible.

There are some exceptions to this rule, C4 photo-autotrophs show quantum yield responses largely independent of oxygen concentration, with some C4 species also demonstrating negligible temperature dependence over intermediate temperature gradients (Ehleringer *et al.* 1977). These differences, relative to C3 plants, are associated with the fact photorespiration has almost entirely been eradicated from C4 species (Chollet & Ogren 1975; Ehleringer *et al.* 1977; Rumpho *et al.* 1984); thus, regardless of partial pressures of oxygen, there is reduced 'competition' between carboxylation and photorespiration which is likely to influence the overall temperature dependence of quantum yield. Also within C3 photo-autotrophs, perhaps more pertinent in aquatic taxa, there are examples of mechanisms that have been acquired to further increase affinity for carbon dioxide fixation and therefore increasing the carboxylation to photorespiration ratio. These are known as Carbon Concentrating Mechanisms (CCMs) (Raven *et al.* 2008); and it is possible that their signature is seen in the activation energies that have been characterized for photosynthesis in aquatic ecosystems and phytoplankton communities whereby $E_a{}^P$estimates have been observed to be greater than the "effective" activation energy of 0.32eV (Yvon-Durocher *et al.* 2010; Regaudie-De-Gioux & Duarte 2012).

Despite studies that have investigated the differences in $E_a{}^P$ and $E_a{}^R$ at the community and ecosystem level (Lopez-Urrutia *et al.* 2006; Yvon-Durocher *et al.* 2010, 2012; Regaudie-De-Gioux & Duarte 2012) there is still limited work at the species level. Recent experimental studies on freshwater green algae have demonstrated that whilst in agreement with previous work that $E_a{}^R$ is greater than $E_a{}^P$ (Padfield *et al.* 2016; Schaum *et al.* 2017), the magnitude of the activation energies differ from the "universal" expectations, with estimates for

$E_a{}^R$ and $E_a{}^P$ much higher than previous estimates (~ 1 to 1.2eV for $E_a{}^R$ and ~0.65 to 0.75eV for $E_a{}^P$). To better understand this phenomenon whereby $E_a{}^R > E_a{}^P$ seems to be universal across phytoplankton communities and marine phytoplankton taxa, it is crucial to conduct similar experiments on a wider range of marine phytoplankton, representing the diversity of the different phylogenetic groups; including, cyanobacteria and phyla from the red and green "super-families". This seemingly ubiquitous observation is crucial for understanding how net carbon flux from ecosystems will respond to both short and long-term warming (Yvon-Durocher *et al.* 2012), but also at the individual level it can help to understand the underlying metabolic constraints of thermal tolerance and the potential metabolic mechanisms of thermal adaptation (Padfield *et al.* 2016; Schaum *et al.* 2017).

As marine phytoplankton are ectothermic, their thermal tolerance of growth is best characterised by a unimodal thermal tolerance curve (Thomas *et al.* 2012). If metabolic rates of photosynthesis and respiration also tend to have a unimodal response to temperature, then to improve understanding of how metabolic performance may underpin thermal tolerance it is best to parameterise these responses with the same model, and over the same range of temperatures (Pawar *et al.* 2016; García-Carreras *et al.* 2018). Unlike the monotonic Eppley curve, which assumes that maximal growth rates continue to increase with temperature, this approach at the species level allows for a more realistic interpretation of enzyme function, whereby high temperature can be rate limiting (see Figure.1.3a). Recent studies on specific phytoplankton species have had success by fitting a Sharpe-Schoolfield equation for high temperature inactivation to both phytoplankton growth rates and mass-specific metabolic rate responses to temperature (Padfield *et al.* 2016; Schaum *et al.* 2017, 2018). By combining Eq.1.1 with the Sharpe-Schoolfield equation it is possible to derive a set of parameters that describe these responses (Sharpe & DeMichele 1977; Schoolfield *et al.* 1981):

$$\ln\big(b(T)\big) = E_a\left(\frac{1}{kT_c} - \frac{1}{kT}\right) + \ln\big(b(T_c)\big) - \ln\left(1 + e^{E_h\left(\frac{1}{kT_h} - \frac{1}{kT}\right)}\right) \qquad (1.2)$$

where b is either the rate of growth, or mass specific photosynthesis or respiration, k is Boltzmann's constant, E_a is the activation energy (eV), T is temperature in Kelvin (K), E_h is the deactivation energy which characterizes

decrease in rates above T_h where half the enzymes have become non-functional and $b(T_c)$ is rate normalized to an arbitrary common temperature where there is no low or high temperature inactivation. Eq. 1.2 can also be used to derive an optimum temperature (T_{opt}) where a maximum rate is expected:

$$T_{opt} = \frac{E_h T_h}{E_h + kT_h \ln\left(\frac{E_h}{E_a} - 1\right)} \quad (1.3)$$

The parameters $b(T_c)$, E_a, E_h, and T_{opt} therefore all characterise the unimodal response of biological rates to temperature change (see Figure.1.3a).

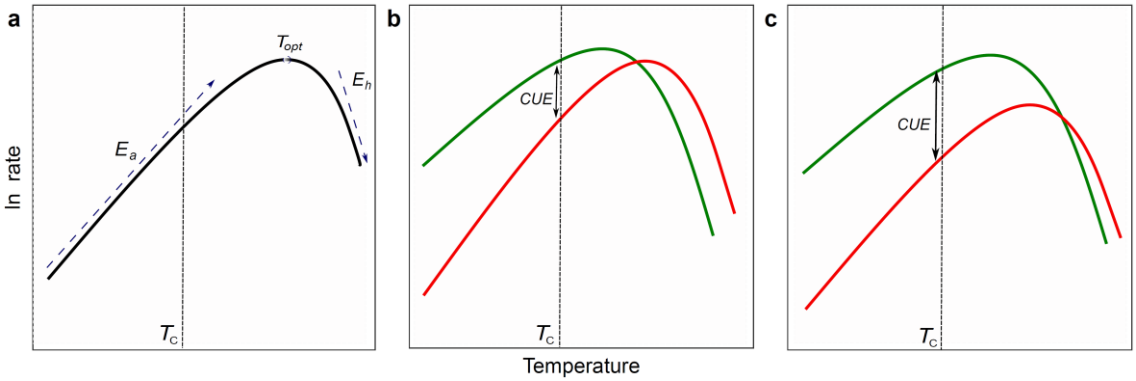

Figure 1.3. Thermal performance parameters (also applicable to thermal tolerance curves), and a hypothesised mechanism of thermal adaptation: **(a)** an illustration of the different parameters derived from fitting the Sharpe-Schoolfield model (see Eq.1.2 and 1.3) to either thermal tolerance curves or metabolism thermal performance curves, where E_a is the activation energy (eV), E_h is the deactivation energy, T_c is an arbitrary common temperature and T_{opt} is the optimum temperature of the physiological rate **(b)** an example of the differing thermal performance curves of respiration (red) and photosynthesis (green), where activation energy of respiration is greater than photosynthesis, and therefore as temperature increases towards peak rates CUE (carbon-use efficiency) decreases **(c)** an example of how phytoplankton may adapt to warmer temperatures, by increasing CUE through downregulation of respiration rates.

Though the empirical work at the species level in this field is limited to just a few studies (Padfield *et al.* 2016; Schaum *et al.* 2017, 2018), the modelling of the thermal performance of both respiration and photosynthesis has proved insightful for understanding the implications this has for growth, but also the mechanisms of thermal adaptation. As it is generally shown that ${E_a}^R > {E_a}^P$, then as temperature increases so does the relative magnitude of respiration to photosynthesis. Whilst both respiration and photosynthesis are necessary for

the production of ATP to fuel biosynthesis (Raven 1976; Shuter 1979; Raven & Geider 1988; Geider & Osborne 1989), dark respiration is also responsible for 'maintenance' and repair (Raven 1976; Geider & Osborne 1989). It is therefore considered that the majority of energy used to fuel biosynthesis comes from photosynthesis (Raven 1976; Geider & Osborne 1989). As a consequence of ${E_a}^R > {E_a}^P$, there is a greater increase of respiratory costs relative to photosynthetic carbon fixation as temperatures approach peak performance; consequently, it could be deduced that this results in a decrease in the potential for carbon allocation to growth (see Figure. 1.3b). This has been expressed in previous studies by the carbon-use efficiency (Padfield *et al.* 2017; Schaum *et al.* 2018):

$$CUE = 1 - \left(\frac{R}{P}\right) \quad (4)$$

Whereby, if respiration, R, is assumed to increase by a greater amount per unit temperature relative to photosynthesis, P, then it can be expected that carbon-use efficiency, CUE, will correlate negatively with temperature. Given the seemingly ubiquitous trend that R is more temperature dependent than P, it is therefore reasonable to assume that in order for taxa to acclimate and adapt to higher temperatures it is necessary to somehow overcome this metabolic constraint. Indeed, the aforementioned studies have also been able to associate increased thermal tolerance and improved fitness in growth rate responses over evolutionary time scales with down regulation of metabolic rates, and more specifically greater down regulation of respiration rates relative to photosynthesis rates, resulting in an improved CUE (Padfield *et al.* 2016; Schaum *et al.* 2018) (see Figure. 1.3b and 1.3c).

Experimental evolution and phytoplankton

Unlike terrestrial plants, phytoplankton make for ideal candidates in experimental evolution studies. This is mainly due to the fact that phytoplankton are unicellular organisms with relatively fast generation times and high population densities (Collins 2011; Reusch & Boyd 2013). Thus far, experimental evolution studies have demonstrated that phytoplankton can show

rapid evolution to increased carbon dioxide concentrations, and that over hundreds, to thousands, of generations this is demonstrated by changes in overall fitness and plasticity of a range of phenotypic traits (Collins & Bell 2004; Lohbeck *et al.* 2012; Schaum *et al.* 2012; Schlüter *et al.* 2014). More recently there have been a handful of studies that have investigated thermal adaptation of marine phytoplankton. These studies have shown that phytoplankton can rapidly adapt to stressful warmed environments over ~100 generations (Padfield *et al.* 2016) or more (Schlüter *et al.* 2014; Listmann *et al.* 2016; Baker *et al.* 2018; O'Donnell *et al.* 2018; Schaum *et al.* 2018), and typically this is illustrated through increased fitness over the duration of the experiment (i.e. increased growth rates) in response to the elevated temperature, as well as overall changes to the thermal tolerance curves of the warm adapted strains (normally higher optimal and maximal growth temperatures). However, so far there has been relatively poor coverage in such experiments of the diversity of marine phytoplankton.

All of these previous studies have focussed on single species making it difficult to draw comparisons about the ability of one species to adapt versus another, owing to the different experimental timeframes and methodological techniques employed by different researchers. Furthermore, only two of these studies (Padfield *et al.* 2016; Schaum *et al.* 2018) have attempted to gain an insight into the metabolic mechanisms that may be associated with the observed adaptation to high temperatures. Both of these studies identified that in coincidence with improvements of growth rates in response to the high temperatures, the warm adapted taxa appeared to show greater down regulation of mass-specific respiration rates relative to photosynthesis rates, resulting in an improved carbon-use efficiency, and thus inferring a metabolic mechanism of thermal adaptation that is driven by the greater temperature dependence of respiration relative to photosynthesis. Given the findings of previous experimental evolution studies, it is therefore pertinent to explore whether differences in the temperature dependence of respiration and photosynthesis occur across a wider range of more ecologically relevant phytoplankton, but also whether the associated metabolic mechanisms of thermal adaptation are similar given the universal metabolic constraints on thermal tolerance observed thus far. In addition to this, it is highly possible that

adaptation to high temperatures will also result in intraspecific trade-offs of key functional traits, with potential implications for bio-geochemical cycles and ecosystem functioning; for example, size and nutrient affinity (Litchman & Klausmeier 2008). However, only a few of these previous experimental evolution studies have provided evidence of such trade-offs (Baker *et al.* 2018; O'Donnell *et al.* 2018; Schaum *et al.* 2018), and therefore further work is required to explore how changes in such traits may manifest for different phytoplankton species.

A final point for consideration, in relation to previous empirical studies on phytoplankton thermal adaptation, is that different approaches are often taken to control genetic diversity at the start of the evolution experiments. One approach is to start such experiments with replicated 'clonal' populations, whereby the genetic diversity has been reduced to, in theory, one genotype, from which subsequent experimental populations grow and mutations arise. This approach has been employed by a few previous phytoplankton thermal adaptation studies (Listmann *et al.* 2016; O'Donnell *et al.* 2018; Schaum *et al.* 2018), whilst others have started their experiments without controlling for standing genetic variation (Padfield *et al.* 2016; Baker *et al.* 2018). A key argument for starting such experiments with replicated clonal populations is that it allows independent populations to develop and new mutations to arise, and thus can reflect whether the direction and magnitude of adaptation is consistent across the replicates, despite starting from the same genetic diversity. That is to say, if for example all replicates were showing a comparable level of thermal adaptation at the end of a set time-period experiment then it suggests similar mutations have been selected for, and at a similar rate. Whereas, if for example, all replicates were showing very different levels of thermal adaptation by the end of the same time-period then this might suggest otherwise. Taking such an approach is also advantageous if wanting to conduct subsequent molecular work to understand the genetic changes associated with thermal adaptation, as the clonal ancestor can be used for comparison with each experimental replicate to see how much the individual populations have diverged from the original genotype (Schaum *et al.* 2018). Contrary to this, there are also valid arguments for not using clonal populations. Firstly, as there is high standing genetic variation in natural populations, then arguably to be more reflective of

'real world' observations, it is relevant to investigate experimental evolution of populations with high genetic variation (Reusch & Boyd 2013; Padfield *et al.* 2016). Secondly, due to the greater genetic diversity, this increases the potential for beneficial mutations to arise, which subsequently increases the pace of evolution; which from a practical point of view is likely to reduce the experimental time-frame before thermal adaptation is observable in physiological responses. Critically, given these differences in approach (i.e. non-clonal versus clonal starting populations), when comparing the thermal adaptation observed across different taxa, and across different studies, this key part of the experimental design is likely to play a pivotal role in the pace and magnitude of thermal adaptation that has been reported.

Research rationale

In summary of this introductory discussion, three key problems or limitations in the current state of the field were identified, providing rationale for this thesis:

1) There is currently limited understanding of what sets the limits of thermal tolerance in different marine phytoplankton taxa. Though recent application of MTE on a few studies at the species level suggest a universal metabolic constraint, whereby respiration is more temperature sensitive than photosynthesis, better understanding is required that captures the full limits of thermal tolerance along with the metabolic performance over a similar range of temperatures. To gain a handle on whether the trends observed so far are universal (e.g. $E_a{}^R > E_a{}^P$), in spite of the multi-facetted evolutionary history of marine phytoplankton, a more diverse representation of taxa is required that encompasses cyanobacteria and the sub-lineages of the red and green super-families. This could not only aid the inclusion of marine phytoplankton in climate-change related models, but also it allows for greater understanding of the potential metabolic mechanisms that may underpin thermal adaptation.

2) Current inclusion of marine phytoplankton in ecosystem models and biogeochemical models is generalised by the Eppley coefficient, which was derived from a meta-analyses. It is unknown whether this across-species temperature dependence is representative of the average

temperature dependence at the species level, and furthermore its use overlooks the possibility of different mechanisms of adaptation across-species, which in some instances could reflect temperature invariance of the maximal performance. Consequently, it is possible that use of this coefficient may under or over-predict species responses and wider community responses if applied at a finer scale. Furthermore, despite giving an indication of how different taxa may perform in terms of growth rate in response to higher temperatures, there is little understanding of the inter-specific differences in traits associated with taxa that have higher thermal tolerance. Therefore a more detailed interpretation of an across versus within species temperature dependence is required to critique the use of the Eppley coefficient, but to also understand the inter-specific functional trait trade-offs associated with thermal adaptation and potential community restructuring.

3) Though there has been a recent flurry of studies investigating how phytoplankton adapt to warming, these studies have been limited to single taxa and, with a couple of exceptions, do not go beyond the observed improvements in thermal tolerance to try and explain the possible underlying metabolic mechanisms. Furthermore, only a few of the previous studies have associated functional trait trade-offs with warm adaptation (e.g. cell size and nutrient affinity). Therefore there is a need for studies that investigate experimental evolution for a wider range of taxa, that combine this with observations of metabolic performance and that apply the same experimental methods across the taxa. Such work would help to identify the potential for different species to improve their fitness and thermal tolerance in response to high temperature stress, and to inform whether there really are universal metabolic constraints that influence the mechanisms of thermal adaptation. In addition, it could inform on the intra-specific functional trait trade-offs associated with thermal adaptation, and thus the potential implications for the wider ecosystem functioning and biogeochemical cycles.

Research aims

In response to each of the limitations mentioned above, this thesis had three main research aims:

a) To measure the thermal tolerance of growth, and thermal performance of respiration and photosynthesis, for an array of marine phytoplankton taxa that covers their diverse evolutionary history. This will help to understand whether there are common metabolic constraints that underpin the limits of thermal tolerance.

b) Using the species level estimates of thermal tolerance, a direct comparison can be made between the species level temperature dependence of growth and the across-species temperature dependence of maximal growth rates. This will help to validate the use of an across-species temperature dependence, such as the Eppley coefficient, to account for phytoplankton responses to temperature increase in ecological and biogeochemical models. Furthermore, the inter-specific functional trait trade-offs associated with higher thermal tolerance can be inferred; allowing for likely implications for biogeochemical cycles and ecosystem function to be deduced.

c) For a selection of phytoplankton taxa, representing different phylogenetic groups, experimental evolution will be used to assess the ability to adapt to high temperature stress. This will help to understand the rate and magnitude of adaptation across the different taxa, but also the possible underlying mechanisms along with any intra-specific trait trade-offs.

The following three chapters present the findings for each of these research aims. Each chapter is written in the style of a manuscript, and thus each chapter is written with its own stand-alone materials and methods sections. The relevant supporting information for each chapter can be found in Appendices A to C, for chapters 2 to 4, respectively.

Chapter 2: Universal metabolic constraints on the thermal tolerance of marine phytoplankton

Abstract

Marine phytoplankton are responsible for over 45% of annual global net primary production. Ocean warming is expected to drive massive reorganisation of phytoplankton communities, resulting in pole-ward range shifts and sharp declines in species diversity, particularly in the tropics. The impacts of warming on phytoplankton species depend critically on their physiological sensitivity to temperature change, characterised by thermal tolerance curves. Local extinctions arise when temperatures exceed species' thermal tolerance limits. The mechanisms that determine the characteristics of thermal tolerance curves (e.g. optimal and maximal temperatures) and their variability among the broad physiological diversity of marine phytoplankton are however poorly understood. Here we show that differences in the temperature responses of photosynthesis and respiration establish physiological trade-offs that constrain the thermal tolerance of 18 species of marine phytoplankton, spanning cyanobacteria and phyla of the red and green super-families. Across all species we found that rates of respiration were more sensitive to increasing temperature and typically had higher optimal temperatures than photosynthesis. Consequently, the fraction of photosynthetic energy available for allocation to growth (carbon-use efficiency) declined exponentially with rising temperatures with a sensitivity that was invariant among the 18 species. Furthermore, the optimal temperature of growth was generally lower than that of photosynthesis and as a result, supra-optimal declines in growth rate were associated with temperature ranges where the carbon-use efficiency exhibited accelerated declines. These highly conserved patterns demonstrate that the limits of thermal tolerance in marine phytoplankton are underpinned by common metabolic constraints linked to the differential temperature responses of photosynthesis and respiration.

Introduction

The planet's oceans are changing at an unprecedented rate (Henson *et al.* 2017); over the past half-century average sea surface temperatures have been increasing by 0.1 ºC per decade (IPCC 2013) and are projected to rise by a further 3ºC or more by the end of the century (Collins *et al.* 2013). Ocean warming is thought to be a key driver of recent declines in phytoplankton productivity (Behrenfeld *et al.* 2006; Boyce *et al.* 2010; Capuzzo *et al.* 2018), and models of marine biogeochemistry predict further reductions in productivity over the 21st century as temperatures exceed limits of thermal tolerance and nutrient limitation increases in warmer, more stratified oceans (Laufkotter *et al.* 2015). Thermal tolerance curves of marine phytoplankton (like all ectotherms) exhibit characteristic unimodality and left-skew, meaning that fitness declines more sharply above the optimum temperature than below (Thomas *et al.* 2012). Marine phytoplankton species exhibit substantial variability in their thermal tolerance. Optimal temperatures for growth range between approximately 2 to 38ºC and are positively correlated with the average temperature of the environment, indicating a global pattern of thermal adaptation (Thomas *et al.* 2012, 2016). Ocean warming is expected to result in major reorganisation of marine phytoplankton communities as temperatures exceed the thermal optima of some species but not others. In particular, tropical and sub-tropical regions are projected to experience pronounced declines in species diversity and productivity (Thomas *et al.* 2012, 2016) because many of the taxa in these areas already exist close to their limits of thermal tolerance. Despite its importance for predicting the impacts of global warming on marine phytoplankton communities, we currently understand very little about the physiological processes that determine the limits of thermal tolerance in marine phytoplankton.

To address this fundamental knowledge gap we carried out a large-scale experiment to investigate the physiological mechanisms that set the limits of thermal tolerance in marine phytoplankton. Our experiments span a representative sample of the broad physiological and phylogenetic diversity of the marine phytoplankton; including 18 species belonging to ecologically important functional groups – Cyanobacteria, Diatoms, Dinoflagellates, Coccolithophores, Rhodophytes and Chlorophytes (see Appendix A Table.1).

These species were chosen to encompass the putative primary and secondary endosymbionts of both the red and green super-families, and thus reflect the complex evolutionary histories of marine phytoplankton (Falkowski *et al.* 2004; Keeling 2004). This allowed for us to investigate whether, in spite of such physiological diversity, similar physiological constraints underpin the limits of thermal tolerance across a broad range of phytoplankton taxa.

Materials and Methods

Culturing of marine phytoplankton strains

18 marine phytoplankton strains were obtained from CCAP (The Culture Collection of Algae and Protozoa) and RCC (Roscoff Culture Collection) between autumn 2015 and spring 2016. Strains of eukaryotic phytoplankton were selected from phylogenetic groups of both the red and green super-families (Falkowski *et al.* 2004; Keeling 2004), in addition to two strains of cyanobacteria. We tried to work with organisms that had been well studied in the literature, were known to be globally abundant and play crucial roles for marine ecology and global carbon cycling. The strains were originally isolated from a range of latitudes and some have since been in culture for up to 65 years (see Appendix A Table.1). Therefore, since isolation, these cultures were unlikely to have experienced many major fluctuations to their growth conditions compared to in their natural environment; thus, it is largely unknown what effect the lab-history has had on the original thermal tolerance of each strain. Stocks of each of the strains were cultured on their previous culture collection medium using artificial sea water. The following media were used: Guillard's F/2 and F/2 + Si, Keller's K, K + Si and K/2, and PCR-S11 Red Sea medium (with Red Sea salts). All stock cultures were incubated in Infors HT incubators at 20°C, under a 12:12 hour light-dark cycle with a PAR intensity of 45-50 µmol m^2 s^{-1} and shaken at 65rpm. Where possible we tried to obtain strains from the culture collections that matched, or were close to, these conditions. The red alga *Porphyridium purpureum* was an exception, which we cultured at 20-25 µmol m^2 s^{-1}. Cultures were kept under exponential, nutrient replete, growth conditions for ~ 2 months before any physiological data was collected. This was to allow the cultures some time to adjust to their new lab conditions; when we collected our thermal

tolerance data we did not want our organisms to already be in a state of acclimation in response to other abiotic variables, for example adjusting to slightly different light sources and shaking regimes compared to their previous culture collection conditions.

Measuring the thermal tolerance curve

For each species, a minimum of 3 technical replicates were inoculated with the same starting density into fresh growth medium across a range of temperatures (15°C - 37°C). Cell counts were made daily using flow cytometry (Accuri C6 flow cytometer, BD Scientific), and population density was tracked until cultures reached carrying capacity. Per capita growth rates (μ) were quantified from a modified Baranyi growth model without the lag phase(Baranyi & Roberts 1994), using non-linear least squares regression via the 'nlsMicrobio' package in R statistical software (v3.3.1). Models were fitted using the 'nlsLoop' function in the R github package 'nlsLoop'. This draws on the 'nlsLM' function in the 'minpack.lm' R package, which uses a modified Levenberg-Marquardt optimisation algorithm. Model parameters were determined by running 2000 random combinations of estimated starting parameters, which were then selected using the Akaike Information Criterion (AIC) to determine the set of parameters that best characterised the data. Growth rates derived for each technical replicate at each growth temperature were then used to determine the thermal tolerance curves (see Figure.2.1A).

Estimates of Cell Carbon and Nitrogen

For each species, an exponentially growing culture from the 20°C stock was divided into 3 technical replicates and centrifuged at 3500rpm, at 4°C for 30 minutes. The resultant pellets were rinsed with deionised water and re-spun 3 times to remove any artificial sea water residue. For the calcifying organisms (*Emiliania huxleyi, Gephyrocapsa oceanica, Thoracosphaera heimii* i.e. those with a calcium carbonate coccoliths) it was necessary to dissolve the extra-cellular inorganic carbon (Ho *et al.* 2003; Biermann & Engel 2010). This was achieved by treating these pellets with 0.5 mL of 3M HCl for 1 hour before being rinsed with deionised water and re-pelleted. All pellets were freeze-dried using a CoolSafe (95-15 PRO, ScanVac) over 24 hours and then weighed to obtain dry weight. Samples were placed in tin cups and sent to Elemtex (Elemtex Ltd,

Cornwall, UK, PL17 8QS) for elemental analysis of %C and %N using a SerCon Isotope Ratio Mass Spectrometer (CF-IRMS) system (continuous flow mode). For each technical replicate we then calculated the C:N ratio as well as $\mu g\ C\ cell^{-1}$ (micrograms of carbon per cell) (see Appendix A Table.3).

Measuring the metabolic thermal response curves

Measurements of photosynthesis and dark respiration were collected across a range of assay temperatures (7°C to 49°C) for a minimum of 3 biological replicates per species. We used a clark-type oxygen electrode as part of a Chlorolab 2 system (Hansatech Ltd, King's Lynn, UK) to measure net rates of oxygen evolution in the light (net primary production, NP) and oxygen consumption in the dark (dark respiration); both in units of μmol O_2 mL^{-1} s^{-1}. All biological replicates were sampled from the stock cultures, which had all been growing at 20°C and were taken at the mid-logarithmic growth phase to ensure that the samples were not substrate limited. To improve the signal to noise ratio when measuring rates, all biological replicate samples were concentrated by centrifugation at 1500rpm, 20°C, for 15 minutes and re-suspended into an adequate volume of fresh growth medium. Prior to running a sample at each assay temperature, all samples were given ~ 15 minutes to adjust to the assay temperature in the dark before any data was collected. This also gave the electrode system sufficient time to stabilise before metabolic rates were measured. This was necessary for two reasons, i) as the sample adjusts to the assay temperature this will naturally cause changes in the dissolved oxygen concentration, ii) the electrode system results in oxygen signal drift, and this too is temperature dependent. We measured rates of oxygen depletion from 21 sterilised artificial seawater samples across a range of temperatures 4°C - 44°C and found that the impact of drift was minimised after ~15 minutes of stabilisation time. Nevertheless, signal drift was linearly temperature dependent after this time. To account for drift in our dataset we corrected all our raw data using the following empirically derived relationship:

$$drift = (-0.392 \times T) - 6.51 \qquad (2.1)$$

Where *T* is assay temperature (°C), and *drift* is the non-biological depletion in oxygen concentration measured in units μmolO_2 mL^{-1} s^{-1} after approximately 15 minutes of stabilisation. The raw O_2 flux data was then corrected by subtracting

the estimated drift. Rates of net photosynthesis, measured as O_2 evolution, were collected across a range of light intensities from 0 to 1800 µmol m^2 s^{-1} with increments of 50 µmol m^2 s^{-1} between 0 to 200 µmol m^2 $s^{-1,}$ 100 µmol m^2 s^{-1} between 200 and 1000 µmol m^2 s^{-1}, followed by 1200 µmol m^2 s^{-1}, 1500 µmol m^2 s^{-1} and finally 1800 µmol m^2 s^{-1}. This enabled us to model a photosynthesis-irradiance (PI) curve for each assay temperature, and therefore obtain an estimate of light saturated net photosynthesis, NP_{max}, see Eq. 2.2. Respiration (*R*) was measured as oxygen consumption in the dark, over a 3-minute period directly following the light response outlined above. The photosynthesis-irradiance curve was then quantified by fitting Eiler's photoinhibition model to the data using non-linear least squares regression (as described above) (Eilers & Peeters 1988; Edwards *et al.* 2016):

$$NP(I) = \frac{NP_{max} I}{\frac{NP_{max}}{\alpha {I_{opt}}^2} I^2 + \left(1 - 2\frac{NP_{max}}{\alpha I_{opt}}\right) I + \frac{NP_{max}}{\alpha}} \qquad (2.2)$$

Where $NP(I)$ is the rate of net primary production at light intensity, I, NP_{max} is the maximum rate of NP at the optimal light intensity, I_{opt}, and α is the rate in which NP increases up to NP_{max}.

Light saturated gross primary production (*P*) was then calculated for each assay temperature as:

$$P = NP_{max} + R \qquad (2.3)$$

To investigate the effect of light limitation on the temperature dependence of photosynthesis we used Eq. 2.2 to determine the predicted NP at half the light saturated irradiance ($0.5 \times I_{opt}$). Thus replacing in NP_{max} in Eq. 2.3 with this prediction we derived $P_{0.5}$, a light limited value of gross primary production at half the saturating irradiance for each assay temperature response.

Metabolic rates were then converted from units µmol O_2 mL^{-1} s^{-1} to µg C µg C^{-1} $hour^{-1}$. We achieved this using the following equation:

$$b(\mu g\ C\ \mu g\ C^{-1}\ h^{-1}) = \frac{b(\mu mol\ O_2\ cell^{-1}\ h^{-1}) \times 32 \times M \times (\frac{12}{44})}{\mu gC\ cell^{-1}} \qquad (2.4)$$

Where b is the metabolic rate (either *P* or *R*), 32 is the molecular weight of O_2, M is a species specific assimilation quotient for CO_2:O_2 (Falkowski *et al.* 1985)

which is used to describe consumption or fixation of C in the cell per unit of O_2 , and 12/44 is the ratio of molecular weight of C to CO_2, thus $32 \times M \times \frac{12}{44}$ converts from $\mu mol\ O_2$ to μgC. Samples from each strain were analysed to determine species-specific $\mu g\ C\ cell^{-1}$ values and the number of $cells\ mL^{-1}$ was measured for each biological replicate using flow cytometry. The calculation of *M* is based on the assumption of the following balanced growth equation, where:

$$nCO_2 + (n+1)H_2O + HNO_3 \rightarrow (CH_2O)_n\ NH_3 + (n+2)O_2 \qquad (2.5)$$

If the *C:N* ratio (*n*) of the phytoplankton is calculated in moles then the ratio of CO_2:O_2, or *M*, will be equal to *n/n+2* (Falkowski *et al.* 1985). Our calculated values of *M* ranged from ~0.71 to ~0.89 (see Appendix A Table.3).

Quantifying the thermal response curves

The thermal response curves for rates of growth, photosynthesis (at both saturated and half saturated irradiance) and respiration were quantified using a modified version of the Sharpe-Schoolfield equation (Sharpe & DeMichele 1977; Schoolfield *et al.* 1981):

$$\ln\big(b(T)\big) = E_a\left(\frac{1}{kT_c} - \frac{1}{kT}\right) + \ln\big(b(T_c)\big) - \ln\left(1 + e^{E_h\left(\frac{1}{kT_h} - \frac{1}{kT}\right)}\right) \qquad (2.6)$$

where b is either the rate of growth (d^{-1}), photosynthesis or respiration ($\mu g\ C\ \mu g\ C^{-1}\ h^{-1}$), *k* is Boltzmann's constant (8.62×10^{-5} eV K^{-1}), E_a is the activation energy (eV), indicative of the steepness of the slope leading up to the thermal optima, *T* is temperature in Kelvin (K), E_h is the deactivation energy which characterizes temperature-induced decrease in rates above T_h where half the enzymes have become non-functional and $b(T_c)$ is rate normalized to an arbitrary reference temperature, here T_c = 20ºC (+ 273.15), where no low or high temperature inactivation is experienced. Eq. 2.6 can be used to derive an optimum temperature where the maximum rate is predicted:

$$T_{opt} = \frac{E_h T_h}{E_h + kT_h \ln\left(\frac{E_h}{E_a} - 1\right)} \qquad (2.7)$$

The parameters $b(T_c)$, E_a, E_h, T_h, and T_{opt}, can be considered as traits that characterise the unimodal response of biological rates to temperature change. We expect these traits to differ across the diverse taxa analysed in this study, owing to their diverse evolutionary histories and ancestral temperature regimes (given that they have been isolated from different latitudes/oceans). To test this assumption, we fitted the data for growth, photosynthesis and respiration across all species to Eq. 2.6 using non-linear mixed effects modelling with the 'nlme' package in R. We used separate analyses to assess the thermal responses of growth, photosynthesis and respiration. All models included each of the parameters in Eq. 2.6 as fixed effects, which quantify the average value of the parameter across all species and replicates. For the analysis of the thermal response of growth rate, we included 'species' as a random effect on each parameter, which quantifies species-specific deviations from the average across all species (i.e. the fixed effect) that are assumed to be normally distributed with a mean of zero. For the analyses of photosynthesis and respiration, we included 'replicate' nested within 'species' to account for the fact that we measured a minimum 3 replicate thermal response curves for each species. Here the random effect quantifies species-specific deviations from the fixed effects as well as those attributable to variance among the replicates of each species.

Because the Sharpe-Schoolfield equation can only take non-zero and positive rate values, in instances where either no observed growth rate, or a negative growth rate were measured (typically the highest and lowest temperature) we set the rate to the minimum value measured for the species in order to fit the model.

Quantifying the carbon-use efficiency and modelling the break-point temperature

The carbon-use efficiency (CUE) was calculated as:

$$\mathrm{CUE} = 1 - R/P \qquad (2.8)$$

Due to the non-linear temperature response of the CUE, with accelerated declines at high-temperatures, we fitted a segmented linear regression model to estimate the break-point in the temperature response after which the CUE exhibited an accelerated decline. We fitted the segmented linear regression

model to CUE values derived from the fitted Sharpe-Schoolfield curves for each species enabling us to derive an estimate of CUE at every 1°C increment across the range of assay temperatures where metabolic rates were measured for each species (see Figure.2.2). We fitted the break-point model to the CUE values using the 'segmented' package in R, where the breakpoint estimate is defined in the segmented model as the intersection where there is significant difference in slopes (Muggeo 2003), determined by the Davies test for performing hypothesis (Davies 1977). It is for this reason that it was necessary to use the predicted values of respiration and photosynthesis to derive the break-point, as the measured data in most cases only provided one or two data points beyond the inflection point, and this would not have been sufficient to accurately model the second slope beyond this point (see Figure.2.3). The model returned an estimate of the CUE break-point temperature and the 95% confidence intervals surrounding this value for each species (see Appendix A Table.7).

Determining the temperature dependence of the CUE

We characterized the temperature dependence of the CUE up to the CUE breakpoint temperature for each species using the Arrhenius equation,

$$\ln \mathrm{CUE}(T) = E_a{}^{CUE}\left(\frac{1}{kT_c} - \frac{1}{kT}\right) + \ln \mathrm{CUE}(T_c) \qquad (2.9)$$

where $\ln \mathrm{CUE}(T)$ is the natural logarithm of the CUE at temperature T (in Kelvin), $E_a{}^{CUE}$ is the apparent activation energy characterising the temperature dependence of CUE. We centred the temperature data using an arbitrary reference temperature T_c = 283 K = 20ºC, so that $\ln \mathrm{CUE}(T_c)$ is the CUE at T_c. We fitted Eq. 2.9 to all the measurements of CUE, up to the CUE break-point temperature identified for each species (see Figure.2.4, and Appendix A Table.8) using a linear mixed effects model. This allowed us to derive an average value for $E_a{}^{CUE}$ and $\ln \mathrm{CUE}(T_c)$ across the 18 species. We also included random effects of 'replicate' nested within 'species' in the model to account for the fact we measured a minimum of 3 replicate responses of respiration and photosynthesis for each species. This allowed us to capture the species-specific estimates $E_a{}^{CUE}$ and $\ln \mathrm{CUE}(T_c)$ (see Appendix A Table.8).

Results & Discussion

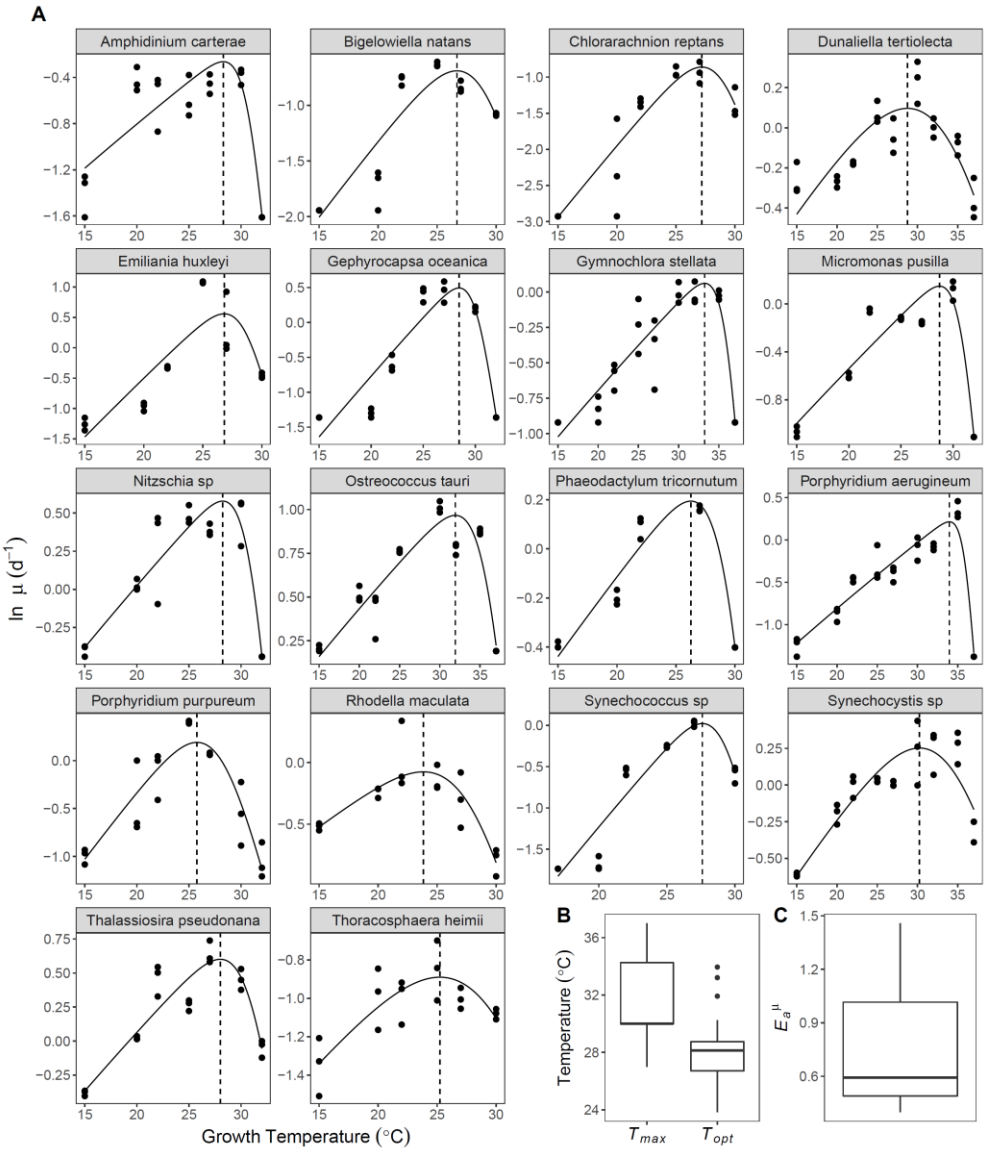

Figure.2.1 Thermal tolerance curves for 18 species of marine phytoplankton. (A) Thermal reaction tolerance curves for all 18 species used in this study. The data points presented are the natural logarithm of per capita growth rate, μ, for each replicate (n= minimum of 3 technical replicates per assay temperature for each species). The fitted lines are from the predicted random effect of species derived from non-linear mixed effects modelling with a Sharpe-Schoolfield model. The vertical dashed lines correspond with the optimal temperatures of growth. **(B)** Boxplot distributions of optimal growth temperatures (T_{opt}) and maximum temperatures of growth (T_{max}) across all 18 species. **(C)** Boxplot distribution of growth activation energy, or temperature dependence ($E_a{}^{\mu}$), across all 18 species (see Appendix A Table.2). The bold horizontal line corresponds to the median value, the top and bottom of the box correspond to the 75th and 25th percentiles and the whiskers extend to the largest and smallest values no greater or less than $1.5\times$ the interquartile range, beyond which the points are plotted as outliers.

We first characterised variability in thermal tolerance curves among taxa by measuring growth rates for each species across a temperature gradient spanning 15 to 37°C and fitting the Sharpe-Schoolfield equation for high temperature inactivation to the data using non-linear mixed effects modelling (Sharpe & DeMichele 1977; Schoolfield *et al.* 1981) (see Figure.2.1). The upper limits of thermal tolerance varied across the taxa, with $T_{max}{}^{\mu}$ (maximum temperature of observed growth), ranging from 27°C to 37°C. The optimal temperature of growth, $T_{opt}{}^{\mu}$, ranged from 23.8°C to 34.0°C and the activation energy, $E_a{}^{\mu}$ – which characterises the increase in rate up to $T_{opt}{}^{\mu}$ – ranged from 0.40 eV to 1.46 eV, with an average $E_a{}^{\mu}$ of 0.77eV (95% CI: 0.58 to 0.97) (see Figure.2.1, and Appendix A Table.2). These $E_a{}^{\mu}$ values highlight that the temperature dependence of growth at the species level is significantly higher than previously reported temperature dependence parameters, such as the canonical Eppley coefficient (equivalent to $E_a{}^{\mu} \approx 0.3$ eV), that are derived by comparing maximum growth rates across many species and are the standard way in which the impacts of warming on phytoplankton productivity are represented in models of marine biogeochemistry (Eppley 1972; Chen & Laws 2017; Kremer *et al.* 2017). These findings suggest that the Eppley coefficient (and other values from similar analyses (Kremer *et al.* 2017)), which capture the broad-scale, macroecological impacts of temperature along geographic gradients, might significantly under estimate the impacts of temperature fluctuations on phytoplankton growth at local to regional scales.

To determine the physiological processes that shape the thermal tolerance curves, in particular those that determine the optimum temperature and supra-optimal declines in growth rate, it is essential to understand how the key metabolic pathways that drive biomass synthesis respond to warming. Despite having diverse evolutionary histories, all unicellular phytoplankton share common, key metabolic pathways (Quigg *et al.* 2003) and their ability to sequester carbon, and therefore grow, is ultimately determined by photosynthesis and respiration (Shuter 1979; Raven & Geider 1988). The light-dependent reactions of photosynthesis account both for the processes that convert inorganic carbon to organic carbon stores and those that facilitate the production of ATP and reductant used to fuel biomass synthesis (Raven 1976). The dark reactions in respiration can be conceptually divided into ‘growth’ and

‘maintenance’ components (Raven 1976; Shuter 1979; Raven & Geider 1988; Geider & Osborne 1989). ‘Growth-respiration’ provides the ATP, reductant and carbon skeletons required for producing new biomass and is expected to be proportional to the rate of growth. By contrast, ‘maintenance-respiration’ provides the ATP for macromolecular turnover and the maintenance of solute gradients, and is proportional to cell biomass (Raven 1976). Whilst dark respiration clearly plays an important role in photolithotrophic growth in microalgae, the majority of the energy used to fuel biosynthesis (between 60 – 90%) is thought to derive from photosynthesis (Raven 1976; Geider & Osborne 1989). To understand the physiological constraints that shape the variability in phytoplankton thermal tolerance, we quantified temperature-dependent variation in rates of photosynthesis and dark respiration in the 18 species of marine phytoplankton.

For each species, we measured the acute responses of gross photosynthesis and dark respiration across a temperature gradient spanning 7°C to 49°C, and quantified the resultant thermal response curves by fitting the Sharpe-Schoolfield equation for high temperature inactivation to the data using non-linear mixed effects modelling (see Methods). We found consistent differences in the parameters characterising the thermal responses of photosynthesis and respiration across all the species in this study despite their diverse evolutionary histories (see Figure.2.2, and Appendix A Figure.3 and Figure.4). The activation energy for respiration was greater than that of photosynthesis in all 18 species (i.e. $E_a{}^R > E_a{}^P$; see Figure.2.2B, and Appendix A Figure.3 and Figure.4). Pooling the parameters across species yielded an average activation energy for photosynthesis of $E_a{}^P$= 0.74 eV (95% CI: 0.69 to 0.79), whilst the average for respiration was $E_a{}^R$ = 1.07 eV (95% CI: 0.98 to 1.15). Critically, the average activation energy for photosynthesis was statistically indistinguishable from that of growth rate ($E_a{}^\mu$ = 0.77eV, 95% CI: 0.58 to 0.97). These results demonstrate that respiratory costs become an increasingly large proportion of photosynthetic carbon fixation and biomass synthesis as temperatures rise toward the peak of the thermal response curves. We also found that for most species, the optimum temperature for respiration was higher than that of photosynthesis (i.e. $T_{opt}{}^R > T_{opt}{}^P$), with the average thermal optimum for photosynthesis, $T_{opt}{}^P$ = 31.18°C ± 0.83 (s.e.m.) and

respiration, $T_{opt}{}^{R}$ = 32.91°C ± 0.48 (s.e.m.) (see Figure.2.2C, and Appendix A Figure.3 and Figure.4). Furthermore, in all species, the deactivation energy, which characterises the speed that rates decline past the optimum, was lower for respiration relative to photosynthesis (i.e. $E_h{}^{P} > E_h{}^{R}$), with the average across species for photosynthesis $E_h{}^{P}$ = 6.08 (95% CI: 5.04 to 7.12) and respiration $E_h{}^{R}$ = 2.62 (95% CI: 2.31 to 2.93) (see Figure.2.2D, and Appendix A Figure.3 and Figure.4). Thus, as temperatures rise beyond T_{opt}, rates of photosynthesis decline faster than rates of respiration. Overall these findings show remarkable consistency across diverse taxa (see Appendix A Figure.3 and Figure.4) in how differences in the parameters that characterise the thermal responses of photosynthesis and respiration result in increasing respiratory expenditure of carbon fixed by photosynthesis as temperatures rise.

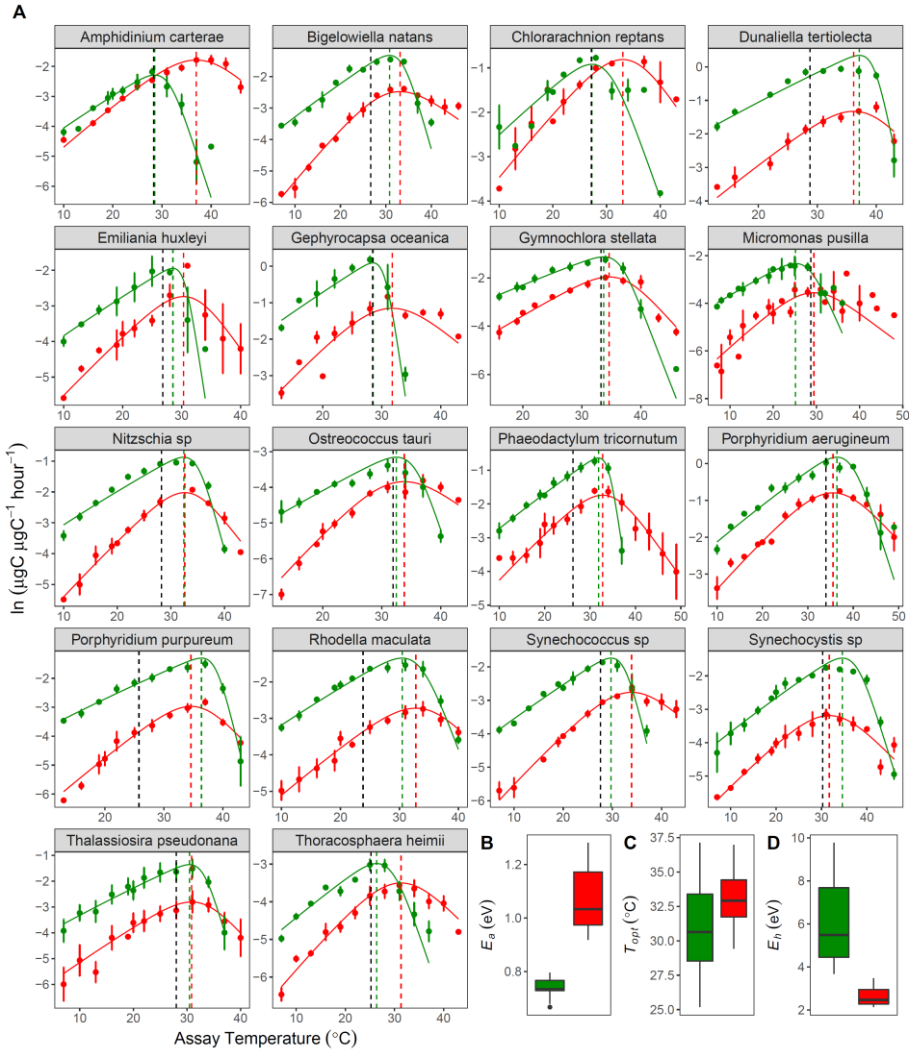

Figure.2.2 Thermal performance curves for respiration and gross photosynthesis in 18 species of marine phytoplankton. (A) Metabolic thermal performance curves for all 18 species used in this study. Green

colouring denotes gross photosynthesis, red colouring denotes respiration. The data points presented are the natural logarithm of mean metabolic, with error bars denoting ± s.e.m (*n* = minimum of 3 biological replicates per response for each species). The fitted lines for each species are from the random effects of a non-linear mixed effects model fitted to the rate data using the Sharpe-Schoolfield equation (see Methods). The vertical dashed lines correspond with the optimal temperatures for each metabolic flux, with the black dashed line added to show optimal growth temperature. **(B, C and D)** Boxplots showing the distribution of the estimated values for activation energy (E_a), optimal temperature (T_{opt}) and deactivation energy (E_h) for photosynthesis and respiration across the 18 species (see Appendix A Table.4 and Table.5).

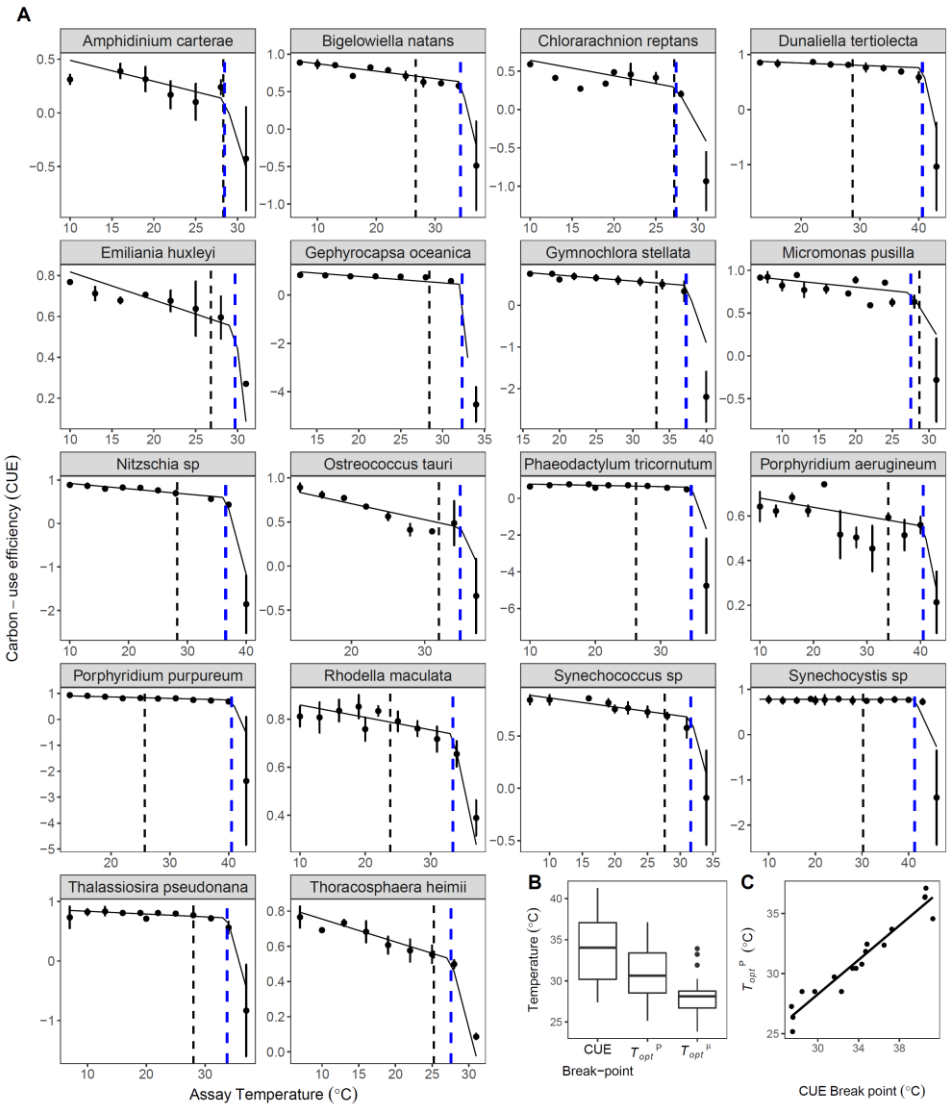

Figure.2.3 Carbon-use efficiency breakpoints constrain the optimal temperature of growth. (A) Segmented linear regression models fitted to the predicted carbon use efficiency (CUE), derived from the thermal performance parameters of respiration and photosynthesis for each species (Figure.2.2). The modelled response is presented here alongside the calculated mean CUE at each assay temperature, with error bars denoting ± s.e.m (*n* = minimum of 3 biological replicates per response for each species). The dashed vertical blue line represents the predicted break-point in the model, where there was a

significant change in the slope of the CUE thermal response. The dashed vertical black line represents the estimate optimal temperature of growth (Figure.2.1). In most cases this either coincides with the break-point, falling within the 95% CIs of the break-point, or was lower than the break-point**. (B)** Boxplots showing the distribution of the estimated values for the CUE break-point temperature, optimal temperature of gross photosynthesis ($T_{opt}{}^{P}$) and optimal temperature of growth ($T_{opt}{}^{\mu}$) across the 18 species (see Appendix A Tables.2, 5 and 7) **(C)** The significant coupling between the CUE and $T_{opt}{}^{P}$, illustrating that the sharp declines in CUE are determined by the universal metabolic constrains identified in Figure.2.2.

The carbon-use efficiency (CUE = 1-*R*/*P*), is an estimate of the fraction of photosynthetic energy (*P*) that can be allocated to growth after accounting for respiration (*R*). Recent work on both marine and freshwater phytoplankton species suggests that declines in CUE at high temperature may be linked to impaired performance at supra-optimal temperature (Padfield *et al.* 2016; Schaum *et al.* 2018). Furthermore, observations that the evolution of elevated thermal tolerance are coupled with adaptive shifts in metabolic traits that increase CUE at high temperature (Padfield *et al.* 2016; Schaum *et al.* 2017, 2018), imply an important role for CUE in constraining thermal tolerance that could provide a general explanation for high-temperature impairment of growth across the diversity of the phytoplankton. To determine whether the differential thermal responses of photosynthesis and respiration can help explain the physiological processes that constrain the thermal tolerance curves of diverse phytoplankton, we quantified how the CUE varied as a function of temperature. Consistent with previous work, we found that the CUE decreased with increasing temperature in all 18 species. Declines in the CUE with rising temperature were however highly non-linear; because $T_{opt}{}^{R} > T_{opt}{}^{P}$ and $E_h{}^{P} > E_h{}^{R}$ for most species, as temperature rose beyond $T_{opt}{}^{P}$ the CUE exhibited an accelerated decline at high temperatures. To quantify this non-linear response and the location of the inflection point where declines in CUE become accelerated, we fitted a break-point model to the thermal responses of the CUE. We found a significant break-point in the thermal response of the CUE for all 18 species that was tightly coupled with $T_{opt}{}^{P}$ (see Figure.2.3). As $E_a{}^{R} > E_a{}^{P}$ for all species, temperature dependent declines in CUE up to the break-point were universal across the species (see Figure.2.4) with an average activation energy, $E_a{}^{CUE}$, of -0.12eV (95% CI: -0.16 to -0.08). Furthermore, in all

18 species the optimum temperature for growth ($T_{opt}{}^{\mu}$) either coincided with the CUE break-point (i.e. the 95% CIs of the CUE break-point included $T_{opt}{}^{\mu}$), or was lower than the CUE break-point (see Figure.2.3). This finding suggests that temperature-driven declines in the CUE, linked to fundamental differences in the intrinsic thermal responses of photosynthesis and respiration, could play an important role in constraining the thermal tolerance of diverse marine phytoplankton. Because the metabolic costs for repair and maintenance are largely accounted for by dark respiration (Raven 1976; Geider & Osborne 1989) the temperature-driven declines in the CUE likely reflect increases in the costs associated with maintenance and repair of heat-induced cellular damage that eventually exceed the rate of substrate supply by photosynthesis, causing rates of growth to decline at supra-optimal temperatures.

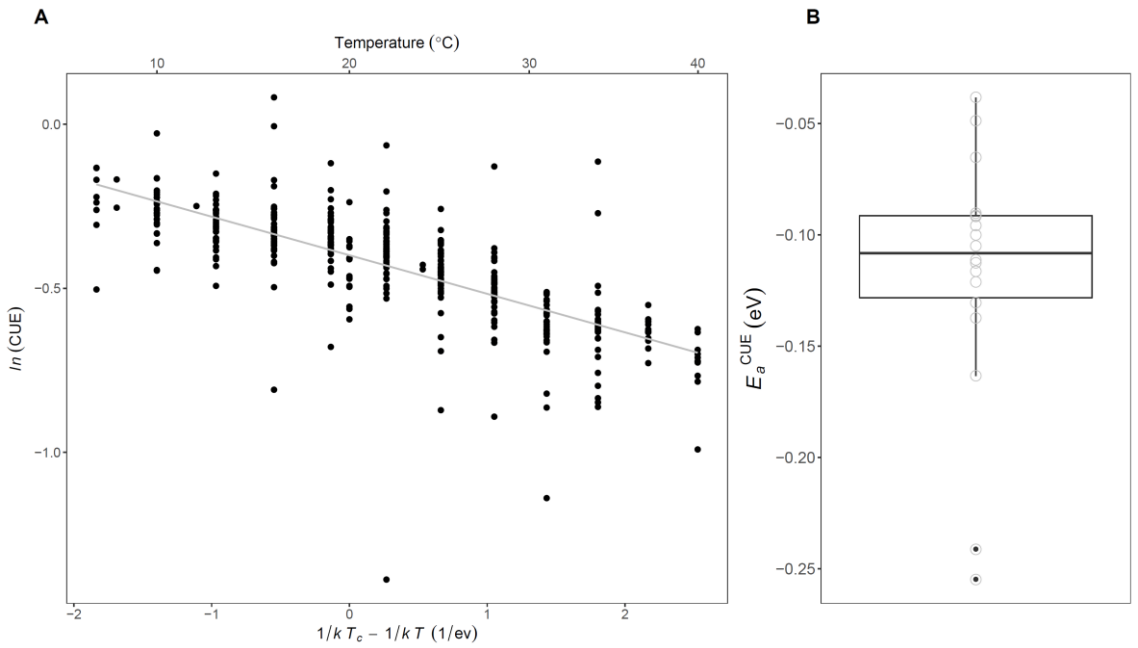

Figure.2.4 The temperature dependence of the carbon-use efficiency. (A) A scatterplot showing the relationship between the natural logarithm of the carbon-use efficiency (CUE) and standardised Boltzmann temperature up to the CUE break-point (see Figure.2.3) for the pooled dataset of 18 species, where T_c = 20°C and k is the Boltzmann constant (8.62×10^{-5} eV). The fitted line represents the fixed effect of a linear mixed effects model fitted to the data using the Boltzmann-Arrhenius equation (see Methods). Values of ln(CUE) have been standardised by dividing by the species-specific intercept derived from the random effects of the mixed effects model. This standardisation was for visualisation of the data only. The plot demonstrates that the CUE decreases up to the CUE break-point temperature with a consistent temperature dependence, equating to an average activation energy ($E_a{}^{CUE}$) of -0.12eV. **(B)** Boxplot of the species-specific $E_a{}^{CUE}$ values derived from the linear mixed effects model.

It is important to note that our experiments were conducted under nutrient replete conditions. A recent study has suggested that the temperature sensitivities of photosynthesis and respiration (Marañón *et al.* 2018) in some marine phytoplankton may decline under nutrient limitation and that the differential temperature sensitivities of photosynthesis and respiration may be negligible under limited conditions. This work however quantified the temperature sensitivities of photosynthesis and respiration at only 3 or 4 temperatures leading to estimates of thermal sensitivities with large error margins and a high probability of generating type II errors (i.e. accepting the null hypothesis of no difference in the thermal sensitivity of photosynthesis and respiration). Furthermore, measurements were made only under resource limited conditions precluding a quantitative comparison with nutrient replete conditions via the same methodology. Whilst we expect that the absolute values of the thermal sensitivities of photosynthesis and respiration are likely to decline under resource limitation, it is highly improbable that the intrinsic differences between photosynthesis and respiration documented in this study under nutrient replete conditions will be erased under nutrient limitation. Indeed, our analyses demonstrate that light limitation had a negligible impact on the temperature sensitivity of photosynthesis and in particular, the fundamental differences in the impacts of temperature on photosynthesis and respiration were preserved under light limited conditions (see Appendix A Figure.2 and Table.6). We therefore anticipate that the supra-optimal declines in growth linked to temperature-driven decoupling between photosynthesis, respiration and biomass synthesis that we have shown here, apply equally under nutrient replete and limited conditions. Whilst large areas of the global ocean are under nutrient limited conditions for long periods (Moore *et al.* 2013), understanding the impacts of temperature under nutrient replete conditions (as we have done here) remains critically important because a large proportion of marine primary productivity occurs during episodic bloom events driven by short periods of increased nutrient concentrations (Pingree *et al.* 1975; Townesend *et al.* 1994; Bruland *et al.* 2005). Clearly, significant further work is required to understand the interplay between temperature and nutrient availability on phytoplankton physiology and to assess whether the patterns we have shown here apply to conditions of nutrient limitation, given that current experimental evidence (Marañón *et al.* 2018) is not sufficient to draw meaningful conclusions.

Conclusions

Overall, our findings highlight marked similarities in the temperature dependence of photosynthesis and respiration across diverse taxonomic groups, spanning the cyanobacteria and red and green super-families and suggest that common physiological trade-offs underpin the thermal tolerance of marine phytoplankton. We found that rates of respiration were more sensitive to temperature, had higher thermal optima and declined less abruptly past the optimum than those of photosynthesis. Consequently, the fraction of photosynthetic energy available for allocation to growth (the CUE) exhibited an accelerated decline with rising temperatures in a manner that was highly conserved among the 18 species investigated. We also found that the optimal temperature for growth coincided with, or was lower than, an inflection point in the temperature dependence of the CUE, which marked a transition that led to accelerated declines at high temperatures. These patterns suggest that universal metabolic constraints driven by the differential temperature sensitivity of photosynthesis and respiration play a key role in setting the limits of thermal tolerance of diverse marine phytoplankton. Our results therefore help pave the way for improving representations of phytoplankton biodiversity in models of ocean biogeochemistry by providing a process-based understanding of the factors that shape the limits of temperature tolerance for diverse species of marine phytoplankton, which can be used to aid predictions of immigration and local extinctions driven by global warming.

Chapter 3: Quantifying the temperature dependence of growth rate in marine phytoplankton within and across species

Abstract

Models of marine biogeochemistry capture the effects of temperature on phytoplankton growth via the monotonic, exponential Eppley coefficient, without considering the physiological or evolutionary processes that underpin this emergent, across-species temperature response. Here we investigate both the within- and across-species temperature dependence of growth rate for 18 species of marine phytoplankton. We find that the temperature dependence of growth rate derived across-species was lower than the average temperature response within-species. This finding supports a "partial compensation" model of thermal adaptation and suggests that adaptation can partially compensate for the underlying thermodynamic effects of temperature on physiological rates observed within-species. We also find that thermal tolerance traits systematically covary with a host of key functional traits. Consequently, turnover in species composition in a warmer ocean linked to thermal tolerance traits could be associated with major shifts in the functional trait composition of marine phytoplankton communities with far reaching implications for ecosystem functioning.

Introduction

Marine phytoplankton play a critical role in regulating the ocean's biogeochemical cycles (Falkowski *et al.* 1998, 2008) and contribute to approximately 50% of global primary productivity (Field *et al.* 1998). Models of ocean biogeochemistry predict that global warming could result in significant declines in net primary production by marine phytoplankton throughout the 21st century (up to 20%). These declines are driven by increases in grazing and nutrient limitation in warmer, more stratified oceans and occur in spite of the assumption that phytoplankton growth will continue to increase exponentially with rising temperatures (Stock *et al.* 2014; Laufkotter *et al.* 2015).

The temperature dependence of phytoplankton productivity commonly applied in models of marine biogeochemistry is the canonical Eppley curve (Thomas *et al.* 2012; Stock *et al.* 2014; Laufkotter *et al.* 2015). The Eppley curve, and more recent derivations (Bissinger *et al.*, 2008; Kremer *et al*., 2017), are fundamentally an across-species characterisation of the thermal sensitivity of phytoplankton maximal growth rates, that assume a monotonic, exponential increase in rates with rising temperature (Eppley 1972), defined by a Q_{10} value (which quantifies the increase in rate per 10°C rise in temperature) of ≈1.88. The Eppley coefficient and similar derivations, are based on maximal growth rate estimates across a diverse range of taxa from contrasting environments (Eppley 1972; Bissinger *et al.*, 2008; Kremer *et al*., 2017). Consequently, they capture an emergent temperature dependence that is unlikely to be driven by the thermodynamic impacts of temperature on physiology alone. Rather, such coefficients are a phenomenological representation of the impacts of temperature on phytoplankton productivity, which encompasses broad physiological differences among taxa adapted to diverse thermal environments.

It is widely recognised that the temperature dependence of phytoplankton growth at the species level is unimodal and demonstrates negative-skewness (see Figure 3.1), whereby rates rise exponentially up to a maximal rate at the thermal optimum, beyond which rates decline much more rapidly (Schoolfield *et al.* 1981; Kingsolver 2009; Thomas *et al.* 2012). The application of the Eppley coefficient and similar monotonic functions, therefore assume that there is a continual increase in maximal growth rate as temperatures rise. Indeed, in the evolutionary biology literature, such patterns

have been termed, the “hotter is better” or the “thermodynamic constraints” hypotheses (Frazier *et al.* 2006; Kingsolver 2009). According to these hypotheses, organisms are unable to escape the thermodynamic impacts of temperature on biochemical kinetics and thus species adapted to cold environments inevitably have lower maximal growth rates than those from warmer climates. An alternative suite of hypotheses – e.g. “biochemical adaptation” (Somero & Hochachka 1971) or “complete compensation” – suggest that either via acclimation or adaptation, organisms can adjust their physiology to compensate for the thermodynamic effects of temperature, up-regulating rates in colder climates and down-regulating in warmer conditions. Importantly, these hypotheses lead to testable predictions that can be used to understand how evolution influences the temperature dependence of growth rate within and across species. For instance, the “hotter is better” hypothesis implies that the biochemical impacts of temperature are the same within and across species, thus the average temperature dependence derived from species-level thermal performance curves should be equal to the temperature dependence derived across species by comparing maximal rates across optimal temperatures (Frazier et al. 2006; Knies et al. 2009; see Figure 3.1a) . Conversely, “complete compensation” implies that evolutionary adaptation to different thermal regimes can compensate for the thermodynamic impacts of temperature, meaning that whilst rates of performance are expected to be strongly temperature dependent when any given species experiences temperature variation, optimal rates should be independent of temperature across species adapted to warm or cool environments resulting in equalisation of performance across diverse thermal regimes (Padfield et al. 2017; see Figure 3.1c). An intermediate scenario is clearly also possible, where maximal rates increase with rising increasing optimal temperatures but the temperature response derived across species is weaker than that derived within species; we refer to this intermediate scenario as “partial compensation” (Padfield et al. 2017; see Figure 3.1b). Understanding which of these evolutionary hypotheses best describe the impacts of temperature on the growth rate of marine phytoplankton is key to improving representations of phytoplankton physiology in models of marine biogeochemistry but so far remains unexplored.

A key physiological factor that can lead to systematic variation in maximal growth rates across phytoplankton taxa is cell size. It is well

established that as a general rule, across a broad range of organisms (including: vertebrates, invertebrates, protists and plants) growth rates tend to scale with size following a negative quarter-power law, such that smaller species grow at a faster rate (Brown *et al.* 2004; Savage *et al.* 2004a). Evidence for quarter-power scaling of growth rate in phytoplankton however is equivocal. Whilst some studies have demonstrated that phytoplankton growth rates approximate quarter-power scaling (Banse 1976; Savage *et al.* 2004b; Edwards *et al.* 2012), others that have explored the size scaling across a much wider range of size classes and phylogenetic groups, have found a divergence from the expected scaling and favour a much weaker relationship between maximum growth rate and cell size (Banse 1982; Sommer 1989; Tang 1995; Maranón *et al.* 2007; Huete-Ortega *et al.* 2012; Sal *et al.* 2015; Kremer *et al.* 2017). If cell size varies systematically with temperature, such that species from warmer environments with higher thermal optima tend to also be smaller (Sal *et al.* 2015), then accounting for any size scaling of metabolic rate is critical for understanding the processes that contribute to the across-species temperature dependence of growth rate in marine phytoplankton. Indeed, a recent meta-analysis has shown that after accounting for the size scaling the temperature dependence of maximal growth rates of phytoplankton yields an activation energy of 0.3 eV, analogous to a Q_{10} of 1.53, concluding that the Eppley coefficient is likely to overestimate the temperature response of maximal growth rates (Kremer *et al.* 2017) owing to systematic covariance between cell size and thermal adaptation.

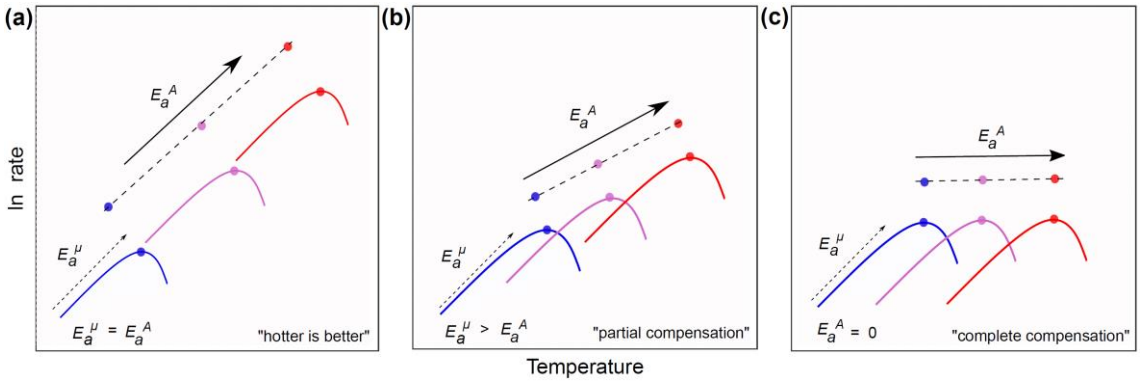

Figure. 3.1. An illustration of the unimodal response of growth rate to temperature increase and the different mechanisms of thermal adaptation. Blue colouring denotes cold adaptation and red warm adaptation. Data points reflect the maximal growth rate observed at the respective optimal growth temperatures. (a) Shows a perfect “hotter is better” scenario for thermal

adaptation whereby the across-species activation energy of maximal growth rates, E_a^A, is equal to the within species activation energy, E_a^{μ}. This favours the "thermo-dynamic constraint hypothesis" whereby warm adapted organisms out-perform cold adapted organisms at their optimal temperatures. (b) Shows a "partial compensation" scenario, whereby the within species activation energy is greater than the across-species activation energy of maximal rates, this is driven by down regulation of rates in order to adapt to higher temperatures and/or upregulation to adapt to cold temperatures. (c) Shows a "complete compensation" scenario whereby there is a temperature invariance of the maximal rates across cold and warm adapted taxa, and thus the across-species activation energy is not significantly different from zero.

It is expected that increases in global temperature will drive reorganisation of phytoplankton communities, resulting in latitudinal range shifts and declines in species diversity, particularly in warm tropical regions where taxa regularly experience environmental conditions in excess of their thermal optima (Barton *et al.* 2010; Norberg *et al.* 2012; Thomas *et al.* 2012). The impacts of temperature-driven turnover in phytoplankton community composition on ecosystem functioning will depend on the extent to which key functional traits covary with thermal tolerance traits. Such 'functional' traits can be considered morphological (e.g. cell size and shape), physiological (e.g. metabolic performance, thermal tolerance, nutrient uptake), behavioural (e.g. motility) or associated with life history (e.g. sexual or asexual reproduction); all of which can have a consequential bearing on ecosystem dynamics and biogeochemical cycling (Litchman & Klausmeier 2008). Cell size is often considered as a "master trait" owing to its influence on numerous other functional traits (Edwards *et al.* 2012). For instance, cell size is often strongly correlated with the macromolecular composition of phytoplankton cells, with larger individuals often containing less carbon, nitrogen, phosphorus and chlorophyll per unit volume (Verity *et al.* 1992; Montagnes *et al.* 1994; Menden-Deuer & Lessard 2000). Rates of nutrient uptake, photosynthesis and respiration are also tightly coupled with cell size (Chisholm 1992; Raven 1998; Yoshiyama & Klausmeier 2008). Thus, if cell size and thermal tolerance are linked across species of marine phytoplankton, then temperature-driven changes in taxonomic composition linked to thermal traits may also have far reaching effects on marine biogeochemistry because major changes in the functional trait composition of communities may be expected. It is however currently unclear whether key

functional traits in marine phytoplankton are indeed linked to thermal tolerance traits.

Here we carry out a large scale laboratory study to investigate the interplay between thermal adaptation, cell size and functional traits across 18 species of marine phytoplankton spanning five orders of magnitude from 0.1 to 10^3 μm^3 in cell volume, and representing key functional groups of both the red and green super-families (Falkowski *et al.* 2004; Keeling 2004) including: cyanobacteria, rhodophyta, chlorophyta, chlorarachniophyta, dinoflagellata, haptophyta and heterokonta (see Appendix B Table.1). Specifically, we provide the first test of the "hotter is better" and biochemical adaptation hypotheses in marine phytoplankton by comparing the temperature dependence of growth rate within vs. across species after accounting for the size scaling of growth rate. We also assess the extent to which key functional traits covary with cell size and thermal tolerance across the 18 species, to provide insight into how the functioning of phytoplankton communities may change as the oceans continue to warm in the coming decades.

Materials and Methods

Selection of the different species and culturing techniques

All 18 marine phytoplankton strains were sourced from CCAP (The Culture Collection of Algae and Protozoa) and RCC (Roscoff Culture Collection). Where possible, species were obtained that had been well studied in the literature and play crucial roles for marine ecology and global carbon cycling (see Appendix B Table.1). Stocks of each of the strains were cultured on their previous culture collection medium using artificial seawater, including: Guillard's F/2 and F/2 + Si, Keller's K, K + Si and K/2, and PCR-S11 Red Sea medium (with Red Sea salts).

All stock cultures were incubated in Infors HT incubators at 20°C, under a 12:12 hour light-dark cycle with a PAR intensity of 45-50 µmol m^2 s^{-1} and shaken at 65rpm. The red alga *Porphyridium purpureum* was an exception and was cultured at 20-25 µmol m^2 s^{-1}. All stocks were maintained under exponential, nutrient replete, growth conditions for ~ 2 months before any collection of physiological data.

Cell volume estimates

For each species, samples were taken from the stock populations in the exponential growth phase and fixed with a final concentration of 3% glutaraldehyde and 0.3% formaldehyde. Confocal microscope images were taken for a minimum of ~50 cells. ImageJ software (Schneider *et al.* 2012) was used to record cell dimensions and geometric models that best resembled the morphology of each species were then used to estimate cell volume (Hillebrand *et al.* 1999; Sun & Liu 2003), see Appendix B for extended methods on taxa specific volume calculations and Table.3 for estimates.

Cellular carbon and nitrogen estimates

For each species, samples of a known cell density in the exponential growth phase were divided into 3 technical replicates, each of 100ml, and centrifuged at 3500rpm, at 4°C for 30 minutes. Pellets were rinsed with deionised water, vortexed, and re-spun 3 times to remove residue of artificial sea water. For the calcifying organisms (*Emiliania huxleyi, Gephyrocapsa oceanica, Thoracosphaera heimii*) it was necessary to dissolve the extra-cellular inorganic carbon. We treated these pellets by adding 0.5 mL of 3M HCl and leaving for 1 hour before being rinsed with deionised water and re-pelleted (Ho *et al.* 2003). Pellets were then freeze-dried using a CoolSafe (95-15 PRO, ScanVac) over 24 hours and weighed to obtain dry weight. Samples were wrapped in tin cups and sent to Elemtex (Elemtex Ltd, Cornwall, UK, PL17 8QS) for elemental analysis of %C and %N using a SerCon Isotope Ratio Mass Spectrometer (CF-IRMS) system (continuous flow mode). For each technical replicate we could then calculate $\mathrm{pgC\ cell^{-1}}$, $\mathrm{pgN\ cell^{-1}}$ and the C:N ratio (see Appendix B Table.3).

Chlorophyll *a* estimates

For each species, 50ml of an exponentially growing culture of known cell density was centrifuged at 3500rpm, for 30 minutes at 4°C. The resultant pellets were re-suspended in 6ml of ethanol (100%) by vortexing, and all samples were then kept refrigerated in the dark for 24 hours. Following the extraction period, samples were vortexed again and cell debris was removed by centrifugation at 3500rpm for 3 minutes. Using a spectrophotometer (Jenway 7315) we measured absorbance of the supernatant from 610nm to 750nm for a minimum

of three technical replicates per species. Blanks were measured across the same wavelength range to correct for the ethanol absorbance. We then used well established absorbance coefficients to obtain estimates of pg chlorophyll *a* cell^{-1} for each of the species (Ritchie 2006; Henriques *et al.* 2007), see Appendix B for extended methods and Table.3 for the estimates.

Growth rate measurements

A minimum of 3 technical replicates of each species were inoculated with the same starting density into fresh growth medium across a range of temperatures (15°C - 37°C) from exponentially growing stock cultures. Cell counts were made daily following inoculation using flow cytometry (Accuri C6 flow cytometer, BD Scientific), and population density was monitored until cultures reached carrying capacity. For many responses there was an initial lag period, characterised by a period of no growth or a decline in population density before exponential growth was observed. For consistency, all growth rate measurements were taken following this lag period (if there was one). We assume that such lag periods followed by growth are reflective of 'acclimation', and therefore our measurements of population growth and the resultant thermal tolerance curves are the outcome of acclimation at each temperature. Per capita growth rates (μ) were quantified from a modified Baranyi growth model (Baranyi & Roberts 1994), using non-linear least squares regression via the 'nlsMicrobio' package in R statistical software (v3.3.1). Models were fitted using the 'nlsLoop' function in the R github package 'nlsLoop', this applies the 'nlsLM' function in the 'minpack.lm' R package which uses a modified Levenberg-Marquardt optimisation algorithm. Growth model parameters were determined by running 2000 random combinations of estimated starting parameters, which were then selected using the Akaike Information Criterion (AIC) to determine the combination of parameters that best characterised the data for each technical replicate. Growth rates derived for each technical replicate at each growth temperature were then used to determine the thermal tolerance curves (see modelling thermal performance curves section below).

Modelling thermal tolerance curves

Thermal tolerance curve for growth rate was quantified for each species using a modified version of the Sharpe-Schoolfield equation (Sharpe & DeMichele 1977;

Schoolfield *et al.* 1981):

$$\ln\left(b(T)\right) = E_a\left(\frac{1}{kT_c} - \frac{1}{kT}\right) + \ln\left(b(T_c)\right) - \ln\left(1 + e^{E_h\left(\frac{1}{kT_h} - \frac{1}{kT}\right)}\right) \quad (3.1)$$

where b is the rate of growth (d^{-1}), k is Boltzmann's constant, E_a is the within species activation energy (eV), characterising the steepness of the slope up to the thermal optima, T is temperature in Kelvin (K), E_h is the deactivation energy which characterizes decrease in rates above T_h where half the enzymes have become non-functional and $b(T_c)$ is rate normalized to an arbitrary reference temperature, here T_c = 20ºC (+ 273.15), where there is no low or high temperature inactivation. Eq. 3.1 can also be used to derive an optimum temperature where a maximum rate is expected:

$$T_{opt} = \frac{E_h T_h}{E_h + kT_h \ln\left(\frac{E_h}{E_a} - 1\right)} \quad (3.2)$$

The parameters $b(T_c)$, E_a, E_h, T_h, and T_{opt} all characterise the unimodal response of growth rates to temperature change. These traits are likely to differ across the diverse taxa analysed in this study. To test this, we fitted the data for growth to Eq. 3.1 using non-linear mixed effects modelling with the 'nlme' package in R. The model included each of the parameters in Eq. 3.1 as fixed effects, enabling us to quantify the average value of each parameter across all species combined. We included 'species' as a random effect on each of the model parameters, returning species-specific deviations from the overall average (i.e. the fixed effect). Because the Sharpe-Schoolfield equation can only take non-zero and positive rate values, in instances where either no observed growth rate, or a negative growth rate were measured (typically the highest and lowest temperature) we set the rate to the minimum value measured for the species in order to fit the model (see Figure 3.2 and Appendix B Figure.1 and Table.2).

Size correction of the across-species temperature dependence of maximal growth rates

Eq. 3.1 was used to determine the maximal growth rate at the optimal growth temperature, $b\left({T_{opt}}^{\mu}\right)$ (see Appendix B Table.6). We then quantified the size

scaling of maximal growth rate using a linear mixed effects model via the 'lmer' function from the 'lme4' package in R (see Figure 3.3a and Appendix B Table.5).

$$\ln\left(b\left({T_{opt}}^{\mu}\right)\right) = \alpha^{\mu}\ln(M) + \ln(b_0) + \varepsilon \quad (3.3)$$

Where $b\left({T_{opt}}^{\mu}\right)$ is the maximal growth rate at the optimal growth temperature, M is the size of the organism (in this case mean cell volume), α^{μ} is the size scaling exponent of maximal growth rates, $\ln(b_0)$ is the normalisation constant (zero intercept) and ε represents the random effect of phyla (e.g. cyanobacteria, rhodophyta, chlorophyta, chlorarachniophyta, dinoflagellata, haptophyta and heterokonta) on the intercept. Inclusion of the random effect of phyla accounted for non-independence in the model's residuals among phylogenetically similar taxa (Sal *et al.* 2015).

We then used the size scaling relationship to correct the maximal growth rates, $b\left({T_{opt}}^{\mu}\right)$, for the effect of size (Brown *et al.* 2004)

$$b\left({T_{opt}}^{\mu}\right)_{cor} = \frac{b\left({T_{opt}}^{\mu}\right)}{M^{-\alpha^{\mu}}} \quad (3.4)$$

Where, $b\left({T_{opt}}^{\mu}\right)_{cor}$ is the size corrected maximal growth rate at the optimal growth temperature (see Figure 3.3b and Appendix B Table.6). We then used $b\left({T_{opt}}^{\mu}\right)_{cor}$ to quantify the across-species temperature dependence of maximal growth rate (see Appendix B Table.5).

$$\ln\left(b\left({T_{opt}}^{\mu}\right)_{cor}\right) = {E_a}^{A}(1/kT_c - 1/kT) + \ln(b(T_c)) + \varepsilon \quad (3.5)$$

Where ${E_a}^{A}$ is the estimated across-species activation energy characterising the increase in the natural logarithm of $b\left({T_{opt}}^{\mu}\right)_{cor}$ with temperature, k is the Boltzmann constant (8.62 * 10^{-5} eV K^{-1}), T is optimal growth temperature (in Kelvin) and T_c is the mean optimal growth temperature across all species (in Kelvin), which yields, $\ln(b(T_c))$ as the natural logarithm of predicted growth rate at T_c; ε represents the random effect of phyla on the intercept.

Measuring optimal light intensity of photosynthesis

Measurements of photosynthesis were made at the optimal growth temperature (to the nearest 1°C) in 3 biological replicates of each species. We used a clark-

type oxygen electrode in combination with a Chlorolab 2 system (Hansatech Ltd, King's Lynn, UK) to measure net rates of oxygen evolution in the light (net primary production, NP) in units of µmol O_2 mL^{-1} s^{-1}. All biological replicates were taken from the stock cultures during mid-logarithmic growth phase so that samples were not substrate limited.

Net photosynthesis rates, measured as O_2 evolution, were collected across a gradient of light intensities from 0 to 1800 µmol m^2 s^{-1} with increments of 50 µmol m^2 s^{-1} between 0 to 200 µmol m^2 $s^{-1,}$ 100 µmol m^2 s^{-1} between 200 and 1000 µmol m^2 s^{-1}, followed by 1200 µmol m^2 s^{-1}, 1500 µmol m^2 s^{-1} and finally 1800 µmol m^2 s^{-1}. This allowed us to model a photosynthesis-irradiance (PI) curve and therefore obtain an estimate of light saturated net photosynthesis, NP_{max} , see Eq. 3.6. The PI curve was then quantified by fitting Eiler's photoinhibiton model (Eilers & Peeters 1988; Edwards *et al.* 2016) to the data using non-linear least squares regression (as described above for growth rate measurements):

$$NP(I) = \frac{NP_{max} I}{\frac{NP_{max}}{\alpha {I_{opt}}^2} I^2 + \left(1 - 2\frac{NP_{max}}{\alpha I_{opt}}\right) I + \frac{NP_{max}}{\alpha}} \quad (3.6)$$

Where $NP(I)$ is the rate of net primary production at light intensity, I, NP_{max} is the maximum rate of NP at the optimal light intensity, I_{opt} (the light intensity at which NP is maximal), and α is the rate in which NP increases up to NP_{max}.

Trait correlations and covariance

Patterns of trait covariance were examined across the 18 species using principal component analysis (PCA), using the 'prcomp' function in R (see Figure 3.4a). This analysis was performed on the following traits: mean cell volume (μm^3), picograms carbon per cell ($\mathrm{pgC}\ cell^{-1}$), picograms nitrogen per cell ($\mathrm{pgN}\ cell^{-1}$), picograms chlorophyll *a* per cell (pg Chl*a* $cell^{-1}$), optimal growth temperature (${T_{opt}}^{\mu}$), optimal irradiance of photosynthesis at ${T_{opt}}^{\mu}$ (I_{opt}) and rate of growth at ${T_{opt}}^{\mu}$ ($b\left({T_{opt}}^{\mu}\right)$) for each species. The first two principal components, which combined accounted for >75% of the total variance, were used to define the axes onto which results were projected. The loadings scores for each of the traits were derived and plotted on the same axis to demonstrate any putative negative or positive covariance of the traits. Following the PCA, we

carried out linear regression analyses to assess the correlations of both $T_{opt}{}^{\mu}$ and cell volume with the first principal component values (i.e. the primary axis of variation). Though it was expected that a number of traits are strongly size dependent, this also allowed for us to investigate the variance of key functional traits with differences in thermal tolerance – characterized by $T_{opt}{}^{\mu}$ (see Figure 3.4b and c and Appendix B Table.7). Linear mixed effects modelling was used to assess the correlations between per capita carbon, nitrogen and chlorophyll *a* and cell volume, (see Appendix B Figure.3 and Table.8), as well as the direct correlation between $T_{opt}{}^{\mu}$ and cell volume (see Appendix B Figure.4 and Table.9); in each case we included random effect of phyla on the intercept of the linear regressions.

Results

Temperature dependence of growth rates within and across species

At the species level, we found substantial variance in both the activation energy, $E_a{}^{\mu}$, and the optimal temperature of growth, $T_{opt}{}^{\mu}$, across the 18 species (see Figure 3.2, Appendix B Figure.1 and Table.2). We found that $E_a{}^{\mu}$ ranged across the taxa from 0.40 to 1.46eV, with an average (fixed effect) of 0.77eV (95% CI: 0.58 to 0.97). Pooling the data at the functional group level, we found that chlorophytes and dinoflagellates had the lowest average activation energies of 0.49eV (± 0.09 s.e.m) and 0.52eV(± 0.04 s.e.m), respectively. Whereas, haptophytes and cyanobacteria had the largest average activation energies of 1.34eV (0.07 s.e.m) and 1.01eV (0.44 s.e.m) ,respectively (see Appendix B Figure.2). Across all taxa, the estimated $T_{opt}{}^{\mu}$ ranged from 23.83°C to 33.96°C, with a mean of 28.29°C (± 0.63 s.e.m).

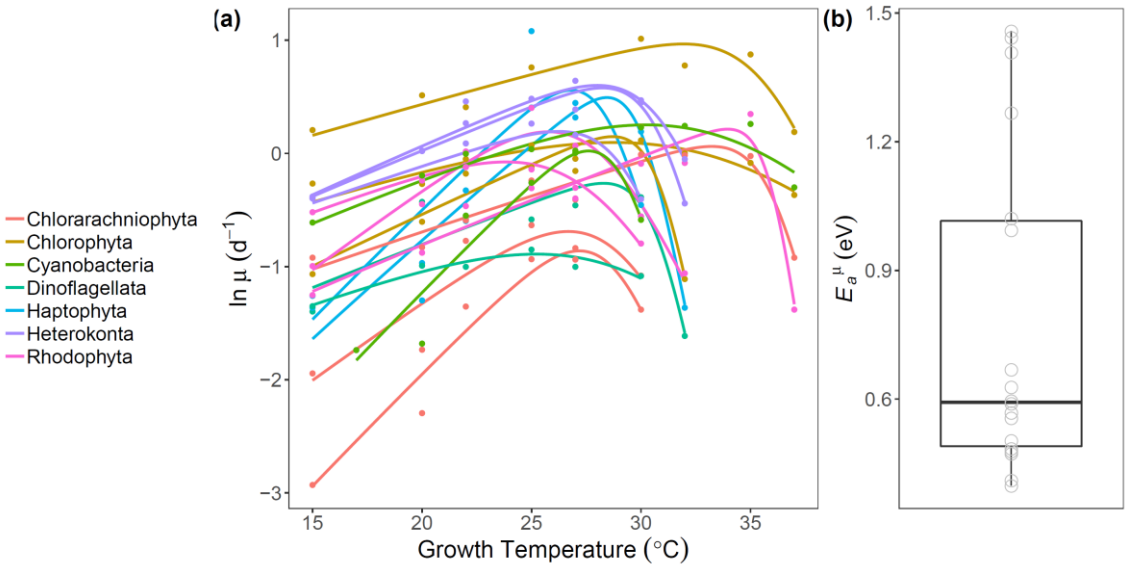

Figure. 3.2 Estimates of within-species temperature dependence (a) The modelled thermal tolerance curves of natural logarithm growth rates at the species level. The colours denote the different phylogenetic groups, and each line a different species. Data points are of mean growth rate across a minimum of 3 technical replicates for each species. (b) A box and whisker plot to demonstrate the variance in the species level activation energies. The bold horizontal line corresponds to the median value, the top and bottom of the box correspond to the 75th and 25th percentiles and the whiskers extend to the largest and smallest values no greater or less than the 1.5 × the interquartile range. The faded grey circles represent the individual species activation energies.

We then quantified the size scaling of the maximal growth rates and found a significant log-log relationship between $b(T_{opt}{}^{\mu})$ and cell volume ($\chi^2 = 3.99,\ p = 0.046$), with a size scaling exponent, α^{μ}, of -0.088 (95% CI: -0.173 to -0.002) (see Figure 3.3a, Appendix B Table.5). Next, we corrected the maximal growth rates for the effect of size, and found a significant relationship between the size-corrected maximal growth rates, $b(T_{opt}{}^{\mu})_{cor}$ and standardised optimal growth temperature ($\chi^2 = 5.12,\ p = 0.02$), yielding an across-species activation energy of maximal growth rates, $E_a{}^{A}$, of 0.50eV (95% CI: 0.1 to 0.90) (see Figure 3.3b and Appendix B Table.5), which was lower than the within species average $E_a{}^{\mu}$ of 0.77eV (95% CI: 0.58 to 0.97). Given the large confidence intervals surrounding our estimate of α^{μ}, we also determined size-corrected estimates of $E_a{}^{A}$ for both the upper and lower 95% confidence intervals of α^{μ}, -0.002, and -0.173 respectively. The estimated activation

energy ranged between 0.36 and 0.62 eV using the lower and upper 95% confidence intervals of the size-scaling coefficient for size correction.

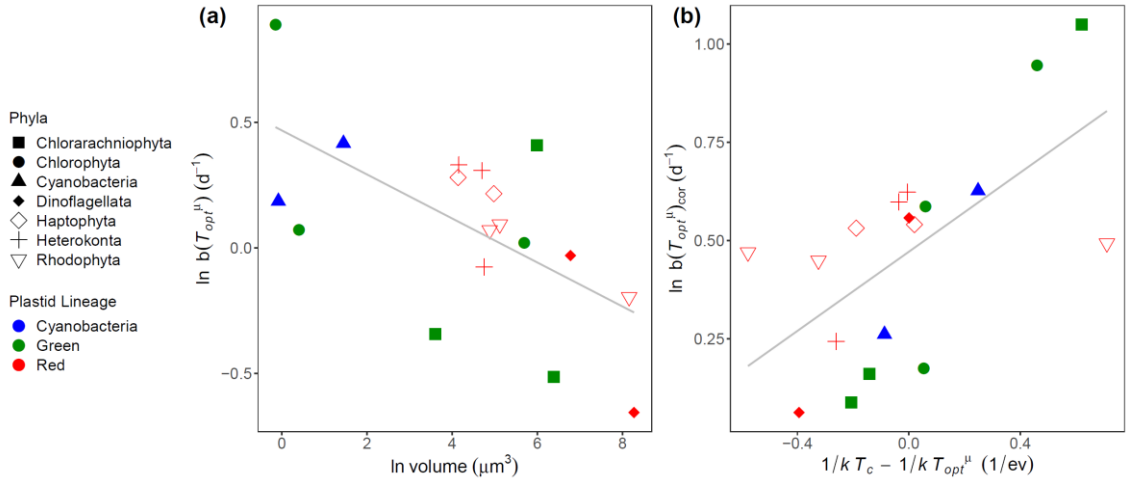

Figure 3.3 Across-species size scaling and temperature dependence (a) A scatter plot of natural logarithm maximal growth rate, $b(T_{opt}{}^{\mu})$, against natural logarithm mean cell volume. We found a significant effect of volume on the maximal growth rates, deriving a size scaling exponent, α^{μ}, of -0.088, represented by the gradient of the fitted line, with a conditional r^2 = 0.56. (b) A scatterplot of natural logarithm size corrected maximal growth rates, $b(T_{opt}{}^{\mu})_{cor}$, plotted against standardised Boltzmann optimal growth temperatures. The gradient of the fitted line, derived as the fixed effect of a linear mixed effect model fitted to the Boltzmann-Arrhenius equation, yields an across-species activation energy of 0.50eV, with a conditional r^2 = 0.70. Rates (y-axes) are presented as standardised rates, which control for phylogenetic differences in the intercept for visualisation of the statistical model. This entailed dividing each rate by the intercept for each phyla and adding the global (fixed effect) intercept.

Trait correlations and covariance

We carried out a PCA to illustrate the general co-variance of thermal and functional traits across the taxa. We found that size was the primary driver for variation in the data, with both positive and negative correlations of most of the traits with size (see Figure 3.4a). We found positive correlations between cell volume and per capita carbon, nitrogen, and chlorophyll *a* content; as expected, these log-log correlations were sub-linear, meaning in each case concentration per unit volume decreased with greater cell size (see Appendix B Figure.3) By contrast, cell size was weakly positively correlated with I_{opt}, illustrating that smaller cells show more effective light utilisation. In agreement with the derived size scaling exponent and across-species temperature dependence, growth

rate at ${T_{opt}}^{\mu}$, $b({T_{opt}}^{\mu})$, was negatively correlated with volume and positively correlated with optimal growth temperature. Critically, we found that optimal growth temperature, ${T_{opt}}^{\mu}$ was negatively correlated with cell size such that larger species tended to have lower thermal tolerance (see Figure 3.4a, Appendix B Figure.4). We support these conclusions by demonstrating that cell volume is strongly negatively correlated with the first principal component values ($F - statistic = 17.32,\ p < 0.001$, see Figure 3.4b and Appendix B Table.7), whereas ${T_{opt}}^{\mu}$ is significantly positively correlated with the first principal component values ($F - statistic = 9.45,\ p = 0.007$, see Figure 3.4c and Appendix B Table.7); thus, both size and ${T_{opt}}^{\mu}$ appear to have an opposing, but significant, effect on the primary axis of variance, implying a negative correlation between greater ${T_{opt}}^{\mu}$ and cell size. Nonetheless, linear mixed effects modelling did not find the negative correlation between ${T_{opt}}^{\mu}$ and cell volume to be significant ($\chi^2 = 2.22,\ p = 0.136,$ 95% CI: -0.83 to 0.12). With a more extensive dataset, where *n* > 18, this finding could be more adequately scrutinised (see Appendix B Figure.4 and Table.9).

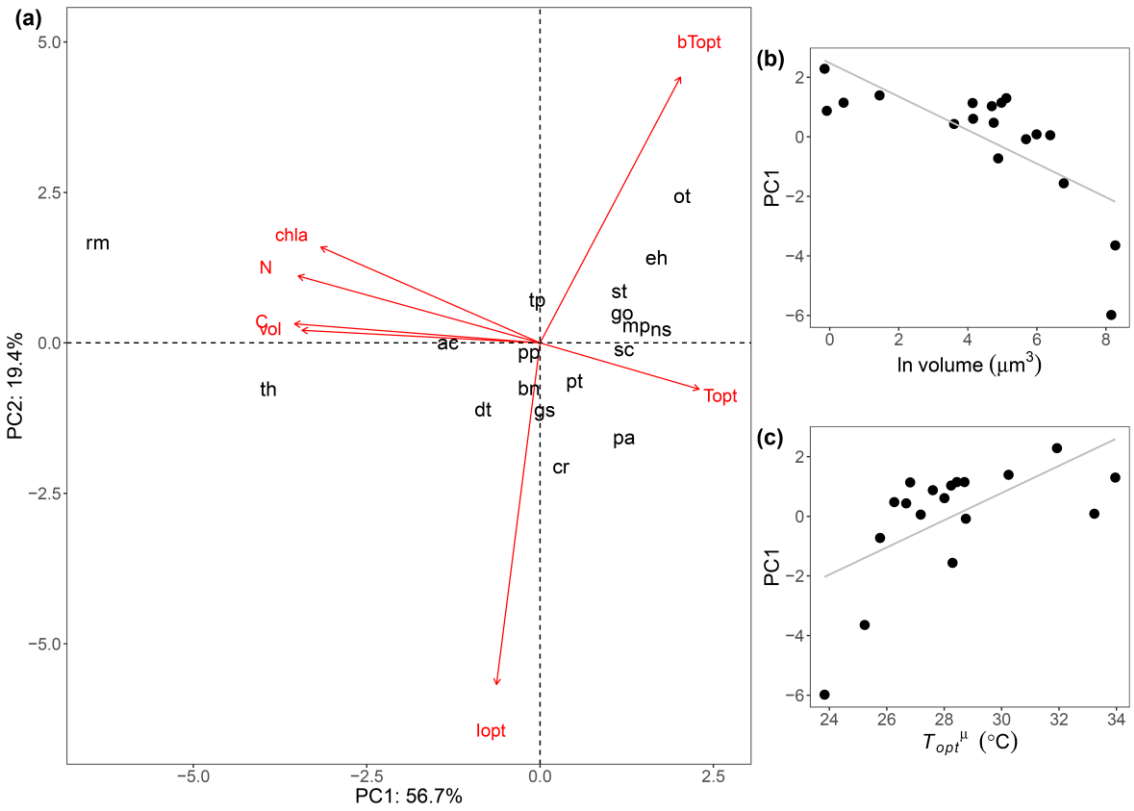

Figure 3.4. Principal component analysis of inter-specific trait covariance (a) Principal component analysis of trait covariance. The first two principal components account for >75% of the total variance. The loadings for each of the variables illustrate the covariance among the thermal and functional traits, where: vol = mean cell volume, C = $\mathrm{pgC}\,cell^{-1}$, N = $\mathrm{pgN}\,cell^{-1}$ chla = pg chlorophyll *a* $cell^{-1}$, Topt = optimal growth temperature, Iopt = optimal light intensity of photosynthesis and bTopt = growth rate at optimal temperature. The length of each loading vector reflects the combined weighting of each variable in the first two principal components. Species abbreviations are: ac = *A.carterae,* bn = *B.natans,* cr = *C.reptans,* dt = *D.tertiolecta,* eh = *E.huxleyi,* go = *G. oceanica,* gs = *G.stellata,* mp = *M. pusilla,* ns = *Nitzschia* sp., ot = *O. tauri,* pt = *P. tricornutum,* pa = *P. aerugineum,* pp = *P. purpureum,* rm = *R. maculata,* sc = *Synechococcus* sp., st = *Synechocystis* sp., tp = *T. pseudonana and* th = *T. heimii.***(b)** Principal component 1 values plotted against natural logarithm of mean cell volume, illustrating the significant negative effect of cell volume on the primary axis of trait variation (see Appendix B Table.7). **(c)** Principal component 1 values plotted against optimal growth temperature ($T_{opt}{}^{\mu}$), illustrating the significant positive effect of $T_{opt}{}^{\mu}$ on the primary axis of trait variation see Appendix B Table.7).

Discussion

Current representations of the thermal response of phytoplankton productivity in models of marine biogeochemistry employ phenomenological, monotonic exponential functions, which implicitly assume that the impacts of temperature on algal growth rate are the same within vs. across species (Eppley, 1972; Stock *et al.*, 2014; Laufkotter *et al.*, 2015). The application of these types of models to capture the effects of temperature on phytoplankton production at all scales (e.g. local to global), rests on the assumption embodied by the "hotter is better" hypothesis from evolutionary biology (though never stated as such in the marine ecology literature); namely that organisms are unable to escape the thermodynamic effects of temperature on growth and thus species adapted to cold environments have inherently slow maximal growth rates, while those from warm environments grow much more rapidly – i.e. evolution has little capacity to modulate the effects of temperature on metabolism and growth (Frazier *et al.* 2006; Knies *et al.* 2009). In this study we assess how thermal adaptation influences the temperature scaling of growth rate across 18 species of marine phytoplankton, spanning a diverse range of phyla measured using common laboratory protocols. We found support for "partial compensation" (Figure 3.1b), with the temperature dependence of maximum growth rate derived across-species being lower than the average within-species temperature dependence across the 18 species. This suggests that evolutionary adaptation has the capacity to partially offset the underlying effects of temperature on maximal growth rates. Our results also emphasise that a host of key functional traits were correlated with the thermal tolerance traits across the species, suggesting that temperature-driven changes in phytoplankton community composition could have major implications for the functioning of marine phytoplankton communities in a warmer ocean.

Within-species vs. across-species temperature dependence

Before quantifying the across-species temperature dependence of phytoplankton growth, we first derived the size scaling of maximum growth rate. We found an exponent, α^{μ}, of -0.088 (95% CI: -0.173 to -0.002), which was similar to previous work on phytoplankton (Banse 1982; Sommer 1989; Tang 1995; Maranón *et al.* 2007; Huete-Ortega *et al.* 2012; Sal *et al.* 2015; Kremer *et*

al. 2017), and was lower than the expected negative quarter power scaling predicted by metabolic scaling theory (Banse 1976; Brown *et al.* 2004; Savage *et al.* 2004a; Edwards *et al.* 2012). Previous work has hypothesised that this may be due to a non-linear size scaling of growth rates, whereby smaller phytoplankton (picophytoplankton) taxa actually demonstrate lower growth rates than intermediate sized taxa (Marañón *et al.* 2013; López-Sandoval *et al.* 2014). We found that the size scaling relationship in our dataset was best described by a linear model (on log scales), after taking into account the variance in the intercept among phyla. This approach is supported by the work of Sal *et al*., (2015), which has shown that after correction for phylogenetic differences, the size scaling of phytoplankton growth rates was best described by a linear model, rather than a unimodal model. We then used our derived size scaling exponent to account for the effects of interspecific differences in size when deriving the temperature response of maximal growth rates.

After size correction, the temperature dependence of maximum growth rate was well characterised by the Boltzmann-Arrhenius equation, with an activation energy, $E_a{}^A$ of 0.50eV (see Figure 3.3b). At the species level, we found that the temperature dependence of growth rate, characterised by the activation energy, $E_a{}^{\mu}$, ranged from 0.40eV to 1.46eV, with an average of 0.77eV (see Figure 3.2). These results demonstrate that on average the effects of temperature on phytoplankton growth are greater within than across species, and provide support for the "partial compensation" hypothesis. An activation energy of ~0.50 eV implies a Q_{10} of 1.96 at 25ºC, which is greater than the Eppley coefficient (Q_{10} = 1.88) and other more recent derivations (Bissinger *et al.* 2008; Kremer *et al.* 2017). However, it should be noted that the 95% confidence intervals around the across-species activation energy were large, spanning 0.1 to 0.9 eV (Q_{10} = 1.14 to 3.37), similarly the range of within-species activation energies were also significant, from 0.40eV to 1.46 eV (Q_{10} = 1.69 to 6.72). Thus, whilst our results suggest a "partial compensation" mechanism of thermal adaptation (Figure 3.1b), our statistical analyses do not allow us to rule out the "hotter is better" hypothesis (Figure 3.1a). Furthermore, we investigated the effect of a stronger or weaker size scaling on the size-corrected across-species temperature dependence by taking into account the upper and lower confidence intervals surrounding our estimate of α^{μ} (see Appendix B Table.5).

With our upper size scaling estimate (-0.002) this increased our size-corrected value of $E_a{}^A$ to 0.62eV and thus closer to our within-species average. Contrary to this, correcting for a stronger effect of size, with the lower size scaling estimate (-0.173), resulted in a temperature dependence with an approximated $E_a{}^A$ of 0.36eV; much closer to the Eppley coefficient

. These findings are consistent with a recent meta-analysis which demonstrated that at the functional group level (including, heterokonts, dinoflagellates, cyanobacteria, chlorophytes and haptophytes) the temperature dependence of growth was generally greater than the average temperature dependence modelled across a pooled dataset which included all functional groups (Chen & Laws 2017). In this study, at the level of phyla, average estimates of $E_a{}^{\mu}$, ranged from 0.49eV to 1.34eV (see Appendix B Figure.2). Cyanobacteria, chlorarachniohytes, haptophytes and rhodophytes all had average activation energies that were greater than the modelled across-species activation energy of 0.50eV. Whereas, chlorophytes dinoflagellates and heterokonts all had average activation energies that were much closer to the across-species average.

The large range of activation energies derived at the species level in this study (0.40eV to 1.46eV) also highlights a key limitation of applying an across-species temperature dependence in models of marine biogeochemistry where the goal is to make local and regional scale predictions about the impacts of temperature change (Stock *et al.* 2014; Laufkotter *et al.* 2015). Our results emphasise a wide range of temperature sensitivities that deviate substantially from the across species temperature response. Echoing the conclusions drawn from the meta-analysis by Chen and Laws (2017), these results imply that applying a common temperature coefficient will often under- or over-estimate the impacts of temperature changes on phytoplankton productivity depending on which taxa dominate locally at the community scale. A more robust approach would be to get better empirical constraints on variability in the within-species temperature responses among the key groups of marine phytoplankton, and use this information to parameterise models that allow flexible temperature sensitivity depending on the dominant phyla or functional group in a given location. In addition to this, our within-species estimates of activation energy and thermal optima were all derived from acute growth rate responses from

cultures that had all come from the stocks maintained at 20°C. Given that recent experimental evidence has been able to demonstrate that phytoplankton can modulate metabolism, and thus growth rate, as rapid adaptive responses to long-term warming (Padfield *et al.* 2016; Schaum *et al.* 2018), it would also be useful to determine within-species temperature dependence and optima following experimental adaptation to different temperatures regimes. Indeed, it was demonstrated by Schaum *et al*. (2018) that adaptation of the diatom *Thalassiosira pseudonana* to moderate, severe and fluctuating warming treatments resulted in clear shifts in thermal optima as well as activation energy of growth rate. Thus, this suggests that thermal adaptation at an intra-specific level is also likely to play out in across-species interpretations of phytoplankton temperature dependence, especially if estimates encompass taxa from a range of ancestral environments with different thermal regimes, for example – across a latitudinal gradient.

Trait covariance and implications for ecosystem function

We found that maximal growth rates in marine phytoplankton increase with increasing optimal temperatures after controlling for the effects of size. This type of across-species temperature response is the common way in which the effects of temperature on phytoplankton productivity are captured in models of marine biogeochemistry (Stock *et al.* 2014; Laufkotter *et al.* 2015). However, the application of an across-species temperature response to predicting the impacts of warming on phytoplankton productivity implicitly assumes that there will be a continual replacement of species that is linked to their variability in thermal tolerance as environmental temperatures rise (Follows *et al.* 2007). A key factor that is missed when applying this type of temperature dependence model is that other traits may be inherently associated with a turnover in taxonomic composition moving from species with low- to high thermal tolerance. A rich body of work has demonstrated extensive correlations and putative trade-offs between key traits that are both important for determining phytoplankton physiology and ecological dynamics as well as constraining key ecosystem scale functions (e.g. nutrient cycling) (Litchman *et al.* 2007; Edwards *et al.* 2012). From the first principal component of our PCA we demonstrate that most variance in the traits is driven by cell size and, conversely to cell size, by the limits of thermal tolerance (or $T_{opt}{}^{\mu}$) . Thus, we deduce that cell size was

negatively correlated with the optimum temperature for growth (Figure 3.4, and Appendix B Figure.4), such that the smallest taxa were often those with the highest thermal tolerance. Whilst we acknowledge that our dataset is limited to laboratory strains of a select range of taxa, this finding supports numerous conclusions in the literature that suggest smaller phytoplankton will be at an advantage with ocean warming (Bopp *et al.* 2005; Morán *et al.* 2010; López-Urrutia & Morán 2015). The most commonly supported argument for success of smaller phytoplankton taxa, is that warming will lead to increased stratification of the oceans and therefore greater nutrient limitation of the euphotic zone (Bopp *et al.* 2005; Behrenfeld *et al.* 2006). Typically, smaller phytoplankton have higher nutrient affinity than larger phytoplankton (Chisholm 1992; Raven 1998; Litchman & Klausmeier 2008), and are therefore more likely to maintain growth at lower nutrient levels than larger competitors (Edwards *et al.* 2012; Barton *et al.* 2013). In addition, observations have also found that abundance of picophytoplankton, as well as proportion of phytoplankton biomass made up of picophytoplankton, increases with temperature (Li 2002; Li *et al.* 2006; Morán *et al.* 2010) and that nutrient concentrations fail to explain all the variation in mean phytoplankton size (López-Urrutia & Morán 2015). In conjunction with the current support for increases in abundance of small phytoplankton with warming, our study suggest that smaller phytoplankton may also succeed under warming as they have evolved to have faster growth rates at higher thermal optima.

Critically, cell size was the dominant axis explaining variation in a number of other functional traits in the 18 species analysed in this study (Figure 3.4a). Thus, the negative correlation between the thermal optimum and cell size could have profound implications for global biogeochemical cycles and trophic interactions in the ocean. As smaller cells tend to have much lower sinking velocities (Falkowski *et al.* 1998; Litchman & Klausmeier 2008), it could be expected that expansion of oligotrophic ocean (Falkowski *et al.* 1998; Irwin & Oliver 2009) in combination with increases in picophytoplankton abundance would lead to reduced carbon sequestration and weakening of the ocean's biological carbon pump (Falkowski *et al.* 1998; Morán *et al.* 2010). Furthermore, reduction in cell size is also related to reduced resistance to grazing, and thus a shift in community structure to those dominated by smaller phytoplankton sizes could have implications for energy flow in pelagic food webs (Raven 1998; Li *et*

al. 2006; Litchman & Klausmeier 2008). Within our dataset we were also able to demonstrate that warming may have direct implications for the turnover of carbon and nitrogen by phytoplankton communities. In agreement with previous work (Verity *et al.* 1992; Montagnes *et al.* 1994; Menden-Deuer & Lessard 2000; Montagnes & Franklin 2001; Marañón *et al.* 2013), we found that taxa with a smaller cell volume tended to have more carbon, nitrogen and chlorophyll *a* content per unit volume (see Appendix B Figure.3). Thus, if phytoplankton communities were to become increasingly dominated by smaller taxa this could have implications for the cycling of these key nutrients, as the overall biomass of the communities may be more carbon and nitrogen rich. Our data therefore suggest that temperature driven turnover of phytoplankton community composition could have far reaching implications for the functioning of marine ecosystems, that extend beyond the simple effect of temperature on maximum growth rate. A systematic shift to species with small cell size is likely to be associated with change in the distribution of a host of functional traits that can have ecosystem-wide effects – e.g. elemental composition, photophysiology – and this covariance between functional and thermal traits are not currently accounted for in models of marine biogeochemistry (Stock *et al.* 2014; Laufkotter *et al.* 2015).

Chapter 4: Adaptation of marine phytoplankton to warming; a comparative experimental study across three ecologically relevant marine taxa

Abstract

Understanding the adaptive responses of marine phytoplankton to increases in ocean temperatures is crucial for improving global biogeochemical models. In recent years experimental evolution studies have been providing strong evidence that indicates phytoplankton can display rapid thermal adaptation, characterised by increased fitness at warmed temperatures and overall shifts in their thermal tolerance. Whilst these studies can be influential for informing modellers, they all employ slightly different experimental techniques and are normally focussed on just one species. This makes it difficult to make inter-specific comparisons about the rates of thermal adaptation across diverse taxa of marine phytoplankton, from ecologically and bio-geochemically important functional groups. Furthermore, only a few of these studies have attempted to understand the metabolic mechanisms that are underlying the observed thermal adaptation. In this study we attempted to address a few of these limitations of previous work by conducting an experimental evolution study that explored the effects of high temperature stress on clonal isolates of three diverse taxa of marine phytoplankton; the cyanobacteria *Synechococcus* sp*.,* the chlorophyte *Ostreococcus tauri* and the diatom *Phaeodoactylum tricornutum*. Over a set experimental time period of 22 weeks we found differing levels of thermal adaptation across the three taxa. Whilst *Phaeodoactylum tricornutum* showed potential to acclimate to high temperature, populations rapidly crashed within a couple of weeks and did not recover. *Ostreococcus tauri* did adapt to the warmed temperature and increased its thermal optima, but failed to reach comparable growth rates to those observed under ambient conditions. *Synechococcus* sp. also adapted to the warmed temperature, shifting its thermal optima to higher temperatures, with a widening of its tolerance curve and with maximal growth rates that were comparable to those observed under ambient conditions. For both *Ostreococcus tauri* and *Synechococcus* sp. adaptation was facilitated by down-regulated mass specific metabolism, and in agreement with previous work we found that *Synechococcus* sp. down-

regulated its respiration rates by a greater magnitude than photosynthesis resulting in an improved carbon-use efficiency; which we deduce allowed for greater carbon allocation to growth. In combination with these findings, we also observed clear trends of increased body size associated with thermal adaptation, and with this we can associate warm adaptation to changes in a range of other physiological traits such as per capita carbon, nitrogen and chlorophyll. Subsequently, in support of previous findings, this study demonstrates the validity and importance of conducting such experiments to understand the potential for, and characteristics of, evolved thermal tolerance and the associated implications for ecosystem function.

Introduction

There is a growing field of research looking into the long-term responses of phytoplankton to warming through experimental evolution studies (Schlüter *et al.* 2014; Listmann *et al.* 2016; Padfield *et al.* 2016; Baker *et al.* 2018; O'Donnell *et al.* 2018; Schaum *et al.* 2018). Understanding thermal adaptation of phytoplankton is critical for incorporating such responses into global biogeochemical models (Thomas *et al.* 2012; Laufkotter *et al.* 2015). Along with greater ocean stratification and increased grazing (Bopp *et al.* 2005; Behrenfeld *et al.* 2006; Chen *et al.* 2012; Laufkotter *et al.* 2015), it is expected that warming will drive reductions in marine primary production (Behrenfeld *et al.* 2006; Boyce *et al.* 2010; Capuzzo *et al.* 2018) and extinctions of phytoplankton taxa, particularly at lower latitudes, where temperatures may exceed thermal tolerance limits (Thomas *et al.* 2012, 2016). Thus far, experimental evolution studies have indicated that phytoplankton can demonstrate rapid thermal adaptation, over 100 generations or more (Padfield *et al.* 2016), to both warmed and fluctuating temperature environments, providing strong evidence to support the inclusion of evolutionary changes into such models. However, to date, this work has been limited to a couple of model species of freshwater green algae (Padfield *et al.* 2016; Schaum *et al.* 2017) and relatively few marine taxa, covering just three of the key functional groups; the diatom *Thalassiosira pseudonana* (O'Donnell *et al.* 2018; Schaum *et al.* 2018), the coccolithophore

Emiliania huxleyi (Schlüter *et al.* 2014; Listmann *et al.* 2016) and the dinoflagellate *Amphidinium massartii* (Baker *et al.* 2018).

Typically, the extent to which organisms have adapted to a high temperature treatment is expressed in such experiments by measuring thermal tolerance curves of growth rate for both ambient and warm adapted strains, which characterise the changes in thermal limits of acclimation (Listmann *et al.* 2016; Schaum *et al.* 2017, 2018; Baker *et al.* 2018; O'Donnell *et al.* 2018). Most of these studies demonstrate a clear shift in the tolerance curve in response to warming, generally to higher optimal ($T_{opt}{}^{\mu}$) and maximal ($T_{max}{}^{\mu}$) growth temperatures (Listmann *et al.* 2016; Schaum *et al.* 2017, 2018; Baker *et al.* 2018; O'Donnell *et al.* 2018), but often with a cost to performance at lower temperatures (Baker *et al.* 2018; O'Donnell *et al.* 2018; Schaum *et al.* 2018). This often reflects the "specialist-generalist" theory for evolution of thermal tolerance, whereby adaptation results in a specialisation to one range of environmental conditions at a cost to performance in another range of environmental conditions (Angilletta *et al.* 2003). Some of these studies have also investigated the trade-offs of other physiological traits associated with high temperature adaptation. For example, changes in nutrient affinity (Baker *et al.* 2018; O'Donnell *et al.* 2018), which is crucial for understanding the implications of thermal adaptation on the functioning of the organism and the biogeochemical cycles that they mediate (Falkowski *et al.* 1998; Litchman & Klausmeier 2008). However, only a few of these studies have attempted to understand the potential metabolic mechanisms of adaptation to high temperatures (Padfield *et al.* 2016; Schaum *et al.* 2017, 2018).

Given that there are increasing observations at both the individual and community scale of a universal difference in the temperature dependence of respiration and photosynthesis, whereby phytoplankton tend to have a greater thermal sensitivity of respiration relative to photosynthesis (Lopez-Urrutia *et al.* 2006; Yvon-Durocher *et al.* 2012; Padfield *et al.* 2016; Schaum *et al.* 2017; Barton *et al.* 2018) resulting in a decrease in carbon use efficiency (CUE) as temperatures increase over a mesophilic range (Padfield *et al.* 2016; Barton *et al.* 2018; Schaum *et al.* 2018), then the possibility that different phytoplankton taxa may adjust their metabolism in a similar direction to overcome this universal constraint is something that requires further exploration. Gaining a

handle on the metabolic mechanisms that facilitate thermal adaptation across a diverse range of taxa is therefore crucial for discussions into whether models can be developed to infer directions of thermal adaptation from metabolism datasets alone (García-Carreras *et al.* 2018). To date, a couple of the experimental evolution studies have demonstrated that phytoplankton down-regulate their metabolic rates in response to long-term exposure to high temperatures, and have found that it tends to be due to greater down regulation of mass specific respiration rate relative to gross primary production that results in improved efficiency of carbon allocation to growth (Padfield *et al.* 2016; Schaum *et al.* 2018). In qualitative agreement with this, a recent study that worked on isolated strains of the freshwater green alga *Chlamydomonas reinhardtii* from a 10 year mesocosm experiment has also shown that greater thermal performance of warm adapted isolates is associated with increased net photosynthesis (Schaum *et al.* 2017). Nonetheless, despite these recent studies being in general agreement with the idea that shifts in thermal tolerance are underpinned by metabolic traits, direct comparisons should be made with caution owing to the difference in timescale of the experiments (years versus months) and because these studies represent poor coverage of the diversity of phytoplankton. Thus far, being limited to two model species of freshwater green algae (Padfield *et al.* 2016; Schaum *et al.* 2017) and one marine diatom (Schaum *et al.* 2018); therefore providing limited coverage of the different evolutionary histories of phytoplankton, and the wide range of phylogenies represented by the faceted branches of primary and secondary endosymbionts of the red and green super-families (Falkowski *et al.* 2004; Keeling 2004).

Given the limited representation of key marine taxa in experimental evolution studies, as well as the nuances of different experimental methods, here we attempted to add to the current knowledge in this field by investigating both the magnitude and metabolic mechanisms of thermal adaptation, following the same experimental protocol, for three taxa of marine phytoplankton. Over a period of 22 weeks we ran an evolution experiment on clonal strains of *Synechococcus* sp. - a globally abundant cyanobacteria (Flombaum *et al.* 2013) , *Ostreococcus tauri* – a chlorophyte and the smallest known eukaryote (Courties *et al.* 1994; Derelle *et al.* 2006) and *Phaeodactylum tricornutum* – a prevalent diatom in coastal marine ecosystems (Bowler *et al.* 2008), at both a

control and a warmed treatment. We monitored the weekly change in growth rate over the 22 weeks to demonstrate the rate at which fitness was changing in response to elevated temperature. Previous experimental evolution studies on phytoplankton tend to use number of generations to infer adaptive changes, with evolutionary responses often observed within ~100 generations (Schlüter *et al.* 2014; Padfield *et al.* 2016; Schaum *et al.* 2018). Here we used a set period of time to compare the changes in thermal tolerance across the taxa, primarily because it is difficult to accurately calculate number of generations passed when there are large lag phases in population growth during the initial response to a stressful environment, when death rate is more than, or equal to, specific growth rate and when selection pressure is greatest (for example, see Figure.4.3a and Appendix C Figures.2a and 3a, where *Synechococcus* sp*.* at 30 °C demonstrated no positive growth for the first ~ 25 days). Furthermore, this approach also allowed for intrinsic differences in average generation time across the three taxa to play out in the magnitude of thermal adaption observed over the set time period. Following the 22 weeks we measured the thermal tolerance curves of growth for both the ambient and warmed treatment strains for each of the taxa to see if the overall thermal tolerance of the taxa had shifted. To better understand potential changes in the thermal tolerance, we then investigated the metabolic performance of each of the strains with full reciprocal transplant assays to assess how the metabolic performance may be constraining the parameters observed in the thermal tolerance curves. In addition to this, we also collected data to estimate cell size, along with measurements of carbon, nitrogen and chlorophyll *a* per cell to further understand the possible functional implications of thermal adaptation across the taxa.

Materials and Methods

Experimental design

The strains of *Synechococcus* sp. (CCMP 2370, WH8102) and *Ostreococcus tauri* (RCC 4221) were originally obtained from RCC (Roscoff culture collection), and the strain of *Phaeodactylum tricornutum* (CCAP 1052/1B, CCMP 2558)

from CCAP (The Culture Collection of Algae and Protozoa). Stock cultures of each of the three species in this study had been maintained in the lab under similar conditions to those of their respective culture collection for a minimum of one year before the experiment commenced. Cultures were kept under nutrient replete conditions at an ambient temperature of 20°C, on a 12:12 hour light-dark cycle at approximately 45-50umol m^2 s^{-1} and at a constant agitation of 65rpm in an Infors HT incubator. Each of the strains were grown on their long-term culture collection mediums; PCR-S11 for *Synechococcus* sp., Keller's K for *Ostreococcus tauri* and Guillard's F/2 + Si for *Phaeodactylum tricornutum*. Before starting the experiment we identified 'stressful' high temperatures to be used for our warmed treatments by obtaining thermal tolerance curves for each of the taxa. This was achieved by making growth rate estimates for a minimum of three technical replicates across a range of assay temperatures, from 18 to 33°C (see section below for details on measuring growth rates and modelling the thermal tolerance curves). From the modelled thermal tolerance curves of the pre-clonal stock populations (see Figure.4.2) we were then able to identify a supra-optimal temperature for each of the taxa where rates were approximately 50% the magnitude of maximal growth rates at the optimal temperature; for *Synechococcus* sp. this was identified as 30°C, for *Ostreococcus tauri* this was 33°C and for *Phaeodactylum tricornutum* this was 27°C. By taking this approach we had a quantitative justification for the selection of the high temperature treatments, allowing us to make fairer comparisons of the extent of observed thermal adaptation across the taxa over a set time period. We obtained clonal starting populations for each of the taxa by serial dilution-to-extinction, in three 24-well plates for each taxa; with an approximation of one individual inoculated per well. Once clonal growth was evident, we then chose a single clonal population for each of the taxa to be the ancestral population for our experiment. The clonal ancestor was distributed into 6 replicates at both the ambient control temperature, 20°C, and the identified high temperature treatment for each taxa. Conducting the experiment from a clonal founder population allowed us to investigate whether the direction, magnitude and mechanism of thermal adaptation is consistent across the biological replicates of each species, in spite of starting from the same, bottle-necked genetic diversity and thus with less mutations within the populations for selection to act on. With exception to the change in temperature for the warmed treatments, culturing conditions were

kept as they were for the original stock cultures (as described above). The biological replicates at each temperature were maintained in semi-continuous batch culture, and always transferred during the exponential growth phase back to the same original starting density in 100ml for each species. This allowed for calculation of specific growth rates between transfers (see section below on growth rate trajectories), which was essential for tracking changes in fitness of the warm adapted replicates relative to the control. This was achieved at each transfer by measuring average cell densities of each replicate using flow cytometry, which also gave us an estimate of average cell length that could be used to monitor changes in cell volume throughout the experiment (see section on cell size below). After the minimum 22 week experimental period all additional physiological data was collected over an additional 5 week period for each of the biological replicates (see Figures.4.3 and 4.4, and Appendix C Figure.2), including: measurements of thermal tolerance curves, full reciprocal transplant assays of growth, respiration and gross photosynthesis rates and measurements of per capita mass of organic carbon, nitrogen and chlorophyll *a*.

For a schematic breakdown of the full experimental design see Figure 4.1.

Flow cytometry

We used an Accuri C6 flow cytometer (BD Scientific) to measure population density of our experimental replicates, but also to obtain estimates of cell size. Population density estimates were made for each biological replicate to determine specific growth rate (see below). Mean forward scatter (FSC) was used to obtain mean cell length by calibrating FSC against calibration beads of a known size along with 18 marine phytoplankton taxa of a known average length (see Appendix C Figure.1). Following this we could estimate cell length and cell volume for each of the taxa, assuming spherical cell geometry (see below).

Specific growth rate for growth rate trajectories

Using the estimates of population density, at the beginning and end of each transfer period obtained from flow cytometry, we calculated specific growth rate (μ, day^{-1}) using the following equation (Wood *et al.* 2005):

$$\mu = \frac{\ln(N_{t1} - N_{t0})}{\Delta t} \quad (4.1)$$

Where N_{t1} is the population density at the end of the transfer period (when cells are still in exponential phase), N_{t0} is the inoculation density and Δt is the time passed in days since the inoculation.

Approximate number of generations passed between each transfer period could then be calculated from the estimated doubling time:

$$\textit{Approximate number of generations} = \Delta t \ / \ (\frac{0.6931}{\mu}) \quad (4.2)$$

Where, 0.6931/μ (or log(2)/μ) gives the calculated doubling time based on the estimated specific growth rate, μ, assuming mortality is zero, and Δt is the time passed in days since the inoculation.

FSC conversion factor and cell volume calculation

As described above we calibrated FSC against beads and taxa of a known length. This allowed us to derive the following conversion factor (see Appendix C Figure.1):

$$\ln\ cell\ length(\mu m) = (0.57 \times \ln FSC) - 5.93 \quad (4.3)$$

Where cell length is measured in μm, and FSC represents mean forward scatter measured by the flow cytometer simultaneously to the population density measurements. Assuming a spherical geometry, we then used the following equation to derive cell volume of the taxa at the time of each transfer (Hillebrand *et al.* 1999; Sun & Liu 2003) :

$$cell\ volume\ (\mu m^3) = \frac{\pi}{6} \times cell\ length\ (\mu m)^3 \quad (4.4)$$

Growth rate trajectories

We used the specific growth rate calculated at each transfer to track the changes in fitness of the replicates over the 22 week period (27 weeks, including the time period where additional physiological data was collected, see Figure.4.3). As the cytometry data provided estimates of population density during exponential growth and average cell volume, we also tracked these

parameters over the duration of the experiment (see Figure.4.4 and Appendix C Figure.2). Crucially, we were interested in investigating the effect of growth temperature on these trajectories. Due to the different shape of the trajectories across the treatments, and the taxa, we used generalized additive mixed effects models (GAMMs) to assess the effect of the growth temperature. These were fitted to the data using the "gamm4" package in R (v3.5.1). This approach allowed for us to account for the hierarchal nature of our data, whereby for each of the taxa, in each treatment, we had 6 individual biological replicates with their own unique trajectories. Therefore we treated replicate as a random effect on the intercept of the all the models, meaning that deviations of the replicates from the fixed effect (modelled intercept) were normally distributed with a mean that is equal to zero. The most complex models included the fixed effect of treatment temperature (i.e. control temperature and warmed temperature) on both the intercept (characterizing the median value of the response variable) and the shape of the time-series response (which is modelled using a cubic regression spline, to vary across the treatments). A model selection process was then followed to determine the best model, and to conclude the overall effect of the treatment on the trajectories. This entailed sequentially fitting models to the data, starting from the most complex model, then a model with just the effect of treatment on intercept but not shape, followed by just the effect of treatment on shape and not intercept, and finally no effect of treatment on either the intercept of the shape. The best model was selected by computing sample-size corrected Akaike Information Criterion scores (AICc) and then comparing these across all of the models, with the best model having the lowest AICc score that was more than 2 ΔAICc scores lower than the second best model. AICc weights also identified the strength of the best model relative to the others. These model comparisons were made using the "MuMIn" package in R. This process was repeated for the specific growth rate trajectories of each species, along with the trajectories of exponential phase population density and estimated cell volume (see Figures.4.3 and 4.4, and Appendix C Figure.2). The selection process is summarised by Appendix C Table.2.

Thermal tolerance curves

Following the 22 week experimental period we measured the thermal tolerance curves of each of the treatment replicates for each taxa. This entailed

inoculating each biological replicate into fresh growth medium with the same starting density, and placing them in incubators at a range of assay temperatures; from 15 to 35°C. Daily cell density measurements were made using flow cytometry, until replicates had reached carrying capacity. Where no positive growth was observed, and cell densities had dropped considerably following inoculation and not recovered within approximately 5 days, we deemed this data unsuitable for measuring thermal limits of acclimation and thus dropped the data for these assay responses from the analysis.

We modelled growth rate for each replicate at each assay temperature by log transforming the density measurements and running linear regressions through the exponential growth data, returning us a specific-growth rate for each experimental replicate at each assay temperature (see Eq.4.1). This was achieved through linear mixed effects modelling, using the "lme4" package in R, whereby we included the random effect of each specific biological replicate (across all taxa and treatments) on both the slope and intercept of the relationship between the natural logarithm transformed cell density and the number of days at the assay temperature. This returned us replicate specific deviations of both the slope and intercept from the overall response, with the slope coefficients derived for each replicate being used here as our specific growth rate estimates.

A modified version of the Sharpe-Schoolfield equation, which assumes that the rate of growth is limited by an enzyme catalysed reaction, was then used to quantify the unimodal thermal tolerance curves of growth rate for each of the treatments (Sharpe & DeMichele 1977; Schoolfield *et al.* 1981):

$$\ln\big(b(T)\big) = E_a\left(\frac{1}{kT_c} - \frac{1}{kT}\right) + \ln\big(b(T_c)\big) - \ln\left(1 + e^{E_h\left(\frac{1}{kT_h} - \frac{1}{kT}\right)}\right) \quad (4.5)$$

where b is the specific growth rate (d^{-1}), k is Boltzmann's constant, E_a is the activation energy (eV), characterising the steepness of the slope up to the thermal optima, T is temperature in Kelvin (K), E_h is the deactivation energy which characterizes decrease in rates above T_h where half the enzymes have become non-functional and $b(T_c)$ is rate normalized to an arbitrary reference temperature, here T_c = 22ºC (+ 273.15), where there is no low or high temperature inactivation. Eq. 4.5 can also be used to derive an optimum

temperature where a maximum rate is expected:

$$T_{opt} = \frac{E_h T_h}{E_h + k T_h \ln\left(\frac{E_h}{E_a} - 1\right)} \quad (4.6)$$

The parameters $b(T_c)$, E_a, E_h, T_h, and T_{opt} all characterise the unimodal response of growth rates to temperature increase. We modelled Eq.4.5 to each of the biological replicates of each species using a non-linear least squares regression analysis. This approach required the "nls.multstart" package in R, which applies the 'nlsLM' function in the 'minpack.lm' package and uses a modified Levenberg-Marquardt optimisation algorithm. Growth model parameters were determined by running 1000 random combinations of estimated starting parameters, which were then selected using AIC scores to determine the combination of parameters that best characterised the data for each biological replicate. We were then able to plot the predicted responses for each biological replicate using the returned parameters (see Figure.4.5a and 4.5f). We also obtained treatment level fits for visualisation of the overall effect of the experimental treatment, this required calculating the mean growth rate across all 6 biological replicates at each assay temperature, and re-running the above procedure to derive a set of parameters specific to the average treatment response (see Figure.4.5a and 4.5f). To determine whether there was a significant change in any of the parameters across the treatments for each species, we used linear mixed effects modelling and compared the full model, which included the fixed effect of treatment and random effect of replicate on the intercept, against a null hypothesis which included no fixed effect of treatment and just random effect of replicate. Analysis of variance (ANOVA) was used to compare models, and this is summarised in Appendix C Table.5, along with the replicate parameter estimates and their 95% confidence intervals (see Appendix C Tables.3 and 4). As mentioned in the experimental design section, the thermal performance of the pre-clonal stocks was also modelled for each of the taxa to identify a suitable temperature for our warmed treatments. However, unlike the method outlined above, we could only model the thermal performance parameters at the level of species, as the replication of growth measurements at each assay temperature were only technical with all inoculations coming from the same stock of each species (i.e. no biological replication).

Thermal plasticity of cell size

By estimating the mean cell volume at each assay temperature (obtained from flow cytometry data when making the cell density counts), we were able to observe any phenotypic changes in cell size across the temperature range used to measure thermal tolerance, and therefore compare thermal plasticity of size across the experimental treatments. To best demonstrate the changes in cell size associated with each assay temperature, for each biological replicate at each assay temperature we only used volume estimates from the last time-point that corresponds to the final stages of exponential growth before carrying capacity was reached for each replicate. This meant that each replicate had the maximum time to acclimate, before carrying capacity was reached and thus before nutrients became limited. The acclimated cell sizes at each assay temperature for all replicates were then plotted as boxplots to qualitatively interpret the plasticity of each of the replicates from each of the treatments (see Figure.4.6).

Growth reciprocal transplant assays

We carried out full reciprocal transplant assays for each of the taxa to determine changes in performance in response to both the control temperature and warmed temperature. We achieved this by inoculating all six replicates from each treatment into fresh growth medium at both the control and warmed temperatures. We tracked the cell density each day and then modelled specific-growth rate for each of the replicates as described above for the thermal tolerance curves. We then analysed the differences in growth rate between the control and warmed treatments at each temperature using linear mixed effects modelling and ANOVAs, as described above for testing the effect of treatment on the thermal tolerance parameters (see Figure.4.8, and Appendix C Table.6).

Estimates of Carbon and Nitrogen per cell

For each biological replicate, whilst in exponential growth, 50 to 100ml of culture of known density was aliquoted into falcon tubes and centrifuged at 3500rpm, at 4°C for 45 minutes. The resultant pellets were rinsed with deionised water and re-spun 3 times to remove any artificial sea water residue. All pellets were freeze-dried using a CoolSafe (95-15 PRO, ScanVac) over 24 hours and then

weighed to obtain dry weight. Samples were placed in tin cups and sent to Elemtex (Elemtex Ltd, Cornwall, UK, PL17 8QS) for elemental analysis of %C and %N using a SerCon Isotope Ratio Mass Spectrometer (CF-IRMS) system (continuous flow mode). For each biological replicate we then calculated $\mathrm{pg\ C\ cell^{-1}}$ (picograms of carbon per cell), $\mathrm{pg\ N\ cell^{-1}}$ (picograms of nitrogen per cell) and the C:N ratio (the carbon to nitrogen ration, in moles). Corresponding flow cytometry data was used to estimate the average cell volume for each of the replicates; from this we could then estimate changes in carbon and nitrogen per unit volume. ANOVAs were subsequently used to test for a significant shift in sub-cellular carbon, nitrogen and C:N ratio across the treatments (see Figure.4.9 and Appendix C Figure.4, Tables.8 to 10).

Chlorophyll a per cell measurements

For each biological replicate, whilst in exponential growth, 50ml of culture of a known cell density was centrifuged at 3500rpm, for 45 minutes at 4°C. The resultant pellets were re-suspended in 6ml of ethanol (100%) by vortexing, and all samples were then kept refrigerated in the dark for 24 hours. Following the extraction period, samples were vortexed again and cell debris was removed by centrifugation at 3500rpm for 3 minutes. Using a spectrophotometer (Jenway 7315) we measured absorbance of the supernatant from 610nm to 750nm for a minimum of three technical replicates per biological replicate. Blanks were measured across the same wavelength range to correct for the ethanol absorbance. We then used well established absorbance coefficients to obtain estimates of mean pg chlorophyll *a* cell^{-1} for each of the biological replicates. Due to differences in the pigment composition between the taxa, different equations were used (Ritchie 2006):

Cyanobacteria (*Synechococcus* sp.):

$$\mu g\ Chlorophyll\ a\ cell^{-1} = \frac{(11.9035\ A_{665} - A_{730})v/(lV)}{cells\ ml^{-1}} \quad (4.7)$$

Chlorophytes (*Ostreococcus tauri*):

$$\mu g\ Chlorophyll\ a\ cell^{-1} = \frac{(-5.2007\ A_{649} + 13.5275\ A_{665} - A_{730})v/(lV)}{cells\ ml^{-1}} \quad (4.8)$$

Where A_{xxx} is the absorbance at xxx nm (A_{730} represents the background absorbance), v is the volume of solvent used for the extractions (in this case 6ml of ethanol), l is the length of the spectrophotometric cell (cm), V is the original sample volume (in this case 50ml) and $cells\ ml^{-1}$ is the cell density of the original culture in exponential growth phase (Ritchie 2006; Henriques *et al.* 2007). As we also had corresponding flow cytometry data, again this was used to estimate the average cell volume for each of the replicates; and from this we could then estimate chlorophyll per unit volume. ANOVAs were subsequently used to test for significant shifts in cell chlorophyll *a* across the treatments (see Figure.4.9 and Appendix C Figure.4, and Tables.8 to 10).

Metabolism reciprocal transplant assays

Assay measurements of photosynthesis and dark respiration were collected at both the ambient and warmed treatment temperatures for all biological replicates, thus allowing us to compare the metabolic performance of each of the treatment replicates at each of treatment temperatures. We used a clark-type oxygen electrode as part of a Chlorolab 2 system (Hansatech Ltd, King's Lynn, UK) to measure net rates of oxygen evolution in the light (net primary production, NP) and oxygen consumption in the dark (dark respiration); both in units of μmol O_2 mL^{-1} s^{-1}. All biological replicates were sampled during mid-logarithmic growth phase to ensure that the samples were not substrate limited. To improve the signal to noise ratio when measuring rates, all biological replicate samples were concentrated by centrifugation at 1500rpm, 20°C, for 15 minutes and re-suspended into an adequate volume of fresh growth to make the assay temperature measurements (approximately 3mL). Prior to running a sample at each assay temperature, all samples were given ~ 15 minutes to pre-acclimate to the assay temperature in the dark before any data was collected. This also gave the electrode system sufficient time to stabilise before metabolic rates were measured. This was necessary for two reasons, i) as the sample adjusts to the assay temperature this will naturally cause changes in the dissolved oxygen concentration, ii) the electrode system results in oxygen signal drift, and this too is temperature dependent. We measured rates of oxygen depletion from 21 sterilised artificial seawater samples across a range

of temperatures 4°C - 44°C and found that the impact of drift was minimised after ~15 minutes of stabilisation time. Nevertheless, signal drift was linearly temperature dependent after this time. To account for drift in our dataset we corrected all our raw data using the following empirically derived relationship:

$$drift = (-0.392 \times T) - 6.51 \quad (4.9)$$

Where *T* is assay temperature (°C), and *drift* is the non-biological depletion in oxygen concentration measured in units $\mu molO_2\ mL^{-1}\ s^{-1}$ after approximately 15 minutes of stabilisation. The raw O_2 flux data was then corrected by subtracting the estimated drift.

Rates of net photosynthesis, measured as O_2 evolution, were collected across a range of light intensities from 0 to 1800 μmol $m^2\ s^{-1}$; starting with 20 μmol $m^2\ s^{-1}$, followed by the growth light level, 45μmol $m^2\ s^{-1}$ and then increments of 50 μmol $m^2\ s^{-1}$ between 100 to 200 μmol $m^2\ s^{-1}$, 100 μmol $m^2\ s^{-1}$ between 200 and 1000 μmol $m^2\ s^{-1}$, followed by 1200 μmol $m^2\ s^{-1}$, 1500 μmol $m^2\ s^{-1}$ and finally 1800 μmol $m^2\ s^{-1}$. This enabled us to model a photosynthesis-irradiance (PI) curve for each assay temperature, and therefore obtain an estimate of light saturated net photosynthesis, NP_{max}, see Eq.4.10. Respiration (*R*) was measured as oxygen consumption in the dark, over a 4-minute period directly following the light response outlined above. The photosynthesis-irradiance curve was then quantified, for each assay temperature response of each biological replicate, by fitting Eiler's photoinhibition model (Eilers & Peeters 1988; Edwards *et al.* 2016) to the data using non-linear least squares regression, as described previously for fitting the thermal tolerance curves, using the "nls.multstart" package:

$$NP(I) = \frac{NP_{max} I}{\frac{NP_{max}}{\alpha {I_{opt}}^2} I^2 + \left(1 - 2\frac{NP_{max}}{\alpha I_{opt}}\right) I + \frac{NP_{max}}{\alpha}} \quad (4.10)$$

Where $NP(I)$ is the rate of net primary production at light intensity, I, NP_{max} is the maximum rate of NP at the optimal light intensity, I_{opt}, and α is the rate in which NP increases up to NP_{max}. Light saturated gross primary production (P_{max}) was then calculated for each assay temperature as:

$$P_{max} = NP_{max} + R \quad (4.11)$$

Prior to running the photoinhibition model, rate units were then converted from μmol O_2 mL^{-1} s^{-1} to μg C μg C^{-1} $hour^{-1}$. We achieved this using the following equation:

$$b(\mu g\ C\ \mu g\ C^{-1}\ h^{-1}) = \frac{b(\mu mol\ O_2\ cell^{-1}\ h^{-1}) \times 32 \times M \times (\frac{12}{44})}{\mu gC\ cell^{-1}} \quad (4.12)$$

Where b is the metabolic rate (either *NP* or dark respiration), 32 is the molecular weight of O_2, M is a replicate specific assimilation quotient for CO_2:O_2 (Falkowski *et al.* 1985) which is used to describe consumption or fixation of C in the cell per unit of O_2, and 12/44 is the ratio of molecular weight of C to CO_2, thus $32 \times M \times \frac{12}{44}$ converts from $\mu mol\ O_2$ to μgC. Biological replicates were analysed to determine replicate specific $\mu g\ C\ cell^{-1}$ values (see previous section on estimating carbon and nitrogen per cell), and the number of $cells\ mL^{-1}$ was measured for each biological replicate using flow cytometry. The calculation of *M* assumes the following balanced growth equation, where:

$$nCO_2 + (n+1)H_2O + HNO_3 \rightarrow (CH_2O)_n\ NH_3 + (n+2)O_2 \quad (4.13)$$

If the *C:N* ratio (*n*) of the phytoplankton is calculated in moles then the ratio of CO_2:O_2, or *M*, will be equal to *n/n+2* (Falkowski *et al.* 1985). Our calculated values of *M* ranged from ~0.75 to ~0.79 for *Ostreococcus tauri* and from ~ 0.73 to ~0.75 for *Synechococcus* sp. (Appendix C Table.8).

Calculation of carbon-use efficiency

Carbon use efficiency (CUE), which we discuss here as the potential for carbon allocation growth, was calculated from the gross photosynthesis, P_{max}, and respiration, R, data for each biological replicate response to each assay temperature, where:

$$CUE = 1 - (\frac{R}{P_{max}}) \quad (4.14)$$

Statistical analysis of metabolism data

For all estimates of P_{max}, R and CUE we then analysed the effect of treatment on the metabolic responses to each assay temperature. This was also carried out using linear mixed effects modelling and ANOVAs, as described above for

the reciprocal transplant assays of growth rates (see Figure.4.7, and Appendix C Table.7).

Principal Components Analysis

Variance in different phenotypic traits across the taxa and treatments were examined using principal component analysis (PCA), this was conducted using the 'prcomp' function in the in-built 'stats' package in R. This analysis was performed on the following traits: mean cell volume, $\mathrm{pgC}\,\mu\mathrm{m}^{-3}$ (picograms of carbon per unit volume) mean $\mathrm{pgN}\,\mu\mathrm{m}^{-3}$ (picograms of nitrogen per unit volume), mean pg chlorophyll *a* $\mu\mathrm{m}^{-3}$ (picograms of chlorophyll *a* per unit volume) , $T_{opt}{}^{\mu}$ (optimal growth temperature) and the C:N ratio (carbon to nitrogen ratio, in moles). All variables were natural logarithm transformed to normalise the values and therefore not to inflate the variances. The first two principal components, which combined accounted for >75% of the total variance, were used to define the axes of the plot onto which results were projected. Loadings scores for each of the variables were derived and plotted on the same axis to demonstrate any possible negative or positive covariance of the traits. Ellipses were plotted as a visual guide to the clustering of the different treatment replicates, and reflect 95% confidence intervals around the centroid of each cluster giving us an indication of whether the treatment replicates can be uniquely identified by the traits included in the PCA (see Figure.4.10, and Appendix C Figure.5 for PCA including per capita estimates of C, N and chlorophyll *a*).

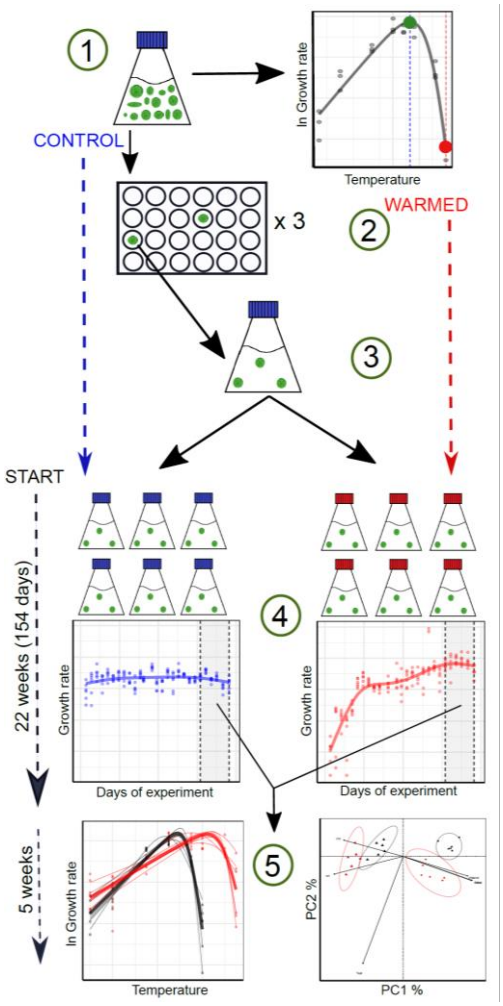

Figure.4.1. Schematic diagram of the experimental design for each species. (1) Stock cultures of each species were maintained under nutrient replete, exponential, growth conditions at the control temperature of 20°C (their ancestral lab culture conditions). We measured the thermal tolerance of each stock culture and identified a stressful 'warmed' temperature (red dot) for each species where growth rates were approximately 50% of the rate at the optimal temperature (green dot), see Figure 4.2.(2) We then used a serial dilution-to-extinction method, where we approximately inoculated 1 cell into 2ml of growth medium per well, and repeated this for three 24 well-plates, (3) Once growth was observed we selected one colony (from one random well) for inoculation into a larger volume of media; this was our clonal founder population (4) From the clonal founder population we then inoculated 6 biological replicates into 100ml of growth medium at both the control temperature and the identified warmed temperature. These biological replicates were maintained under nutrient replete, exponential, growth at each temperature and weekly growth rate measurements were made to demonstrate changes in fitness over time, see Figure 4.3.. We tracked growth rates for 22 weeks, or 154 days. (5) Following this experimental period, over a further 5 weeks we then collected extensive physiological datasets from the 6 replicates of each treatment (e.g. thermal tolerance curves, metabolism reciprocal transplant assays and sub-cellular carbon, nitrogen and chlorophyll *a* measurements, see Figures 4.5-4.10).

Results

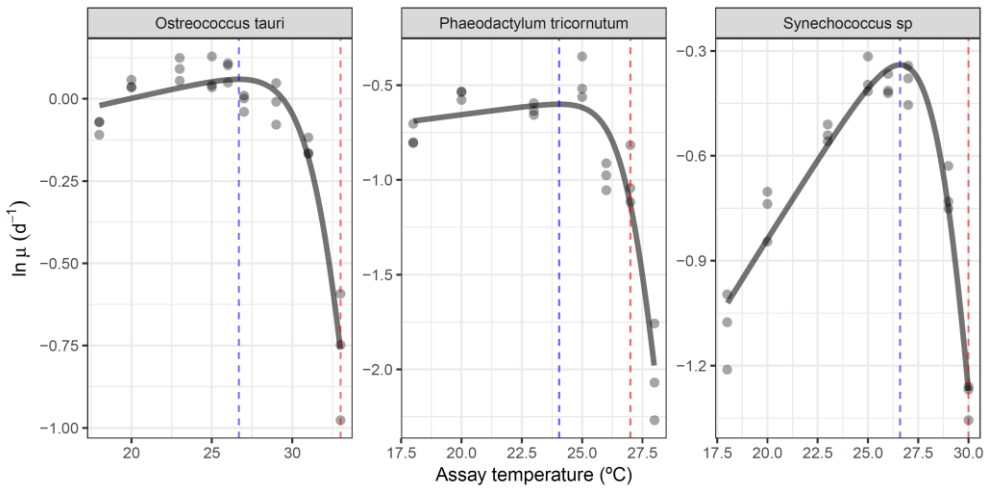

Figure.4.2. Thermal tolerance curves of pre-clonal stock populations for each of the taxa in this study. Data points represent natural logarithm growth rates for a minimum of 3 technical replicates per assay temperature. Model lines were derived from fitting a modified Sharpe-Schoolfield model to the datasets of each taxa independently, using a non-linear least squares regression approach, that selected the best fit from a range of random starting parameters using AIC scoring (as described in the methods section for modelling thermal tolerance curves). Parameters for each of the fits are summarised in Appendix C Table.1. The dashed blue line highlights the modelled thermal optima for each of the taxa: 26.7°C for *Ostreococcus tauri*, 24.0°C for *Phaeodactylum tricornutum* and 26.6 °C for *Synechococcus* sp. These fits were used to determine a supra-optimal growth temperature that returned rates that were approximately 50% of the rates at the optimal temperature for each taxa, this gave us a quantitative approach for determining the high temperature treatment for each of the taxa, highlighted by the dashed red line; 33°C for *Ostreococcus tauri*, 27°C for *Phaeodactylum tricornutum* and 30 °C for *Synechococcus* sp.

Pre-clonal tolerance curves

We found clear variation in the thermal tolerance of each of the taxa prior to making them clonal (see Figure.4.2, and Appendix C Table.1). Between assay temperatures of 18°C and 33°C we found that *Phaeodactylum tricornutum*, had the narrowest thermal niche with a maximum growth temperature (T_{max}) of 28°C, followed by *Synechococcus* sp. with a T_{max} of 30°C and lastly *Ostreococcus tauri*, with a T_{max} of 33°C. This was also reflected by the differences in the optimal temperature , ${T_{opt}}^{\mu}$, for each of the taxa; 24.0°C for *Phaeodactylum tricornutum*, 26.6 °C for *Synechococcus* sp. and 26.7°C for

Ostreococcus tauri. Whilst we also see clear differences in E_a^{μ} across the taxa, which characterises the rate at which specific growth rate increases up to the maximum growth temperature, the primary interest in modelling these responses was to identify a supra-optimal temperature for each of the taxa where rates were 50% of their rate at the optimum (see Experimental Design in the Methods section). From estimating the specific growth rate at the optimal temperature we determined these supra optimal temperatures as 33°C for *Ostreococcus tauri*, 30 °C for *Synechococcus* sp. and 27°C for *Phaeodactylum tricornutum* (see Appendix C Table.1). Critically, Figure.4.2 demonstrates that prior to clonal isolation, the stock populations of all taxa demonstrated positive growth at the identified high temperature treatments, reflecting the thermal limits of acclimation of the diverse stock populations.

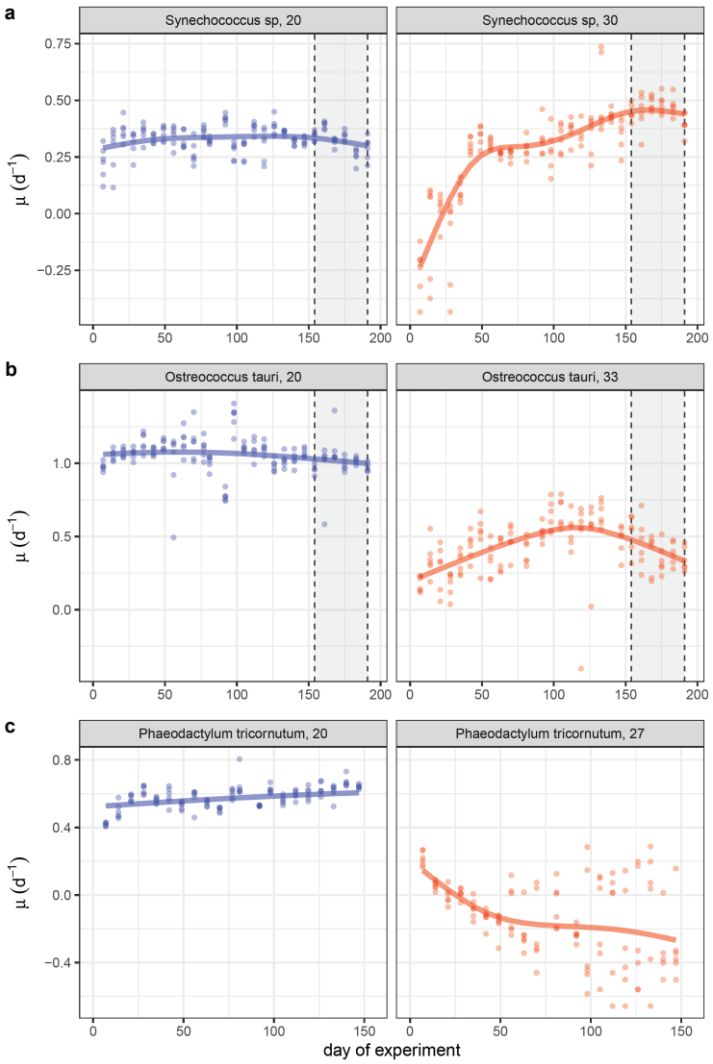

Figure.4.3. Growth rate projections for each of the taxa at each of their respective treatment temperatures. Plots on the left present the changes in specific growth rate at the control temperature for each of the taxa, denoted by

blue colouring, plots on the right present the changes in specific growth rate at the warmed temperature treatment for each of the taxa, denoted by red colouring. The lower of the dashed vertical lines highlight the end of the 22 week experimental period, and the shaded area represents the 5 week period during which all other physiological data was collected, up to the second vertical dashed line at the 27 week mark. Data points represent specific growth rate measurements for the 6 biological replicates at each treatment temperature, and the fitted line for each of the treatments represents the best fits of the selected GAMM for each of the taxa (See Methods). There was a significant effect of treatment on both the shape and intercept of the responses for each of the taxa (see Appendix C Table.2). **(a)** The projections for *Synechococcus* sp. **(b)** The projections for *Ostreococcus tauri* **(c)** The projections for *Phaeodactylum tricornutum*. Unlike the other two species, data collection for *Phaeodactylum tricornutum* ceased after 22 weeks. This was due to both very low and negative growth rates for most of the experimental period and very low population densities (Appendix C Figure.2) at the high temperature treatment, making it unfeasible to collect any additional physiological data.

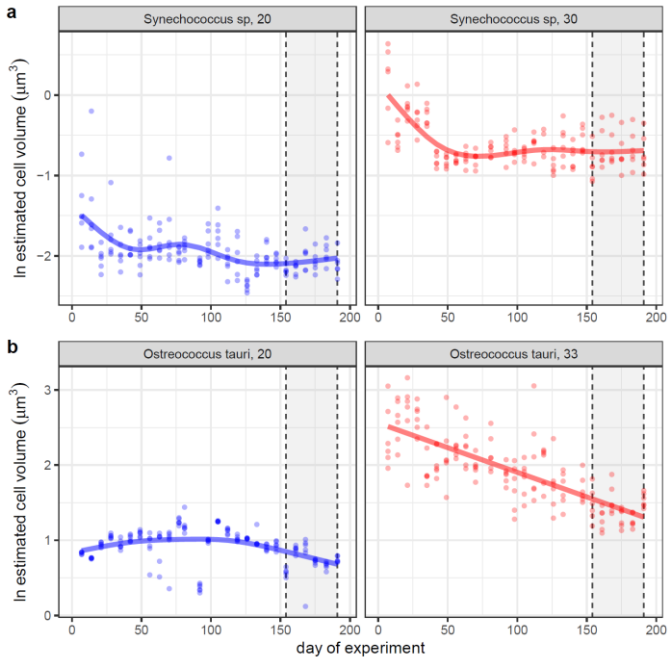

Figure.4.4. Natural logarithm cell volume projections for each of the taxa at each of their respective treatment temperatures. Plots on the left present the changes in cell volume at the control temperature for each of the taxa, denoted by blue colouring, plots on the right present the changes in cell volume at the warmed temperature treatment for each of the taxa, denoted by red colouring. Data points represent cell volume estimates for the 6 biological replicates at each treatment temperature, and the fitted line for each of the treatments represents the best fits of the selected GAMM for each of the taxa (See Methods). There was a significant effect of treatment on both the shape and intercept of the responses for each of the taxa (see Appendix C Table.2). **(a)** The projections for *Synechococcus* sp. **(b)** The projections for *Ostreococcus tauri.*

Grow rate, density and size projections

Across all taxa we found that there was a significant effect of experimental treatment on both the intercept and shape of the specific growth rate time series (see Figure.4.3 and Appendix C Table.2). For *Synechococcus* sp. at the control temperature we observed no overall change in specific growth rate over the duration of the experiment, with specific growth rates across all 6 biological replicates fluctuating around $0.3d^{-1}$. In response to the high temperature treatment, we measured negative specific growth rates for all biological replicates over the first 2 to 3 weeks, following this there was a rapid increase in growth rates up to day 50 of the experiment where rates reached a similar magnitude to the control treatment, and then growth rates continued to gradually increase up to the final 5 weeks of the experiment, where they reached a magnitude that was higher than the control (see Figure.4.3a). Likewise, for *Ostreococcus tauri* at the control temperature we observed very little change in the growth rate across all replicates, with rates fluctuating around 1 to 1.1 d^{-1}. In response to the warmed treatment, unlike *Synechococcus* sp., the warmed replicates of *Ostreococcus tauri* maintained positive specific growth rates but at a magnitude that was lower than the control. Over the first half of the experiment the specific growth rates gradually increased, reaching a maximum of approximately 0.6 d^{-1}. Following this the growth rates then gradually declined to approximately 0.3 d^{-1} by the end of the experimental period (see Figure.4.3b). For *Phaeodactylum tricornutum* at the control temperature we observed a very slight increase in growth rates over the duration of the experiment, from approximately 0.5 d^{-1} to 0.6 d^{-1}. However, at the warmed temperature there was a clear indication that there had been no thermal adaptation. For the first couple of weeks growth rates remained positive, albeit at a much lower magnitude to the control, indicating that there may have initially been some thermal acclimation to the elevated temperature. Following this, for most of the replicates, negative specific growth rates were then observed over the duration of the experiment (see Figure.4.3c).

These growth rate projections are complemented by very similar projections of population density (see Appendix C Figure.2), where we also found a significant effect of treatment on both the shape and intercept of the time series for each of the taxa (see Appendix C Table.2). This was to be expected as the changes in

growth rate between replicate transfers, where replicates were always being diluted back to the same starting density, were therefore proportional to the change in population density of the cultures between transfers.

We also found a significant effect of treatment on both the intercept and slope of the estimated cell volume of the clonal replicates throughout the course of the experiment (see Figure 4.4). For *Synechococcus* sp*.* at the control temperature we found that average cell volume decreased slightly over the first couple of weeks, but following this cell volume was relatively stable at approximately 0.15µm^3 throughout the rest of the experiment. In response to the warmed treatment however there was a rapid increase in cell volume within the first week, with average cell volume reaching approximately 1 µm^3. Over the next 50 days the volume gradually decreased, and then stabilised when it reached approximately 0.45 µm^3, where it remained at a greater volume than the control for the rest of the experimental period (see Figure.4.4a). For *Ostreococcus tauri* there was also a relative stability at the control temperature, where the volume fluctuated between 2 µm^3 to 3 µm^3 throughout the course of the experiment. At the warmed temperature, as with *Synechococcus* sp*.* there was a rapid initial increase in volume within the first week to approximately 12µm^3. Throughout the duration of the experiment the volume then gradually declined, and by the end of the experimental period had reached a volume of approximately 3.5 µm^3 (see Figure.4.4b). Thus, unlike *Synechococcus* sp*.*, the shift to a larger cell size was not maintained, and with a longer experimental period the estimated volume at the high temperature looked set to have reached volumes that were of a similar magnitude to the control.

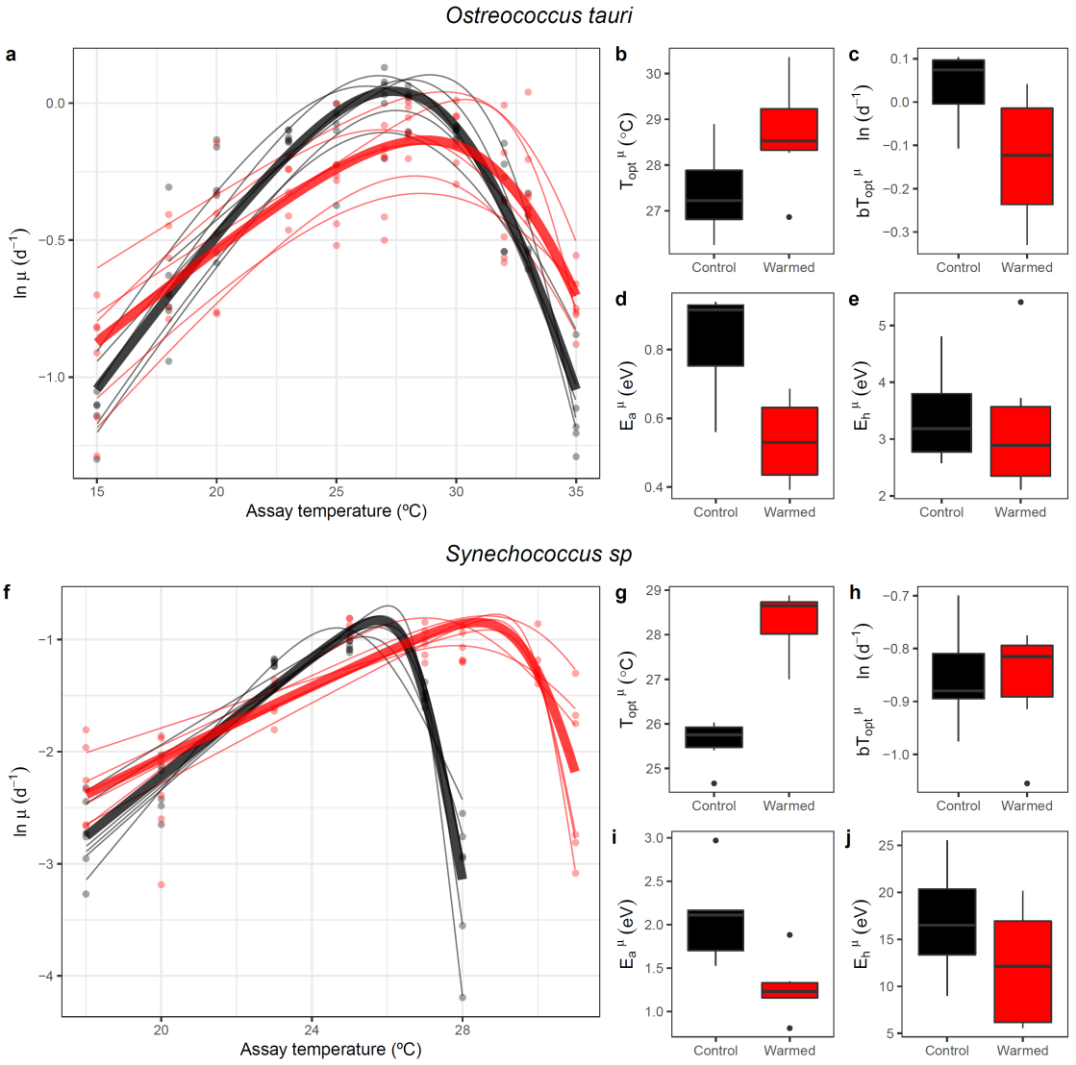

Figure.4.5. Thermal tolerance curves and the modelled Sharpe-Schoolfield parameters for both the control and warmed treatment replicates of *Ostreococcus tauri* (a – e) and *Synechococcus* sp. (f – j). Black colouring denotes control treatment data, and red denotes the warmed treatment data. In each case model lines were derived from independently fitting a modified Sharpe-Schoolfield model to the natural logarithm growth rate responses of each biological replicate, using a non-linear least squares regression approach, that selected the best fit from a range of random starting parameters using AIC scoring (as described in the methods section for modelling thermal tolerance curves). For visualisation purposes only, parameters were also derived for the mean growth rate responses for each treatment at each assay temperature. Replicate fits are visualised by finer lines, and the average fit by the bold lines. The box and whisker plots for each of the taxa illustrate the resultant divergences in the thermal performance parameters following approximately 22 weeks at each treatment, and tests for significant differences are summarised in Appendix C Table.5. The bold horizontal line corresponds to the median parameter value, the top and bottom of the box correspond to the 75th and 25th percentiles and the whiskers extend to the largest and smallest values no greater or less than the 1.5 × the interquartile range.

Post-experiment thermal tolerance curves

Due to the lack of an adaptive response observed for *Phaeodactylum tricornutum* over the experimental time period in response to the warmed treatment, and the resultant low cell densities, it was not feasible to conduct measurements of thermal performance for this species. Nonetheless, we were able to measure the thermal tolerance curves of replicates from the control and warmed treatments of *Ostreococcus tauri* and *Synechococcus* sp. (see Figure.4.5). For *Ostreococcus tauri*, we observed an overall shift in the thermal tolerance curve to a higher ${T_{opt}}^{\mu}$, with an average control ${T_{opt}}^{\mu}$ of 27.36°C and an average warmed ${T_{opt}}^{\mu}$ of 28.72°C. We also modelled an overall decrease in the ${E_a}^{\mu}$ of the warmed replicates, with an average control ${E_a}^{\mu}$ of 0.83eV and an average warmed ${E_a}^{\mu}$ of 0.50eV. In combination with a raised optimal temperature, the warmed replicates also demonstrated reduced maximal growth rates (${bT_{opt}}^{\mu}$) at the optimal temperature. For both treatments we were able to measure acclimated growth rates of *Ostreococcus tauri* across the temperature range of 15°C to 35°C. This demonstrates that despite the overall changes in the thermal performance parameters, the thermal limits of acclimation measured over the same temperature range were maintained following the warm adaptation. For *Synechococcus* sp. we observed a much greater shift in the tolerance curve, with an average control ${T_{opt}}^{\mu}$ of 25.76°C and an average warmed ${T_{opt}}^{\mu}$ of 28.39°C. We also modelled an overall decrease in the ${E_a}^{\mu}$of the warmed replicates, with an average control ${E_a}^{\mu}$ of 1.98eV and an average warmed ${E_a}^{\mu}$ of 1.20eV. Unlike *Ostreococcus tauri* there was not an overall decrease in ${bT_{opt}}^{\mu}$ of the warm adapted replicates, with no significant difference in ${bT_{opt}}^{\mu}$ between the two treatments. Furthermore, we were able to measure acclimated growth rates for the warm adapted replicates between 18°C to 31°C but for the control replicates we could only measure acclimated rates between 18°C to 28°C. Thus, as a consequence of the adaptation to the higher temperature the warm adapted replicates of *Synechococcus* sp. demonstrated a wider niche of thermal tolerance relative to the replicates at the control temperature. Tests for significant difference in the thermal tolerance

parameters across the treatments for each species are summarised in Appendix C Table.5.

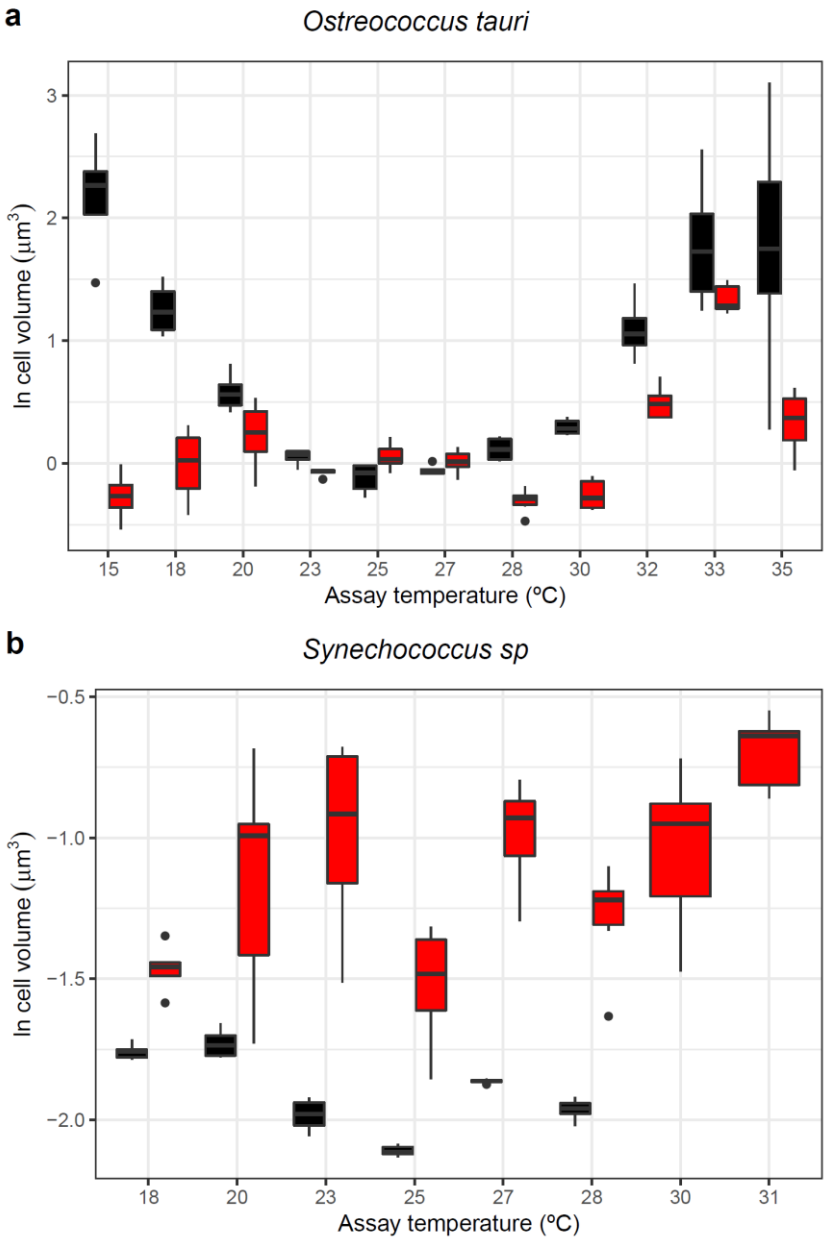

Figure.4.6. Thermal performance response of natural logarithm cell volume for both *Ostreococcus tauri* (a) and *Synechococcus* sp. (b). This data was collected simultaneously to the growth rate data used to model the thermal tolerance curves of each strain (see Figure.4.5) and therefore reflects the acclimation response of cell size, during exponential growth phase, following short-term exposure to a range of temperatures. In each plot, black colouring denotes the control treatment responses, and red for the warmed treatment responses.

Thermal plasticity of size

For both taxa we see that there has clearly been an effect of growth temperature on the thermal plasticity of cell size. For *Ostreococcus tauri* the control replicates show a decrease in cell size with warming between 15°C and 27°C, beyond which we see an increase in cell size up to 35°C (see Figure.4.6a). This acclimation response characterised by larger cell size is in agreement with the experimental time series data, where we show an initial shift to larger cell size in response to 33°C within the first couple of weeks (see Figure.4.4b). Contrary to the control treatment response, the warm adapted replicates of *Ostreococcus tauri* seem to show a decrease in cell size in response to cooling. Between 33°C and 28°C there is a sharp decline in size, however between 28°C and 15°C the cell sizes fluctuate, but all at much lower volumes than the response at the ancestral temperature of 33°C. However, in response to 35°C there is also a shift to smaller cell size (see Figure.4.6a).

Synechococcus sp. also illustrates clear differences in the thermal plasticity of the replicate size across the treatments (see Figure.4.6b). Unlike *Ostreococcus tauri* where there is more overlap in the cell size response across the replicates from both treatments, for *Synechococcus* sp. in response to all assay temperatures the cell size of the warm adapted replicates is always greater than the control. This is supported by the fact that size, in response to the warmed treatment over the experimental period, appeared to stabilise at a larger volume than the control after approximately 50 days (see Figure.4.4a), suggesting that there has been an overall adaptation to larger cell size. In relation to the plastic response, for the control replicates there is an overall decrease in cell volume between the assay temperatures of 18°C and 28°C, however we did not observe any acclimated growth rates for the control strain beyond 28°C. Similarly to *Ostreococcus tauri*, the warm adapted replicates of *Synechococcus* sp. appear to illustrate an overall decrease in volume between the high temperature, 31°C, and the lowest temperature, 18°C.

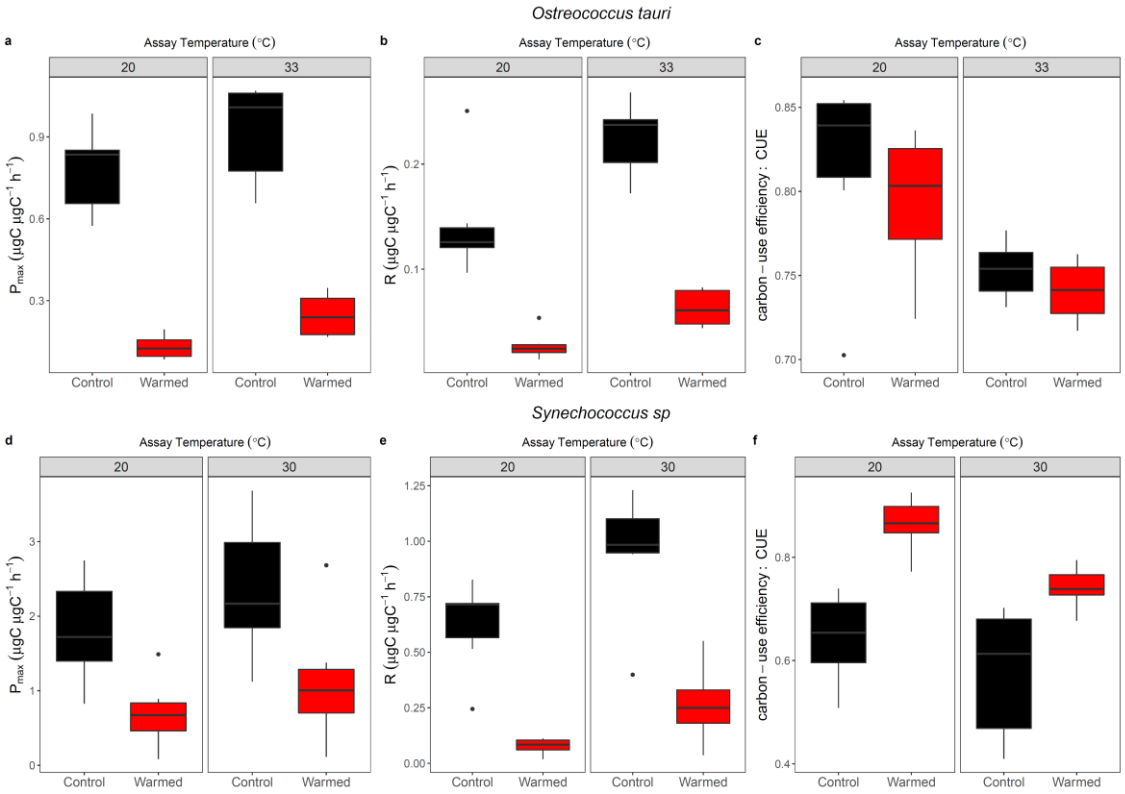

Figure.4.7. Reciprocal transplant assay measurements of gross photosynthesis (P_{max}), respiration (R) and carbon-use efficiency (CUE) for both control and warm adapted replicates of *Ostreococcus tauri* (**a – c**) and *Synechococcus* sp. (**d – f**). For both taxa the warmed treatments reflect lower mass-specific metabolic rates of P_{max} and R relative to the control, reflecting a down-regulation of metabolic rates in response to the higher temperature (a,b,d,and e). *Synechococcus* sp. replicates from the warmed treatment demonstrate higher CUE at both the control and warmed assay temperatures relative to replicates at the control treatment (f), whereas for *Ostreococcus tauri* there is no difference between the CUE of the warmed treatment replicates and control replicates in response to each of the assay temperatures (c). We deduce that this is due to *Synechococcus* sp. showing greater down-regulation of mass-specific R relative to down regulation of P_{max}, resulting in greater potential for carbon allocation growth in the warm adapted replicates. Tests for significant differences in the responses displayed in this figure, i.e. difference in treatment responses to each assay temperatures are summarised in Appendix C Table.7.

Metabolism and Carbon-use efficiency reciprocal transplant assays

In response to acute temperature change we identified clear differences in mass-specific metabolic rates at both the control temperature and warmed temperature for each of the taxa. Critically, we observed overall decrease in mass-specific metabolism for both of the taxa as a result of adaptation to higher temperatures. Of significance for understanding the thermal tolerance curves we identify that *Synechococcus* sp. was able to increase its carbon-use

efficiency in response to the high temperature, relative to the control, whereas *Ostreococcus tauri* only adjusted its metabolism to have similar carbon-use efficiency to the control (see Figure.4.7). For *Ostreococcus tauri* we observed significant down-regulation of both mass-specific gross photosynthesis and respiration for the warm adapted replicates. In response to the 20°C assay temperature the mean mass-specific P_{max} of the warmed replicates was 83% lower than the control, likewise in response to the 33°C assay temperature the mean mass-specific P_{max} of the warmed replicates was 73% lower than the control. Similarly, for mass-specific R, at the 20°C assay temperature the mean rate was 81% lower than the control for the warm adapted replicates, and in response to the 33°C assay temperature the mean rate was 72% lower than the control for the warm adapted replicates. Thus, the down-regulation of metabolism for the warm adapted strains was similar for both P_{max} and R, and in response to both assay temperatures (see Figure.4.7a and 4.7b). Consequently, despite the down-regulated metabolic rates, the calculated CUE was not significantly different between the control replicates and the warm adapted replicates of *Ostreococcus tauri* in response to both assay temperatures (see Figure.4.7c, see Appendix C Table.7). Contrary to this we observed a significant improvement in the CUE of the warmed strains of *Synechococcus* sp*.* in response to both assay temperatures. Similarly to *Ostreococcus tauri* we did observe a down-regulation of mass-specific metabolic rates, but by a greater proportion for R relative to P_{max} (see Figure.4.7d and 4.7e). In response to the 20°C assay temperature the mean mass-specific P_{max} of the warmed replicates was 61% lower than the control, likewise in response to the 30°C assay the mean mass-specific P_{max} of the warmed replicates was 52% lower than the control. For mass-specific R, at the 20°C assay temperature the mean rate was 88% lower than the control for the warm adapted replicates, and in response to the 30°C assay temperature the mean rate was 72% lower than the control for the warm adapted replicates. As a result, the smaller down-regulation of P_{max} relative R, in response to both assay temperatures, resulted in a greater CUE of the warm adapted replicates relative to the control (see Figure.4.7f). Tests for significance in the differences in the metabolic performances are summarised in Appendix C Table.7.

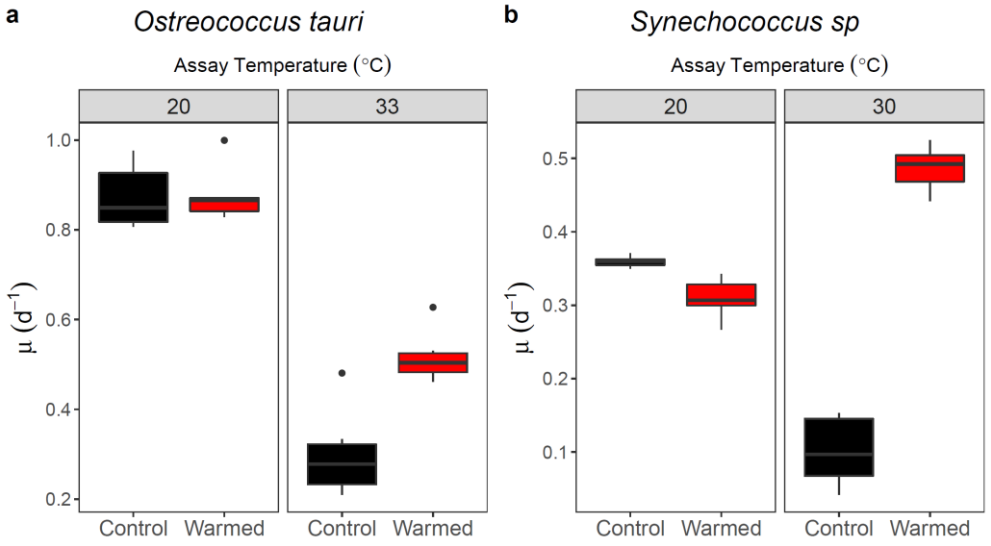

Figure.4.8. Reciprocal transplant assay measurements of specific growth rate for both control and warm adapted strains of *Ostreococcus tauri* (a) and *Synechococcus* sp. (b). For *Ostreococcus tauri* we observe an overall poorer performance of both the control and warmed strain in response to the warmed assay temperature, 33°C. However, the performance of the warmed strain at 33°C is significantly better than the control, indicating thermal adaptation to the high temperature. We also see a similar performance between the two strains in response to the control temperature, 20°C, and this suggests that there has not been evolutionary cost for the performance at lower temperatures following adaptation to the high temperature. For *Synechococcus* sp. we observe a poorer performance of the control strain at 30°C, but a massively improved performance of the warmed strain with growth rates that were higher than the control performance at the control temperature, thus reflecting clear thermal adaptation. However, the performance of the warmed strain at 20°C is significantly lower than the control, indicating that there has been a cost to the performance at low temperatures in association with the thermal adaptation to the high temperature. Tests for significant differences in the responses displayed in this figure are summarised in Appendix C Table.6.

Growth rate reciprocal transplant assays

We found a clear difference in the levels of adaptation observed from the reciprocal transplant assays of growth rate measurements between *Synechococcus* sp. and *Ostreococcus tauri*. For *Ostreococcus tauri* we observed that replicates from both treatments displayed a weaker performance at the warmed assay temperature relative to the control assay temperature (see Figure.4.8a), reflecting the overall lower growth rates of the warmed treatment replicates (see Figure.4.3b). Nonetheless, thermal adaptation was apparent due to significantly higher growth rates of the warmed replicates in response to the warmed assay temperature relative to the control. Furthermore, this adaptation to the warmed treatment appears to have come at no cost to the performance at

the lower control temperature, where we found no difference between the performances of replicates from both treatments. Unlike *Ostreococcus tauri*, we observed that the response of the warm adapted replicates of *Synechococcus* sp. to the warmed treatment temperature was significantly better than the control response (see Figure.4.8b), and furthermore was significantly better than the control response at the control temperature. This is in agreement with the projected growth rates from the experimental time series, where we demonstrated an increase in the warmed treatment growth rates to a greater magnitude than the control (see Figure.4.3a). As a possible cost of the warmed adaptation, for *Synechococcus* sp. we also see a poorer performance of the warm adapted replicates at the control temperature relative to the control replicates. Tests for significance in the differences in the growth rate performances are summarised in Appendix C Table.6.

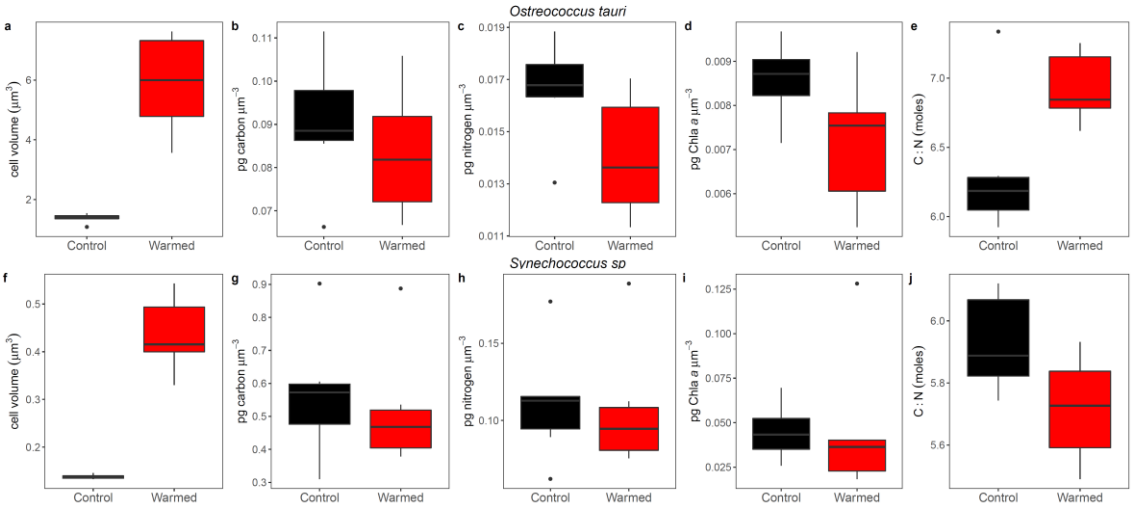

Figure.4.9. Phenotypic trait differences between the control and warm adapted treatment replicates of both *Ostreococcus tauri* (a – e) and *Synechococcus* sp. (f – j). For both taxa the warmed replicates reflect increased cell volume (a,f) and no significant difference in the volume specific carbon content relative to the control (b,g). Warm adapted *Synechococcus* sp. shows no change in the volume specific nitrogen content relative to the control (h), however the warm adapted *Ostreococcus tauri* shows a shift to lower nitrogen per unit volume (c). Likewise, for chlorophyll *a* per unit volume there is not a significant difference between the control and warmed *Synechococcus* sp. (i), however for *Ostreococcus tauri* there appears to be a shift to less chlorophyll *a* per unit volume in the warm adapted replicates (d). Furthermore, we see a significant increase in the C:N ratio of the warmed replicates of *Ostreococcus tauri* (e) but not for *Synechococcus* sp., where there is a decrease in the C:N ratio for most replicates (j). Tests for significant differences in the traits displayed in this figure are summarised in Appendix C Table.10.

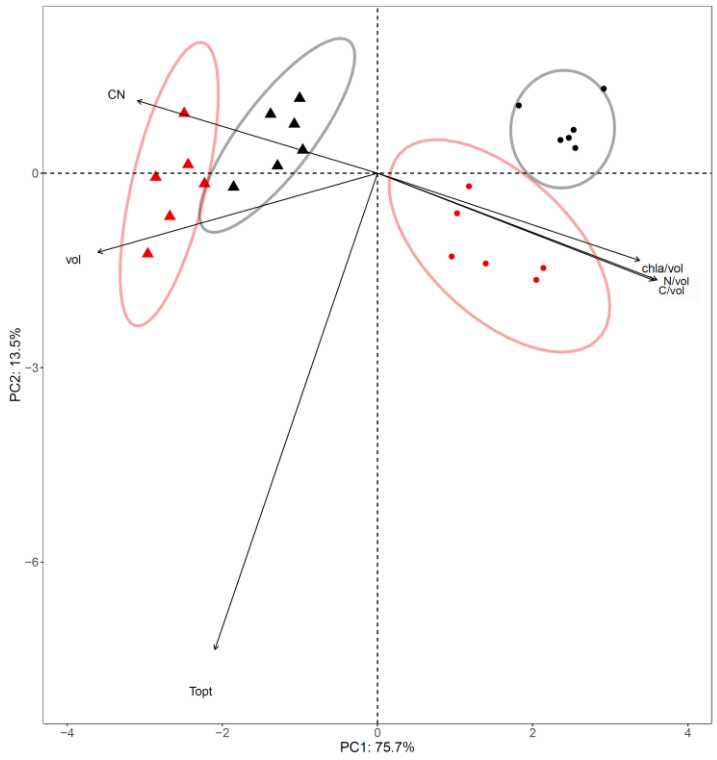

Figure.4.10. Principal component analysis of the trait data for each of the control and warm adapted replicates of both *Ostreococcus tauri* and *Synechococcus* sp. Triangles denote *Ostreococcus tauri* biological replicates, and circles denote *Synechococcus* sp. biological replicates, with black and red colouring denoting control and warmed treatments, respectively. The principal component axes are derived from the first two principal components and make up >75% of the total variance in the data. The loadings for each of the variables included in the analysis are plotted to demonstrate the correlations and covariance of physiological traits, where: vol = estimated cell volume, Topt = optimal growth temperature, CN = C:N ratio in moles, C/vol = $\mathrm{pgC\ \mu m^{-3}}$, N/vol = $\mathrm{pgN\ \mu m^{-3}}$ and chla/vol = $\mathrm{pg\ chlorophyll}\ a\ \mathrm{\mu m^{-3}}$. The length of each loading vector reflects the combined weighting of each variable in the first two principal components. Here, all loadings were multiplied by a constant for visualisation purposes. Ellipses were plotted as a visual guide to the clustering of the different treatment replicates, and reflect 95% confidence intervals around the centroid of each cluster giving us an indication of whether the treatment replicates can be uniquely identified by the traits included in the PCA. All variables were natural logarithm transformed to normalise the values and therefore not to inflate the variances. The PCA highlights clear differentiation of the two species, as well as their respective control and warmed treatments, in relation to the physiological traits provided (for boxplots of these traits see Figures.4.5 and 4.9).

Phenotypic trait differences and covariance

Across both of the taxa we found a significantly greater cell volume for our warm adapted replicates, and this is in agreement with our time-series projections of cell volume. In correlation with greater volume we also found that the warm adapted replicates also returned significantly higher measurements of $\mathrm{pgC\ cell^{-1}}$ (picograms of carbon per cell) and $\mathrm{pgN\ cell^{-1}}$ (picograms of carbon per cell) for both taxa. However, for pg chlorophyll *a* cell^{-1} we only observed significantly higher concentrations in the warm adapted strains of *Synechococcus* sp., whereas there was no significant difference in the pg chlorophyll *a* cell^{-1} between the warm adapted and control replicates of *Ostreococcus tauri* (see Appendix C Figure.4). We also observed a significantly greater carbon to nitrogen ratio (C:N) in the warm adapted strains of *Ostreococcus tauri* relative to the control, whereas for *Synechococcus* sp. the C:N was generally lower for the warm adapted strain (see Figure.4.9). Given the differences in volume being the likely driving factor behind some of these findings, we were also able to calculate differences in carbon, nitrogen and chlorophyll *a* per unit volume, and therefore investigate the effect of treatment temperature on the volume specific concentrations (see Figure.4.9). For both taxa we found no significant effect of treatment on $\mathrm{pgC\ \mu m^{-3}}$ (picograms of carbon per unit volume), however we do observe a shift to lower $\mathrm{pgN\ \mu m^{-3}}$ (picograms of nitrogen per unit volume) for *Ostreococcus tauri* but not so much for *Synechococcus* sp. Similarly, we find a shift to lower $\mathrm{pg\ chlorophyll}\ a\ \mathrm{\mu m^{-3}}$ (picograms of chlorophyll *a* per unit volume) for the warm adapted strain of *Ostreococcus tauri* but this is less evident for *Synechococcus* sp. Thus, the differences observed in the C:N between the warmed and control treatment across the taxa could be driven by the lower chlorophyll *a* per capita and per unit volume observed for the warm adapted *Ostreococcus tauri*. Tests for significance in the differences in these traits across the treatment replicates are summarised in Appendix C Tables.9 and 10. Based on these findings, the PCA (see Figure.4.10) illustrates clear differentiation between the warm adapted replicates and the control replicates for each of the taxa. Most of the differences are driven by the changes in volume across the treatments, but we also show that the shift in volume is also positively correlated with the increase in $T_{opt}{}^{\mu}$ of

the warm adapted strains, and that the C:N ratio is negatively correlated with $\mathrm{pg\ chlorophyll}\ a\ \mu\mathrm{m}^{-3}$.

Discussion

Unlike previous studies that have investigated thermal adaptation of phytoplankton using an experimental evolution approach, a key strength of this study is that we present an interpretation of thermal adaptation, over a set time period, for three different marine taxa, each of which represent globally abundant and ecologically important functional groups of phytoplankton. Though previous studies have shared a general agreement in the direction of thermal adaptation (Listmann *et al.* 2016; Schaum *et al.* 2017, 2018; Baker *et al.* 2018; O'Donnell *et al.* 2018), i.e. increases in thermal optima and maximum temperature, it could be argued that a key constraint to having multiple studies on just single taxa is that the experimental time-frame differs across the studies, and it typically lasts long enough until thermal adaptation is observed. Whilst this can give an indication of the pace of adaptation for a particular species, it is difficult to make direct comparisons and inferences about the ability of one species to adapt versus another. Similarly, there is not a common approach for selecting a high temperature treatment throughout these previous studies. Subsequently, the levels of thermal stress will differ across the taxa and therefore likely influence the extent of thermal adaptation observed. In this study we dealt with these two issues by firstly comparing thermal adaptation observed across the taxa over a set experimental time period, and secondly we used the same quantitative method for selecting a high temperature treatment for our taxa (i.e. a supra-optimal temperature where growth rates were approximately 50% of the optimal rate). In addition to this, some previous studies also initiated their experiments with clonal isolates (Listmann *et al.* 2016; O'Donnell *et al.* 2018; Schaum *et al.* 2018) whilst others have not (Padfield *et al.* 2016; Baker *et al.* 2018). In favour of not using clonal isolates is the argument that there is high standing genetic variation in natural populations and thus responses measured are more reflective of natural populations, and therefore it could be expected that this maximises the potential for, and pace of, thermal adaptation (Reusch & Boyd 2013; Listmann *et al.* 2016; Padfield *et al.* 2016). On the other hand, it is

arguably beneficial to use replicated clonal starting populations as it can reflect whether the direction and magnitude of adaptation is consistent, across the replicates, regardless of having the same bottlenecked starting diversity. Furthermore, using a clonal starting population can offer valuable insight into the genetic changes that are facilitating the observed thermal adaptation (Schaum *et al.* 2018), though this was not explored in this study. Therefore, in summary, our approach allowed us to take into account the fact that the extent of thermal adaptation and its mechanisms are both time and taxa dependent, thus offering a unique comparative study into thermal adaptation of a diverse selection of marine phytoplankton.

Time-series projections

It is clear from our time-series projections (Figure.4.3, Figure.4.4 and Appendix C Figure.2) that there were different extents of thermal adaptation observed across the three taxa over the experimental time frame. Firstly, for *Phaeodactylum tricornutum* we conclude that in response to the high temperature treatment, despite initially reflecting thermal acclimation with positive growth rates for the first couple of weeks, population size continued to decline beyond this point and did not recover throughout the duration of the experiment. This could be an outcome of starting with a clonal population, as growth rates of approximately 0.35 d^{-1} were observed at 27°C for the non-clonal stock prior to deriving clonal isolates (see Figure.4.2), and therefore the reduced genetic diversity perhaps limited the potential for adaptation. Furthermore, if our experimental time period had lasted longer it is possible that we may have witnessed evolutionary rescue, whereby evolution can counteract population decline to an environmental stressor and therefore prevent the possibility of extinction (Bell & Gonzalez 2009; Bell 2013). This was observed for the diatom *Thalassiosira pseudonana* in the recent study by Schaum et al (2018), whereby evolutionary rescue in their high temperature treatment did not happen for more than one year after the primary inoculation. Nonetheless, a key purpose of this study was to investigate the ability of clonal isolates of different taxa to adapt to similar stressful high temperature within a set time period, therefore in comparison to the other two taxa, *Phaeodactylum tricornutum* was unable to adapt over the 22 week duration of the experiment. We were able to infer thermal adaptation of *Ostreococcus tauri* in response to warming. The

time-series projection of growth rates indicates, that despite growth rates at the high temperature remaining lower than the control replicates, for over half of the experimental time period they continually increased in response to the warm treatment, reaching growth rates that were approximately double the starting magnitude by day 100. This clear improvement in fitness during the experimental time period can be associated with the passing of approximately 100 generations (see Appendix C Figure.3), thus we can infer thermal adaptation to the warmed environment for *Ostreococcus tauri* (Padfield *et al.* 2016). For *Synechococcus* sp. we observed a greater extent of thermal adaptation during the experimental time period. Whilst there was an initial period of approximately 25 days where there was negative population growth, this was followed by a rapid increase in growth rates. By day 50 they were performing just as well as the control, and by the end of the experimental period had reached specific growth rates that were greater than the control.

Effect of complexity?

These findings demonstrate an interesting trend. The largest and most complex organism, *Phaeodactylum tricornutum* (Bowler *et al.* 2008) failed to adapt. The second largest of the taxa, *Ostreococcus tauri* (albeit the smallest known eukaryote (Courties *et al.* 1994; Derelle *et al.* 2006; Palenik *et al.* 2007)), did adapt but failed to attain growth rates that were comparable to those observed at its ancestral temperature. Finally, the smallest, and arguably most simplistic of the taxa, *Synechococcus* sp. (Palenik *et al.* 2003), showed the strongest thermal adaptation in the set time period, reaching growth rates that were higher than at its ancestral temperature. Arguably these findings support theory that more complex organisms, with a larger genome size (Lynch *et al.* 2003), are likely to reflect slower rates of adaptation (Orr 2000). As we started from clonal isolates, the probability that beneficial mutations would arise in the smaller taxa was likely to be higher given the greater population sizes of both *Synechococcus* sp. and *Ostreococcus tauri* (Hao *et al.* 2015; Ashander *et al.* 2016; Schaum *et al.* 2018). Furthermore, it is also considered that picophytoplankton (which in definition encompasses both *Ostreococcus tauri* and *Synechococcus* sp., as phytoplankton with an average diameter of less than 2µm) have greater nutrient affinity relative to larger taxa (Chisholm 1992; Raven 1998; Finkel *et al.* 2010). In addition to this, it is also hypothesised that

smaller taxa demonstrate more effective light utilisation, whereby larger taxa experience more self-shading by pigment molecules and more complex cell structures, known as the “package-effect” (Raven 1998; Finkel 2001; Malerba *et al.* 2018). Whilst we conducted this experiment under nutrient replete conditions, and at constant light levels across all treatments for all taxa, we might conclude that these factor contribute to faster growth rates of the smaller taxa (Raven 1998), and thus aid the rate in which mutations associated with improved fitness spreads through the population. Nonetheless, though this observation of different levels of thermal adaptation across the taxa is novel and provides a unique comparison of the pace and magnitude of thermal adaptation, it is limited to just three taxa that were grown in monoculture and therefore more studies on a wider range of taxa would be highly valuable to further scrutinise these findings.

Evolution of thermal tolerance

Of greater relevance to understanding the direction of thermal adaptation in comparison to previous thermal adaptation studies of phytoplankton it is necessary to discuss the thermal tolerance curves and the underlying metabolic mechanisms associated. Though it is predicted that warming could drive poleward range shifts (Follows *et al.* 2007; Barton *et al.* 2010; Poloczanska *et al.* 2013) and potential extinctions of phytoplankton, particularly in lower latitudes (Thomas *et al.* 2012), the findings presented here support a growing body of knowledge that illustrates potential for rapid thermal adaptation of phytoplankton in response to warming. Overall, in agreement with previous work (Listmann *et al.* 2016; Schaum *et al.* 2017, 2018; Baker *et al.* 2018; O’Donnell *et al.* 2018), we observe a shift in thermal optima, $T_{opt}{}^{\mu}$, to higher temperatures for both *Ostreococcus tauri* and *Synechococcus* sp. (see Figure.4.5). The tolerance curves reflect the observations made from the growth rate projections throughout the course of the experiment, that *Synechococcus* sp. was able to show a greater increase in fitness relative to *Ostreococcus tauri*; for *Synechococcus* sp. this is illustrated by the fact we observed an expansion of the thermal niche to a higher maximal temperature, $T_{max}{}^{\mu}$, relative to the control temperature, as well as maximal growth rates, $bT_{opt}{}^{\mu}$, that were indistinguishable from the control performance; whereas for *Ostreococcus tauri*,

$bT_{opt}{}^{\mu}$ was lower for the warm adapted replicates but the thermal limits of tolerance were the same as the control. Therefore, despite this data strongly supporting the notion that phytoplankton are capable of rapid thermal adaptation, we also provide evidence to suggest that some taxa will demonstrate greater expansion of their limits of acclimation, at a faster pace, and with overall greater magnitudes of maximal growth rate relative to other taxa. Though our tolerance curve data is confined to the assay temperatures where growth rates were observed, the clear difference in shape of the curves between the control and warmed treatment of *Synechococcus* sp*.* is far more reflective of a "specialist-generalist" evolution signature, when compared alongside the tolerance curves of *Ostreococcus tauri*. This is primarily driven by the observed shift in thermal tolerance to the right (higher temperatures), but we also see an overall flattening of the response, signified by the lower activation energy of growth rates, $E_a{}^{\mu}$, of the warm adapted replicates, indicating that the control replicates show greater thermal sensitivity and also, over a portion of the sub-optimal temperature range, a greater performance than the warm adapted replicates. For *Ostreococcus tauri* we can be far less conclusive given the fact that acclimated growth rates were observed across all temperatures for both the control and warm adapted replicates, thus without additional data we could not identify whether there was a difference in the thermal limits of tolerance between the treatments. Nonetheless, in a similar way to *Synechococcus* sp*.* but far less pronounced, along with a shift to a higher $T_{opt}{}^{\mu}$ there was also a shift to a lower $E_a{}^{\mu}$ for the warmed replicates and subsequently there is a large portion of the sub-optimal temperature range where the control replicates displayed greater performance. In addition to this, in the case of *Ostreococcus tauri* the shift to higher $T_{opt}{}^{\mu}$ has come at a trade-off for lower maximal growth rates, $bT_{opt}{}^{\mu}$; whereas this is not the case for *Synechococcus* sp*.*.

These different trade-offs in the tolerance curves were also illustrated by the reciprocal transplant assays for growth rate (see Figure.4.8). This approach is often used to infer intra-specific adaptive change of a particular physiological trait by investigating differences in performance across "home" and "away" environments (Kawecki & Ebert 2004; Blanquart *et al.* 2013; O'Donnell *et al.* 2018). For *Synechococcus* sp*.* thermal adaptation is inferred here, not only by a

better performance of the warmed replicates versus the control replicates in the warmed environment, but a worse performance of the warmed replicates versus the control replicates in the control environment. This provides further support of the "specialist-generalist" evolution signature shown by *Synechococcus* sp. Contrary to this, the warmed replicates of *Ostreococcus tauri* do perform better than the control replicates in the warmed environment, but not significantly different to the control in the control environment. This signifies that there has been an increase in thermal tolerance of the warm adapted replicates, but this has not come at a cost to performance at lower temperatures.

Adaptive and plastic changes in cell size

In addition to the changes in thermal tolerance we also observed that the warmed *Synechococcus* sp*.* replicates adapted to have an overall larger cell volume, but this was not as clear for the warm adapted *Ostreococcus tauri*. The cell volume projections throughout the duration of the experiment illustrate initial increases in cell size in response to the warmed environment for both *Synechococcus* sp*.* and *Ostreococcus tauri*. Throughout the majority of the experimental time period *Synechococcus* sp*.* maintained a larger volume relative to the control, whereas the warmed replicates of *Ostreococcus tauri* gradually decreased in size to a magnitude that was a lot closer to, but still larger than, the control (see Figure.4.4). As differences in body size are known to directly influence metabolic rate, whereby larger individuals often show lower mass-specific metabolism (Gillooly 2001; Brown *et al.* 2004; Savage *et al.* 2004a), it was necessary to take the evolutionary changes in body size into account when considering the potential metabolic mechanisms associated with the thermal adaptation. Indeed, this was corrected for by making our metabolism measurements mass-specific.

In relation to the thermal plasticity of cell size we also observed some interesting trends across the two taxa (see Figure.4.6). For the *Ostreococcus tauri* replicates taken from the control temperature, cell size decreased with warming between 15°C and 27°C and this is in agreement with the temperature size rule, whereby size of an individual of the same species is expected to decrease with increasing environmental temperature (Atkinson & Sibly 1997). However, between 27°C and 35°C the control replicates of *Ostreococcus tauri*

increased in cell volume, to a magnitude that was comparable to the warm adapted replicates. Overall this response of the control replicates across the full temperature is the inverse of what we see for the thermal tolerance curve of growth rates (see Figure.4.5), and thus the larger cell sizes are associated with acclimation to the more stressful cold and warm temperatures. This would suggest that larger cell sizes are observed when growth rates are therefore lower, and when conditions are more stressful. Contrary to the control replicates however, the warm adapted replicates of *Ostreococcus tauri* have a very different plasticity profile, whereby cell volume appears to decrease with cooling between 33°C and 15°C. The temperature size rule would predict the opposite. Overall, the difference in the shape of the profile suggests that thermal adaptation has affected the thermal plasticity of cell size for *Ostreococcus tauri*, but without more detailed data collection, for example microscopy, it is hard to determine exactly what was driving these unexpected trends. For *Synechococcus* sp*.* we also found that thermal adaptation of the warmed strain had affected the plasticity of cell size (see Figure.4.6b). Whilst the control replicates, in agreement with the temperature size rule, showed the expected decrease in cell size between 18°C and 28°C, the warmed replicates also showed a decrease in cell size between 31°C and 18°C. Similarly to the warm adapted replicates of *Ostreococcus tauri*, this is counter-intuitive to the temperature size rule. However, unlike *Ostreococcus tauri*, the warm adapted *Synechococcu*s sp*.* replicates always acclimated with a larger cell size than the control replicates in response to all assay temperatures. This suggests that despite the differences in thermal plasticity between the treatments, *Synechococcus* sp*.* appears to have adapted to a larger cell size in response to the warmed treatment. This finding is in agreement with the work by Schaum et al (2018) where they found that adaptation to high temperature by the marine diatom *Thalassiosira pseudonana* resulted in larger cell size.

The temperature size rule is typically applied to ectothermic metazoans (Atkinson & Sibly 1997), and it is also predicted to be the prevalent trend in unicellular organisms (Forster *et al.* 2013) and for aquatic ectotherms in general (Forster *et al.* 2012); therefore, we have observed something unexpected here. Whilst our data does show partial agreement with the temperature size rule, especially for the control replicates and their responses to intermediate warming,

we find evidence that questions this assumption for both taxa over the full temperature and following warm adaptation. It could be related to the temperature range over which measurements were made in this study, and thus previous studies with smaller temperature ranges of assay temperature may not have observed the acclimated shifts to greater size in response to higher levels of sub-optimal, and supra-optimal, thermal stress (see Figure.4.6). Nonetheless, recent work on phytoplankton that has observed plasticity of cell size on warm and cold adapted strains, over similar temperature ranges to this study, have found evidence to support the temperature size rule following measurements of cell size in response to acute temperature change (Montagnes & Franklin 2001; Schaum *et al.* 2017, 2018). However, much of the experimental work that has studied the acute effect of temperature on cell size in response to temperature has been focussed on different taxa to this study, particularly diatoms (Olson *et al.* 1986; Montagnes & Franklin 2001; Schaum *et al.* 2018), green algae (Schaum *et al.* 2017) and coccolithophores (Olson *et al.* 1986). Only one study reports the short term effect of temperature on the cell size of *Ostreococcus tauri*, but this covers a much smaller range of temperatures (Kulk *et al.* 2012). Therefore, despite our findings showing some strong disagreement with the temperature size rule, there is no previous work on either *Synechococcus* sp. or *Ostreococcus tauri* over a similar range of temperatures that we can use to directly compare these findings at the species level. Furthermore, the evidence presented here, and by previous work (Schaum *et al.* 2018), suggests that over evolutionary timescales, at an intra-specific level, the temperature size rule is not always observed.

Metabolic mechanisms of adaptation

Only a few studies have also attempted to understand the metabolic mechanisms behind observed thermal adaptation in marine phytoplankton (Padfield *et al.* 2016; Schaum *et al.* 2017, 2018). Previous findings suggest that thermal adaptation is characterised by down-regulated mass-specific metabolism, whereby greater down regulation of respiration relative to photosynthesis results in higher CUE and thus greater carbon availability for allocation to growth (Padfield *et al.* 2016; Schaum *et al.* 2018). The need to down-regulate respiration by a greater amount than photosynthesis (or down-regulate photosynthesis less than respiration) in order to acclimate, and

ultimately adapt, in response to stressful high temperatures is primary driven by the differences in the temperature dependence (or activation energy) of photosynthesis and respiration. A growing number of studies have illustrated this phenomenon both at the individual level (Padfield *et al.* 2016; Schaum *et al.* 2017; Barton *et al.* 2018) and at the community and ecosystem level (Lopez-Urrutia *et al.* 2006; Yvon-Durocher *et al.* 2010, 2012; Regaudie-De-Gioux & Duarte 2012). Indeed, the recent work by Barton et al (2018) illustrates this trend for the three taxa in this study, whereby the temperature dependence of respiration for the same culture collection strains of *Ostreococcus tauri, Synechococcus* sp. and *Phaeodactylum tricornutum* was found to be greater than that of photosynthesis. Furthermore, the same study also found that the optimal temperature of respiration is greater than that of photosynthesis for all three of these species. Due to this, at temperatures beyond the optimal temperature of photosynthesis there is likely to be a rapid decrease in CUE. Barton et al (2018) qualitatively suggests that the optimal temperature and upper limits of thermal tolerance are restricted to temperatures below the inflection point in CUE. Therefore, in order to adapt and increase thermal tolerance the organism must need to overcome this metabolic constraint.

In this dataset, similarly to our thermal tolerance curves, our metabolism data also suggests a clearer metabolic mechanism of adaptation for *Synechococcus* sp. relative to *Ostreococcus tauri* (see Figure.4.7) In agreement with previous work (Padfield *et al.* 2016; Schaum *et al.* 2018), for both of the taxa there was clearly a down-regulation of mass-specific rates for both photosynthesis and respiration. For *Synechococcus* sp., in response to the full reciprocal transplant assay, at both assay temperatures (the control and warmed), greater down-regulation of respiration relative to photosynthesis was observed. The fact that we see this in response to both assay temperatures suggests that the warmed replicates have down-regulated their entire thermal performance curve by a greater magnitude for respiration. Consequently, in response to both assay temperatures we observe increased CUE for the warm adapted replicates of *Synechococcus* sp. relative to the control. The story is slightly different for *Ostreococcus tauri*; the down-regulation of respiration is similar to the down-regulation of photosynthesis in response to both assay temperatures. Therefore, the difference in CUE across the replicates of both treatments in response to

each assay temperature was not significant for *Ostreococcus tauri*. We can infer from this that *Ostreococcus tauri* has been able to overcome the initial metabolic constraints at the high temperature by down-regulating the metabolic responses to a level where CUE was similar to that of the ambient environment. Perhaps this is why we do not see growth rates at the warmed temperature reaching the same magnitude, or higher, than the control. However, for *Synechococcus* sp., the increase in CUE relative to the control is perhaps the reason for the elevated growth rates observed in the projections (Figure.4.3a), but also the maximal performance that was indistinguishable from the maximal performance of the control (Figure.4.5f and 4.5h). Thus, in conclusion, *Synechococcus* sp. improved its tolerance and performance at higher temperatures and this can be associated with greater down-regulation of respiration relative to photosynthesis. Whereas *Ostreococcus tauri* improved its tolerance to higher temperatures but not its performance, and this was associated by down-regulation of both photosynthesis and respiration to a level that resembled the CUE of the control replicates.

Physiological trait trade-offs of intra-specific adaptation

Beyond the mass-specific metabolic rates, with this dataset it is not possible to probe the finer details of the genetic changes and the phenotypic expressions associated with the mechanisms of thermal adaptation. We can however make the assumption that one driving factor for the decreased mass-specific rates in response to the warmed temperature, for both taxa, was the increase in cell size (see Figure.4.4, 4.9 and 4.10). Another observation that may have been associated with the lower down-regulation of photosynthesis rates of *Synechococcus* sp., when compared to *Ostreococcus tauri*, was the greater chlorophyll *a* content per cell of the warm adapted replicates, which after taking into account the change in volume also indicated no significant difference in the chlorophyll *a* concentration relative to the control (Figure.4.9 and Appendix C Figure.4). However for *Ostreococcus tauri* we observed no significant difference in the per cell content of chlorophyll *a* between the warm adapted replicates and the control, but once made volume specific we see a shift to lower chlorophyll *a* concentration in the warm adapted strains. This finding is also in agreement with recent work that indicates warm adapted isolates of *Chlamydomonas reinhardtii* also had more chlorophyll *a* per cell, and like *Synechococcus* sp.

here, this is reflected by greater photosynthetic performance relative to ambient adapted isolates (Schaum *et al.* 2017). This difference in chlorophyll content perhaps manifests itself through the observed greater carbon to nitrogen ratio (C:N) in the warm adapted *Ostreococcus tauri* relative to the control, with lower chlorophyll content driving up the C:N (Evans 1989; Montagnes *et al.* 1994). Conversely, the lower C:N values for *Synechococcus* sp. could be because smaller taxa are also associated with reduced carbon storage as well as greater relative abundance of nitrogen containing molecules of non-scalable cellular components (Raven 1994; Marañón *et al.* 2013).

Whilst it is crucial to improve understanding of the pace, magnitude and underlying metabolic mechanisms of marine phytoplankton adaption to warming for better inclusion in ecological models (Thomas *et al.* 2012; Reusch & Boyd 2013), it is also important to understand the implications of thermal adaption on the functional performance of marine taxa and the subsequent implications for key bio-geochemical cycles. Physiological trade-offs associated with high temperature adaptation are likely to have implications for bio-geochemical cycles because functional traits, such as cell size and nutrient uptake, are known to change as a result of thermal adaptation (Falkowski *et al.* 1998; Litchman & Klausmeier 2008). From our data we have been able to show that in combination with the intrinsic interspecific differences between the two taxa, the effect of thermal adaptation has resulted in a clear change in the overall physiologically of the taxa, as shown by the clearly defined clustering from the PCA (see Figure.4.10 and Appendix C Figure.5). We find that warm adapted strains of both *Ostreococcus tauri* and *Synechococcus* sp. increase their volume, and with this they increase their per cell content of carbon and nitrogen. Thus, per capita it could be argued that there has been an overall increase in the nitrogen and carbon demand, which is somewhat in agreement with the findings of Baker et al (2018) where they found greater requirements for carbon, nitrogen and phosphorous in their warm adapted *Amphidinium massartii*. Implications of increasing cell size could be reduced efficiency of nutrient uptake, along with increased sinking velocity (Chisholm 1992; Raven 1998; Litchman & Klausmeier 2008) and weaker light utilisation (Raven 1998; Finkel 2001), but possible benefits of a larger cell size are improved grazer resistance and greater carbon storage capacity (Litchman & Klausmeier 2008). In relation

to bio-geochemical cycles, provided that population size is not reduced as a consequence of the increase in individual size (and here that doesn't seem to be the case for *Synechococcus* sp., but may be the case for *Ostreococcus tauri*, see size projections in Appendix C Figure.2), the increase in per capita carbon (which is not associated with a change in volume specific carbon concentration relative to the control for both taxa) could mean that as a result of warming the uptake of atmospheric carbon may well have been improved. Nonetheless, in terms of carbon that actually gets sequestered on the ocean floor, the role of picophytoplankton is thought to be much lower compared to larger taxa, such as diatoms and coccolithophores, as a consequence of slower sinking velocities (Falkowski *et al.* 1998; Litchman & Klausmeier 2008; Morán *et al.* 2010); however, there is some contrasting evidence that suggests the role of picophytoplankton in deep ocean burial of carbon could be greater than expected (Richardson & Jackson 2007). Overall, though this dataset is confined to just two picophytoplankton with relatively similar functioning, we see some clear intraspecific divergences in physiological traits which could have profound effects on ecosystem function. Thus, moving forward, it would be of great value to conduct similar experiments on a wider range of taxa to gain a handle on the intraspecific trade-offs associated with thermal adaptation of other key functional groups.

Conclusions

In light of previous work that demonstrates that phytoplankton is capable of rapid thermal adaptation, we were able to clearly illustrate that the pace, magnitude and mechanisms of thermal adaptation are highly taxa dependent. We found that the least complex organism, the cyanobacteria *Synechococcus* sp. showed the most rapid improvements in performance in response to the high temperature treatment. This was demonstrated by an overall shift in thermal tolerance characterised by a higher optimal growth temperature and maximal growth rates comparable to those observed under ambient conditions. Underlying these improvements in thermal tolerance was a clear metabolic mechanism that resulted in greater carbon-use efficiency. The slightly more complex eukaryotic chlorophyte, *Ostreococcus tauri* did adapt to the high

temperature treatment but was not able to increase growth rates to a magnitude that were comparable to those observed under ambient conditions. The improved performance at the higher temperature was characterised by an overall shift to a higher optimal temperature but not a shift in the limits of thermal tolerance. Underlying the thermal adaptation of *Ostreococcus tauri* were down-regulated respiration and photosynthesis rates that resulted in a carbon-use efficiency that was comparable to observations under ambient conditions. The most complex organism, the diatom *Phaeodactylum tricornutum* did show signs of acclimating to the high temperature treatment but this could not be sustained and populations crashed within a couple of weeks. As a result of thermal adaptation we were able to identify clear divergences in physiological traits of both *Ostreococcus tauri* and *Synechococcus* sp., mainly driven by changes in cell size. Such findings indicate the potential for evolution to higher temperatures to result in intra-specific trade-offs that could pose implications for ecosystem functioning. Therefore it would be of great value for future work to conduct similar experiments on a wider range of taxa, with high relevance for ecosystem functioning and biogeochemical cycling, to gain a handle on the trade-offs associated with thermal adaptation and the wider implications. Furthermore, the differing levels of thermal adaptation observed in this study were restricted to taxa grown in monoculture, therefore similar work could be conducted that looks at a greater range of taxa in community warming experiments, thereby making interactions possible and allowing for the competitive advantages of some taxa over others to be identified in a more informative manner.

Chapter 5: Discussion

In summary, this research attempted to tackle some of the major limitations to the current understanding of how marine phytoplankton respond to short and long-term warming. The nature of the research allowed for a narrative to emerge across the three complimentary data chapters. Whereby, in Chapter 2, we first investigated thermal tolerance of growth and thermal performance of both photosynthesis and respiration for a diverse range of ecologically relevant phytoplankton taxa. This was then directly useful for Chapter 3 where we attempted to estimate an across-species temperature dependence of maximal growth rates, allowing for a comparison with the Eppley coefficient, as well as inferring inter-specific mechanisms of thermal adaption and the likely physiological trait covariance associated with greater thermal tolerance. For chapter 4, we could then investigate this in further detail at the intra-specific level by taking a subset of the species used in the previous chapters and exploring how thermal tolerance changed as an adaptive response to warmer temperatures, along with the underlying metabolic mechanisms that may have facilitated improved thermal tolerance and the associated physiological trait trade-offs.

General findings

Following up on the initial aims of this research (see Chapter 1); here is a summary of the main research findings from each chapter:

Chapter 2

- Across all 18 species we found large variance in the parameters of thermal tolerance. Maximum temperature of growth, $T_{max}{}^{\mu}$, ranged from 27°C to 37°C. The optimal temperature of growth, $T_{opt}{}^{\mu}$, ranged from 23.8°C to 34.0°C and the activation energy, $E_a{}^{\mu}$, ranged from 0.40 eV to 1.46 eV, with an average $E_a{}^{\mu}$ of 0.77eV. This demonstrates clear inter-specific differences in thermal tolerance, but also it illustrates that the temperature dependence of growth varies substantially from the

canonical Eppley coefficient ($E_a{}^{\mu}$ ≈ 0.3 eV), which is commonly used to represent phytoplankton growth responses in models of ocean warming. This provided the premise for Chapter 3.

- Whilst we found deviance from previous estimates of activation energy for photosynthesis, $E_a{}^{P}$, and respiration, $E_a{}^{R}$, across all taxa spanning we found ubiquitous evidence that $E_a{}^{R}$ was always greater than $E_a{}^{P}$. Furthermore, we also found that the optimal temperature for respiration, $T_{opt}{}^{R}$, tended to be greater than that of photosynthesis, $T_{opt}{}^{P}$, with lower deactivation energy of rates past the optima for respiration relative to photosynthesis. Therefore there were similar patterns in the differences between thermal performance of respiration and photosynthesis. Consequently, across all taxa we found consistent trends in the reduction of carbon-use efficiency with temperature increase.

- We can infer from this that there appears to be universal metabolic constraints across all diverse marine phytoplankton that are likely to influence the limits of thermal tolerance. In agreement with previous work, we can therefore use this knowledge to help understand the metabolic mechanisms of thermal adaptation, and this was explored in further detail in Chapter 4.

Chapter 3

- Using the thermal tolerance curves derived from Chapter 2 we were able to estimate an across-species activation energy of maximal growth rates of ~0.50eV, which is greater than the Eppley coefficient (≈ 0.3 eV). However, the confidence intervals of this estimate ranged from 0.10 to 0.90eV, and furthermore the species level estimates of $E_a{}^{\mu}$ ranged from 0.40 to 1.46eV. Therefore, despite our across-species activation energy being greater than the Eppley coefficient, it was still within the confidence margins of our estimates. However, our average species level $E_a{}^{\mu}$ was ~ 0.77eV, which is greater than our across-species estimate of ~0.50eV,

implying from our dataset that an across-species temperature dependence may not be suitable for general application to global models that are trying to predict phytoplankton productivity responses to warming.

- As our across-species temperature dependence (0.50ev) was lower than our average within-species temperature dependence (0.77eV), we also conclude that the data presented here reflects a “partial compensation” mechanism of thermal adaptation This supports conclusions that adaptation has the capacity to partially offset the underlying effects of temperature on phytoplankton maximal growth rates at an inter-specific level.

- Finally, we also found that a number of key functional traits, most noticeably cell size, covary with traits of thermal tolerance, and from this we deduce possible implications for ecosystem function and biogeochemical cycles following the likely community restructuring in response to warming.

Chapter 4

- From our evolution experiments we were able to demonstrate that different species, representing different phylogenetic groups, showed clear variation in their pace, magnitude and mechanisms of thermal adaptation. Overall, we observed a trend whereby the most complex and largest species, the diatom – *Phaeodactylum tricornutum*, failed to adapt. The second most complex species, the green picophytoplankton - *Ostreococcus tauri,* did appear to adapt to the warmed environment but was unable to reach similar levels of fitness to that observed under ambient conditions. The smallest, and least complex species, the cyanobacteria – *Synechococcus* sp*.*, showed adaptation to the warm environment by reaching levels of fitness that were comparable, if not greater than, those observed under ambient conditions. Critically, this finding can inform about the potential for adaptation intra-specifically, but also inter-specifically as the same experimental techniques were employed for all three species.

- In terms of thermal tolerance, both warm adapted *Ostreococcus tauri and Synechococcus* sp*.* increased their thermal optima. However, *Synechococcus* sp*.* was also able to increase its upper limits of thermal tolerance to temperatures beyond the thermal tolerance of the ambient replicates. Furthermore, warm adapted *Synechococcus* sp*.* also exhibited maximal growth rates that were of the same magnitude as the ambient replicates, whereas for *Ostreococcus tauri* the maximal growth rates were lower for the warm adapted replicates than the ambient replicates.

- We were also able to show that in-light of the findings from Chapter 2, both *Ostreococcus tauri and Synechococcus* sp*.* were able to overcome the underlying metabolic constraints in response to higher temperatures. Both species were able to down-regulate their metabolism. For *Ostreococcus tauri* respiration rates and photosynthesis rates were down-regulated, returning a carbon-use efficiency for the warm adapted replicates that was indistinguishable from the ambient replicates. However, warm adapted *Synechococcus* sp*.* replicates down-regulated respiration rates by a greater proportion than photosynthesis rates, and subsequently this resulted in a greater carbon-use efficiency of the warm adapted replicates relative to those grown under ambient conditions.

- Finally we also observed that both *Ostreococcus tauri and Synechococcus* sp*.* increased their mean cell volume in response to the warmed environment, and this persisted throughout the course of the experiment. We deduce that a change to large cell size positively correlated with an increase in optimal temperature; with this we were able to infer a number of other intra-specific trait trade-offs in response to warm adaptation, highlighting the possible implications for biogeochemical cycles and ecosystem function.

Metabolic performance and the limits of thermal tolerance

Whilst it has previously been demonstrated for aquatic ecosystems (Lopez-Urrutia *et al.* 2006; Yvon-Durocher *et al.* 2010; Regaudie-De-Gioux & Duarte 2012) and specific phytoplankton species (Padfield *et al.* 2016; Schaum *et al.* 2017) that respiration is more temperature dependent than photosynthesis i.e. $E_a^R > E_a^P$, this study provides the most detailed and wide ranging evidence at the species level, spanning cyanobacteria and phytoplankton of both the red and green super-families, that suggests that this metabolic phenomenon is likely to be ubiquitous across all marine phytoplankton. Furthermore, we also show that respiration performs better at high temperatures than photosynthesis, and this is characterised by optimal respiration temperatures that tended to be higher than those measured for photosynthesis, in combination with lower deactivation energy of respiration rates at supra-optimal temperatures. These findings suggest that the process of photosynthesis in phytoplankton is more susceptible to decline under high temperature than respiration. This is in agreement with the functioning of photosynthesis in terrestrial plants, which is considered to be more susceptible to thermal stress than dark respiration (Berry & Bjorkman 1980; Mathur *et al.* 2014).

Due to this universal trend, across all taxa we see a decrease in carbon-use efficiency as temperature rises, with accelerated declines when temperatures exceed the optimal temperature of photosynthesis. Therefore, given that carbon-use efficiency is an indicator of carbon available for allocation to growth following respiratory costs, which include maintenance and repair as well as biosynthesis (Raven 1976; Shuter 1979; Geider & Osborne 1989), then in order to adapt to higher temperatures it is highly likely that phytoplankton will need to overcome this metabolic constraint. Previous studies have shown that the freshwater green alga *Chlorella vulgaris* (Padfield *et al.* 2016) and the marine diatom *Thalassiosira pseudonana* (Schaum *et al.* 2018) both adapted to high temperatures by down regulating respiration by a greater relative proportion than photosynthesis. Here we show agreement with these previous findings, not only by demonstrating a similar underlying metabolic constraint across all species (Chapter 2), but also by showing that at the intra-specific level thermal adaptation is facilitated by down-regulation of metabolic rates (Chapter 4).

Unlike most previous work, for each of our 18 species we also measured thermal tolerance curves. This allowed us to qualitatively demonstrate how metabolism may set the limits of thermal tolerance, as illustrated by our carbon-use efficiency breakpoint analysis (see Chapter 2, Figure.2.3). However, we cannot demonstrate any coupling between the metabolic responses and the thermal tolerance responses with any certainty. The biggest limitation with deducing such conclusions from this dataset is that our metabolism measurements were of acute responses of photosynthesis and dark respiration to temperature change made over time-frames of less than one hour, whereas our growth rate measurements were reflective of 'acclimated' responses where phenotypic adjustments would have taken place over days. Subsequently, it is not possible for us to directly associate our acute thermal performance of metabolism with our acclimated thermal tolerance without making assumptions about the changes in phenotype that may have taken place over such time scales. We could have scaled up our metabolism measurements to diurnal rates, and this would have allowed us to directly couple our estimated metabolism rates with growth rates (Geider & Osborne 1989), however this would also require making assumptions about the data. For example, we measured dark respiration immediately following our photosynthesis-irradiance curves and therefore the respiration rates measured were unlikely to be substrate limited; however, over much longer periods in the dark the rate of respiration is known to decrease due to eventual substrate limitation (Azcón-Bieto & Osmond 1983). Therefore scaling our acute dark respiration measurements over a 12 hour dark period would overlook the effect of substrate limitation that is likely to play out during longer time periods in the dark, and therefore exaggerate the diurnal dark respiration rates.

Arguably, the acute metabolic responses measured in Chapter 2 are more reflective of how metabolism sets the limits of thermal acclimation (or tolerance), and are therefore not reflective of acclimated metabolism that is directly associated with the observed thermal tolerance. An area for further work would be to obtain metabolism measurements after acclimation to each assay temperature, enabling metabolic thermal performance of acclimated cultures to be modelled. This could offer less assumptive direct coupling between the metabolism responses and the measurements of growth from the thermal

tolerance curves, providing an improved understanding of how acclimated metabolism sets the limits of observed thermal tolerance.

Across- versus within- species temperature dependence: Is hotter better?

Our dataset allowed us to directly question the validity of using an across-species temperature dependence to account for phytoplankton responses to warming in ecosystem and ocean biogeochemistry models (Thomas *et al.* 2012; Stock *et al.* 2014; Laufkotter *et al.* 2015). In summary, we were able to demonstrate that our data provided an estimate of across-species temperature dependence that was slightly larger than previous estimates (~0.50eV), but after taking into account the confidence intervals it was statistically indistinguishable from the canonical Eppley coefficient (≈ 0.3 eV) (Eppley 1972; Bissinger *et al.* 2008). However, the across-species activation energy was lower than the average within species activation energy (~ 0.77eV). As well as limitations of its application at local scales, where particular phytoplankton with higher or lower temperature dependence may dominate, these findings also question the application of an across-species temperature dependence when applied to determine phytoplankton responses at a global scale. It is worth noting however that, unlike previous estimates, our across-species temperature dependence was derived from maximal growth rate data where the same experimental techniques were applied across all species, whereas the Eppley curve is a meta-analysis of both freshwater and marine phytoplankton which has intrinsic limitations due to the difference culturing and experimental techniques applied by different laboratories.

These findings support the “partial compensation” hypothesis for thermal adaptation, suggesting that biochemical adaptation at the inter-specific level has acted to partially offset the underlying thermodynamic effect of temperature; which still results in higher maximal growth rates at higher optimal growth temperatures but with a temperature dependence that is weaker across-species than within-species. (Kingsolver 2009; Angilletta *et al.* 2010).. However, we did not see any evidence for either a “hotter is better” or “partial compensation” mechanism of thermal adaptation at an intra-specific level, as shown in Chapter 4. Our warm adapted *Ostreococcus tauri* expressed growth rates at its elevated

optimal temperature that were lower than the ambient strains. Whereas warm adapted *Synechococcus* sp. expressed maximal growth rates at its optimal temperature that were statistically indistinguishable from the ambient strains, reflective of the "complete compensation" or "biochemical adaptation" mechanisms of thermal adaptation, where the response to the high temperature was to down regulate metabolism, and thus maximal performance (Somero & Hochachka 1971; Clarke 2003). It is possible that the "hotter is better" or "partial compensation" mechanisms do not emerge unless evolution is given more time to act. As far as experimental evolution studies go this one was relatively short, < 1 year and approximately 100 generations for each warmed treatment. It could also be dependent on how stressful the warm environment is for each species, or strain. Indeed, it has been shown by Schaum et al (2018) in their recent study on the marine diatom *Thalassiosira pseudonana,* that with moderate warming, and after approximately 300 generations, adaptation resulted in increased optimal growth temperatures and increased maximal growth rates. However with extreme warming they saw an overall decline in maximal growth rates, despite an increase in the optimal growth temperature. There are only a few other studies where elevated growth rate at optimal temperatures has been observed for particular taxa following high temperature adaptation; in a separate lab study on *Thalassiosira pseudonana* (O'Donnell *et al.* 2018)*,* for the marine dinoflagellate *Amphidinium massartii* (Baker *et al.* 2018) and for isolates of *Chlamydomonas* taken from experimental mesocosms after 10 years of warming (Schaum *et al.* 2017).

Given the limited literature in this field it is hard to conclude anything meaningful at the intra-specific level about the evolution of maximal growth rates for different species of marine phytoplankton. This is an important area for further study as the current model inclusion of an across-species temperature dependence, the canonical Eppley coefficient, overlooks the intra-specific mechanisms of thermal adaptation. One suggestion for further work could be to investigate the changes in maximal growth rate for a particular phylogenetic group of phytoplankton, or more specifically a particular genus or species, isolated across a latitudinal transect where there is likely to be strong intra-specific adaptation to the natural thermal gradient (Thomas *et al.* 2012; Boyd *et al.* 2013). Similarly, rather than a 'natural' experiment, this could also be

explored by adapting a particular species to a wider range of temperatures through experimental evolution (thus far, most evolution studies, including the one in this research, have tended to focus one or two high temperature treatments), allowing for an intra-specific temperature dependence of maximal growth rates to be tested more accurately.

Does warming favour the small?

In conjunction with showing that taxa with higher thermal optima also demonstrate higher maximal growth rates, in Chapter 3 we also show that size negatively correlates with optimal growth temperature. Therefore, at an inter-specific level, this research suggests that smaller phytoplankton tend to have higher optimal growth temperatures and this could therefore be an indicator that smaller taxa may have greater tolerance, or ability to adapt, to high temperatures. If community restructuring under warming scenarios was to favour small phytoplankton taxa then this is likely to have strong influence on ecosystem function and biogeochemical cycles because reduction in phytoplankton size is known to be associated with trade-offs of a number of other physiological traits, for example; reduced resistance to grazing, reduced carbon storage, reduced sinking velocity and improved light utilisation (Raven 1998; Litchman *et al.* 2007; Litchman & Klausmeier 2008). In support of this finding, in Chapter 4 we also demonstrate that across our three species, in response to warmed treatments, the smallest and least complex organism, the cyanobacteria *Synechococcus* sp*.,* demonstrated the greatest improvement in fitness as well as the biggest shift in its thermal tolerance curve to higher temperatures when compared to the slightly larger eukaryote, *Ostreococcus tauri*, and the diatom, *Phaeodactylum tricornutum* (three orders of magnitude in cell volume greater).

Nonetheless, at an intra-specific level, in Chapter 4 we also show that a physiological change associated with warm adaptation for both *Synechococcus* sp*.* and *Ostreococcus tauri* was an increase in average body size. This was observed in the study by Schaum et al (2018), whereby over evolutionary timescales the diatom *Thalassiosira pseudonana* also increased its average cell size in response to warming treatments. These findings are somewhat counter-intuitive to the temperature-size rule, which suggests that body size of a species

is negatively correlated with the temperature of its environment (Atkinson & Sibly 1997; Forster *et al.* 2012). Whilst we observed that *Ostreococcus tauri* shifted its size to a greater volume in response to the warmed treatment, throughout the duration of the experiment its average volume gradually decreased, albeit not quite reaching the same size as the ambient strains (see Chapter 4, Figure.4.4b). This might suggest that the initial shift to a greater size could have been a shock response, and that over a longer timeframe cell size may have decreased to an expected smaller size; however without a longer experimental time frame there is no way of knowing. Moreover, this does not seem to have been the case for *Synechococcus* sp., where after approximately 50 days of the experiment cell size stabilised at a greater volume than the ambient strains (see Chapter 4, Figure.4.4a). Despite, the intra-specific observations of increased cell size presented here, this is not supported by previous evolution studies on freshwater green algae, where long-term warming has had a negligible effect on cell size (Padfield *et al.* 2016; Schaum *et al.* 2017).

Cell size can also fluctuate as an acclimation response to short term temperature change. We demonstrate that over shorter time scales, the temperature-size rule was evident as a plastic response for our ambient strains of both *Synechococcus* sp. and *Ostreococcus tauri* when exposed to moderate warming, but at extreme temperatures (i.e. supra-optimal) it appears that the temperatures size rule was reversed. This was especially apparent for *Ostreococcus tauri*. Furthermore, the warm adapted strains of both *Synechococcus* sp. and *Ostreococcus tauri*, when exposed to colder temperatures appeared to show a decrease in cell size; again, this is in contrast with the temperature size rule (see Chapter 4, Figure.4.6). These findings are also in disagreement with previous experimental evolution studies where, despite long-term warming, taxa still obeyed the temperature size-rule as a plastic response to acute temperate change (Schaum *et al.* 2017, 2018). It might be possible that as a response to high temperature stress, where we observe lower growth rates, that cells were aggregating or not dividing efficiently. Recent work with *Thalassiosira pseudonana* has shown that high temperature stress can encourage such aggregation and eventual bio-filming, and this is considered to aid adaptation in response to warming (Schaum 2018).

If this was the case for this study then it is likely to have influenced the measurements of population size determined from the flow cytometry. For *Synechococcus* sp. we observed comparable population sizes across the warm adapted strains and ambient strains, suggesting that aggregation of cells or inefficient cell divisions is unlikely. Whereas for *Ostreococcus tauri* we did observe lower overall population size for the warm adapted strains (see Appendix C Figure.2), but this could just be a taxon specific response of reduced fitness to high temperature (for example, higher per capita nutrient demand causing a reduced carrying capacity) and unrelated to aggregation of cells or poor cell division. Without further measurements however, e.g. microscopy data, it is hard to disentangle exactly what is going on in relation to these counter intuitive intra-specific increases in cell size to warming over both short and long term responses.

Though we present strong inter-specific evidence that warm adapted phytoplankton tend to be of a smaller size, the findings here suggest that it is important to gain a clearer understanding of how cell size changes intra-specifically as an adaptive response to warming. Similarly to understanding whether warm adaptation also results in greater maximal growth rates at the species level, understanding of intra-specific shifts in cell size could be vastly improved by further experimental evolution studies that cover a much wider range of treatment temperatures. This could also be investigated in the 'real world' where latitudinal ranges provide natural temperature gradients. Thus far, from observations of phytoplankton communities in 'natural' ecosystems (Winder *et al.* 2009; Yvon-Durocher *et al.* 2010), and over latitudinal gradients (Morán *et al.* 2010), warming has been shown to be correlated with smaller average phytoplankton size. However, to date, there has been no comprehensive study that investigates the intra-specific changes in cell size of particular species as a response to thermal adaptation over natural gradients. This would make for an insightful and extremely useful future study, which would enhance understanding as to whether the interspecific association of smaller cell size and higher optimal temperatures, as shown by this research, is also present at the species level for a variety of ecologically important phytoplankton. Gaining a handle on such knowledge is crucial for understanding the implications of warming for ecosystem function, as size is a 'master trait'

that implicates many other functional traits of ecological and biogeochemical relevance (Raven 1998; Litchman & Klausmeier 2008).

Universal metabolic mechanisms of thermal adaptation?

In order to better understand whether respiration being more temperature dependent than photosynthesis is the main driving factor that underpins mechanisms of adaptation to high temperatures, we studied the metabolic performance of warm adapted strains and ambient adapted strains to see how phytoplankton overcome this potentially ubiquitous metabolic constraint. Given that experimental evolution and adaptation of phytoplankton to warming is an emergent field, there are limited comparable studies at the species level. Of the available research in the literature, it has been shown that the freshwater green alga, *Chlorella vulgaris* (Padfield *et al.* 2016) and the marine diatom *Thalassiosira pseudonana* (Schaum *et al.* 2018) are able to increase growth rate and thermal tolerance as an adaptive response to high temperature with down regulated mass-specific metabolic rates; whereby respiration is down-regulated by a greater proportion than photosynthesis. Subsequently, this increases the availability of photosynthetically fixed carbon for allocation to growth following respiratory costs. This mechanism directly works to counter-act the fact that respiration is more temperature dependent than photosynthesis (see Figure.1.3, Chapter 1). In our experimental evolution study we show partial support of these previous findings. Similarly, we find that *Synechococcus* sp. increased its growth rates in response to the high temperature treatment, as well as increasing its upper limits of thermal tolerance. We can associate this improvement in fitness at higher temperatures with greater down regulation of mass-specific respiration rates relative to photosynthesis rates, resulting in an improved carbon-use efficiency. Nonetheless, for *Ostreococcus tauri*, whilst we observed down regulation of mass-specific metabolism, this was by the same proportion for both photosynthesis and respiration, and subsequently there was no significant improvement in carbon-use efficiency relative to the ambient strains.

It is possible that the differences observed could simply be relatable to the magnitude of adaptation shown by the thermal tolerance curve. For example, warm adapted *Synechococcus* sp. shifted to a higher tolerance range with a

greater optimal temperature and expressed similar maximal growth rates to the ambient treatment; this can be associated with an improvement in carbon-use efficiency at the warmed assay temperature relative to the control. Whereas for the warm adapted *Ostreococcus tauri*, despite the increase in the thermal optimum, the maximal growth rates remained lower than the control treatment and there was no indication of an increase in the upper limits of thermal tolerance; this we associate with carbon-use efficiency that was indistinguishable from the control treatment in response to the warmed assay temperature.

Although our experimental design allowed for us to compare the magnitude of adaptation across the three different species over a set experimental time period, which is useful for understanding the inter-specific differences in rate of evolution, this approach meant that we didn't observe any further changes that are likely to have taken place beyond this time frame. Given that most evolution studies track more than 100 generations of growth before interpreting physiological traits of thermal adaptation (Listmann *et al.* 2016; Baker *et al.* 2018; O'Donnell *et al.* 2018; Schaum *et al.* 2018), this study was relatively short and similarly to Padfield et al (2016) only lasted for approximately 100 generations for each of our warmed treatments. Therefore it is possible that with more time we may have observed a greater increase in the growth rates of *Ostreococcus tauri,* and with this we may have also observed a comparable metabolic adjustment to previous findings. However, whilst we tried to follow an experimental approach where the magnitude of the stressful environment was comparable across the taxa, achieved by determining a supra-optimal temperature where growth rates for non-clonal populations were approximately 50% of their rate at the optimum temperature, it is possible once the populations were made clonal and the standing genetic variance had been reduced that the warmed treatment was subsequently more 'stressful' than it would have been for the non-clonal populations. This may also explain why we did not observe an adaptive response at all for the *Phaeodactylum tricornutum,* despite observing positive growth rates of the non-clonal population at this temperature. Furthermore, with a longer experimental time frame it may have been possible to observe evolutionary rescue of this species in the warmed environment, as

has been observed in the recent study on *Thalassiosira pseudonana* (Schaum *et al.* 2018).

In summary, the differences in metabolic mechanism of thermal adaptation observed across the taxa in this study both agree and disagree with previous findings. Whilst we could argue that this evidence suggests that the metabolic mechanisms of thermal adaptation are taxa specific, it is also highly likely to be dependent on how stressful the experimental treatment was, the duration of the experiment and whether starting populations were made clonal. We can conclude with some certainty, however, that it was the least complex and smallest of the taxa, *Synechococcus* sp., that demonstrated the largest improvement in fitness and thermal tolerance over the experiment, and therefore it is perhaps of no surprise that this species also demonstrated a metabolic mechanism of adaptation that increased carbon availability to growth in response to warming.

Areas for further research

Whilst this research has contributed to our understanding of how phytoplankton responds to warming, it has not been without limitations and furthermore it has raised some ideas on how the findings here can be enhanced by future research:

- Following on from Chapter 2, it would be incredibly useful to obtain an additional dataset of 'acclimated' metabolic rate measurements that would provide a firmer understanding of the metabolic performance that directly underpins the thermal tolerance curve.

- To advance on the findings from Chapter 3, it is important to gain a handle on the intra-specific adaptation of thermal tolerance curves, and therefore future work could focus on obtaining species specific or phyla specific estimates of maximal growth rates from isolates adapted to a natural temperature gradient or phytoplankton strains adapted to a much wider range of temperatures than previous experimental evolution studies.

- In a similar vein to the previous point, this could also offer insight into the intra-specific changes in cell size that are associated with thermal adaptation over a greater range of temperatures. This would be of great relevance for understanding whether the across-species observation of higher optimal temperatures showing negative correlation with cell size also holds true at the species level. As phytoplankton size is a physiological trait with great relevance to wider ecosystem function and biogeochemical cycles then understanding how cell size changes as an adaptive response is critical for predicting the implications of warming on the ecological role played by specific functional groups.

- Though in chapter 4 we present novel findings of how thermal adaptation compares across three very different phytoplankton species, under the same experimental protocol, this was not without limitations. For future evolution experiments to be more reflective of 'real world' scenarios there are also many other abiotic factors to take into account. The biggest limitation for this study was time, ideally we would have conducted the experiment over a much longer time period, making it more comparable with most previous experimental evolution studies (>1 year and >100 generations) and allowing for further evolutionary changes to take place (please note: the experiment is still being maintained in the Yvon-Durocher laboratory; it was time that demanded that I cease experimenting, the phytoplankton seem happy enough to keep going). Though warming treatments are useful for understanding evolutionary responses to the likely increases in average ocean temperatures, it is also important for future work to consider temperature fluctuations, similar to the work by Schaum et al (2018), as this is more reflective of 'natural' temperature regimes. Furthermore, as ocean warming is indirectly driven by atmospheric increase in carbon dioxide concentration, it is also important to consider the direct effect of carbon dioxide and increased ocean acidity on phytoplankton adaptation. Therefore, a further experimental treatment to be considered, in combination with warming, is increased atmospheric carbon dioxide concentration. Many experimental evolution studies on phytoplankton have looked at adaptation to elevated carbon dioxide concentration (Collins & Bell 2004;

Lohbeck *et al.* 2012; Schaum *et al.* 2012), but only one study has investigated evolution in response to increased warming in combination with elevated carbon dioxide concentrations (Schlüter *et al.* 2014; Listmann *et al.* 2016). Finally, as warming is predicted to create more stratified oceans and consequently greater nutrient limitations for the photic zone (Behrenfeld *et al.* 2006; Irwin & Oliver 2009), it would pertinent for future studies to also investigate the effects of warming in combination with nutrient limitation.

Concluding remarks

This research contributes novel insights into the responses of marine phytoplankton to experimental warming. It has improved our understanding of the metabolic responses of phytoplankton to temperature change by demonstrating, that across the great diversity of marine phytoplankton taxa, there are remarkable consistencies in the acute thermal performance of respiration and photosynthesis; such understanding is incredibly useful for understanding the potential metabolic constraints on thermal tolerance and mechanisms of thermal adaptation.

This work has also provided an estimate for an across-species temperature dependence of maximal growth rates that is weaker than the average species level temperature dependence of growth rates; raising questions about the application of a generalised across-species temperature dependence in global scale models. Despite being greater than previous across-species estimates, this finding can be used to encourage important discussions about the use of the Eppley coefficient in models of ocean biogeochemistry – which at the moment is likely to be misinterpreting phytoplankton responses, especially at more local scales. Furthermore, at an across-species level, our findings suggest that smaller phytoplankton taxa tend to have greater thermal optima, and with this we can infer the likely trait trade-offs associated with community restructuring in response to warming and the associated implications for ecosystem functioning and biogeochemical cycles.

Finally, at the species level we have been able to demonstrate that different taxa will vary in their evolutionary responses to a similar magnitude of warming and over similar timeframes. From this study it seems that the smaller and least complex phytoplankton will show faster rates of evolutionary change, and with greater increases in thermal tolerance relative to larger and more complex phytoplankton. This supports the suggestion that ocean warming may favour the small.

Personal standpoint

As a species we face an uncertain future due to anthropogenically induced climate change. If there is one thing that is for certain however, it's that whatever the climate does, phytoplankton will adjust with it; just as they have done for millions of years. Thus, the big question here, and of more concern for our species and other complex life, is how will they adjust? I hope the knowledge acquired from these experiments can, in some small way, help to answer this question.

Conducting this research, at times, has been an incredibly humbling and rewarding process. Nonetheless, one of the motivations for pursuing with this subject area is because I believe it to be of critical importance for understanding the implications of anthropogenically induced climate change on the wider functioning of the seemingly self-regulating Earth systems that we are very much a part of. Billions of years of evolution have diversified the first oxygenic oxygenic – photosynthesisers into today's phytoplankton assemblages and terrestrial plants. We have them to thank for providing the atmospheric composition that has enabled complex life to succeed on Earth. Whilst research like this can help us understand how phytoplankton may function in response to unprecedented rates of warming, it is also crucial for our species to act in a manner that allows phytoplankton to serve the Earth systems in a way that has permitted the great diversity of complex life to flourish. It could therefore be said that it is we who are accountable for the greater uncertainty when trying to understand how the climate, and subsequently phytoplankton, will respond to warming. Indeed, we have complex choices to make, but phytoplankton will remain, as ever, transient drifters.

Appendix A (for Chapter 2)

Appendix A: Tables

	Phyla	Species (strain identification synonyms)	Location/Year of isolation		Growth medium
	Cyanophyceae	*Synechococcus* sp. (CCMP 2370 , WH8102)	North Atlantic - Sargasso Sea	1981	PCR-S11 Red Sea Salt
		Synechocystis sp. (RCC 1773, R56)	North Atlantic - English Channel	1975	PCR-S11 Red Sea Salt
Green	Chlorophyceae/ Prasinophyceae	*Dunaliella tertiolecta* (CCAP 19/5)	North Atlantic - English Channel	1967	F/2
		Micromonas pusilla (CCMP1545, RCC 834)	North Atlantic - English Channel	1950	K
		Ostreococcus tauri (OTH95, RCC 4221)	Mediterranean - Gulf of Lion	1995	K
	Chlorarachniophyceae	*Gymnochlora stellata* (CCMP2057, RCC 626)	West Pacific Ocean	N/A	F/2
		Bigelowiella natans (CCMP621, RCC 623)	North Atlantic - Sargasso Sea	1981	F/2
		Chlorarachnion reptans (CCAP 815/1 , CCMP239)	North Pacific - Gulf of California	1966	F/2
Red	Rhodophyceae	*Rhodella maculata* (CCAP 1388/2, SAG 45.85)	North Atlantic - English Channel	1965	F/2
		Porphyridium purpureum (CCAP 1380/11)	Japan	1987	F/2
		Porphyridium aerugineum (RCC 652, SAG 110.79)	North Atlantic - North Sea	1980	K
	Bacillariophyceae	*Thalassiosira pseudonana* (CCMP 1335)	North Atlantic - Moriches Bay	1958	F/2 + Si
		Nitzschia sp (RCC 80, ROS97004)	North Atlantic - English Channel	1997	K + Si
		Phaeodactylum tricornutum (CCAP 1052/1B, CCMP 2558)	North Atlantic	N/A	F/2 + Si
	Prymnesiophyceae	*Gephyrocapsa oceanica* (RCC 1303, AC300, LK7)	North Atlantic - Arcachon Bay	1999	K/2
		Emiliania huxleyi (CCMP 1516, CCMP 2090)	South Pacific Ocean	1991	K/2
	Dinophyceae	*Amphidinium carterae* (CCMP 1314)	North Atlantic - Nantucket Sound	1954	F/2
		Thoracosphaera heimii (AC214, Nap17 , RCC 1512)	Mediterranean - Tyrrhenian Sea	2000	K/2

Appendix A:Table.1 Phytoplankton strains. All strains were obtained from CCAP (The Culture Collection of Algae and Protozoa) and RCC (Roscoff Culture Collection). The above table divides strains into phylogenetic groups as well as showing which of the red or green super-families they belong to, with the exception of Cyanophyceae. Growth mediums were prepared according to the medium recipes referred to in the methods section.

	$ln.c^{\mu}$			E_a^{μ}			E_h^{μ}			T_h^{μ}			T_{opt}^{μ}	T_{max}^{μ}
Amphidinium carterae	**-0.80**			**0.56**			**8.84**			**303.85**			**28.29**	**30.00**
Bigelowiella natans	**-1.32**			**0.99**			**4.59**			**302.01**			**26.68**	**30.00**
Chlorarachnion reptans	**-1.95**			**1.44**			**6.00**			**301.84**			**27.18**	**30.00**
Dunaliella tertiolecta	**-0.14**			**0.41**			**1.96**			**307.31**			**28.76**	**37.00**
Emiliania huxleyi	**-0.50**			**1.41**			**7.59**			**301.48**			**26.81**	**30.00**
Gephyrocapsa oceanica	**-0.77**			**1.27**			**9.71**			**303.13**			**28.44**	**30.00**
Gymnochlora stellata	**-0.69**			**0.48**			**7.96**			**309.20**			**33.23**	**35.00**
Micromonas pusilla	**-0.54**			**0.67**			**9.53**			**304.00**			**28.71**	**30.00**
Nitzschia sp	**0.02**			**0.59**			**7.46**			**303.99**			**28.24**	**30.00**
Ostreococcus tauri	**0.43**			**0.40**			**4.99**			**309.06**			**31.93**	**35.00**
Phaeodactylum tricornutum	**-0.11**			**0.47**			**5.91**			**302.64**			**26.26**	**27.00**
Porphyridium aerugineum	**-0.81**			**0.60**			**12.49**			**309.07**			**33.96**	**35.00**
Porphyridium purpureum	**-0.33**			**1.02**			**4.41**			**301.02**			**25.77**	**32.00**
Rhodella maculata	**-0.17**			**0.50**			**3.45**			**300.93**			**23.83**	**30.00**
Synechococcus **sp.**	**-1.23**			**1.46**			**7.81**			**302.23**			**27.60**	**30.00**
Synechocystis **sp.**	**-0.23**			**0.57**			**2.31**			**307.29**			**30.24**	**37.00**
Thalassiosira pseudonana	**0.06**			**0.63**			**5.39**			**304.13**			**28.01**	**32.00**
Thoracosphaera heimii	**-1.00**			**0.49**			**2.37**			**302.84**			**25.23**	**30.00**
Standard deviation	0.57			0.40			3.30			3.10			n/a	n/a
		lower	upper		lower	upper		lower	upper		lower	upper		
Fixed effect	**-0.56**	-0.83	-0.29	**0.77**	0.58	0.97	**6.27**	4.49	8.05	**304.22**	302.67	305.77	**28.29**	n/a

Appendix A:Table.2 Species level, and fixed effect estimates of the growth thermal tolerance parameters, predicted from nonlinear mixed effects modelling. Lower and upper values are for 95% confidence intervals surrounding the fixed effect values. Standard deviations for each parameter are for the random effect of species.

	$\mu gC\ cell^{-1}$	(± s.e.m)	$\mu gN\ cell^{-1}$	(± s.e.m)	$C:N$	(± s.e.m)	M	(± s.e.m)
Amphidinium carterae	**7.21E-05**	1.34E-05	**9.18E-06**	1.51E-06	**9.21**	0.97	**0.82**	0.02
Bigelowiella natans	**4.06E-06**	6.75E-07	**5.42E-07**	1.06E-07	**9.23**	1.67	**0.81**	0.03
Chlorarachnion reptans	**4.81E-06**	7.09E-07	**6.00E-07**	4.45E-08	**9.29**	0.94	**0.82**	0.01
Dunaliella tertiolecta	**2.43E-05**	5.32E-06	**3.91E-06**	7.24E-07	**7.16**	0.36	**0.78**	0.01
Emiliania huxleyi	**4.59E-06**	2.07E-06	**4.24E-07**	1.99E-07	**13.50**	0.98	**0.87**	0.01
Gephyrocapsa oceanica	**3.17E-06**	8.56E-07	**3.74E-07**	1.03E-07	**9.91**	0.16	**0.83**	0.00
Gymnochlora stellata	**2.95E-05**	2.71E-06	**4.90E-06**	2.10E-07	**6.99**	0.33	**0.78**	0.01
Micromonas pusilla	**1.02E-06**	2.67E-07	**8.13E-08**	2.05E-08	**14.35**	0.69	**0.88**	0.01
Nitzschia sp	**6.10E-06**	1.88E-06	**9.41E-07**	1.47E-07	**7.13**	1.45	**0.77**	0.04
Ostreococcus tauri	**1.44E-06**	5.84E-07	**2.47E-07**	1.05E-07	**7.30**	0.59	**0.78**	0.01
Porphyridium aerugineum	**7.78E-06**	1.25E-06	**7.47E-07**	1.83E-07	**12.76**	1.89	**0.86**	0.02
Porphyridium purpureum	**3.37E-05**	2.16E-05	**4.51E-06**	2.22E-06	**7.47**	1.28	**0.78**	0.03
Phaeodactylum tricornutum	**8.17E-06**	3.00E-06	**1.25E-06**	3.56E-07	**7.00**	1.14	**0.77**	0.03
Rhodella maculata	**1.11E-04**	3.79E-05	**1.83E-05**	6.84E-06	**7.28**	0.28	**0.78**	0.01
***Synechococcus* sp.**	**2.12E-06**	8.52E-07	**4.26E-07**	1.59E-07	**6.15**	0.51	**0.75**	0.01
***Synechocystis* sp.**	**1.77E-06**	3.11E-07	**4.22E-07**	7.42E-08	**4.93**	0.38	**0.71**	0.01
Thoracosphaera heimii	**1.16E-04**	4.72E-05	**6.72E-06**	2.29E-06	**18.05**	3.16	**0.89**	0.02
Thalassiosira pseudonana	**2.37E-05**	3.00E-06	**2.94E-06**	6.00E-08	**9.38**	1.00	**0.82**	0.02

Appendix A:Table.3 Carbon and nitrogen per cell measurements, the calculated *M* (carbon assimilation quotient) and C:N ratios (in moles)

	$\ln R(T_c)$			E_a^R			E_h^R			T_h^R			T_{opt}^R
Amphidinium carterae	**-3.34**			**0.97**			**2.32**			**311.31**			**36.97**
Bigelowiella natans	**-3.67**			**1.18**			**2.13**			**305.43**			**33.13**
Chlorarachnion reptans	**-2.05**			**1.02**			**2.66**			**307.65**			**33.04**
Dunaliella tertiolecta	**-2.94**			**0.99**			**2.80**			**311.07**			**36.14**
Emiliania huxleyi	**-3.87**			**1.17**			**3.25**			**304.88**			**30.33**
Gephyrocapsa oceanica	**-2.26**			**1.16**			**2.37**			**305.05**			**31.78**
Gymnochlora stellata	**-3.56**			**1.04**			**3.46**			**309.76**			**34.62**
Micromonas pusilla	**-4.28**			**1.12**			**2.33**			**302.82**			**29.43**
Nitzschia sp	**-3.61**			**1.28**			**3.27**			**306.82**			**32.58**
Ostreococcus tauri	**-5.32**			**1.25**			**2.37**			**306.58**			**33.82**
Porphyridium aerugineum	**-2.10**			**0.93**			**2.20**			**309.83**			**35.54**
Porphyridium purpureum	**-4.75**			**1.20**			**3.20**			**309.05**			**34.59**
Phaeodactylum tricornutum	**-2.90**			**0.97**			**2.68**			**307.62**			**32.79**
Rhodella maculata	**-3.81**			**0.93**			**2.56**			**307.72**			**32.79**
***Synechococcus* sp.**	**-4.03**			**1.06**			**2.26**			**307.47**			**33.91**
***Synechocystis* sp.**	**-4.04**			**0.92**			**2.17**			**306.01**			**31.72**
Thoracosphaera heimii	**-4.38**			**1.02**			**2.22**			**305.02**			**31.31**
Thalassiosira pseudonana	**-3.79**			**0.97**			**3.00**			**305.96**			**30.85**
Standard deviation	0.89			0.15			0.54			2.70			n/a
		lower	upper		lower	upper		lower	upper		lower	upper	
Fixed effect	**-3.60**	-4.02	-3.17	**1.07**	0.98	1.15	**2.62**	2.31	2.93	**307.23**	305.80	308.65	32.91

Appendix A:Table.4 Species level, and fixed effect estimates of the thermal performance parameters for respiration, predicted from nonlinear mixed effects modelling. Lower and upper values are for the 95% confidence intervals surrounding the fixed effect values. Standard deviations for each parameter are for the random effect of species.

	$\ln P(T_c)$			E_a^P			E_h^P			T_h^P			T_{opt}^P
Amphidinium carterae	**-2.98**			**0.77**			**4.99**			**304.36**			**28.51**
Bigelowiella natans	**-2.23**			**0.75**			**5.09**			**306.72**			**30.81**
Chlorarachnion reptans	**-1.43**			**0.77**			**3.67**			**303.25**			**27.27**
Dunaliella tertiolecta	**-1.06**			**0.68**			**8.18**			**312.73**			**37.12**
Emiliania huxleyi	**-2.74**			**0.79**			**9.76**			**303.64**			**28.52**
Gephyrocapsa oceanica	**-0.71**			**0.80**			**9.77**			**303.63**			**28.52**
Gymnochlora stellata	**-2.29**			**0.73**			**6.23**			**309.51**			**33.71**
Micromonas pusilla	**-2.64**			**0.73**			**4.14**			**301.20**			**25.18**
Nitzschia sp	**-1.99**			**0.77**			**6.29**			**308.08**			**32.39**
Ostreococcus tauri	**-4.09**			**0.67**			**5.04**			**308.65**			**32.47**
Porphyridium aerugineum	**-1.13**			**0.71**			**4.18**			**312.72**			**36.40**
Porphyridium purpureum	**-2.72**			**0.72**			**8.02**			**311.92**			**36.36**
Phaeodactylum tricornutum	**-1.69**			**0.74**			**8.65**			**307.22**			**31.86**
Rhodella maculata	**-2.16**			**0.73**			**4.40**			**306.55**			**30.46**
***Synechococcus* sp.**	**-2.53**			**0.73**			**5.86**			**305.55**			**29.74**
***Synechocystis* sp.**	**-2.66**			**0.73**			**4.59**			**310.73**			**34.59**
Thoracosphaera heimii	**-3.40**			**0.73**			**3.98**			**302.43**			**26.37**
Thalassiosira pseudonana	**-2.27**			**0.76**			**6.63**			**306.08**			**30.45**
Standard deviation	0.84			0.08			1.96			3.61			n/a
		lower	upper		lower	upper		lower	upper		lower	upper	
Fixed effect	**-2.26**	-2.66	-1.87	**0.74**	0.69	0.79	**6.08**	5.04	7.12	**306.94**	305.25	308.64	**31.18**

Appendix A:Table.5 Species level, and fixed effect estimates of the thermal performance parameters for light saturated gross photosynthesis at the optimal light irradiance, predicted from nonlinear mixed effects modelling. Lower and upper values are for the 95% confidence intervals surrounding the fixed effect values. Standard deviations for each parameter are for the random effect of species.

	$\ln P_{0.5}(T_c)$			$E_a^{P_{0.5}}$			$E_h^{P_{0.5}}$			$T_h^{P_{0.5}}$			$T_{opt}^{P_{0.5}}$
Amphidinium carterae	**-3.06**			**0.80**			**5.20**			**303.78**			**28.04**
Bigelowiella natans	**-2.46**			**0.81**			**6.36**			**306.82**			**31.24**
Chlorarachnion reptans	**-1.56**			**0.82**			**4.95**			**302.67**			**26.97**
Dunaliella tertiolecta	**-1.16**			**0.70**			**6.30**			**312.16**			**36.25**
Emiliania huxleyi	**-2.83**			**0.82**			**8.33**			**302.97**			**27.73**
Gephyrocapsa oceanica	**-0.81**			**0.82**			**7.04**			**303.55**			**28.13**
Gymnochlora stellata	**-2.48**			**0.77**			**6.64**			**309.36**			**33.71**
Micromonas pusilla	**-2.71**			**0.74**			**5.45**			**301.13**			**25.36**
Nitzschia sp	**-2.07**			**0.78**			**8.02**			**308.62**			**33.20**
Ostreococcus tauri	**-4.15**			**0.73**			**5.31**			**304.20**			**28.30**
Porphyridium aerugineum	**-1.19**			**0.73**			**4.50**			**311.61**			**35.45**
Porphyridium purpureum	**-2.77**			**0.73**			**8.32**			**311.89**			**36.40**
Phaeodactylum tricornutum	**-1.75**			**0.75**			**7.53**			**307.20**			**31.69**
Rhodella maculata	**-2.21**			**0.75**			**4.78**			**306.30**			**30.32**
***Synechococcus* sp.**	**-2.62**			**0.75**			**5.77**			**305.10**			**29.32**
***Synechocystis* sp.**	**-2.73**			**0.72**			**4.97**			**310.46**			**34.38**
Thoracosphaera heimii	**-3.45**			**0.76**			**4.88**			**302.25**			**26.39**
Thalassiosira pseudonana	**-2.33**			**0.78**			**5.80**			**305.53**			**29.81**
Standard deviation	0.83			0.08			1.54			3.61			n/a
		lower	upper		lower	upper		lower	upper		lower	upper	
Fixed effect	**-2.35**	-2.74	-1.96	**0.76**	0.71	0.82	**6.12**	5.16	7.08	**306.42**	304.73	308.12	**30.72**

Appendix A:Table.6 Species level, and fixed effect estimates of the thermal performance parameters for gross photosynthesis at half the light saturated irradiance ($P_{0.5}$), predicted from nonlinear mixed effects modelling. Lower and upper values are for the 95% confidence intervals surrounding the fixed effect values. Standard deviations for each parameter are for the random effect of species.

	CUE break-point temperature	lower	upper
Amphidinium carterae	**28.43**	28.16	28.71
Bigelowiella natans	**34.34**	34.12	34.56
Chlorarachnion reptans	**27.42**	27.02	27.81
Dunaliella tertiolecta	**40.61**	40.49	40.74
Emiliania huxleyi	**29.70**	29.66	29.75
Gephyrocapsa oceanica	**32.33**	32.14	32.51
Gymnochlora stellata	**37.33**	37.09	37.56
Micromonas pusilla	**27.52**	27.21	27.83
Nitzschia sp	**36.51**	36.35	36.66
Ostreococcus tauri	**35.29**	35.00	35.58
Porphyridium aerugineum	**40.53**	39.79	41.28
Porphyridium purpureum	**40.51**	40.36	40.66
Phaeodactylum tricornutum	**34.69**	34.57	34.81
Rhodella maculata	**33.43**	33.17	33.69
***Synechococcus* sp.**	**31.61**	31.45	31.77
***Synechocystis* sp.**	**41.29**	40.94	41.65
Thoracosphaera heimii	**27.55**	27.26	27.85
Thalassiosira pseudonana	**33.75**	33.61	33.89

Appendix A:Table.7 Estimates of the carbon-use efficiency (CUE) break-point temperatures (°C) for each species, with lower and upper values of the 95% confidence intervals. Break-point estimates were derived from fitting a segmented linear regression model to predicted CUE values, derived from the species level parameters of respiration and photosynthesis. The breakpoint estimate is defined in the segmented model as the intersection where there is significant difference in slopes, determined by the Davies test for performing hypothesis.

	$\ln \mathrm{CUE}(T_c)$			E_a^{CUE}		
Amphidinium carterae	**-1.28**			**-0.24**		
Bigelowiella natans	**-0.29**			**-0.12**		
Chlorarachnion reptans	**-0.86**			**-0.10**		
Dunaliella tertiolecta	**-0.19**			**-0.11**		
Emiliania huxleyi	**-0.42**			**-0.09**		
Gephyrocapsa oceanica	**-0.27**			**-0.11**		
Gymnochlora stellata	**-0.32**			**-0.16**		
Micromonas pusilla	**-0.28**			**-0.10**		
Nitzschia sp	**-0.24**			**-0.13**		
Ostreococcus tauri	**-0.33**			**-0.25**		
Porphyridium aerugineum	**-0.52**			**-0.09**		
Porphyridium purpureum	**-0.17**			**-0.09**		
Phaeodactylum tricornutum	**-0.36**			**-0.11**		
Rhodella maculata	**-0.27**			**-0.07**		
Synechococcus **sp.**	**-0.29**			**-0.12**		
Synechocystis **sp.**	**-0.31**			**-0.04**		
Thoracosphaera heimii	**-0.48**			**-0.14**		
Thalassiosira pseudonana	**-0.30**			**-0.05**		
Standard deviation	0.29			0.07		
		lower	upper		lower	upper
Fixed effect	**-0.40**	-0.54	-0.26	**-0.12**	-0.16	-0.08

Appendix A:Table.8 Species level and fixed effect estimates of $\ln \mathrm{CUE}(T_c)$ (the natural logarithm of carbon-use efficiency at T_c, 20°C) and E_a^{CUE} (the apparent activation energy characterising the temperature dependence of CUE, up to the identified break-point temperature of CUE , see Appendix A: Table.7 and Figure. 2.3 Chapter 2).Lower and upper values are for the 95% confidence intervals sur rounding the fixed effect value. Standard deviation is for the random effect of sp ecies. The relationship between $\ln \mathrm{CUE}$ and temperature was significant – indica ting a strong temperature dependence of $\ln \mathrm{CUE}$ across the temperature range b elow the breakpoint of each species (Figure. 2.4, Chapter 2).

Appendix A: Figures

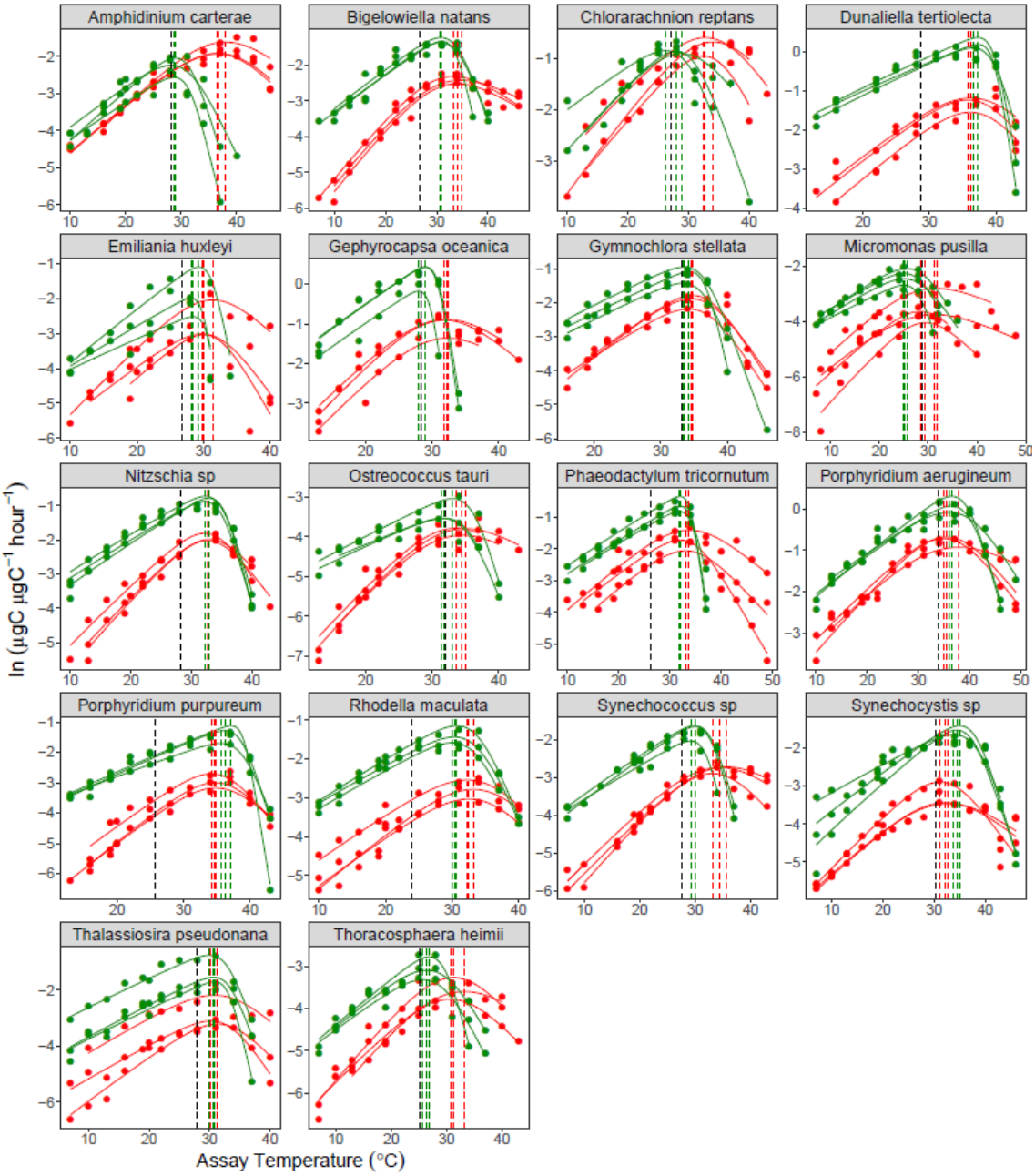

Appendix A:Figure.1 Thermal performance curves for respiration and light saturated gross photosynthesis, displaying the biological replicate variation for 18 species of marine phytoplankton. Metabolic thermal performance curves for the biological replicates of each species used in this study (*n* = minimum of 3 biological replicates per response for each species). Green colouring denotes gross photosynthesis, red colouring denotes respiration. The fitted lines for each replicate are from the random effects of a non-linear mixed effects model fitted to the rate data using the Sharpe-Schoolfield equation. The dashed vertical lines indicate the replicate level variation in the optimal temperature of respiration and photosynthesis, and the black dashed vertical line represents the estimated optimal growth temperature for each species.

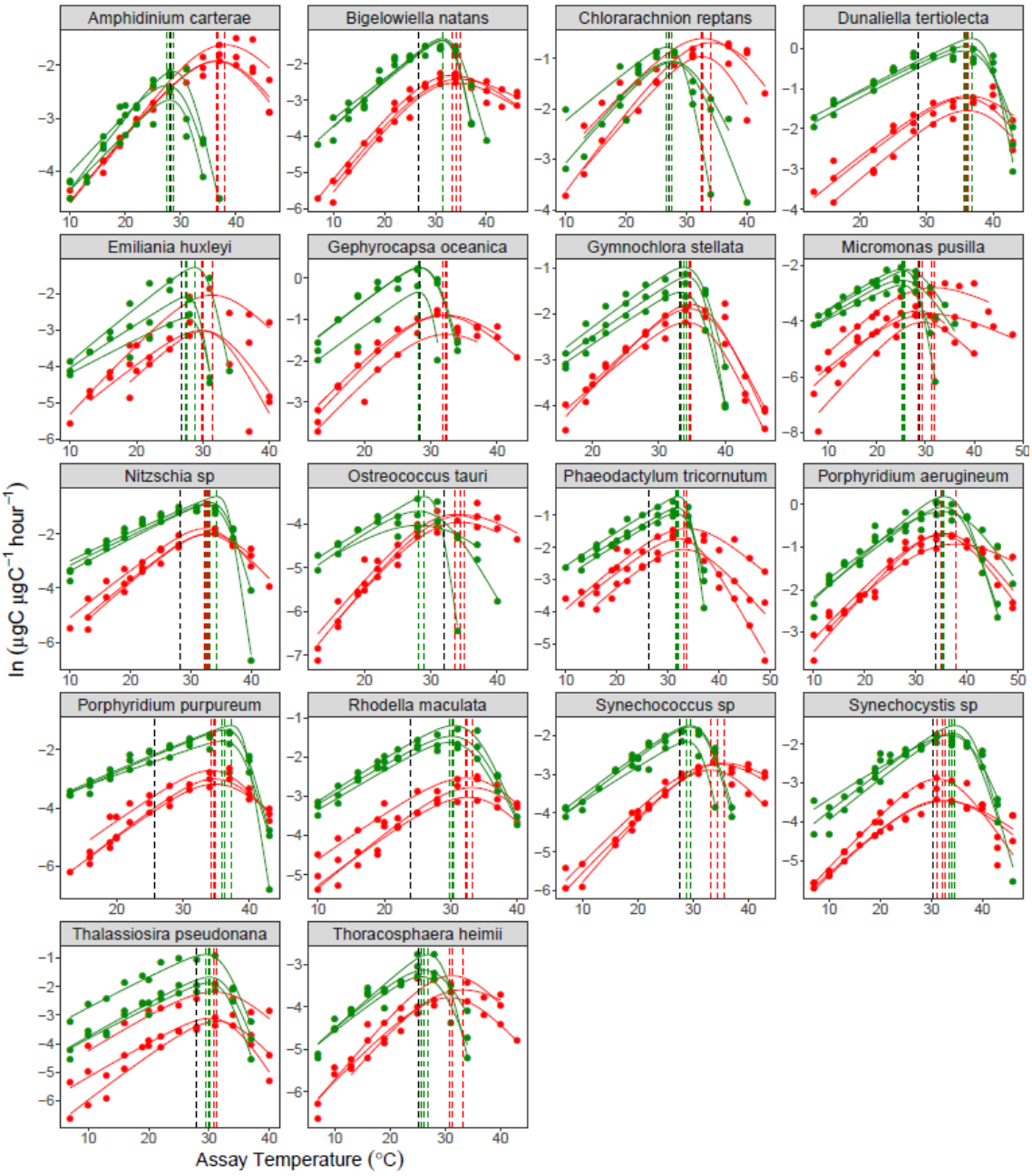

Appendix A:Figure.2 Thermal performance curves for respiration and estimated gross photosynthesis at half the light saturated irradiance, displaying the biological replicate variation for 18 species of marine phytoplankton. Metabolic thermal performance curves for the biological replicates of each species used in this study (*n* = minimum of 3 biological replicates per response for each species). Green colouring denotes gross photosynthesis, red colouring denotes respiration. The fitted lines for each replicate are from the random effects of a non-linear mixed effects model fitted to the rate data using the Sharpe-Schoolfield equation. The dashed vertical lines indicate the replicate level variation in the optimal temperature of respiration and photosynthesis, and the black dashed vertical line represents the estimated optimal growth temperature for each species.

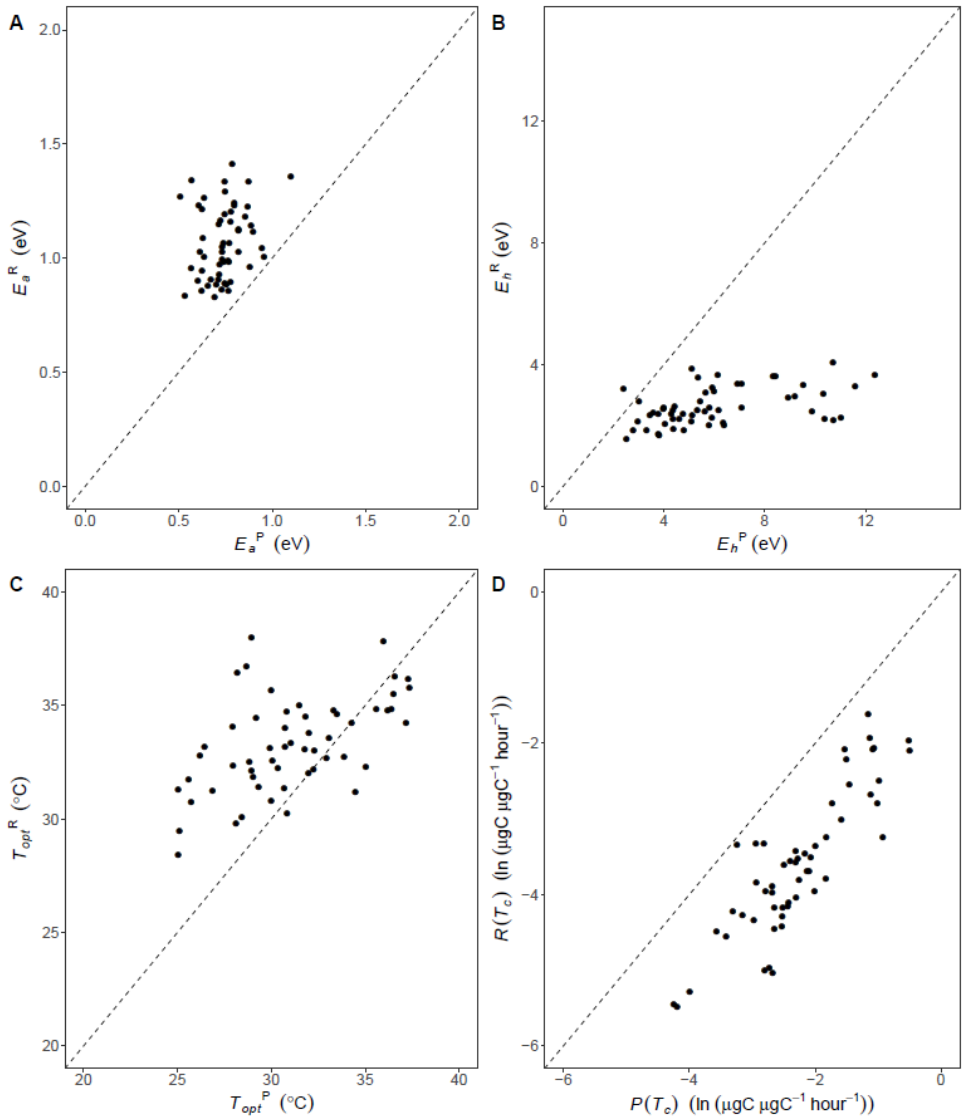

Appendix A:Figure.3 Comparisons of thermal response traits for respiration and gross photosynthesis. (A) shows the difference in the activation energies, where ubiquitously the activation for respiration exceeds that of photosynthesis, $E_a{}^R > E_a{}^P$ **(B)** shows the difference in the deactivation energies, where generally the deactivation energy of photosynthesis exceeds that of respiration, $E_h{}^P > E_h{}^R$ **(C)** shows the difference in the optimal temperatures, where generally the optimal temperature for respiration exceeds that of photosynthesis $T_{opt}{}^R > T_{opt}{}^P$ **(D)** shows the difference in the natural logarithm of metabolic rate at T_c (20ºC), or $b(T_c)$, where ubiquitously the rate of photosynthesis at T_c exceeds that of respiration, $P(T_c) > R(T_c)$. For A-D the dashed line represents the 1:1 line.

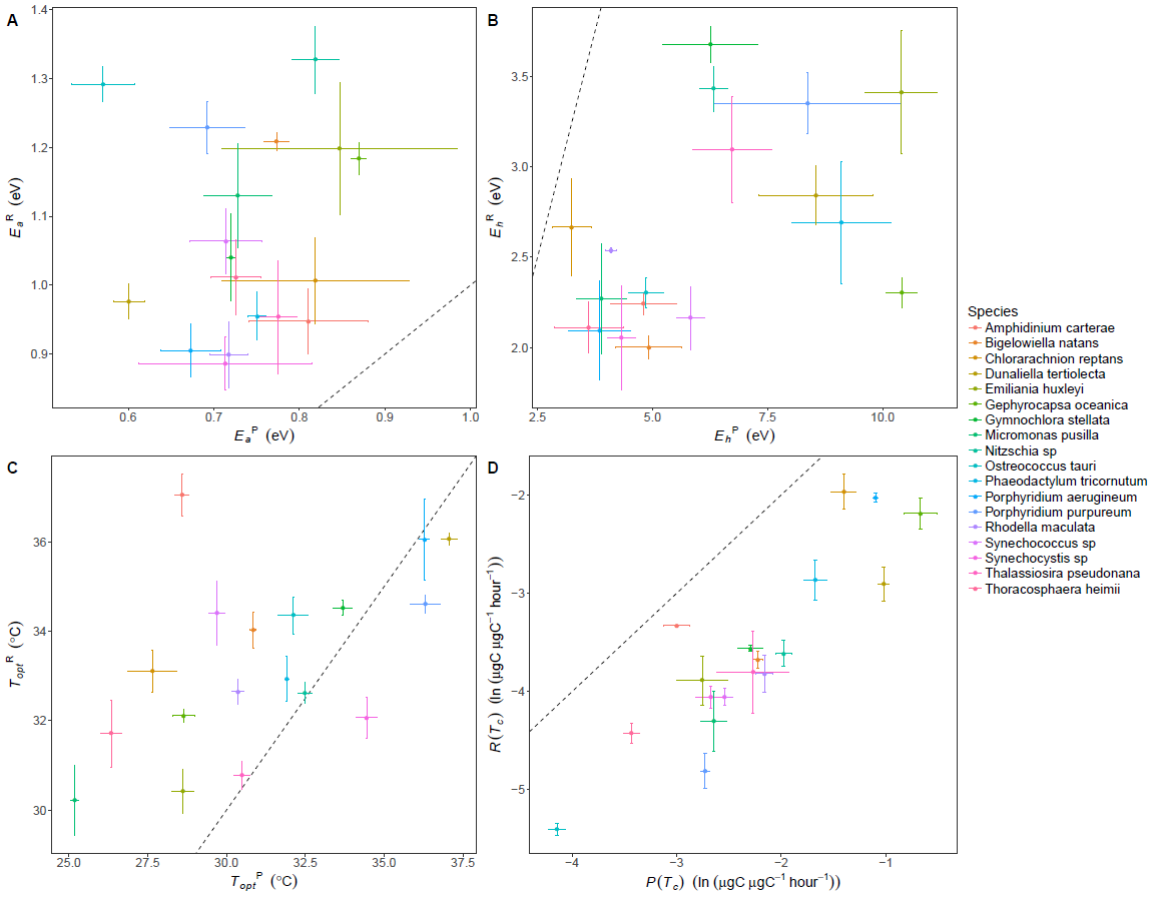

Appendix A:Figure.4 Comparisons of mean thermal response traits for respiration and gross photosynthesis of each species. (A) shows the difference in the mean activation energies at the species level, where ubiquitously the activation energy for respiration exceeds that of photosynthesis, $E_a^R > E_a^P$ **(B)** shows the difference in the mean deactivation energies, where the deactivation energy of photosynthesis exceeds that of respiration, $E_h^P > E_h^R$ for all species **(C)** shows the difference in the mean optimal temperatures, where the optimal temperature for respiration exceeds that of photosynthesis $T_{opt}^R > T_{opt}^P$ for 12 out of the 18 species **(D)** shows the difference in the mean natural logarithm of metabolic rate at T_c (20ºC), or $b(T_c)$, where ubiquitously the rate of photosynthesis at T_c exceeds that of respiration, $P(T_c) > R(T_c)$. For A-D the dashed line represents the 1:1 line and error bars denote ± s.e.m (n = minimum of 3 biological replicates per response for each species) for both x and y parameters.

Appendix B (for Chapter 3)

Appendix B: Extended Materials and Methods

Summary of the calculations used to derive biovolume for the different species

Due to the differing morphology of the species in this study, to approximate cell volume we applied various geometric models (Sun & Liu 2003):

For *Bigelowiella natans*, *Chlorarachnion reptans*, *Emiliania huxleyi*, *Gephyrocapsa oceanica*, *Gymnochlora stellata*, *Ostreococcus tauri*, *Porphyridium aerugineum*, *Porphyridium purpureum*, *Rhodella maculata*, *Synechococcus* sp., *Synechocystis* sp. and *Thoracosphaera heimii* we applied a spherical model.

For *Amphidinium carterae*, *Dunaliella tertiolecta*, *Micromonas pusilla* and *Nitzschia* sp. we applied a prolate-spheroid model.

For *Phaeodactylum tricornutum* we applied a sickle shaped prism model.

For *Thalassiosira pseudonana* we applied a cylinder model.

Summary of algorithms used to estimate Chlorophyll *a* content per cell

As discussed in the Chapter 2 we used previously established absorbance coefficients to estimate µg chlorophyll *a* cell^{-1} for each species. Due to differences in the pigment composition across the taxa, different equations were used for the phylogenetic groups (Ritchie 2006):

Cyanobacteria (*Synechococcus* sp.*, Synechocystis* sp.):

$$\mu g\ Chla\ cell^{-1} = \frac{(11.9035\ A_{665} - A_{730})v/(lV)}{cells\ ml^{-1}}$$

Rhodophyta (*Porphyridium purpureum* , *Porphyridium aerugineum* , *Rhodella maculata*):

$$\mu g\ Chla\ cell^{-1} = \frac{(11.9035\ A_{665} - A_{730})v/(lV)}{cells\ ml^{-1}}$$

Chlorophyta and chlorarachniophyta (*Dunaliella tertiolecta*, *Micromonas pusilla*, *Ostreococcus tauri, Gymnochlora stellata, Bigelowiella natans, Chlorarachnion reptans*):

$$\mu g\ Chla\ cell^{-1} = \frac{(-5.2007\ A_{649} + 13.5275\ A_{665} - A_{730})v/(lV)}{cells\ ml^{-1}}$$

Dinoflagellata and haptophyta (*Amphidinium carterae, Thoracosphaera heimii, Gephyrocapsa oceanica, Emiliania huxleyi*):

$$\mu g\ Chla\ cell^{-1} = \frac{(-2.6094\ A_{629} + 12.4380\ A_{665} - A_{730})v/(lV)}{cells\ ml^{-1}}$$

Heterokonta (*Thalassiosira pseudonana, Nitzschia* sp., *Phaeodactylum tricornutum*):

$$\mu g\ Chla\ cell^{-1} = \frac{(-1.4014\ A_{629} + 12.1551\ A_{665} - A_{730})v/(lV)}{cells\ ml^{-1}}$$

Where A_{xxx} is the absorbance at xxx nm (A_{730} represents the background absorbance), v is the volume of solvent used for the extractions (in this case 6ml of ethanol), l is the length of the spectrophotometric cell (cm), V is the original sample volume (in this case 50ml) and $cells\ ml^{-1}$ is the cell density of the original culture in exponential growth phase (Ritchie 2006; Henriques *et al.* 2007).

Quantifying metabolic rates

All biological replicate samples were concentrated by centrifugation at 1500rpm, 20°C, for 15 minutes and re-suspended into an adequate volume of fresh growth medium. Prior to running a sample at each assay temperature, all samples were given ~ 15 minutes to pre-acclimate to the assay temperature in the dark before any data was collected. This also gave the electrode system sufficient time to stabilise before metabolic rates were measured. This was necessary for two reasons, i) as the sample adjusts to the assay temperature this will naturally cause changes in the dissolved oxygen concentration, ii) the electrode system results in oxygen signal drift, and this too is temperature dependent. We measured rates of oxygen depletion from 21 sterilised artificial seawater samples across a range of temperatures 4°C - 44°C and found that the impact of drift was minimised after ~15 minutes of stabilisation time. Nevertheless, signal drift was linearly temperature dependent after this time. To account for drift in our dataset we corrected all our raw data using the following empirically derived relationship:

$$drift = (-0.392 \times T) - 6.51$$

Where *T* is assay temperature (°C), and *drift* is the non-biological depletion in oxygen concentration measured in units $\mu molO_2\ mL^{-1}\ s^{-1}$ after approximately 15 minutes of stabilisation. The raw O_2 flux data was then corrected by subtracting the estimated drift.

Appendix B: Tables

	Phyla	Species (strain identification synonyms)	Location/Year of isolation		Growth medium
	Cyanobacteria	*Synechococcus* sp. (CCMP 2370 , WH8102)	North Atlantic - Sargasso Sea	1981	PCR-S11 Red Sea Salt
		Synechocystis sp. (RCC 1773, R56)	North Atlantic - English Channel	1975	PCR-S11 Red Sea Salt
Green	Chlorophyta (Chlorophyceae/ Prasinophyceae)	*Dunaliella tertiolecta* (CCAP 19/5)	North Atlantic - English Channel	1967	F/2
		Micromonas pusilla (CCMP1545, RCC 834)	North Atlantic - English Channel	1950	K
		Ostreococcus tauri (OTH95, RCC 4221)	Mediterranean - Gulf of Lion	1995	K
	Chlorarachniophyta	*Gymnochlora stellata* (CCMP2057, RCC 626)	West Pacific Ocean	N/A	F/2
		Bigelowiella natans (CCMP621, RCC 623)	North Atlantic - Sargasso Sea	1981	F/2
		Chlorarachnion reptans (CCAP 815/1 , CCMP239)	North Pacific - Gulf of California	1966	F/2
Red	Rhodophyta	*Rhodella maculata* (CCAP 1388/2, SAG 45.85)	North Atlantic - English Channel	1965	F/2
		Porphyridium purpureum (CCAP 1380/11)	Japan	1987	F/2
		Porphyridium aerugineum (RCC 652, SAG 110.79)	North Atlantic - North Sea	1980	K
	Heterokonta	*Thalassiosira pseudonana* (CCMP 1335)	North Atlantic - Moriches Bay	1958	F/2 + Si
		Nitzschia sp. (RCC 80, ROS97004)	North Atlantic - English Channel	1997	K + Si
		Phaeodactylum tricornutum (CCAP 1052/1B, CCMP 2558)	North Atlantic	N/A	F/2 + Si
	Haptophyta	*Gephyrocapsa oceanica* (RCC 1303, AC300, LK7)	North Atlantic - Arcachon Bay	1999	K/2
		Emiliania huxleyi (CCMP 1516, CCMP 2090)	South Pacific Ocean	1991	K/2
	Dinoflagellata	*Amphidinium carterae* (CCMP 1314)	North Atlantic - Nantucket Sound	1954	F/2
		Thoracosphaera heimii (AC214, Nap17 , RCC 1512)	Mediterranean - Tyrrhenian Sea	2000	K/2

Appendix B:Table.1 Phytoplankton strains. All strains were obtained from CCAP (The Culture Collection of Algae and Protozoa) and RCC (Roscoff Culture Collection). The above table divides strains into phylogenetic groups as well as showing which of the red or green super-families they belong to, with the exception of cyanobacteria. Growth mediums were prepared according to the medium recipes referred to in the methods section.

	$ln.\mu(T_c)$			E_a^{μ}			E_h^{μ}			T_h^{μ}			T_{opt}^{μ}	T_{max}^{μ}
Amphidinium carterae	**-0.80**			**0.56**			**8.84**			**303.85**			**28.29**	**30.00**
Bigelowiella natans	**-1.32**			**0.99**			**4.59**			**302.01**			**26.68**	**30.00**
Chlorarachnion reptans	**-1.95**			**1.44**			**6.00**			**301.84**			**27.18**	**30.00**
Dunaliella tertiolecta	**-0.14**			**0.41**			**1.96**			**307.31**			**28.76**	**37.00**
Emiliania huxleyi	**-0.50**			**1.41**			**7.59**			**301.48**			**26.81**	**30.00**
Gephyrocapsa oceanica	**-0.77**			**1.27**			**9.71**			**303.13**			**28.44**	**30.00**
Gymnochlora stellata	**-0.69**			**0.48**			**7.96**			**309.20**			**33.23**	**35.00**
Micromonas pusilla	**-0.54**			**0.67**			**9.53**			**304.00**			**28.71**	**30.00**
Nitzschia sp	**0.02**			**0.59**			**7.46**			**303.99**			**28.24**	**30.00**
Ostreococcus tauri	**0.43**			**0.40**			**4.99**			**309.06**			**31.93**	**35.00**
Phaeodactylum tricornutum	**-0.11**			**0.47**			**5.91**			**302.64**			**26.26**	**27.00**
Porphyridium aerugineum	**-0.81**			**0.60**			**12.49**			**309.07**			**33.96**	**35.00**
Porphyridium purpureum	**-0.33**			**1.02**			**4.41**			**301.02**			**25.77**	**32.00**
Rhodella maculata	**-0.17**			**0.50**			**3.45**			**300.93**			**23.83**	**30.00**
***Synechococcus* sp.**	**-1.23**			**1.46**			**7.81**			**302.23**			**27.60**	**30.00**
***Synechocystis* sp.**	**-0.23**			**0.57**			**2.31**			**307.29**			**30.24**	**37.00**
Thalassiosira pseudonana	**0.06**			**0.63**			**5.39**			**304.13**			**28.01**	**32.00**
Thoracosphaera heimii	**-1.00**			**0.49**			**2.37**			**302.84**			**25.23**	**30.00**
Standard deviation	0.57			0.40			3.30			3.10			n/a	n/a
		lower	upper		lower	upper		lower	upper		lower	upper		
Fixed effect	**-0.56**	-0.83	-0.29	**0.77**	0.58	0.97	**6.27**	4.49	8.05	**304.22**	302.67	305.77	**28.29**	n/a

Appendix B: Table.2 Species level, and fixed effect estimates of the growth thermal tolerance parameters, predicted from nonlinear mixed effects modelling. $ln.\mu(T_c)$ is the natural log of predicted growth rate at T_c , in this case $T_c = 20°C$. Lower and upper values are for the 95% CI intervals surrounding the fixed effect values. Standard deviations for each parameter are for the random effect of species.

	Volume (μm^3)	(± s.e.m)	pg Chl$a$ $cell^{-1}$	(± s.e.m)	pgC $cell^{-1}$	(±s.e.m)	pgN $cell^{-1}$	(±s.e.m)	C:N	(± s.e.m)
Amphidinium carterae	877.18	57.39	2.43	0.386	72.10	13.431	9.18	1.507	9.21	0.97
Bigelowiella natans	36.70	0.98	0.15	0.067	4.06	0.675	0.54	0.106	9.23	1.67
Chlorarachnion reptans	594.50	41.64	0.40	0.016	4.81	0.709	0.60	0.045	9.29	0.94
Dunaliella tertiolecta	295.11	19.59	2.20	0.027	24.33	5.319	3.91	0.724	7.16	0.36
Emiliania huxleyi	62.59	2.63	0.19	0.020	4.59	2.075	0.42	0.199	13.50	0.98
Gephyrocapsa oceanica	144.98	5.51	0.52	0.130	3.17	0.856	0.37	0.103	9.91	0.16
Gymnochlora stellata	400.30	17.74	3.50	0.072	29.50	2.706	4.90	0.210	6.99	0.33
Micromonas pusilla	1.49	0.24	0.02	0.001	1.02	0.267	0.08	0.021	14.35	0.69
Nitzschia sp	109.38	6.82	0.80	0.047	6.10	1.879	0.94	0.147	7.13	1.45
Ostreococcus tauri	0.86	0.06	0.04	0.001	1.44	0.584	0.25	0.105	7.30	0.59
Porphyridium aerugineum	166.83	4.39	0.70	0.051	7.78	1.249	0.75	0.183	12.76	1.89
Porphyridium purpureum	131.62	2.74	5.12	0.061	33.70	21.552	4.51	2.218	7.47	1.28
Phaeodactylum tricornutum	115.56	11.85	0.39	0.014	8.17	3.004	1.25	0.356	7.00	1.14
Rhodella maculata	3475.09	201.07	17.61	0.759	110.77	37.929	18.27	6.836	7.28	0.28
***Synechococcus* sp.**	0.92	0.04	0.01	0.003	2.12	0.852	0.43	0.159	6.15	0.51
***Synechocystis* sp.**	4.25	0.29	0.05	0.004	1.77	0.311	0.42	0.074	4.93	0.38
Thoracosphaera heimii	3896.80	249.66	2.29	0.831	115.97	47.161	6.72	2.289	18.05	3.16
Thalassiosira pseudonana	63.75	3.68	1.22	0.068	23.70	3.000	2.94	0.060	9.38	1.00

Appendix B: Table.3 Species sub-cellular traits: mean volume, mean *pg* Chlorophyll *a* per cell, mean *pg* carbon (*C*) and nitrogen (*N*) per cell, mean carbon:nitrogen ratio, in moles (C:N) all with standard error of the mean (± s.e.m).

	$T_{opt}{}^{\mu}$	I_{opt} (at $T_{opt}{}^{\mu}$)	(± s.e.m)
Amphidinium carterae	28.29	753.40	134.49
Bigelowiella natans	26.68	770.72	83.46
Chlorarachnion reptans	27.18	1223.91	340.46
Dunaliella tertiolecta	28.76	1196.40	115.61
Emiliania huxleyi	26.81	453.73	224.06
Gephyrocapsa oceanica	28.44	730.90	203.28
Gymnochlora stellata	33.23	1159.37	74.65
Micromonas pusilla	28.71	603.90	20.80
Nitzschia sp	28.24	904.05	123.53
Ostreococcus tauri	31.93	338.36	24.84
Porphyridium aerugineum	33.96	1271.36	320.49
Porphyridium purpureum	25.77	993.20	457.48
Phaeodactylum tricornutum	26.26	1025.24	34.87
Rhodella maculata	23.83	702.74	147.34
***Synechococcus* sp.**	27.60	716.17	37.97
***Synechocystis* sp.**	30.24	425.53	18.73
Thoracosphaera heimii	25.23	957.52	283.22
Thalassiosira pseudonana	28.01	781.97	6.15

Appendix B: Table.4 Mean estimates of optimal light intensity of photosynthesis (I_{opt}) in units µmol m^2 s^{-1} for each species, measured at the optimal temperature of growth ($T_{opt}{}^{\mu}$) to the nearest 1°C.

Model	value	95% Confidence Intervals	*Df*	logLik	AIC	χ^2	*p*
Deriving the size scaling of maximal growth rates:							
ln $b(T_{opt}{}^{\mu})$ ~ ln volume + (1|Phyla)	**-0.088**	**-0.173 to -0.002**	**4**	**-9.04**	**26.07**		
ln $b(T_{opt}{}^{\mu})$ ~ 1 + (1|Phyla)			3	-11.04	28.07	3.99	**0.046**
Deriving the across-species activation energy of size corrected maximal rates, using the modelled size scaling, -0.088:							
ln $b(T_{opt}{}^{\mu})_{cor}$ ~ *T* + (1|Phyla)	**0.50**	**0.1 to 0.9**	**4**	**-6.48**	**20.95**		
ln $b(T_{opt}{}^{\mu})_{cor}$ ~ 1 + (1|Phyla)			3	-9.04	24.08	**5.12**	**0.024**
Deriving the across-species activation energy of size corrected maximal rates, using the lower confidence limit (above), -0.173:							
ln $b(T_{opt}{}^{\mu})_{cor}$ ~ *T* + (1|Phyla)	0.36	-0.2 to 0.9	4	-10.10	28.20		
ln $b(T_{opt}{}^{\mu})_{cor}$ ~ 1 + (1|Phyla)			3	-10.95	27.90	1.70	0.193
Deriving the across-species activation energy of size corrected maximal rates, using the upper confidence limit (above), -0.002:							
ln $b(T_{opt}{}^{\mu})_{cor}$ ~ *T* + (1|Phyla)	**0.62**	**0.2 to 1.0**	**4**	**-7.22**	**22.44**		
ln $b(T_{opt}{}^{\mu})_{cor}$ ~ 1 + (1|Phyla)			3	-10.95	27.91	**7.47**	**0.006**

Appendix B: Table.5 A summary of the linear mixed effects models used to determine the size scaling exponent of maximal growth rates (-0.088) and subsequently the activation energy of size corrected maximal growth rates (0.50eV). The activation energy was also modelled following size correction using the lower(-0.173) and upper (-0.002) 95% confidence interval estimates of the size scaling, this provided a comparison of the possible maximal and minimal activation energies after accounting for the error associated with the size scaling; if the lower estimate is used, the size scaling correction reduces the activation energy to 0.36eV, if the upper estimate is used the activation energy increases to 0.62eV. In each case the most complex model, was compared with a null hypothesis using ANOVA. Bold text indicates a significant correlation. *T* **=** standardised Boltzmann optimal growth temperature.

	$ln\ b(T_{opt}{}^{\mu})$	$b(T_{opt}{}^{\mu})$	$ln\ b(T_{opt}{}^{\mu})_{cor}$	$b(T_{opt}{}^{\mu})_{cor}$
Amphidinium carterae	-0.26	0.77	0.33	1.39
Bigelowiella natans	-0.69	0.50	-0.37	0.69
Chlorarachnion reptans	-0.86	0.42	-0.30	0.74
Dunaliella tertiolecta	0.10	1.10	0.60	1.81
Emiliania huxleyi	0.56	1.75	0.92	2.51
Gephyrocapsa oceanica	0.49	1.64	0.93	2.54
Gymnochlora stellata	0.06	1.06	0.59	1.80
Micromonas pusilla	0.15	1.16	0.18	1.20
***Nitzschia* sp.**	0.58	1.78	0.99	2.69
Ostreococcus tauri	0.97	2.63	0.95	2.60
Porphyridium aerugineum	0.21	1.24	0.66	1.94
Porphyridium purpureum	0.19	1.21	0.62	1.86
Phaeodactylum tricornutum	0.19	1.21	0.61	1.84
Rhodella maculata	-0.08	0.93	0.64	1.90
***Synechococcus* sp.**	0.02	1.02	0.01	1.01
***Synechocystis* sp.**	0.25	1.29	0.38	1.46
Thoracosphaera heimii	-0.89	0.41	-0.16	0.85
Thalassiosira pseudonana	0.60	1.82	0.97	2.63

Appendix B: Table.6 Species level estimates of maximal growth rates (and natural logarithm maximal growth rates) at the optimal growth temperature before size correction, $b(T_{opt}{}^{\mu})$ and after size correction (using the modelled value of -0.088) $b(T_{opt}{}^{\mu})_{cor}$, in units d^{-1}.

Figure 3.4b: **PC1 ~ *ln volume***				
Coefficients	**value**	**Std.Error**	**t value**	**Pr(>|t|)**
Intercept	2.48	0.68	3.63	**0.002**
Slope	-0.56	0.14	-4.16	**<0.001**
Summary:	Multiple R-squared	F-statistic	*p*	
	0.52	**17.32**	**<0.001**	
Figure 3.4c: **PC1 ~ $T_{opt}{}^{\mu}$**				
Coefficients	**value**	**Std.Error**	**t value**	**Pr(>|t|)**
Intercept	-12.91	4.22	-3.06	**0.007**
Slope	0.46	0.15	3.07	**0.007**
Summary:	Multiple R-squared	F-statistic	*p*	
	0.37	**9.45**	**0.007**	

Appendix B: Table.7 A summary of the linear models used to test the significance of the linear relationships between the first principal component values (PC1) obtained from our Principal Component Analysis (see Figure.3.4a, Chapter 3) and both natural logarithm mean cell volume (see Figure.3.4b), and optimal growth temperature (see Figure.3.4c) across all 18 species. Bold text indicates a significant correlation.

Model	value	95% Confidence Intervals	*Df*	logLik	AIC	χ^2	*p*
Appendix B: Figure.3a.							
ln pgC cell^{-1} ~ ln volume + (1|Phyla)	**0.49**	**0.34 to 0.65**	**4**	**-20.72**	**49.44**		
ln pgC cell^{-1} ~ 1 + (1|Phyla)			3	-31.22	68.44	**21.00**	**<0.001**
Appendix B: Figure.3b.							
ln pgN cell^{-1} ~ ln volume + (1|Phyla)	**0.45**	**0.28 to 0.62**	**4**	**-22.95**	**53.90**		
ln pgN cell^{-1} ~ 1 + (1|Phyla)			3	-31.58	69.16	**17.25**	**<0.001**
Appendix B: Figure.3c.							
ln pg Chl*a* cell^{-1} ~ ln volume + (1|Phyla)	**0.74**	**0.55 to 0.92**	**4**	**-23.68**	**55.36**		
ln pg Chl*a* cell^{-1} ~ 1 + (1|Phyla)			3	-37.37	80.73	**27.37**	**<0.001**

Appendix B: Table.8 A summary of the linear mixed effects modelling used to determine the size scaling exponent, and test for the significance, of the relationships of natural logarithm picograms of carbon per cell (pgC cell^{-1}), picograms of nitrogen per cell (pgN cell^{-1}) picograms of chlorophyll *a* per cell (pgN cell^{-1}) against natural logarithm mean cell volume. In each case the most complex model, including the effect of volume, was compared using ANOVA with a model containing no effect of volume. All log-log scaling coefficients were less than 1, implying a negative scaling of per unit volume carbon, nitrogen and chlorophyll *a* with increasing volume. Bold text indicates a significant correlation.

Model	value	95% Confidence Intervals	*Df*	logLik	AIC	χ^2	*p*
Appendix B: Figure.4. $T_{opt}{}^{\mu}$ and ln volume regression:							
$T_{opt}{}^{\mu}$ ~ ln volume + (1|Phyla)	-0.36	-0.83 to 0.12	4	-41.52	91.04		
$T_{opt}{}^{\mu}$ ~ 1 + (1|Phyla)			3	-42.63	91.26	2.22	0.136

Appendix B: Table.9 A summary of the linear mixed effects modelling to test for the significance of the relationship between optimal growth temperature and the natural logarithm mean cell volume. The most complex model, including the effect of volume, was compared using ANOVA with a model containing no effect of size. Despite there being an overall negative correlation between optimal growth temperature and all of the size metrics, we did not find this to be significant.

Appendix B: Figures

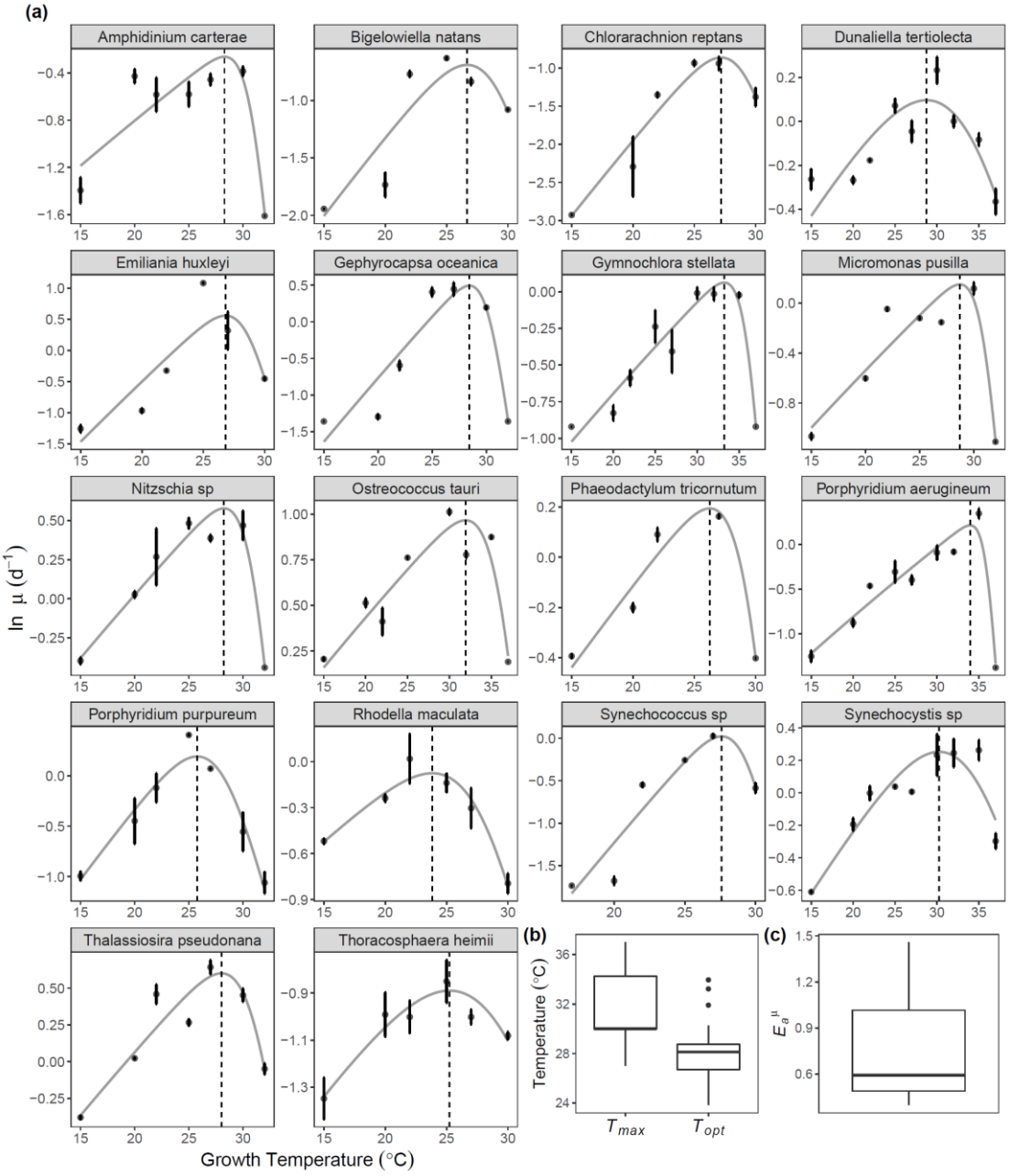

Appendix B: Figure.1 (a) Thermal tolerance curves for all 18 species used in this study (as shown in Figure 3.2a, Chapter 3). The data points presented are the mean natural logarithm of per capita growth rate, μ, with error bars denoting ± s.e.m (n = minimum of 3 biological replicates per growth temperature response for each species). The fitted lines are from the predicted random effect of species derived from non-linear mixed effects modelling with a Sharpe-Schoolfield model. The vertical dashed lines correspond with the optimal temperatures of growth. **(b)** Boxplot distributions of optimal growth temperatures (T_{opt}) and maximum temperatures of growth (T_{max}) across all 18 species. **(c)** Boxplot distribution of growth activation energy, or temperature dependence ($E_a{}^{\mu}$), across all 18 species (see Appendix B Table.2). The bold horizontal line corresponds to the median value, the top and bottom of the box correspond to

the 75th and 25th percentiles and the whiskers extend to the largest and smallest values no greater or less than 1.5 $\times$ the interquartile range, beyond which the points are plotted as outliers.

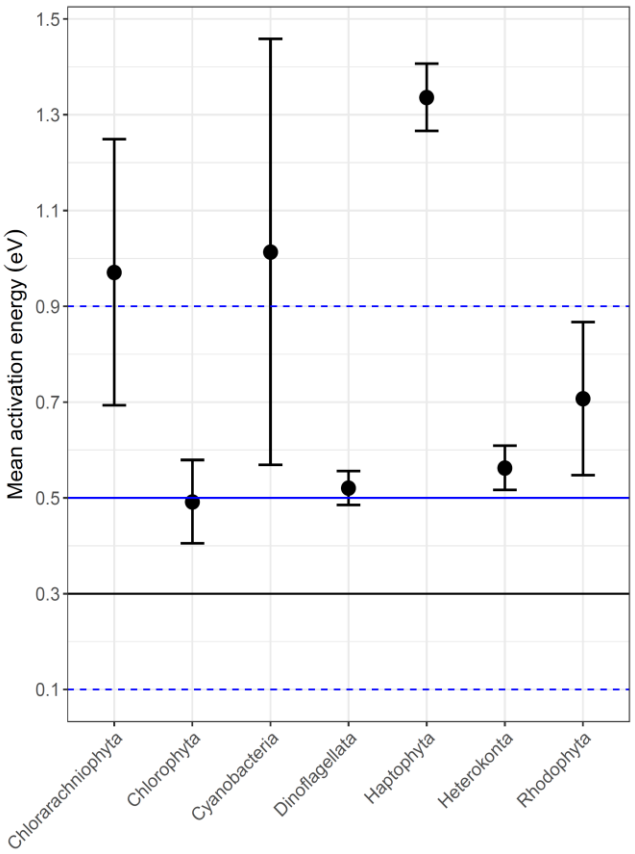

Appendix B: Figure.2 A scatter plot to demonstrate the variance in average activation energy across the seven phyla (or functional groups) represented in this study, and how they differ from our across-species estimate of activation energy. For each group the mean was calculated from the species level activation energies derived from non-linear mixed effects modelling (see Appendix B Table.2 and Figure.1). Datapoints represent the calculated mean, and error bars denote standard error of the mean; for chlorarachniophyta n = 3, chlorophyta n = 3, cyanobacteria n = 2, dinoflagellata n = 2, haptophyta n = 2, heterokonta n = 3 and rhodophyta n = 3. The bold horizontal blue line represents derived the across-species activation energy of 0.5eV, with the dashed blue lines represent the lower and upper 95% confidence intervals. The black horizontal line represents the Eppley coefficient.

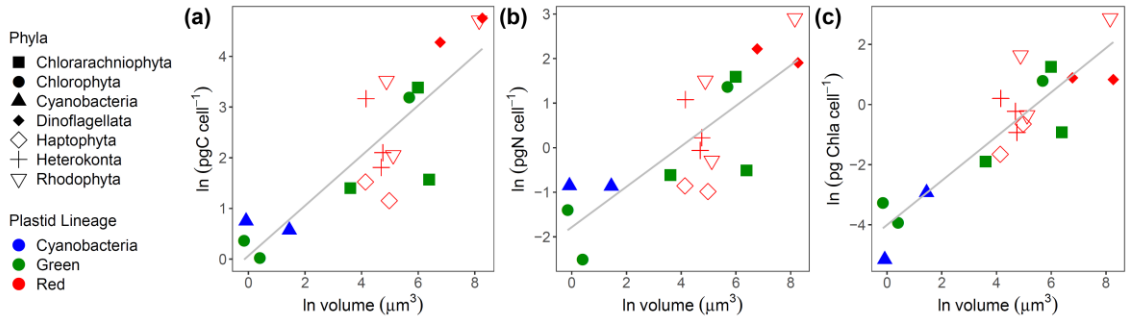

Appendix B: Figure.3 (a) a scatterplot of natural logarithm picograms of carbon per cell against natural logarithm mean cell volume. Linear mixed effects modelling, with random effect of phyla on the intercept of the response, found this relationship to be significant ($\chi^2 = 21.0 \;\; p < 0.001$), returning a sloping coefficient of 0.49 (see Appendix B Table.8), implying a sub-linear relationship whereby concentration of carbon per unit volume decreases with greater cell size. (b) similarly, for picograms of nitrogen per cell we found a significant correlation with volume, returning a sloping coefficient of 0.45 ($\chi^2 = 17.25 \;\; p < 0.001$) (c) finally, we found a significant correlation between picograms chlorophyll *a* and volume with a sloping coefficient of 0.74 ($\chi^2 = 27.37, \; p < 0.001$).

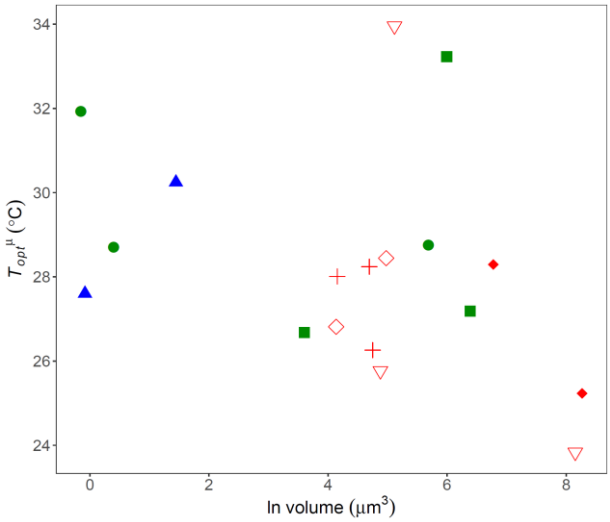

Appendix B: Figure.4 A scatter plot of optimal growth temperature, $T_{opt}{}^{\mu}$, against natural logarithm mean cell volume. Though it could be suggested there is a negative correlation we did not find this to be significant following linear mixed effects modelling ($\chi^2 = 2.22, \;\; p = 0.136,$ see Appendix B Table.9), which encompassed random effect of phyla on the intercept of the response. For a figure legend of the data points, and their respective phylogenetic groups, see Appendix B Figure.3.

Appendix C (for Chapter 4)

Adaptation of marine phytoplankton to warming; a comparative experimental study across three ecologically relevant taxa

Appendix C: Tables

		estimate	lower	upper
Ostreococcus tauri	$E_a{}^{\mu}$	0.08	-0.02	0.18
	$E_h{}^{\mu}$	5.81	3.85	7.78
	$ln.\mu(T_c)$	0.02	-0.02	0.07
	$T_h{}^{\mu}$	305.62	305.14	306.09
	$T_{opt}{}^{\mu}$	26.69	n/a	n/a
	$exp(bT_{opt}{}^{\mu})$	1.06	n/a	n/a
	$0.5(bT_{opt}{}^{\mu})$	33.00	n/a	n/a
Phaeodactylum tricornutum	$E_a{}^{\mu}$	0.12	-0.23	0.47
	$E_h{}^{\mu}$	11.14	6.12	16.16
	$ln.\mu(T_c)$	-0.62	-0.75	-0.50
	$T_h{}^{\mu}$	300.30	299.71	300.90
	$T_{opt}{}^{\mu}$	24.05	n/a	n/a
	$exp(bT_{opt}{}^{\mu})$	0.55	n/a	n/a
	$0.5(bT_{opt}{}^{\mu})$	27.00	n/a	n/a
***Synechococcus* sp.**	$E_a{}^{\mu}$	0.68	0.55	0.80
	$E_h{}^{\mu}$	7.72	5.88	9.55
	$ln.\mu(T_c)$	-0.66	-0.70	-0.61
	$T_h{}^{\mu}$	302.12	301.75	302.49
	$T_{opt}{}^{\mu}$	26.60	n/a	n/a
	$exp(bT_{opt}{}^{\mu})$	0.71	n/a	n/a
	$0.5(bT_{opt}{}^{\mu})$	30.00	n/a	n/a

Appendix C: Table.1 Pre-clonal thermal performance parameters for each species, with lower and upper 95% confidence intervals (see Figure.4.2, Chapter 4). $E_a{}^{\mu}$ = growth activation energy (in eV), $E_h{}^{\mu}$ = growth deactivation energy (in eV), $ln.\mu(T_c)$ = natural logarithm growth rate at the reference temperature, where T_c = 22ºC, $T_h{}^{\mu}$ = the approximate temperature where half the enzymes have become non-functional (in Kelvin), $T_{opt}{}^{\mu}$ = the estimate of optimal growth temperature (in ºC), $exp(bT_{opt}{}^{\mu})$ = the growth rate at $T_{opt}{}^{\mu}$ (d^{-1}) and $0.5(bT_{opt}{}^{\mu})$ = the identified supra-optimal temperature (in ºC) where growth rates are approximately 50% of $exp(bT_{opt}{}^{\mu})$.

(1) formula = μ ~ treatment + s(days, by = treatment, bs = "cr"), random = ~(1 |replicate)

	Model	Intercept	Treatment	s(day of experiment)	df	logLik	AICc	Δ AICc	Weight
Ostreococcus	**4 (full)**	**1.05**	**+**	**+**	**8**	**169.00**	**-321.5**	**0.00**	**1**
	3	0.74		+	7	143.54	-272.7	48.80	0
	2	1.05	+		4	136.84	-265.5	55.97	0
	1	0.74			3	111.63	-217.2	104.34	0
Synechococcus	**4 (full)**	**0.33**	**+**	**+**	**8**	**325.81**	**-635.1**	**0.00**	**0.95**
	3	0.31		+	7	321.89	-629.4	5.74	0.05
	2	0.31			3	142.11	-278.1	357.01	0
	1	0.33	+		4	141.64	-275.1	360.00	0
Phaeodactylum	**4 (full)**	**0.58**	**+**	**+**	**8**	**133.97**	**-251.4**	**0.00**	**1**
	3	0.21		+	7	109.70	-205	46.41	0
	2	0.58	+		4	105.36	-202.6	48.83	0
	1	0.22			3	80.97	-155.8	95.55	0

(2) formula = ln(population size) ~ treatment + s(days, by = treatment, bs = "cr"), random = ~(1 |replicate)

	Model	Intercept	Treatment	s(day of experiment)	df	logLik	AICc	Δ AICc	Weight
Ostreococcus	**4 (full)**	**14.33**	**+**	**+**	**8**	**-492.13**	**1000.7**	**0.00**	**1**
	3	12.26		+	7	-516.92	1048.2	47.48	0
	2	14.33	+		4	-524.97	1058.1	57.34	0
	1	12.25			3	-549.58	1105.2	105.51	0
Synechococcus	**4 (full)**	**13.84**	**+**	**+**	**8**	**-351.02**	**718.5**	**0.00**	**0.97**
	3	13.66		+	7	-355.51	725.4	6.88	0.03
	2	13.84	+		4	-543.97	1096.1	377.57	0
	1	13.66			3	-546.04	1098.2	379.65	0
Phaeodactylum	**4 (full)**	**13.35**	**+**	**+**	**8**	**-269.71**	**556**	**0.00**	**1**
	3	10.38		+	7	-299.94	614.3	58.33	0
	2	13.42	+		4	-418.62	845.4	289.43	0
	1	10.5			3	-448.78	903.6	347.69	0

(3) formula = ln(cell volume) ~ treatment + s(days, by = treatment, bs = "cr"), random = ~(1 |replicate)

	Model	Intercept	Treatment	s(day of experiment)	df	logLik	AICc	Δ AICc	Weight
Ostreococcus	**4 (full)**	**0.92**	**+**	**+**	**8**	**-23.79**	**64.1**	**0.00**	**1**
	3	1.42		+	7	-41.52	97.4	33.35	0
	2	0.92	+		4	-135.61	279.4	215.30	0
	1	1.42			3	-153.40	312.9	248.82	0
Synechococcus	**4 (full)**	**-1.94**	**+**	**+**	**8**	**-6.57**	**29.6**	**0.00**	**1**
	3	-1.28		+	7	-29.93	74.2	44.61	0
	2	-1.94	+		4	-65.47	139.1	109.46	0
	1	-1.28			3	-88.91	183.9	154.29	0

Appendix C: Table.2 Model selection for generalised additive mixed effects models (GAMMs) fitted to (1) specific growth rate data (2) natural logarithm population size data and (3) natural logarithm cell volume estimates for each of the taxa. The GAMMs were used to test primarily for differences in the trajectories of each of the above over the course of the experiment. In each of the models we investigated the effect of treatment on the overall intercept of the response, as well as the shape of the trajectory, s(day of experiment). Random effect of replicate was also included for its effect on intercept only. Model structures were compared using sample-size corrected AIC scores (AICc), where ΔAICc is the difference in AICc score for each model relative to the model structure with the lowest AICc score; the best model is highlighted in bold.

Treatment	replicate	E_a^{μ}	lower	upper	E_h^{μ}	lower	upper	$ln.\mu(T_c)$	lower	upper	T_h^{μ}	lower	upper	T_{opt}^{μ}	$ln(bT_{opt}^{\mu})$
20	1	**0.90**	0.41	1.39	**3.18**	1.82	4.54	**-0.34**	-0.64	-0.04	**302.92**	298.69	307.14	**27.48**	**-0.03**
20	2	**0.93**	0.36	1.50	**2.58**	1.83	3.32	**-0.01**	-0.42	0.41	**301.13**	295.76	306.50	**26.25**	**0.06**
20	3	**0.56**	0.28	0.84	**4.80**	3.03	6.58	**-0.28**	-0.40	-0.15	**305.40**	303.83	306.96	**28.89**	**0.10**
20	4	**0.93**	0.33	1.53	**2.64**	1.19	4.09	**-0.28**	-0.72	0.17	**301.91**	295.62	308.20	**26.96**	**-0.11**
20	5	**0.70**	0.35	1.06	**4.00**	2.22	5.79	**-0.27**	-0.47	-0.08	**304.22**	301.58	306.86	**28.02**	**0.09**
20	6	**0.94**	0.52	1.35	**3.19**	2.32	4.05	**-0.14**	-0.40	0.12	**302.05**	298.78	305.33	**26.76**	**0.10**
	Mean	**0.83**	0.56	1.10	**3.27**	2.46	4.09	**-0.25**	-0.41	-0.08	**303.08**	300.78	305.38	**27.36**	**0.04**
33	1	**0.69**	0.26	1.11	**2.66**	0.96	4.36	**-0.53**	-0.81	-0.25	**304.56**	299.36	309.76	**28.27**	**-0.27**
33	2	**0.65**	0.06	1.23	**2.24**	0.92	3.57	**-0.17**	-0.62	0.28	**303.19**	295.14	311.24	**26.87**	**-0.10**
33	3	**0.39**	0.14	0.65	**3.72**	0.25	7.19	**-0.23**	-0.37	-0.09	**307.21**	304.81	309.61	**29.46**	**0.04**
33	4	**0.59**	-0.03	1.21	**2.11**	-0.21	4.43	**-0.51**	-0.99	-0.02	**305.24**	294.80	315.69	**28.54**	**-0.33**
33	5	**0.47**	0.35	0.59	**5.41**	3.21	7.61	**-0.40**	-0.47	-0.33	**307.00**	306.18	307.82	**30.36**	**0.01**
33	6	**0.42**	0.28	0.56	**3.12**	1.95	4.28	**-0.36**	-0.44	-0.28	**306.39**	304.83	307.94	**28.51**	**-0.15**
	Mean	**0.50**	0.29	0.71	**3.03**	1.47	4.59	**-0.39**	-0.52	-0.27	**306.11**	303.71	308.52	**28.72**	**-0.13**

Appendix C: Table.3 Thermal tolerance parameters for both the control and warmed replicates of *Ostreococcus tauri*, with lower and upper 95% confidence intervals (see Figure.4.5a, Chapter 4). E_a^{μ} = growth activation energy (in eV), E_h^{μ} = growth deactivation energy (in eV), $ln.\mu(T_c)$ = natural logarithm growth rate at the reference temperature, where T_c = 22ºC, T_h^{μ} = the approximate temperature where half the enzymes have become non-functional (in Kelvin), T_{opt}^{μ} = the estimate of optimal growth temperature (in ºC), $ln(bT_{opt}^{\mu})$ = the natural logarithm transformed growth rate at T_{opt}^{μ} (d^{-1}). The above estimates were derived by fitting the Sharpe-Schoolfield model to thermal tolerance data for each treatment specific replicate using non-linear least squares regression. This process was repeated for the average response across all replicates (see Figure.4.5a, Chapter 4).

Treatment	rep	E_a^{μ}	lower	upper	E_h^{μ}	lower	upper	$ln.\mu(T_c)$	lower	upper	T_h^{μ}	lower	upper	T_{opt}^{μ}	$ln(bT_{opt}^{\mu})$
20	1	**2.08**	0.47	3.68	**12.47**	-1.38	26.31	**-1.72**	-2.30	-1.15	**299.55**	297.41	301.69	**25.40**	**-0.98**
20	2	**2.15**	0.05	4.24	**16.98**	-4.94	38.90	**-1.73**	-2.50	-0.97	**299.86**	297.94	301.78	**25.83**	**-0.79**
20	3	**2.17**	0.68	3.67	**25.53**	10.60	40.47	**-1.76**	-2.31	-1.21	**299.89**	299.08	300.71	**26.03**	**-0.70**
20	4	**1.58**	0.66	2.49	**21.49**	10.89	32.09	**-1.61**	-1.95	-1.28	**300.02**	299.35	300.68	**25.95**	**-0.87**
20	5	**1.53**	0.80	2.26	**16.03**	8.04	24.01	**-1.53**	-1.79	-1.26	**299.92**	299.19	300.64	**25.68**	**-0.89**
20	6	**2.97**	0.45	5.49	**9.00**	1.06	16.95	**-1.54**	-2.49	-0.60	**298.42**	294.58	302.26	**24.67**	**-0.90**
	Mean	**1.98**	0.78	3.18	**17.35**	5.19	29.52	**-1.69**	-2.12	-1.25	**299.82**	298.77	300.88	**25.76**	**-0.83**
30	1	**1.18**	0.33	2.02	**7.38**	-10.32	25.08	**-1.63**	-1.97	-1.29	**303.55**	300.77	306.32	**28.62**	**-0.79**
30	2	**1.15**	0.33	1.97	**20.16**	2.66	37.67	**-1.75**	-2.16	-1.33	**303.13**	302.15	304.10	**28.88**	**-0.77**
30	3	**1.35**	0.52	2.17	**16.90**	0.44	33.35	**-1.92**	-2.34	-1.50	**303.04**	301.88	304.21	**28.75**	**-0.82**
30	4	**1.29**	-1.73	4.30	**5.58**	-20.27	31.43	**-1.77**	-2.87	-0.67	**302.66**	289.82	315.50	**27.82**	**-1.05**
30	5	**0.81**	0.38	1.24	**16.95**	6.73	27.17	**-1.57**	-1.79	-1.35	**303.22**	302.58	303.86	**28.68**	**-0.91**
30	6	**1.89**	1.14	2.63	**5.77**	3.12	8.41	**-1.65**	-1.92	-1.38	**301.13**	298.67	303.58	**27.00**	**-0.81**
	Mean	**1.20**	0.50	1.90	**11.65**	-1.67	24.96	**-1.74**	-2.07	-1.41	**303.00**	301.49	304.52	**28.39**	**-0.85**

Appendix C: Table 4 Thermal tolerance parameters for both the control and warmed replicates of *Synechococcus* sp. with lower and upper 95% confidence intervals (see Figure.4.5a, Chapter 4). E_a^{μ} = growth activation energy (in eV), E_h^{μ} = growth deactivation energy (in eV), $ln.\mu(T_c)$ = natural logarithm growth rate at the reference temperature, where T_c = 22ºC, T_h^{μ} = the approximate temperature where half the enzymes have become non-functional (in Kelvin), T_{opt}^{μ} = the estimate of optimal growth temperature (in ºC), $ln(bT_{opt}^{\mu})$ = the natural logarithm transformed growth rate at T_{opt}^{μ} (d^{-1}). The above estimates were derived by fitting the Sharpe-Schoolfield model to thermal tolerance data for each treatment specific replicate using non-linear least squares regression. This process was repeated for the average response across all replicates (see Figure.4.5f, Chapter 4).

Model	Df	logLik	AIC	χ^2	p
Ostreococcus tauri: Figure.4.5b					
$\boldsymbol{T_{opt}}^{\boldsymbol{\mu}}$ **~ T + (1|replicate)**	**4**	**-14.04**	**36.08**		
${T_{opt}}^{\mu}$ ~ 1 + (1|replicate)	3	-18.68	43.36	**9.27**	**0.002**
Ostreococcus tauri: Figure.4.5c					
ln $\boldsymbol{b({T_{opt}}^{\mu})}$ **~ T + (1|replicate)**	**4**	**12.03**	**-16.05**		
ln $b({T_{opt}}^{\mu})$ ~ 1 + (1|replicate)	3	6.74	-7.48	**10.56**	**0.001**
Ostreococcus tauri: Figure.4.5d					
$\boldsymbol{{E_a}^{\mu}}$ **~ T + (1|replicate)**	**4**	**8.98**	**-9.95**		
${E_a}^{\mu}$ ~ 1 + (1|replicate)	3	2.58	0.84	**12.79**	**<0.001**
Ostreococcus tauri: Figure.4.5e					
${E_h}^{\mu}$ ~ T + (1|replicate)	4	-14.79	37.58		
${E_h}^{\mu}$ ~ 1 + (1|replicate)	3	-14.96	35.92	0.34	0.560
Synechococcus sp.: Figure.4.5g					
$\boldsymbol{{T_{opt}}^{\mu}}$ **~ T + (1|replicate)**	**4**	**-8.62**	**25.24**		
${T_{opt}}^{\mu}$ ~ 1 + (1|replicate)	3	-21.62	49.25	**26.01**	**<0.001**
Synechococcus sp.: Figure.4.5h					
ln $b({T_{opt}}^{\mu})$ ~ T + (1|replicate)	4	11.54	-15.07		
ln $b({T_{opt}}^{\mu})$ ~ 1 + (1|replicate)	3	11.53	-17.05	0.020	0.887
Synechococcus sp.: Figure.4.5i					
$\boldsymbol{{E_a}^{\mu}}$ **~ T + (1|replicate)**	**4**	**-3.17**	**14.33**		
${E_a}^{\mu}$ ~ 1 + (1|replicate)	3	-10.30	26.60	**14.27**	**<0.001**
Synechococcus sp.: Figure.4.5j					
${E_h}^{\mu}$ ~ T + (1|replicate)	4	-37.47	82.94		
${E_h}^{\mu}$ ~ 1 + (1|replicate)	3	-38.84	83.69	2.75	0.097

Appendix C: Table.5 A summary of the linear mixed effects modelling to test for the significance of the effect of treatment (T, i.e. growth temperature) on the returned Sharpe-Schoolfield parameters across the replicates of each species (see Figure.4.5 b-e and g-j, Chapter 4). Replicate was therefore included as a random effect on the intercept of the response. In each case the most complex model, which included the effect of treatment (T) was compared with a null hypothesis using ANOVA. Bold text indicates a significant difference in the models, and thus a significant effect of treatment.

Model	Df	logLik	AIC	χ^2	p
Ostreococcus tauri 20°C assay: Figure.4.8a					
μ ~ T + (1|replicate)	4	16.49	-24.98		
μ ~ 1 + (1|replicate)	3	16.48	-26.97	0.01	0.904
Ostreococcus tauri 33°C assay: Figure.4.8a					
μ ~ T + (1|replicate)	**4**	**16.02**	**-24.05**		
μ ~ 1 + (1|replicate)	3	7.28	-8.56	**17.49**	**<0.001**
Synechococcus sp. 20°C assay: Figure.4.8b					
μ ~ T + (1|replicate)	**4**	**30.90**	**-53.80**		
μ ~ 1 + (1|replicate)	3	24.62	-43.24	**12.56**	**<0.001**
Synechococcus sp. 30°C assay: Figure.4.8b					
μ ~ T + (1|replicate)	**4**	**22.67**	**-37.34**		
μ ~ 1 + (1|replicate)	3	2.52	0.96	**40.29**	**<0.001**

Appendix C: Table.6 A summary of the linear mixed effects modelling to test for the significance of the effect of treatment on the specific growth rate at each

reciprocal transplant assay temperature for each species (see Figure.4.8, Chapter 4).

Model	Df	logLik	AIC	χ^2	p
Ostreococcus tauri 20°C assay: Figure.4.7a					
P_{max} ~ T + (1|replicate)	**4**	**9.73**	**-11.47**		
P_{max} ~ 1 + (1|replicate)	3	-4.17	14.34	**27.80**	**<0.001**
Ostreococcus tauri 33°C assay: Figure.4.7a					
P_{max} ~ T + (1|replicate)	**4**	**7.29**	**-6.57**		
P_{max} ~ 1 + (1|replicate)	3	-4.82	15.65	**24.22**	**<0.001**
Ostreococcus tauri 20°C assay: Figure.4.7b					
R ~ T + (1|replicate)	**4**	**22.75**	-37.51		
R ~ 1 + (1|replicate)	3	15.15	-24.30	**15.21**	**<0.001**
Ostreococcus tauri 33°C assay: Figure.4.7b					
R ~ T + (1|replicate)	**4**	**26.74**	**-45.49**		
R ~ 1 + (1|replicate)	3	12.56	-19.11	**28.38**	**<0.001**
Ostreococcus tauri 20°C assay: Figure.4.7c					
CUE ~ T + (1|replicate)	4	19.64	-31.29		
CUE ~ 1 + (1|replicate)	3	19.34	-32.67	0.61	0.433
Ostreococcus tauri 33°C assay: Figure.4.7c					
CUE ~ T + (1|replicate)	4	32.52	-57.04		
CUE ~ 1 + (1|replicate)	3	31.69	-57.37	1.67	0.197
Synechococcus sp. 20°C assay: Figure.4.7d					
P_{max} ~ T + (1|replicate)	**4**	**-10.07**	**28.15**		
P_{max} ~ 1 + (1|replicate)	3	-14.16	34.32	**8.17**	**0.004**
Synechococcus sp. 30°C assay: Figure.4.7d					
P_{max} ~ T + (1|replicate)	4	**-14.81**	**37.63**		
P_{max} ~ 1 + (1|replicate)	3	-17.42	40.83	**5.20**	**0.023**
Synechococcus sp. 20°C assay: Figure.4.7e					
R ~ T + (1|replicate)	**4**	**6.70**	**-5.41**		
R ~ 1 + (1|replicate)	3	-2.83	11.65	**19.06**	**<0.001**
Synechococcus sp. 30°C assay: Figure.4.7e					
R ~ T + (1|replicate)	4	**1.24**	**5.52**		
R ~ 1 + (1|replicate)	3	-6.13	18.26	**14.74**	**<0.001**
Synechococcus sp. 20°C assay: Figure.4.7f					
CUE ~ T + (1|replicate)	**4**	**15.61**	**-23.21**		
CUE ~ 1 + (1|replicate)	3	7.56	-9.12	**16.09**	**<0.001**
Synechococcus sp. 30°C assay: Figure.4.7f					
CUE ~ T + (1|replicate)	**4**	**12.26**	**-16.51**		
CUE ~ 1 + (1|replicate)	3	8.44	-10.88	**7.63**	**0.006**

Appendix C: Table.7 A summary of the linear mixed effects modelling to test for the significance of the effect of treatment on P_{max} (gross photosynthesis), R (dark respiration), and CUE (carbon-use efficiency) rate at each reciprocal transplant assay temperature for each species (see Figure.4.7, Chapter 4). Replicate was included as a random effect on the intercept of the response. In each case the most complex model, including the effect of treatment (T) was compared with a null hypothesis using ANOVA. Bold text indicates a significant difference in the models, and thus a significant effect of treatment.

	Treatment	rep	Volume (µm^3)	pg Chl$a$ $cell^{-1}$	pgC $cell^{-1}$	pgN $cell^{-1}$	C:N	M
Ostreococcus tauri	20	1	1.41	0.023	0.143	0.027	6.25	0.76
	20	2	1.35	0.026	0.119	0.023	6.02	0.75
	20	3	1.08	0.025	0.120	0.019	7.34	0.79
	20	4	1.54	0.020	0.132	0.025	6.12	0.75
	20	5	1.47	0.024	0.097	0.019	5.92	0.75
	20	6	1.39	0.022	0.123	0.023	6.29	0.76
	33	1	4.56	0.028	0.382	0.061	7.25	0.78
	33	2	7.62	0.028	0.530	0.091	6.82	0.77
	33	3	7.59	0.022	0.506	0.086	6.87	0.77
	33	4	3.56	0.027	0.337	0.059	6.62	0.77
	33	5	6.53	0.022	0.522	0.090	6.77	0.77
	33	6	5.47	0.018	0.579	0.093	7.25	0.78
Synechococcus sp.	20	1	0.14	0.006	0.043	0.009	5.83	0.74
	20	2	0.14	0.004	0.080	0.016	5.74	0.74
	20	3	0.15	0.005	0.065	0.013	5.82	0.74
	20	4	0.13	0.003	0.120	0.024	5.95	0.75
	20	5	0.14	0.006	0.079	0.015	6.11	0.75
	20	6	0.13	0.008	0.081	0.015	6.12	0.75
	30	1	0.33	0.008	0.293	0.062	5.49	0.73
	30	2	0.40	0.017	0.184	0.037	5.86	0.75
	30	3	0.52	0.026	0.196	0.040	5.76	0.74
	30	4	0.42	0.018	0.160	0.032	5.93	0.75
	30	5	0.41	0.011	0.221	0.046	5.56	0.74
	30	6	0.54	0.016	0.255	0.052	5.69	0.74

Appendix C: Table.8 Sub-cellular phenotypic traits of each replicate from each treatment, including: estimated volume, mean *pg* Chlorophyll *a* per cell, *pg* carbon (*C*) and nitrogen (*N*) per cell, carbon:nitrogen ratio (C:N), in moles, and M, the estimated carbon assimilation quotient for CO_2:O_2.

Model	Df	logLik	AIC	χ^2	p
Ostreococcus tauri, pgC $cell^{-1}$: Appendix C Figure.4a					
pgC $cell^{-1}$ ~ T + (1|replicate)	**4**	**16.38**	**-24.75**		
pgC $cell^{-1}$ ~ 1 + (1|replicate)	3	11.57	-17.14	**9.61**	**0.002**
Ostreococcus tauri, pgN $cell^{-1}$: Appendix C Figure.4b					
pgN $cell^{-1}$ ~ T + (1|replicate)	**4**	**38.05**	**-68.10**		
pgN $cell^{-1}$ ~ 1 + (1|replicate)	3	33.27	-60.54	**9.56**	**0.002**
Ostreococcus tauri, pgChl$a$ $cell^{-1}$: Appendix C Figure.4c					
pgChl$a$ $cell^{-1}$ ~ T + (1|replicate)	4	53.38	-98.76		
pgChl$a$ $cell^{-1}$ ~ 1 + (1|replicate)	3	53.25	-100.51	0.254	0.615
Synechococcus sp., pgC $cell^{-1}$: Appendix C Figure.4d					
pgC $cell^{-1}$ ~ T + (1|replicate)	**4**	**23.01**	**-38.02**		
pgC $cell^{-1}$ ~ 1 + (1|replicate)	3	18.95	-31.90	**8.13**	**0.004**
Synechococcus sp., pgN $cell^{-1}$: Appendix C Figure.4e					
pgN $cell^{-1}$ ~ T + (1|replicate)	**4**	**41.03**	**-74.06**		
pgN $cell^{-1}$ ~ 1 + (1|replicate)	3	37.08	-68.16	**7.89**	**0.005**
Synechococcus sp., pgChl$a$ $cell^{-1}$: Appendix C Figure.4f					
pgChl$a$ $cell^{-1}$ ~ T + (1|replicate)	**4**	**48.74**	**-89.48**		
pgChl$a$ $cell^{-1}$ ~ 1 + (1|replicate)	3	45.48	-84.95	**6.53**	**0.011**

Appendix C: Table.9 A summary of the linear mixed effects modelling to test for the significance of the effect of treatment (T, i.e. growth temperature) on per capita carbon (pgC $cell^{-1}$), nitrogen (pgN $cell^{-1}$) and chlorophyll *a* (pgChl$a$ $cell^{-1}$) for each taxa (see Appendix C Figure.4). Replicate was included as a random effect on the intercept of the response. In each case the most complex model, including the effect of treatment (T) was compared with a null hypothesis using ANOVA. Bold text indicates a significant difference in the models, and thus a significant effect of treatment.

Model	Df	logLik	AIC	χ^2	p
Ostreococcus tauri, volume: Figure.4.9a					
$\boldsymbol{cell\ volume}$ **~ T + (1|replicate)**	**4**	**-17.86**	**43.72**		
$cell\ volume$ ~ 1 + (1|replicate)	3	-22.05	50.11	**8.39**	**0.004**
Ostreococcus tauri, pgC μm^{-3}: Figure.4.9b					
pgC μm^{-3}~ T + (1|replicate)	4	34.39	-60.77		
pgC μm^{-3} ~ 1 + (1|replicate)	3	34.03	-62.06	0.716	0.397
Ostreococcus tauri, pgN μm^{-3}: Figure.4.9c					
pgN μm^{-3}~ T + (1|replicate)	4	57.61	-107.22		
pgNμm^{-3} ~ 1 + (1|replicate)	3	55.80	-105.59	3.63	0.057
Ostreococcus tauri, pgChl$a$ μm^{-3}: Figure.4.9d					
pgChl$a$ μm^{-3} ~ T + (1|replicate)	4	64.49	-120.98		
pgChl$a$ μm^{-3} ~ 1 + (1|replicate)	3	62.72	-119.44	3.54	0.059
Ostreococcus tauri, $C:N$: Figure.4.9e					
$\boldsymbol{C:N}$ **~ T + (1|replicate)**	**4**	**-5.18**	**18.35**		
$C:N$ ~ 1 + (1|replicate)	3	-7.46	20.93	**4.58**	**0.032**
Synechococcus sp., volume: Figure.4.9f					
$\boldsymbol{cell\ volume}$ **~ T + (1|replicate)**	**4**	**18.52**	**-29.04**		
$cell\ volume$ ~ 1 + (1|replicate)	3	13.70	-21.40	**9.64**	**0.002**
Synechococcus, sp. pgC μm^{-3}: Figure.4.9g					
pgC μm^{-3}~ T + (1|replicate)	4	3.78	0.45		
pgC μm^{-3} ~ 1 + (1|replicate)	3	3.69	-1.37	0.22	0.641
Synechococcus sp., pgN μm^{-3}: Figure.4.9h					
pgN μm^{-3}~ T + (1|replicate)	4	22.62	-37.24		
pgNμm^{-3} ~ 1 + (1|replicate)	3	22.60	-39.19	0.046	0.831
Synechococcus sp., pgChl$a$ μm^{-3}: Figure.4.9i					
pgChl$a$ μm^{-3} ~ T + (1|replicate)	4	25.72	-43.43		
pgChl$a$ μm^{-3} ~ 1 + (1|replicate)	3	25.71	-45.43	0.01	0.924
Synechococcus sp., $C:N$: Figure.4.9j					
$\boldsymbol{C:N}$ **~ T + (1|replicate)**	**4**	**5.70**	**-3.40**		
$C:N$ ~ 1 + (1|replicate)	3	3.70	-1.40	**4.00**	**0.045**

Appendix C: Table.10 A summary of the linear mixed effects modelling to test for the significance of the effect of treatment (T, i.e. growth temperature) on cell volume, per unit volume carbon (pgC μm^{-3}), nitrogen (pgN μm^{-3}), and chlorophyll *a* (pgChl$a$ μm^{-3}), and C:N for each taxa (see Figure.4.9, Chapter 4). Replicate was included as a random effect on the intercept of the response. In each case the most complex model, including the effect of treatment (T) was compared with a null hypothesis using ANOVA. Bold text indicates a significant difference in the models, and thus a significant effect of treatment.

Appendix C: Figures

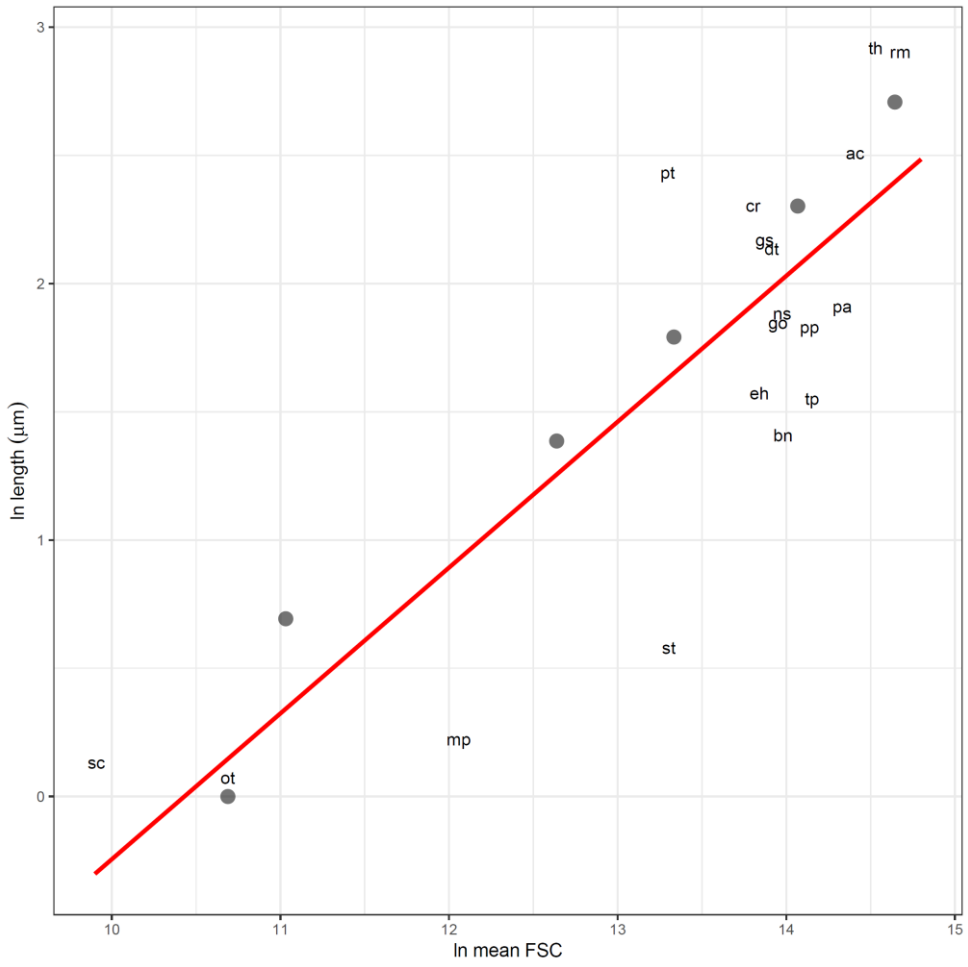

Appendix C: Figure.1 Calibration of natural logarithm FSC to natural logarithm cell length (µm). Grey circles represent calibration beads of known lengths; 1, 2, 4, 6, 10 and 15µm. Text labels refer to 18 different species of marine taxa, with lengths measured and averaged for a minimum of 50 individuals per taxa, where; ac = *A.carterae,* bn = *B.natans,* cr = *C.reptans,* dt = *D.tertiolecta,* eh = *E.huxleyi,* go = *G. oceanica,* gs = *G.stellata,* mp = *M. pusilla,* ns = *Nitzschia sp,* ot = *O. tauri,* pt = *P. tricornutum,* pa = *P. aerugineum,* pp = *P. purpureum,* rm = *R. maculata,* sc = *Synechococcus* sp., st = *Synechocystis* sp., tp = *T. pseudonana and* th = *T. heimii.* Measurements were made using confocal microscopy. The modelled red line represents a linear model fitted to all data points (the 18 taxa and calibration beads combined), this returned an R-squared value of 0.76. The coefficients of the modelled line were then used to derive the conversion factor, to obtain an estimate of cell length: $\ln\ cell\ length(\mu m) = (0.57\ \times \ln FSC) - 5.93.$

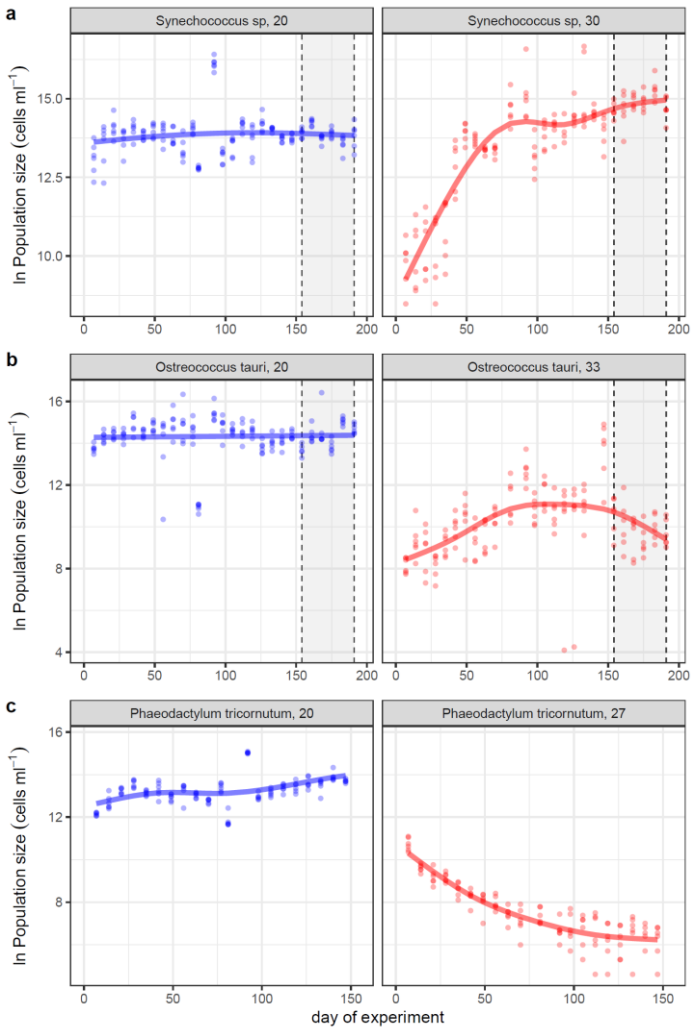

Appendix C: Figure.2 Natural logarithm population size (cells mL^{-1}) projections for each of the taxa at each of their respective treatment temperatures at the mid-log growth phase. Plots on the left present the changes in mid-log cell density at the control temperature for each of the taxa, denoted by blue colouring, plots on the right present the changes in mid-log cell density at the warmed temperature treatment for each of the taxa, denoted by red colouring. The lower of the dashed vertical lines highlight the end of the 22 week experimental period, and the shaded area represents the 5 week period during which all other physiological data was collected, up to the second vertical dashed line at the 27 week mark. Data points represent natural logarithm of mid-log cell density measurements for the 6 biological replicates at each treatment temperature, and the fitted line for each of the treatments represents the best fits of the selected GAMM for each of the taxa (See Methods). There was a significant effect of treatment on both the shape and intercept of the responses for each of the taxa (see Appendix C Table.2). **(a)** The projections for *Synechococcus* sp. **(b)** The projections for *Ostreococcus tauri* **(c)** The projections for *Phaeodactylum tricornutum*. Unlike the other two species, *Phaeodactylum tricornutum* in response to the high temperature demonstrated continuous decline in population size and this made it unfeasible to collect any additional physiological data at the end of the experimental period (hence no shaded region between the 22 and 27 week marks).

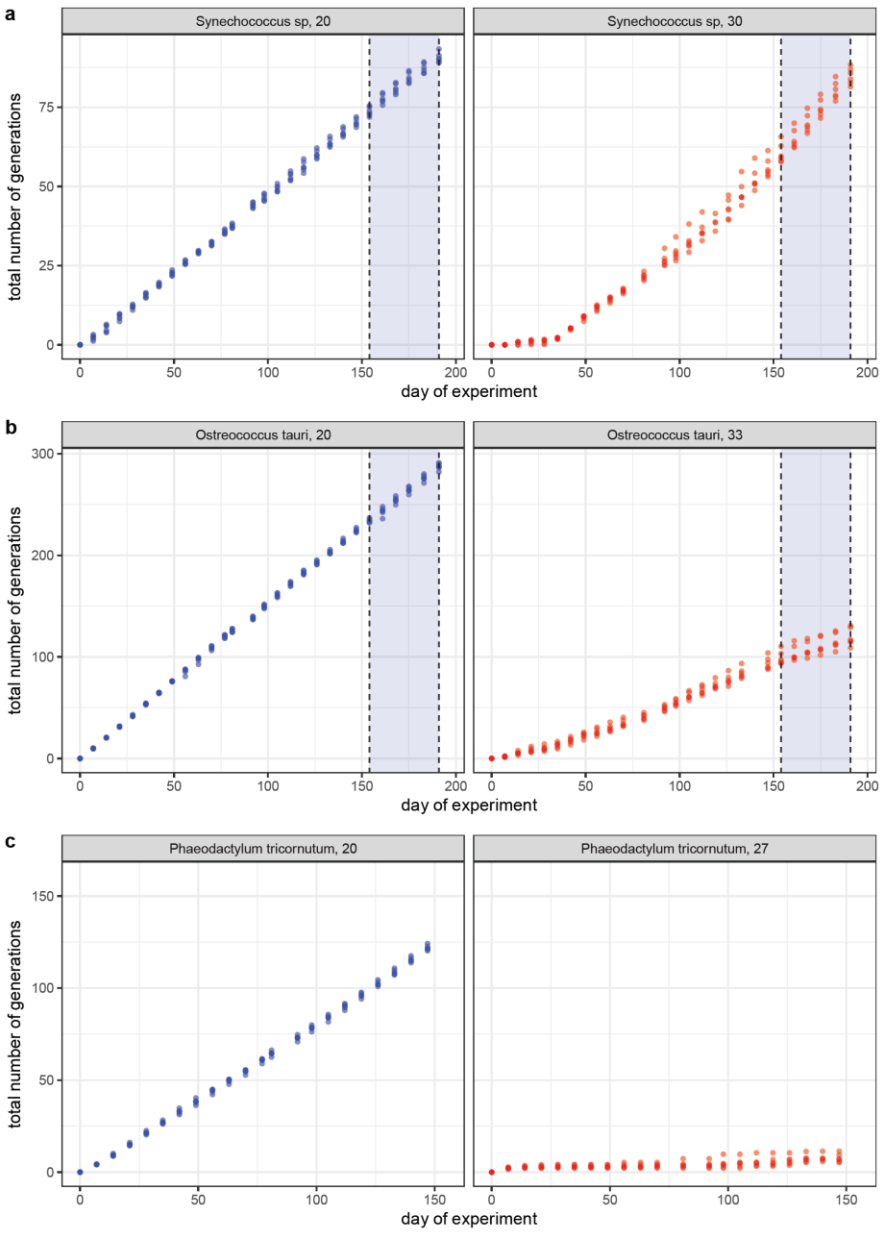

Appendix C: Figure.3 Approximate total number of generations passed throughout the course of the experiment. Plots on the left present the total number of generations passed at the control temperature for each of the taxa, denoted by blue colouring, plots on the right present the total number of generations passed at the warmed temperature treatment for each of the taxa, denoted by red colouring. Data points represent estimates of the total number of generations passed for each of the 6 biological replicates at each treatment temperature. **(a)** The number of generations passed for *Synechococcus* sp. **(b)** The number of generations passed for *Ostreococcus tauri* **(c)** The number of generations passed for *Phaeodactylum tricornutum*. Unlike the other two species, *Phaeodactylum tricornutum* in response to the high temperature demonstrated continuous decline in population size and this made it unfeasible to collect any additional physiological data at the end of the experimental period (hence no shaded region between the 22 and 27 week marks).

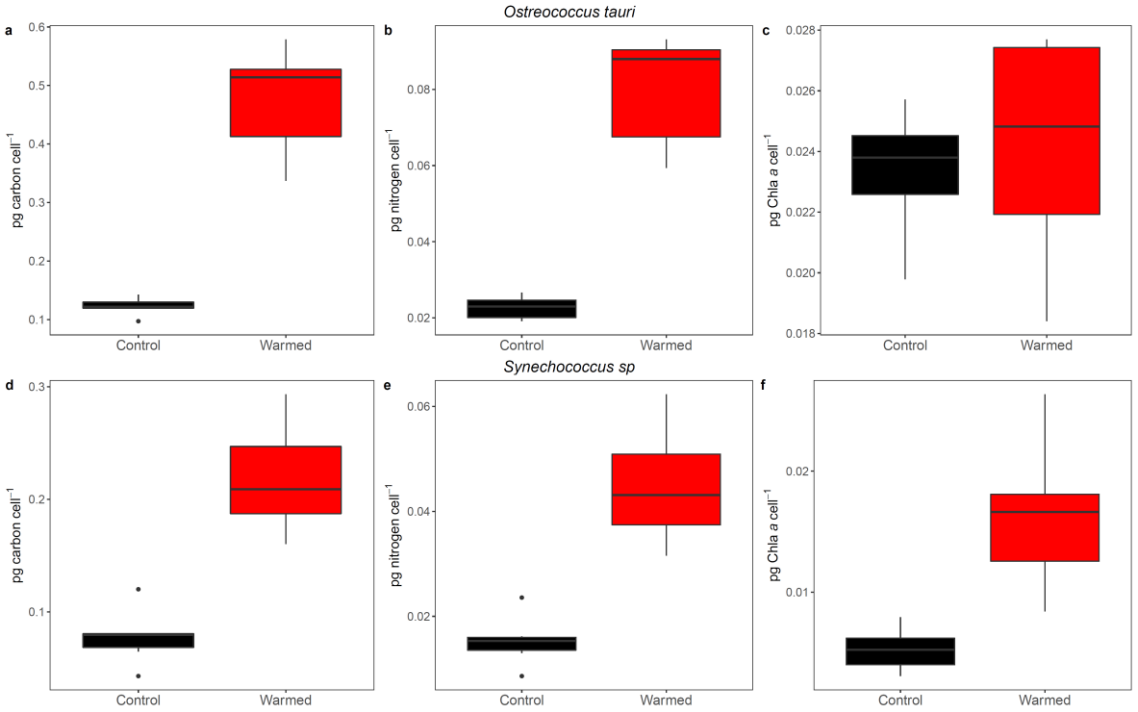

Appendix C: Figure.4 Differences in carbon, nitrogen and chlorophyll *a* per capita between the control and warm adapted strains of both *Ostreococcus tauri* (a – c) and *Synechococcus* sp. (d – f). For both taxa, there is a significant increase in carbon content per cell in the warm adapted replicates (a,d). For both taxa, there is also a significant increase in nitrogen content per cell in the warm adapted replicates (b,e). However there is only a significant increase in the chlorophyll *a* content per cell in the warm adapted *Synechococcus* sp. (f), but for *Ostreococcus tauri* there was no significant difference with the control replicates (c). Tests for significant differences in the traits displayed in this figure are summarised in Appendix C Table.9. For each of the boxes, the bold horizontal line corresponds to the median parameter value, the top and bottom of the box correspond to the 75th and 25th percentiles and the whiskers extend to the largest and smallest values no greater or less than the $1.5 \times$ the interquartile range.

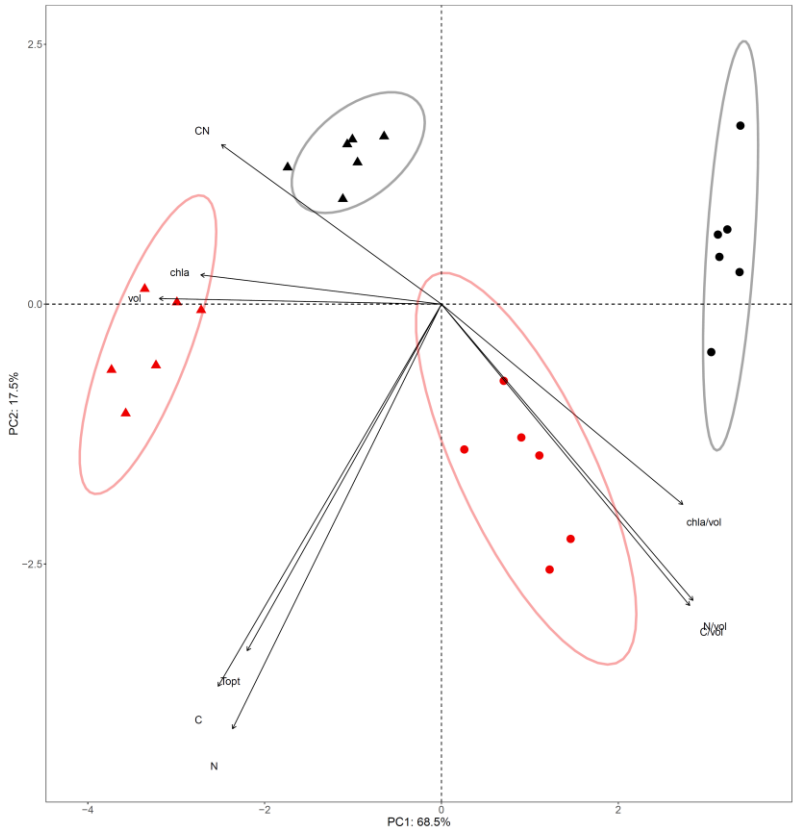

Appendix C: Figure.5 Principal component analysis of the physiological trait data for the control and warm adapted replicates of both *Ostreococcus tauri* and *Synechococcus* sp. Triangles denote *Ostreococcus tauri* biological replicates, and circles denote *Synechococcus* sp. biological replicates, with black and red colouring denoting control and warmed treatments, respectively. The principal component axes are derived from the first two principal components and make up >75% of the total variance in the data. The first, PC1 (68.5% of the variance), returns loading scores of: -0.39 vol, -0.31 CN, -0.32 C, - 0.30 N, -0.34 chla, 0.35 C/vol, 0.36 N/vol, 0.34 chla/vol and -0.27 Topt. The second, PC2 (17.5% of the variance), returns loading scores of: 0.01 vol, 0.19 CN, -0.46 C, - 0.51 N, 0.04 chla, -0.36 C/vol, -0.36 N/vol, -0.24 chla/vol and -0.42 Topt. The loadings for each of the variables included in the analysis are plotted to demonstrate the correlations and covariance of physiological traits, where: vol = estimated cell volume, C = mean $\mathrm{pgC\ cell^{-1}}$, N = mean $\mathrm{pgN\ cell^{-1}}$, chla = mean pg chlorophyll *a* cell^{-1}, Topt = optimal growth temperature, CN = C:N ratio in moles, C/vol = $\mathrm{pgC\ \mu m^{-3}}$, N/vol = $\mathrm{pgN\ \mu m^{-3}}$ and chla/vol = $\mathrm{pg\ chlorophyll\ }a\ \mathrm{\mu m^{-3}}$. The length of each loading vector reflects the combined weighting of each variable in the first two principal components. Here, all loadings were multiplied by a constant for visualisation purposes. Ellipses were plotted as a visual guide to the clustering of the different treatment replicates, and reflect 95% confidence intervals around the centroid of each cluster giving us an indication of whether the treatment replicates can be uniquely identified by the traits included in the PCA. All variables were natural logarithm transformed to normalise the values and therefore not to inflate the variances. The PCA highlights clear differentiation of the two species, as well as their respective control and warmed treatments, in relation to the physiological traits provided.

Bibliography

Allen, A.P., Gillooly, J.F. & Brown, J.H. (2005). Linking the global carbon cycle to individual metabolism. *Funct. Ecol.*, 19, 202–213.

Allen, J.F. & Martin, W. (2007). Evolutionary biology: Out of thin air. *Nature*, 445, 610–612.

Angilletta, M.J., Huey, R.B. & Frazier, M.R. (2010). Thermodynamic Effects on Organismal Performance: Is Hotter Better? *Physiol. Biochem. Zool.*, 83, 197–206.

Angilletta, M.J., Wilson, R.S., Navas, C.A. & James, R.S. (2003). Tradeoffs and the evolution of thermal reaction norms. *Trends Ecol. Evol.*, 18, 234–240.

Ashander, J., Chevin, L.M. & Baskett, M.L. (2016). Predicting evolutionary rescue via evolving plasticity in stochastic environments. *Proc. R. Soc. B Biol. Sci.*, 283.

Atkinson, D. & Sibly, R.M. (1997). Why are organisms usually bigger in colder environments? Making sense of a life history puzzle. *Trends Ecol. Evol.*, 12, 235–239.

Azcón-Bieto, J. & Osmond, C.B. (1983). Relationship between Photosynthesis and Respiration. *Plant Physiol.*, 71, 574–581.

Baker, K.G., Radford, D.T., Evenhuis, C., Kuzhiumparam, U., Ralph, P.J. & Doblin, M.A. (2018). Thermal niche evolution of functional traits in a tropical marine phototroph. *J. Phycol.*

Banavar, J.R., Moses, M.E., Brown, J.H., Damuth, J., Rinaldo, A., Sibly, R.M., *et al.* (2010). A general basis for quarter-power scaling in animals. *Proc. Natl. Acad. Sci.*, 107, 15816–15820.

Banse, K. (1976). Rates of Growth, Respiration and Photosynthesis of Unicellular Algae As Related To Cell Size—a Review. *J. Phycol.*

Banse, K. (1982). Cell volumes, maximal growth rates of unicellular algae and ciliates, and the role of ciliates in the marine pelagial. *Limnol. Oceanogr.*, 27, 1059–1071.

Baranyi, J. & Roberts, T.A. (1994). A dynamic approach to predicting bacterial growth in food. *Int. J. Food Microbiol.*, 23, 277–294.

Barton, A.D., Dutkiewicz, S., Flierl, G., Bragg, J. & Follows, M.J. (2010). Patterns of Diversity in Marine Phytoplankton. *Science*, 327, 1509–1511.

Barton, A.D., Pershing, A.J., Litchman, E., Record, N.R., Edwards, K.F., Finkel, Z. V., *et al.* (2013). The biogeography of marine plankton traits. *Ecol. Lett.*, 16, 522–534.

Barton, S., Jenkins, J., Buckling, A., Schaum, C. & Smirnoff, N. (2018). Universal metabolic constraints on the thermal tolerance of marine phytoplankton. *bioRxiv*, 358002; do.

Behrenfeld, M.J., O'Malley, R.T., Siegel, D.A., McClain, C.R., Sarmiento, J.L., Feldman, G.C., *et al.* (2006). Climate-driven trends in contemporary ocean productivity. *Nature*, 444, 752–755.

Bell, G. (2013). Evolutionary rescue and the limits of adaptation. *Philos. Trans. R. Soc. B Biol. Sci.*, 368, 1–6.

Bell, G. & Gonzalez, A. (2009). Evolutionary rescue can prevent extinction following environmental change. *Ecol. Lett.*, 12, 942–948.

Bernacchi, C.J., Singsaas, E.L., Pimentel, C., Portis, A.R. & Long, S.P. (2001). Improved temperature response functions for models of Rubisco-limited photosynthesis. *Plant, Cell Environ.*, 24, 253–259.

Berry, J. & Bjorkman, O. (1980). Photosynthetic Response and Adaptation to Temperature in Higher Plants. *Annu. Rev. Plant Physiol.*, 31, 491–543.

Bhattacharya, D., Price, D.C., Xin Chan, C., Qiu, H., Rose, N., Ball, S., *et al.* (2013). Genome of the red alga Porphyridium purpureum. *Nat. Commun.*, 4.

Biermann, A. & Engel, A. (2010). Effect of CO2 on the properties and sinking velocity of aggregates of the coccolithophore Emiliania huxleyi. *Biogeosciences*, 7, 1017–1029.

Bissinger, J.E., Montagnes, D.J.S., Sharples, J. & Atkinson, D. (2008). Predicting marine phytoplankton maximum growth rates from temperature: Improving on the Eppley curve using quantile regression. *Limnol. Oceanogr.*, 53, 487–493.

Blanquart, F., Kaltz, O., Nuismer, S.L. & Gandon, S. (2013). A practical guide to measuring local adaptation. *Ecol. Lett.*, 16, 1195–1205.

Bopp, L., Aumont, O., Cadule, P., Alvain, S. & Gehlen, M. (2005). Response of diatoms distribution to global warming and potential implications: A global model study. *Geophys. Res. Lett.*, 32, 1–4.

Bowler, C., Allen, A.E., Badger, J.H., Grimwood, J., Jabbari, K., Kuo, A., *et al.* (2008). The Phaeodactylum genome reveals the evolutionary history of diatom genomes. *Nature*, 456, 239–244.

Boyce, D.G., Lewis, M.R. & Worm, B. (2010). Global phytoplankton decline over the past century. *Nature*, 466, 591–596.

Boyd, P.W., Rynearson, T.A., Armstrong, E.A., Fu, F., Hayashi, K., Hu, Z., *et al.* (2013). Marine Phytoplankton Temperature versus Growth Responses from Polar to Tropical Waters - Outcome of a Scientific Community-Wide Study. *PLoS One*, 8.

Brown, J.H., Gillooly, J.F., Allen, A.P., Savage, V.M. & West, G.B. (2004). Toward a metabolic theory of ecology. *Ecology*, 85, 1771–1789.

Bruland, K.W., Rue, E.L., Smith, G.J. & DiTullio, G.R. (2005). Iron, macronutrients and diatom blooms in the Peru upwelling regime: Brown and blue waters of Peru. *Mar. Chem.*, 93, 81–103.

Capuzzo, E., Lynam, C.P., Barry, J., Stephens, D., Forster, R.M., Greenwood, N., *et al.* (2018). A decline in primary production in the North Sea over 25 years, associated with reductions in zooplankton abundance and fish stock recruitment. *Glob. Chang. Biol.*, 24, e352–e364.

Chen, B., Landry, M.R., Huang, B. & Liu, H. (2012). Does warming enhance the effect of microzooplankton grazing on marine phytoplankton in the ocean? *Limnol. Oceanogr.*, 57, 519–526.

Chen, B. & Laws, E.A. (2017). Is there a difference of temperature sensitivity between marine phytoplankton and heterotrophs? *Limnol. Oceanogr.*, 62, 806–817.

Chisholm, S.W. (1992). Phytoplankton size. In: *Primary Productivity and Biogeochemical Cycles in the Sea*. pp. 213–237.

Chollet, R. & Ogren, W.L. (1975). Regulation of photorespiration in C3 and C4 species. *Bot. Rev.*, 41, 137–179.

Clarke, A. (2003). Costs and consequences of evolutionary temperature adaptation. *Trends Ecol. Evol.*, 18, 573–581.

Collins, M., Knutti, R., Arblaster, J., Dufresne, J.-L., Fichefet, T., Friedlingstein, P., *et al.* (2013). Long-term Climate Change: Projections, Commitments and Irreversibility. *Clim. Chang. 2013 Phys. Sci. Basis. Contrib. Work. Gr. I to Fifth Assess. Rep. Intergov. Panel Clim. Chang.*, 1029–1136.

Collins, S. (2011). Many Possible Worlds: Expanding the Ecological Scenarios in Experimental Evolution. *Evol. Biol.*, 38, 3–14.

Collins, S. & Bell, G. (2004). Phenotypic consequences of 1,000 generations of selection at elevated CO2in a green alga. *Nature*, 431, 566–569.

Courties, C., Vaquer, A., Troussellier, M., Lautier, J., Chrétiennot-Dinet, M.J., Neveux, J., *et al.* (1994). Smallest eukaryotic organism [6]. *Nature*.

Davies, R.B. (1977). Hypothesis Testing when a Nuisance Parameter is Unidentified Under the Alternative. *Biometrika*, 64, 247–254.

Dell, A.I., Pawar, S. & Savage, V.M. (2011). Systematic variation in the temperature dependence of physiological and ecological traits. *Proc. Natl. Acad. Sci.*, 108, 10591–10596.

DeLong, J.P., Okie, J.G., Moses, M.E., Sibly, R.M. & Brown, J.H. (2010). Shifts in metabolic scaling, production, and efficiency across major evolutionary transitions of life. *Proc. Natl. Acad. Sci.*, 107, 12941–12945.

Derelle, E., Ferraz, C., Rombauts, S., Rouze, P., Worden, a. Z., Robbens, S., *et al.* (2006). Genome analysis of the smallest free-living eukaryote Ostreococcus tauri unveils many unique features. *Proc. Natl. Acad. Sci.*, 103, 11647–11652.

Edwards, K.F., Thomas, M.K., Klausmeier, C.A. & Litchman, E. (2012). Allometric scaling and taxonomic variation in nutrient utilization traits and maximum growth rate of phytoplankton. *Limnol. Oceanogr.*, 57, 554–566.

Edwards, K.F., Thomas, M.K., Klausmeier, C.A. & Litchman, E. (2016). Phytoplankton growth and the interaction of light and temperature: A synthesis at the species and community level. *Limnol. Oceanogr.*, 61, 1232–1244.

Ehleringer, J., Björkman, O. & Bjorkman, O. (1977). Quantum yields for CO2 uptake in C3 and C4 plants. *Plant Physiol.*, 59, 86–90.

Eilers, P.H.C. & Peeters, J.C.H. (1988). A model for the relationship between light intensity and the rate of photosynthesis in phytoplankton. *Ecol. Modell.*, 42, 199–215.

Eppley, R.W. (1972). Temperature and phytoplankton growth in the sea. *Fish. Bull.*, 70, 1063–1085.

Evans, J.R. (1989). Photosynthesis and nitrogen relationship in leaves of C3 plants. *Oecologia*, 78, 9–19.

Falkowski, P.G., Barber, R.T. & Smetacek, V. (1998). Biogeochemical Controls and Feedbacks on Ocean Primary Biogeochemical Controls and Feedbacks on Ocean Primary Production. *Science*, 281, 200–207.

Falkowski, P.G., Fenchel, T. & Delong, E.F. (2008). The Microbial Engines That Drive Earth's Biogeochemical Cycles. *Science*, 320, 1034–1039.

Falkowski, P.G., Gan, R. & Wyman, K. (1985). Growth-irradiance relationships in phytoplankton. *Limnol. Oceanogr.*, 30, 311–321.

Falkowski, P.G., Katz, M.E., Knoll, A.H., Quigg, A., Raven, J.A., Schofield, O., *et al.* (2004). The evolution of modern eukaryotic phytoplankton. *Science*, 305, 354–60.

Falkowski, P.G., Katz, M.E., Milligan, A.J., Fennel, K., Cramer, B.S., Aubry, M.P., *et al.* (2005). The Rise of Oxygen over the Past 205 Million Years and the Evolution of Large Placental Mammals. *Science*, 309, 2202–2204.

Farquhar, G.D., Caemmerer, S. Von & Berry, J.A. (1980). A Biochemical Model of Photosynthetic CO2 Assimilation in Leaves of C3 species. *Planta*, 149, 78–90.

Field, C.B., Behrenfeld, M.J., Randerson, J.T. & Falkowski, P.G. (1998). Primary Production of the Biosphere: Integrating Terrestrial and Oceanic Components. *Science*, 281, 237–240.

Finkel, Z. V., Beardall, J., Flynn, K.J., Quigg, A., Rees, T.A. V. & Raven, J.A. (2010). Phytoplankton in a changing world: Cell size and elemental stoichiometry. *J. Plankton Res.*, 32, 119–137.

Finkel, Z.V. (2001). Light absorption and size scaling of light-limited metabolism in marine diatoms. *Limnol. Oceanogr.*, 46, 86–94.

Flombaum, P., Gallegos, J.L., Gordillo, R. a, Rincón, J., Zabala, L.L., Jiao, N., *et al.* (2013). Present and future global distributions of the marine Cyanobacteria Prochlrococcus and Synechococcus. *Pnas*, 110, 9824–9829.

Follows, M.J., Dutkiewicz, S., Grant, S. & Chisholm, S.W. (2007). Emergent Biogeography of Microbial Communities in a Model Ocean. *Science*, 315, 1843–1846.

Forster, J., Hirst, a. G. & Atkinson, D. (2012). Warming-induced reductions in body size are greater in aquatic than terrestrial species. *Proc. Natl. Acad. Sci.*, 109, 19310–19314.

Forster, J., Hirst, A.G. & Esteban, G.F. (2013). Achieving temperature-size changes in a unicellular organism. *ISME J.*, 7, 28–36.

Frazier, M.R., Huey, R.B. & Berrigan, D. (2006). Thermodynamics Constrains the Evolution of Insect Population Growth Rates: “Warmer Is Better.” *Am. Nat.*, 168, 512–520.

Frei, R., Gaucher, C., Poulton, S.W. & Canfield, D.E. (2009). Fluctuations in Precambrian atmospheric oxygenation recorded by chromium isotopes. *Nature*, 461, 250–253.

García, F.C., García-Martín, E.E., Taboada, F.G., Sal, S., Serret, P. & López-Urrutia, Á. (2016). The allometry of the smallest: Superlinear scaling of microbial metabolic rates in the Atlantic Ocean. *ISME J.*, 10, 1029–1036.

García-Carreras, B., Sal, S., Padfield, D., Kontopoulos, D.-G., Bestion, E., Schaum, C.-E., *et al.* (2018). Role of carbon allocation efficiency in the temperature dependence of autotroph growth rates. *Proc. Natl. Acad. Sci.*, 115, E7361–E7368.

Geider, R.J. & Osborne, B.A. (1989). Respiration and microalgal growth : a review of the quantitative relationship. *New Phytol.*, 112, 327–341.

Gillooly, J.F. (2001). Effects of Size and Temperature on Metabolic Rate. *Science*, 293, 2248–2251.

Grzebyk, D., Schofield, O., Vetriani, C. & Falkowski, P.G. (2003). Minireview The Mesozoic Radiation of Eukaryotic Algae: The Portable Plastid Hypothesis. *J. Phycol.*, 267, 259–267.

Hao, Y.Q., Brockhurst, M.A., Petchey, O.L. & Zhang, Q.G. (2015). Evolutionary rescue can be impeded by temporary environmental amelioration. *Ecol. Lett.*, 18, 892–898.

Henriques, M., Silva, A. & Rocha, J. (2007). Extraction and quantification of pigments from a marine microalga : a simple and reproducible method. *Commun. Curr. Res. Educ. Top. Trends Appl. Microbiol.*, 586–593.

Henson, S.A., Beaulieu, C., Ilyina, T., John, J.G., Long, M., Séférian, R., *et al.* (2017). Rapid emergence of climate change in environmental drivers of marine ecosystems. *Nat. Commun.*, 8, 1–9.

Hillebrand, H., Dürselen, C.-D., Kirschtel, D., Pollingher, U. & Zohary, T. (1999). Biovolume Calculation for Pelagic and Benthic Microalgae. *J. Phycol.*, 35, 403–424.

Ho, T., Quigg, A., Zoe, V., Milligan, A.J., Falkowski, P.G. & Morel, M.M. (2003). The Elemental Composition of Some Marine Phytoplankton. *J. Phycol.*, 39, 1145–1159.

Huete-Ortega, M., Cermeño, P., Calvo-Díaz, A. & Marañón, E. (2012). Isometric size-scaling of metabolic rate and the size abundance distribution of phytoplankton. *Proc. R. Soc. B Biol. Sci.*, 279, 1815–1823.

IPCC. (2013). Observations: Ocean Pages. *Clim. Chang. 2013 - Phys. Sci. Basis*, 255–316.

Irwin, A.J. & Oliver, M.J. (2009). Are ocean deserts getting larger? *Geophys. Res. Lett.*, 36, 1–5.

Kattge, J. & Knorr, W. (2007). Temperature acclimation in a biochemical model of photosynthesis: A reanalysis of data from 36 species. *Plant, Cell Environ.*, 30, 1176–1190.

Kawecki, T.J. & Ebert, D. (2004). Conceptual issues in local adaptation. *Ecol. Lett.*, 7, 1225–1241.

Keeling, P.J. (2004). Diversity and evolutionary history of plastids and their hosts. *Am. J. Bot.*, 91, 1481–1493.

Keeling, P.J. (2010). The endosymbiotic origin, diversification and fate of plastids. *Philos. Trans. R. Soc. B Biol. Sci.*, 365, 729–748.

Kingsolver, J.G. (2009). The Well-Temperatured Biologist. *Am. Nat.*, 174, 755–768.

Kleiber, M. (1932). Body size and metabolism. *Hilgardia A J. Agric. Sci.*

Kleiber, M. (1947). Body Size and Metabolic Rate. *Physiol. Rev.*, 27.

Knies, J.L., Kingsolver, J.G. & Burch, C.L. (2009). Hotter Is Better and Broader: Thermal Sensitivity of Fitness in a Population of Bacteriophages. *Am. Nat.*, 173, 419–430.

Knoll, A.H. (1992). The early evolution of eukaryoptes: a geological perspective. *Science*, 256, 622–627.

Kremer, C.T., Thomas, M.K. & Litchman, E. (2017). Temperature- and size-scaling of phytoplankton population growth rates: Reconciling the Eppley curve and the metabolic theory of ecology. *Limnol. Oceanogr.*, 62, 1658–1670.

Kulk, G., de Vries, P., van de Poll, W., Visser, R. & Buma, A. (2012). Temperature-dependent growth and photophysiology of prokaryotic and eukaryotic oceanic picophytoplankton. *Mar. Ecol. Prog. Ser.*, 466, 43–55.

Laufkotter, C., Vogt, M., Gruber, N., Aita-Noguchi, M., Aumont, O., Bopp, L., *et al.* (2015). Drivers and uncertainties of future global marine primary production in marine ecosystem models. *Biogeosciences*, 12, 6955–6984.

Lenton, T. & Watson, A. (2012). *Revolutions That Made the Earth*. 1st edn. Oxford University Press.

Lewis, L.A. & McCourt, R.M. (2004). Green algae and the origin of land plants. *Am. J. Bot.*, 91, 1535–1556.

Li, W.K.W. (2002). Macroecological patterns of phytoplankton in th enorthwestern North Atlantic Ocean. *Nature*, 419, 154–157.

Li, W.K.W., Harrison, W.G. & Head, E.J.H. (2006). Coherent assembly of phytoplankton communities in diverse temperate ocean ecosystems. *Proc. R. Soc. B Biol. Sci.*, 273, 1953–1960.

Listmann, L., LeRoch, M., Schluter, L., Thomas, M.K. & Reusch, T.B.H. (2016). Swift thermal reaction norm evolution in a key marine phytoplankton species. *Evol. Appl.*, 9, 1156–1164.

Litchman, E. & Klausmeier, C.A. (2008). Trait-Based Community Ecology of Phytoplankton. *Annu. Rev. Ecol. Evol. Syst.*, 39, 615–639.

Litchman, E., Klausmeier, C.A., Schofield, O.M. & Falkowski, P.G. (2007). The role of functional traits and trade-offs in structuring phytoplankton communities: Scaling from cellular to ecosystem level. *Ecol. Lett.*, 10, 1170–1181.

Lohbeck, K.T., Riebesell, U. & Reusch, T.B.H. (2012). Adaptive evolution of a key phytoplankton species to ocean acidification. *Nat. Geosci.*, 5, 346–351.

López-Sandoval, D.C., Rodríguez-Ramos, T., Cermeño, P., Sobrino, C. & Marañón, E. (2014). Photosynthesis and respiration in marine phytoplankton: Relationship with cell size, taxonomic affiliation, and growth phase. *J. Exp. Mar. Bio. Ecol.*, 457, 151–159.

López-Urrutia, Á. & Morán, X.A.G. (2015). Temperature affects the size-structure of phytoplankton communities in the ocean. *Limnol. Oceanogr.*, 60, 733–738.

Lopez-Urrutia, A., San Martin, E., Harris, R.P. & Irigoien, X. (2006). Scaling the metabolic balance of the oceans. *Proc. Natl. Acad. Sci.*, 103, 8739–8744.

Lynch, M., Conery, J.S. & Galtier, N. (2003). The origins of genome complexity. *Science*, 302, 1401–4.

Malerba, M.E., Palacios, M.M., Palacios Delgado, Y.M., Beardall, J. & Marshall, D.J. (2018). Cell size, photosynthesis and the package effect: an artificial selection approach. *New Phytol.*, 449–461.

Marañón, E., Cermeño, P., López-Sandoval, D.C., Rodríguez-Ramos, T., Sobrino, C., Huete-Ortega, M., *et al.* (2013). Unimodal size scaling of phytoplankton growth and the size dependence of nutrient uptake and use. *Ecol. Lett.*, 16, 371–379.

Maranón, E., Cermeno, P., Rodríguez, J., Zubkov, M. V. & Harris, R.P. (2007). Scaling of phytoplankton photosynthesis and cell size in the ocean. *Limnol. Oceanogr.*, 52, 2190–2198.

Marañón, E., Lorenzo, M.P., Cermeño, P. & Mouriño-Carballido, B. (2018). Nutrient limitation suppresses the temperature dependence of phytoplankton metabolic rates. *ISME J.*

Martinez, E., Antoine, E., Ortenzio, F. & Gentili, B. (2009). Climate-driven decadal-scale oscillations of Oceanic Phytoplankton. *Science*, 326, 1253–56.

Mathur, S., Agrawal, D. & Jajoo, A. (2014). Photosynthesis: Response to high temperature stress. *J. Photochem. Photobiol. B Biol.*, 137, 116–126.

Medlyn, B.E., Dreyer, E., Ellsworth, D., Forstreuter, M., Harley, P.C., Kirschbaum, M.U.F., *et al.* (2002). Temperature response of parameters of a biochemically based model of photosynthesis. II. A review of experimental data. *Plant, Cell Environ.*, 25, 1167–1179.

Menden-Deuer, S. & Lessard, E.J. (2000). Carbon to volume relatinship for dinoflagellates, diatoms and other protist plankton. *Limnol. Oceanogr.*, 45, 569–579.

Montagnes, D.J.S., Berges, J.A., Harrison, P.J. & Taylor, F.J.R. (1994). Estimating carbon, nitrogen, protein, and chlorophyll a from volume in marine phytoplankton. *Limnol. Oceanogr.*, 39, 1044–1060.

Montagnes, D.J.S. & Franklin, D.J. (2001). Effect of temperature on diatom volume, growth rate, and carbon and nitrogen content: Reconsidering some paradigms. *Limnol. Oceanogr.*, 46, 2008–2018.

Moore, C.M., Mills, M.M., Arrigo, K.R., Berman-Frank, I., Bopp, L., Boyd, P.W., *et al.* (2013). Processes and patterns of oceanic nutrient limitation. *Nat. Geosci.*, 6, 701–710.

Morán, X.A.G., López-Urrutia, Á., Calvo-Díaz, A. & Li, W.K.W. (2010). Increasing importance of small phytoplankton in a warmer ocean. *Glob. Chang. Biol.*, 16, 1137–1144.

Muggeo, V.M.R. (2003). Estimating regression models with unknown break-points. *Stat. Med.*, 22, 3055–3071.

Norberg, J., Urban, M.C., Vellend, M. & Al, E. (2012). Eco-evolutionary responses of biodiversity to climate change. *Nat. Clim. Chang.*, 2, 1–5.

O'Donnell, D.R., Hamman, C.R., Johnson, E.C., Kremer, C.T., Klausmeier, C.A. & Litchman, E. (2018). Rapid thermal adaptation in a marine diatom reveals constraints and trade-offs. *Glob. Chang. Biol.*

Olson, R.J., Vaulot, D. & Chisholm, S.W. (1986). Effects of Environmental Stresses on the Cell Cycle of Two Marine Phytoplankton Species. *Plant Physiol.*, 80, 918–925.

Orr, H.A. (2000). Adaptation and the cost of complexity. *Evolution (N. Y).*, 54, 13–20.

Padfield, D., Lowe, C., Buckling, A., Ffrench-Constant, R., Jennings, S., Shelley, F., *et al.* (2017). Metabolic compensation constrains the temperature dependence of gross primary production. *Ecol. Lett.*, 20, 1250–1260.

Padfield, D., Yvon-Durocher, G., Buckling, A., Jennings, S. & Yvon-Durocher, G. (2016). Rapid evolution of metabolic traits explains thermal adaptation in phytoplankton. *Ecol. Lett.*, 19, 133–142.

Palenik, B., Barahamsha, B., Larimer, F.W., Land, M., Hauser, L., Chain, P., *et al.* (2003). The genomes of a motile marine Synechococcus. *Nature*, 424, 1037–1042.

Palenik, B., Grimwood, J., Aerts, A., Rouze, P., Salamov, A., Putnam, N., *et al.* (2007). The tiny eukaryote Ostreococcus provides genomic insights into the paradox of plankton speciation. *Proc. Natl. Acad. Sci.*, 104, 7705–7710.

Pawar, S., Dell, A.I., Savage, V.M. & Knies, J.L. (2016). Real versus Artificial Variation in the Thermal Sensitivity of Biological Traits. *Am. Nat.*, 187, E41–E52.

Pingree, R.D., Pugh, P.R., Holligan, P.M. & Forster. (1975). Summer phytoplankton blooms and red tides along tidal fronts in the approaches to the English Channel. *Nature*, 258, 672–677.

Poloczanska, E.S., Brown, C.J., Sydeman, W.J., Kiessling, W., Schoeman, D.S., Moore, P.J., *et al.* (2013). Global imprint of climate change on marine life. *Nat. Clim. Chang.*, 3, 919–925.

Le Quere, C., Harrison, S.P., Colin Prentice, I., Buitenhuis, E.T., Aumont, O., Bopp, L., *et al.* (2005). Ecosystem dynamics based on plankton functional types for global ocean biogeochemistry models. *Glob. Chang. Biol.*, 11, 2016–2040.

Quigg, A., Finkel, Z. V, Irwin, A.J., Rosenthal, Y., Ho, T.-Y., Reinfelder, J.R., *et al.* (2003). The evolutionary inheritance of elemental stoichiometry in marine phytoplankton. *Nature*, 425, 291–4.

Raven, J.A. (1976). The Quantitative Role of ' Dark ' Respiratory Processes in Heterotrophic and Photolithotrophic Plant Growth, 587–602.

Raven, J.A. (1994). Why are there no picoplanktonic O 2 evolvers with volumes less than 10 −19 m 3 ? *J. Plankton Res.*, 16, 565–580.

Raven, J.A. (1998). The twelfth Tansley Lecture. Small is beautiful: The picophytoplankton. *Funct. Ecol.*, 12, 503–513.

Raven, J.A., Cockell, C.S. & De La Rocha, C.L. (2008). The evolution of inorganic carbon concentrating mechanisms in photosynthesis. *Philos. Trans. R. Soc. B Biol. Sci.*, 363, 2641–2650.

Raven, J.A. & Geider, R.J. (1988). Temperature and algal growth. *New Phytol.*, 110, 441–461.

Redfield, A.. (1958). The Biological Control of Chemical Factors in the Environment. *Am. Sci.*, 46, 205–221.

Regaudie-De-Gioux, A. & Duarte, C.M. (2012). Temperature dependence of planktonic metabolism in the ocean. *Global Biogeochem. Cycles*, 26, 1–10.

Retallack, G.J. (2001). Cenozoic Expansion of Grasslands and Climatic Cooling. *J. Geol.*, 109, 407–426.

Reusch, T.B.H. & Boyd, P.W. (2013). Experimental Evolution Meets Marine Phytoplankton. *Evolution (N. Y).*, 67, 1849–1859.

Richardson, T.. & Jackson, G.. (2007). Small Phytoplankton and Carbon Export from the Surface Ocean. *Science*, 315, 838–840.

Ritchie, R.J. (2006). Consistent sets of spectrophotometric chlorophyll equations for acetone, methanol and ethanol solvents. *Photosynth. Res.*, 89, 27–41.

Ruddiman, W.F., Ellis, E.C., Kaplan, J.O. & Fuller, D.Q. (2015). Defining the epoch we live in. *Science*, 348, 38–39.

Rumpho, M.E., Ku, M.S.B., Cheng, S.-H. & Edwards, G.E. (1984). Photosynthetic Characteristics of C3-C4 Intermediate Flaveria Species. *Plant Physiol.*, 75, 993–996.

Sagan, L. (1967). On the origin of mitosing cells. *J. Theor. Biol.*, 14, 225–IN6.

Sal, S., Alonso-Saez, L., Bueno, J., Garcıa, F.C. & Lopez-Urrutia, A. (2015). Thermal adaptation, phylogeny, and the unimodal size scaling of marine phytoplankton growth. *Limnol. Oceanogr.*, 60, 1212–1221.

Saunders, G.W. & Hommersand, M.H. (2004). Assessing red algal supraordinal diversity and taxonomy in the context of contemporary systematic data. *Am. J. Bot.*, 91, 1494–1507.

Savage, V., Gillooly, J., Woodruff, W., West, G., Allen, A., Enquist, B.J., *et al.* (2004a). The predominance of quarter • power scaling in biology. *Funct. Ecol.*, 18, 257–282.

Savage, V.M., Gillooly, J.F., Brown, J.H., West, G.B. & Charnov, E.L. (2004b). Effects of Body Size and Temperature on Population Growth. *Am. Nat.*, 163, 429–441.

Schaum, C.-E. (2018). Enhanced biofilm formation aids adaptation to extreme warming and environmental instability in the diatom *Thalassiosira pseudonana* and its associated bacteria. *Limnol. Oceanogr.*, 1–20.

Schaum, C.-E., Barton, S., Bestion, E., Buckling, A., Garcia-Carreras, B., Lopez, P., *et al.* (2017). Adaptation of phytoplankton to a decade of experimental warming linked to increased photosynthesis. *Nat. Ecol. Evol.*, 1, 0094.

Schaum, C.-E., Buckling, A., Smirnoff, N., Studholme, D.J. & Yvon-Durocher, G. (2018). Environmental fluctuations accelerate molecular evolution of thermal tolerance in a marine diatom. *Nat. Commun.*, 1–14.

Schaum, E., Rost, B., Millar, A.J. & Collins, S. (2012). Variation in plastic responses of a globally distributed picoplankton species to ocean acidification. *Nat. Clim. Chang.*, 3, 298–302.

Schirrmeister, B.E., de Vos, J.M., Antonelli, a. & Bagheri, H.C. (2013). Evolution of multicellularity coincided with increased diversification of cyanobacteria and the Great Oxidation Event. *Proc. Natl. Acad. Sci.*, 110, 1791–1796.

Schlüter, L., Lohbeck, K.T., Gutowska, M.A., Gröger, J.P., Riebesell, U. & Reusch, T.B.H. (2014). Adaptation of a globally important coccolithophore to ocean warming and acidification. *Nat. Clim. Chang.*, 1–7.

Schneider, C.A., Rasband, W.S. & Eliceiri, K.W. (2012). NIH Image to ImageJ: 25 years of image analysis. *Nat. Methods*, 9, 671–675.

Schoolfield, R.M., Sharpe, P.J.H. & Magnuson, C.E. (1981). Non-linear regression of biological temperature-dependent rate models based on absolute reaction-rate theory. *J. Theor. Biol.*, 88, 719–731.

Sharpe, P.J.H. & DeMichele, D. (1977). Reaction Kinetics of Poikilotherm Development. *J. Theor. Biol.*, 64, 649–670.

Shuter, B. (1979). A model of physiological adaption in unicellular algae. *J. Theor. Biol.*, 78, 519–552.

Somero, G.N. & Hochachka, P.W. (1971). Biochemical adaptation to the Environment. *Am. Zool.*, 11, 159–167.

Sommer, U. (1989). Maximal growth rates of Antarctic phytoplankton: Only weak dependence on cell size. *Limnol. Oceanogr.*, 34, 1109–1112.

Stock, C.A., Dunne, J.P. & John, J.G. (2014). Global-scale carbon and energy flows through the marine planktonic food web: An analysis with a coupled physical-biological model. *Prog. Oceanogr.*, 120, 1–28.

Sun, J. & Liu, D. (2003). Geometric models for calculating cell biovolume and surface area for phytoplankton. *J. Plankton Res.*, 25, 1331–1346.

Tang, E.P. (1995). The allometry of algal growth rates. *J. Plankton Res.*, 17, 1325–1335.

Thomas, M.K., Kremer, C.T., Klausmeier, C.A. & Litchman, E. (2012). A Global Pattern of Thermal Adaptation in Marine Phytoplankton. *Science*, 338, 1085–1088.

Thomas, M.K., Kremer, C.T. & Litchman, E. (2016). Environment and evolutionary history determine the global biogeography of phytoplankton temperature traits. *Glob. Ecol. Biogeogr.*, 25, 75–86.

Toseland, A., Daines, S.J., Clark, J.R., Kirkham, A., Strauss, J., Uhlig, C., *et al.* (2013). The impact of temperature on marine phytoplankton resource allocation and metabolism. *Nat. Clim. Chang.*, 3, 979–984.

Townesend, D.W., Cammen, L.M., Holligan, P.M., Campbell, D.E. & Pettigrew, N.R. (1994). Causes and consequences of variability in the timing of phytoplankton blooms. *Deep. Res. Part I*, 41, 747–765.

Tréguer, P. & Pondaven, P. (2000). Silica control of carbon dioxide. *Nature*, 406, 358–359.

Verity, P.G., Robertson, C.Y., Tronzo, C.R., Andrews, M.G., Nelson, J.R. & Sieracki, M.E. (1992). Relationship between cell volume and the carbon and nitrogen contentof marine photosynthetic nanoplankton. *Limnol. Oceanogr.*, 37, 1434–1446.

Winder, M., Reuter, J.E. & Schladow, S.G. (2009). Lake warming favours small-sized planktonic diatom species. *Proc. R. Soc. B Biol. Sci.*, 276, 427–435.

Wohlers, J., Engel, A., Zollner, E., Breithaupt, P., Jurgens, K., Hoppe, H.G., *et al.* (2009). Changes in biogenic carbon flow in response to sea surface warming. *Pnas*, 106, 7067–7072.

Wood, A.., Everroad, R.. & Wingard, L.. (2005). Measuring Growth Rates in Microalgal Cultures. In: *Algal Culturing Techniques*. pp. 269 – 287.

Yoshiyama, K. & Klausmeier, C.A. (2008). Optimal Cell Size for Resource Uptake in Fluids: A New Facet of Resource Competition. *Am. Nat.*, 171, 59–70.

Yvon-Durocher, G., Caffrey, J.M., Cescatti, A., Dossena, M., Giorgio, P. Del, Gasol, J.M., *et al.* (2012). Reconciling the temperature dependence of respiration across timescales and ecosystem types. *Nature*, 487, 472–476.

Yvon-Durocher, G., Jones, J.I., Trimmer, M., Woodward, G. & Montoya, J.M. (2010). Warming alters the metabolic balance of ecosystems. *Philos. Trans. R. Soc. B Biol. Sci.*, 365, 2117–2126.